Universidad Autónoma de Madrid
Instituto de Física Teórica
UAM/CSIC

PhD Thesis

The Phenomenological Landscape of Leptophilic ALPs

Arturo de Giorgi

Supervisor
Prof. Dr. Luca Merlo

Madrid, June 19, 2024

A mia nonna Adriana.

Ph.D. Scientific Production

1. J. Alonso-Gonzalez, A. de Giorgi, L. Merlo, and S. Pokorski, *Searching for BSM physics in Yukawa couplings and flavour symmetries*, JHEP **05** (2022) 041, [arXiv:2109.07490]
2. A. de Giorgi and S. Vogl, *Warm dark matter from a gravitational freeze-in in extra dimensions*, JHEP **04** (2023) 032, [arXiv:2208.03153]
3. J. Bonilla, A. de Giorgi, B. Gavela, L. Merlo, and M. Ramos, *The cost of an ALP solution to the neutral B-anomalies*, JHEP **02** (2023) 138, [arXiv:2209.11247]
4. A. de Giorgi, L. Merlo, and S. Pokorski, *The Low-Scale Seesaw Solution to the M_W and $(g-2)\mu$ Anomalies*, Fortsch. Phys. **71** (2023), no. 4-5 2300020, [arXiv:2211.03797]
5. J. Bonilla, A. de Giorgi, and M. Ramos, *Neutral B-anomalies from an on-shell scalar exchange*, arXiv:2211.05135
6. A. de Giorgi and G. Piazza, *A lesson from $R_{\tau\tau}^{K^{(*)}}$ and $R_{\nu\nu}^{K^{(*)}}$ at Belle II*, Fortsch. Phys. **72** (2024), no. 1 2300200, [arXiv:2211.05595]
7. A. de Giorgi, L. Merlo, and J.-L. Tastet, *Probing HNL-ALP couplings at colliders*, Fortsch. Phys. **71** (2023), no. 4-5 2300027, [arXiv:2212.11290]
8. A. de Giorgi, F. Koutroulis, L. Merlo, and S. Pokorski, *Flavour and Higgs physics in Z2-symmetric 2HD models near the decoupling limit*, Nucl. Phys. B **994** (2023) 116323, [arXiv:2304.10560]
9. A. de Giorgi and S. Vogl, *Gravity-matter sum rules in models with a single extra-dimension*, JHEP **05** (2024) 315, [arXiv:2311.01507]
10. A. de Giorgi, L. Merlo, X. Ponce Díaz, and S. Rigolin, *The minimal massive Majoron Seesaw Model*, JHEP **03** (2024) 094, [arXiv:2312.13417]
11. A. de Giorgi, M. F. Zamoro, and L. Merlo, *GeV ALP from TeV Vector-like Leptons*, arXiv:2402.14059

Abstract

In this thesis, we consider model-building and phenomenology related to the simultaneous presence, alongside the Standard Model, of an Axion-Like Particle (ALP) and Heavy Neutral Leptons (HNLs). The former is naturally produced when global symmetries are spontaneously broken; the latter constitutes some of the most appealing candidates to "naturally" explain the smallness of neutrino masses. Altogether, this combination of particles naturally arises in Majoron models. We consider various UV models that could produce such a particle and possible mechanisms that could generate its mass radiatively. Bounds from flavour-, collider- and astro-searches are investigated.

Resumen

En esta tesis, consideramos la construcción de modelos y la fenomenología relacionada con la presencia simultánea, junto al Modelo Estándar, de un Axion-Like Particle (ALP) y de Leptones Neutrales Pesados (HNLs). La primera se produce de forma natural cuando se rompen espontáneamente las simetrías globales; la segunda constituye uno de los candidatos más atractivos para explicar de forma "natural" la pequeñez de las masas de neutrinos. En conjunto, esta combinación de partículas surge de forma natural en los modelos de Majorones. Consideramos varios modelos UV que podrían producir dicha partícula y posibles mecanismos que podrían generar su masa de forma radiativa. Los límites de las búsquedas de sabores, colisionadores y astros son investigado.

Contents

Introduction

The Higgs boson discovery in 2012 at LHC crowned the Standard Model (SM) completion. The number of successes of this theory is truly remarkable, making it perhaps the most successful theory ever created. Despite this, plenty of room exists for research Beyond the SM (BSM). On one side, the Higgs sector scalar potential parameters have not yet been measured with sufficient precision to rule out New Physics (NP) altering the Higgs mechanism. On the other hand, some experimental problems *require* the extension of the SM, the most notable probably being neutrino masses and Dark Matter. The lack of precise data does not point to preferred solutions, leaving space for a wide number of directions in BSM model building. We then have puzzles within the SM: why are the couplings and the structure the way they are? Why are there huge hierarchies within a set of particles that get their masses from the same field? The relation of such questions to NP is not certain, but it is a very enriching study which often deepens our understanding of the SM itself. Where NP will show up first is the hard question, which depends solely on Nature and could surprise us as it did in the early 20th century. As it happens in fundamental research, the usefulness of our research for future generations will be proven only by the "nature" of Nature itself: as a famous Italian author once said, *Ai posteri l'ardua sentenza* [1] ("posterity will judge").

The BSM candidates of this thesis are two of the most motivated NP particles: Heavy Right-Handed neutrinos, or more generically, Heavy Neutral Leptons (HNLs), and Axion-Like Particles (ALPs). The former is perhaps theoretically the most motivated candidate to address the smallness of neutrino masses. HNLs come with a rich phenomenology whose impact depends on their masses and flavour structure. The latter, which amounts to the effective theory of a pseudo-Nambu-Goldstone Boson (pNGB), is the byproduct of Spontaneous Symmetry Breaking (SSB) of global symmetries. The motivations to study such particles are complementary: from the experimental point of view, their lightness is theoretically solid and provided by their pNGB nature allows for them to be produced on-shell in terrestrial and astrophysical

[1] *Il cinque maggio*, A. Manzoni, 1821.

environments. From a more theoretical point of view, one may wonder if SSB is or is not a rare phenomenon in particle physics; if this was common in BSM extensions, the question that naturally arises is: how likely is that a global SSB occurs from the TeV- to the Planck scale? Indeed, it turns out that ALPs arise in many contexts, ranging from flavour models to String Theory. This Thesis explores the consequences of the simultaneous presence of HNLs and ALPs within specific UV models and the context of Effective Field Theory (EFT). Such NP combination is special as it can lead to a mutual enhancement in their potential discoveries.

The structure of the Thesis is the following. In Chapter 1, we summarise the theoretical foundations of the Standard Model (SM), the most relevant features that will be influenced by New Physics (NP), as well as its current problem and puzzles which NP could solve. In Chapter 2, we introduce the two main protagonists of the thesis: Heavy Neutral Leptons (HNLs) (Sec. 2.1), more precisely, heavy right-handed neutrinos, and Nambu-Goldstone Bosons NGBs (Sec. 2.2), with special focus on Axion-Like particles (ALPs) and Majorons. Both sections are structured to present an overview of their theoretical foundations and their phenomenology. Finally, Chapter 3 is dedicated to the selection of papers produced during the PhD, which constitute the original research of this Thesis. Further details about the structure of this manuscript can be found in the table of contents.

Introducción

El descubrimiento del bosón de Higgs en 2012 en el LHC supuso la culminación del Modelo Estándar (SM). El número de éxitos de esta teoría es realmente notable, convirtiéndola quizás en la teoría más exitosa jamás creada. A pesar de ello, aún queda mucho por investigar más allá del SM (BSM). Por un lado, los parámetros del potencial escalar del sector de Higgs aún no se han medido con suficiente precisión como para descartar que la Nueva Física (NF) altere el mecanismo de Higgs. Por otro lado, algunos problemas experimentales *requieren* la ampliación del SM, siendo probablemente los más notables las masas de neutrinos y la materia oscura. La falta de datos precisos no apunta a soluciones preferidas, dejando espacio para un amplio número de direcciones en la construcción del modelo BSM. Así pues, tenemos enigmas dentro del SM: ¿por qué los acoplos y la estructura son como son? ¿Por qué existen enormes jerarquías dentro de un conjunto de partículas que obtienen sus masas del mismo campo? La relación de estas cuestiones con la NF no es segura, pero se trata de un estudio muy enriquecedor que a menudo profundiza nuestra comprensión del propio SM. Dónde aparecerá primero la NF es la pregunta difícil, que depende exclusivamente de la Naturaleza y podría sorprendernos como lo hizo a principios del siglo XX. Como ocurre en la investigación fundamental, la utilidad de nuestra investigación para las generaciones futuras sólo la probará la "naturaleza" de la propia Naturaleza: como dijo una vez un famoso autor italiano, *Ai posteri l'ardua sentenza* [2] ("la posteridad juzgará").

Los candidatos a BSM de esta tesis son dos de las partículas NF más motivadas: Los neutrinos pesados diestros, o más genéricamente, los leptones neutros pesados (HNLs), y partículas de tipo axión (ALPs). El primero es quizás el candidato teóricamente más motivado para abordar la pequeñez de las masas de neutrinos. Los HNL vienen acompañadas de una rica fenomenología cuyo impacto depende de sus masas y estructura de sabor. Esta última, que equivale a la teoría efectiva de un pseudo Bosón de Nambu-Goldstone (pNGB), es el subproducto de la Ruptura Espontánea de Simetría (SSB) de simetrías globales. Las motivaciones para estu-

[2] *Il cinque maggio*, A. Manzoni, 1821.

diar tales partículas son complementarias: desde el punto de vista experimental, su ligereza es teóricamente sólida y su naturaleza de pNGB permite que se produzcan on-shell en entornos terrestres y astrofísicos. Desde un punto de vista más teórico, cabe preguntarse si el SSB es o no un fenómeno raro en la física de partículas; si esto fuera común en las extensiones BSM, la pregunta que surge naturalmente es: ¿hasta qué punto es probable que se produzca un SSB global desde la escala TeV hasta la escala de Planck? De hecho, resulta que los ALP surgen en muchos contextos, desde los modelos de sabores hasta la Teoría de Cuerdas. Esta Tesis explora las consecuencias de la presencia simultánea de HNLs y ALPs dentro de modelos UV específicos y en el contexto de la Teoría de Campo Efectivo (EFT). Tal combinación de HNLs es especial ya que puede conducir a una mejora mutua en sus descubrimientos potenciales.

La estructura de la Tesis es la siguiente. En el Capítulo 1, resumimos los fundamentos teóricos del Modelo Estándar (SM), las características más relevantes que se verán influenciadas por la Nueva Física (NF), así como su problemática actual y los enigmas que la NP podría resolver. En el Capítulo 2, presentamos a los dos protagonistas principales de la tesis: los Leptones Neutros Pesados (HNLs) (Sec. 2.1), más concretamente, los neutrinos pesados diestros, y los Bosones Nambu-Goldstone NGBs (Sec. 2.2), con especial atención a las partículas similares al Axión (ALPs) y a los Majorones. Ambas secciones están estructuradas para presentar una visión general de sus fundamentos teóricos y su fenomenología. Finalmente, el Capítulo 3 está dedicado a la selección de trabajos realizados durante el doctorado, que constituyen la investigación original de esta Tesis. Para más detalles sobre la estructura de este manuscrito, véase el índice.

Chapter 1

The Standard Model, Open Problems and Puzzles

1.1. The Standard Model

The Standard Model (SM) is our current best theory of three (electromagnetic, weak and strong) of the four (gravity) known fundamental interactions in Nature. The SM is a renormalizable Poincaré-invariant quantum chiral gauge field theory. For such a theory to be defined, it needs three elements:

1. the gauge group of the theory;
2. the spectrum, i.e. the fields or particle content;
3. the symmetries of the vacuum, or in other words Spontaneous Symmetry Breaking (SSB) patterns of the gauge group.

The SM is defined by the gauge group $G_{\rm SM} \equiv U(1)_Y \times SU(2)_L \times SU(3)_C$. The associated charges are typically called *hypercharge*, *weak-charge* and *colour*, respectively. The theory spectrum consists of the spin-1 gauge bosons of the corresponding gauge groups, a scalar and chiral 1/2-spin fermions. Their transformation properties under $G_{\rm SM}$ can be seen in Table 1.1. The scalar is usually referred to as *Higgs boson*. The fermions are referred to as *quarks* if they transform under $SU(3)_C$, or *leptons* if not. Both quarks and leptons appear in three copies, typically called 'flavour', distinguished only by their masses.

Field	$U(1)_Y$	$SU(2)_L$	$SU(3)_C$
Q_L^i	$1/6$	**2**	**3**
u_R^i	$2/3$	**1**	**3**
d_R^i	$-1/3$	**1**	**3**
L_L^i	$-1/2$	**2**	**1**
e_R^i	-1	**1**	**1**
H	$1/2$	**2**	**1**

Table 1.1: The particle spectrum of the SM and their representations. Fields with the $L(R)$-subscript transform in the left(right)-representation of the Lorentz group. The superscript $i = 1, 2, 3$ acts as the flavour index of the field. H denotes the Higgs boson.

Finally, the SM gauge group is spontaneously broken by the vacuum expectation value (vev) of the Higgs doublet down to the subgroup

$$G_{\text{SM}} = U(1)_Y \times SU(2)_L \times SU(3)_C \quad \to \quad U(1)_Q \times SU(3)_C \,, \tag{1.1}$$

where the charge $U(1)_Q$ is the *electric* charge.

1.1.1. The SM Lagrangian

The Lagrangian of the theory can be decomposed into four pieces[1]

$$\mathcal{L} = \mathcal{L}_{\text{Gauge}} + \mathcal{L}_{\text{Kinetic}} + \mathcal{L}_{\text{Higgs}} + \mathcal{L}_{\text{Yukawa}} \,. \tag{1.2}$$

The Lagrangian includes all operators allowed by Poincaré and G_{SM} symmetries up to energy dimension four.[2] This ensures the renormalizability and predictivity of the theory. We will consider them separately.

Gauge The pure gauge part of the SM also referred to as the Yang-Mills part [13], reads

$$\mathcal{L}_{\text{Gauge}} = -\frac{1}{4} B^{\mu\nu} B_{\mu\nu} - \frac{1}{4} W^{a\mu\nu} W^a_{\mu\nu} - \frac{1}{4} G^{a\mu\nu} G^a_{\mu\nu} + \theta_{\text{QCD}} \frac{g_s^2}{32\pi^2} G^{a\mu\nu} \widetilde{G}^a_{\mu\nu} \,, \tag{1.3}$$

[1] The Lagrangian of the ghost fields necessary for the gauge fixing is omitted here; it can be found e.g. in Ref. [12].

[2] The effects of operators with energy dimension greater than four in amplitudes are suppressed by energy powers at low-energy where the SM is defined, and are thus not relevant. The extension of the SM with such operators is called SMEFT; we will briefly introduce it in Section 2.1.

where $B_{\mu\nu}$, $W^a_{\mu\nu}$, $G^a_{\mu\nu}$ are the field strength tensors of $G_{\rm SM}$

$$B_{\mu\nu} \equiv \partial_\mu B_\nu - \partial_\nu B_\mu \,, \tag{1.4}$$

$$W^a_{\mu\nu} \equiv \partial_\mu W^a_\nu - \partial_\nu W^a_\mu - g\epsilon^{abc} W^b_\mu W^c_\nu \,, \tag{1.5}$$

$$G^a_{\mu\nu} \equiv \partial_\mu G^a_\nu - \partial_\nu G^a_\mu - g_s f^{abc}_s G^b_\mu G^c_\nu \,, \tag{1.6}$$

$\widetilde{G}^a_{\mu\nu}$ is the dual field strength

$$\widetilde{G}^a_{\mu\nu} \equiv \frac{1}{2}\epsilon^{\mu\nu\rho\sigma} G^a_{\rho\sigma} \,, \tag{1.7}$$

$\epsilon^{\mu\nu\rho\sigma}$ is the antisymmetric Levi-Civita symbol, and g', g and g_s are the gauge couplings of $G_{\rm SM}$, respectively. The constants ϵ^{abc} and f^{abc}_s are the *structure constants* of the corresponding group. Generically, denoted as T^a the generators of the group, the structure constants f^{abc} are defined by the commutator

$$[T^a, T^b] = i f^{abc} T^c \,. \tag{1.8}$$

For $SU(2)$, T^a is defined by the Pauli matrices σ^a, $T^a = \sigma^a/2$, while for $SU(3)$ by the Gell-Mann matrices λ^a, $T^a = \lambda^a/2$.

Kinetic - Fermions The requirement of gauge invariance forces the kinetic terms of the fermionic Lagrangian to also fix their interactions with the gauge bosons. Given a generic field ψ transforming under the fundamental representation of a gauge group with coupling g_Π and bosons Π^a, the covariant derivative is defined as

$$D_\mu \psi \equiv \left(\partial_\mu + i g_\Pi \Pi^a_\mu T^a\right) \psi \,. \tag{1.9}$$

For example, the covariant derivative of Q_L is given by

$$D_\mu Q_L = \left(\partial_\mu + i g' Y_{Q_L} B_\mu + i g \frac{\sigma^a}{2} W^a_\mu + i g_s \frac{\lambda^a}{2} G^a_\mu\right) Q_L \,. \tag{1.10}$$

The kinetic fermionic Lagrangian is then restricted to be

$$\mathcal{L}_{\psi\text{-Kinetic}} = \overline{Q_L} i \not{D} Q_L + \overline{u_R} i \not{D} u_R + \overline{d_R} i \not{D} d_R + \overline{L_L} i \not{D} L_L + \overline{e_R} i \not{D} e_R \,, \tag{1.11}$$

where $\not{D} \equiv \gamma^\mu D_\mu$. Group and flavour indices have been omitted for the sake of readability and will be considered implicit if not stated otherwise. Remarkably, the interactions of fermions with gauge bosons are controlled by the same gauge couplings defined in the Yang-Mills sector.

Higgs The covariant derivative also fixes the interactions of the Higgs doublet with gauge bosons. The Higgs Lagrangian can be written as

$$\mathcal{L} = (D^\mu H)^\dagger (D_\mu H) - V(H), \tag{1.12}$$

where the most generic potential compatible with the gauge symmetries and renormalizability reads

$$V(H) = -\mu^2 H^\dagger H + \lambda (H^\dagger H)^2 \,. \tag{1.13}$$

If $\mu^2 > 0$, the potential has a minimum at $H^\dagger H = \mu^2/2\lambda \equiv v^2/2$ and SSB occurs. Such information can be conveniently encoded into the doublet via the parametrization

$$H = \begin{pmatrix} G^+ \\ \dfrac{v + h + iG_Z}{\sqrt{2}} \end{pmatrix} . \tag{1.14}$$

The fields G_Z and G^+ are the Nambu-Goldstone Bosons (NGBs) stemming from the SSB. Using appropriate gauge fixing (see e.g. Ref. [12]), the NGBs can be absorbed into the massive gauge bosons. This choice goes in the literature under the name of *unitary gauge*; in such a gauge, one effectively can set $G_Z = G^\pm = 0$. This is the Brout–Englert–Higgs mechanism [14, 15, 16]. The remaining neutral field corresponding to the excitation of the vev, h, is the Higgs boson. Its mass is found to be $m_h^2 = 2\mu^2 = 2\lambda v^2$.

The combination of the SM gauge group that survives the SSB is $G_{\rm SM} \to U(1)_Q \times SU(3)_C$. By identifying

$$\begin{cases} A_\mu \equiv B_\mu \cos\theta_W + Z_\mu \sin\theta_W \,, \\ Z_\mu \equiv -B_\mu \sin\theta_W + W_\mu^3 \cos\theta_W \,, \end{cases} \qquad W_\mu^\pm \equiv \frac{W_\mu^1 \mp W_\mu^2}{2} \,, \tag{1.15}$$

one obtains the masses of the gauge bosons

$$M_W = \frac{1}{2} g v \,, \qquad M_Z = \frac{M_W}{\cos\theta_W} \,, \qquad m_A = 0, \tag{1.16}$$

where A is now the photon field of Quantum Electrodynamics (QED) and the *Weinberg angle* is defined as

$$\cos\theta_W \equiv \frac{g'}{\sqrt{g^2 + g'^2}} \,. \tag{1.17}$$

The scalar sector includes 2 new free parameters, e.g. m_h and v.

Yukawa The Yukawa part of the Lagrangian describes the interaction of the fermions with the Higgs doublet and provides them with a mass after SSB. It can be written down as

$$-\mathcal{L}_{\text{Yukawa}} = \overline{Q'_L}\widetilde{H}Y_u u'_R + \overline{Q'_L}HY_d d'_R + \overline{L'_L}HY_e e'_R + \text{h.c.}, \tag{1.18}$$

where $\widetilde{H} \equiv i\sigma^2 H^*$, $Y_{u,d,e}$ are generic 3×3 complex matrices typically dubbed *Yukawa matrices*, and Q_L and L_L are the quark and lepton doublets, respectively,

$$Q_L \equiv \begin{pmatrix} u_L \\ d_L \end{pmatrix}, \qquad L_L \equiv \begin{pmatrix} \nu_L \\ e_L \end{pmatrix}. \tag{1.19}$$

After SSB, the fermions obtain mass terms

$$-\mathcal{L}_{\text{Yukawa}} \supset \overline{u'_L}m'_u u'_R + \overline{d'_L}m'_d d'_R + \overline{e'_L}m'_e e'_R + \text{h.c.}, \tag{1.20}$$

where, henceforth, we employ the notation

$$m'_X \equiv \frac{v}{\sqrt{2}}Y_X\,. \tag{1.21}$$

The matrices $m'_{u,d,e}$ are, in general, not diagonal and thus need to be diagonalized. Given $\psi = u, d, e$, this can be done by redefining the fields via a unitary rotation U

$$\psi' = U_\psi \psi\,, \tag{1.22}$$

such that

$$U^\dagger_{\psi_L} m'_\psi U_{\psi_R} = m^{\text{diag}}_\psi = \text{diag}(m_{\psi_1}, m_{\psi_2}, m_{\psi_3}). \tag{1.23}$$

Unless some symmetry is imposed on the Yukawas, left- and right-handed field-rotations are different. In the leptonic sector, due to the absence of a Yukawa term for neutrinos, the rotations of the full-doublet L'_L and e'_R suffice in diagonalizing the leptonic Yukawa term, that is

$$-\mathcal{L}_{\text{Yukawa}} \supset \frac{\sqrt{2}}{v}\left[\overline{L'_L}Hm'_e e'_R\right] + \text{h.c.} = \frac{\sqrt{2}}{v}\left[\overline{L_L}Hm_e e_R\right] + \text{h.c.}. \tag{1.24}$$

The rotation matrices completely disappear in the mass basis and are therefore unphysical. The same does not happen in the quark sector; since Q'_L appears simultaneously in the up- and down- Yukawa interactions, generically u'_L and d'_L must be rotated differently. This mismatch has physical consequences and is manifested in the theory via the appearance of charged flavour-changing interactions with the

W-boson-

$$-\mathcal{L} \supset \frac{g}{\sqrt{2}} \left(W_\mu^+ \overline{u'_L} \gamma^\mu d'_L + \text{h.c.} \right) = \frac{g}{\sqrt{2}} \left(W_\mu^+ \overline{u_L} V_{\text{CKM}} \gamma^\mu d_L + \text{h.c.} \right) , \tag{1.25}$$

where we defined the Cabibbo–Kobayashi–Maskawa (CKM) unitary matrix

$$V_{\text{CKM}} \equiv U_{u_L}^\dagger U_{d_L} . \tag{1.26}$$

In the following, we will drop the primed notation in the Lagrangian and write everything in the gauge basis (i.e. before performing the rotation to diagonalize the Yukawa matrices) if not specified otherwise. If masses enter observables of amplitudes, they will be referred to as the diagonalized physical masses.

The CKM matrix contains 3 independent angles and 1 complex phase; it can be parameterized as

$$V_{\text{CKM}} = \begin{pmatrix} c_{12}c_{13} & s_{12}c_{13} & s_{13}e^{-i\delta} \\ -s_{12}c_{23} - c_{12}s_{23}s_{13}e^{i\delta} & c_{12}c_{23} - s_{12}s_{23}s_{13}e^{i\delta} & s_{23}c_{13} \\ s_{12}s_{23} - c_{12}c_{23}s_{13}e^{i\delta} & -c_{12}s_{23} - s_{12}c_{23}s_{13}e^{i\delta} & c_{23}c_{13} \end{pmatrix} , \tag{1.27}$$

In terms of magnitude, the central values of its entries are given by [17]

$$|V_{\text{CKM}}| \equiv \begin{pmatrix} |V_{ud}| & |V_{us}| & |V_{ub}| \\ |V_{cd}| & |V_{cs}| & |V_{cb}| \\ |V_{td}| & |V_{ts}| & |V_{tb}| \end{pmatrix} \approx \begin{pmatrix} 0.974 & 0.225 & 0.004 \\ 0.225 & 0.973 & 0.042 \\ 0.009 & 0.041 & 0.999 \end{pmatrix} . \tag{1.28}$$

Despite approaching the identity matrix, the CKM induces non-trivial mixing among different flavours in charged interactions. In the SM, all neutral interactions are flavour-diagonal at tree-level; flavour-changing processes arise only via charged interactions in the quark sector and are CKM-suppressed. Leptonic interactions can only be flavour-diagonal as there is no counterpart of the CKM matrix.

As the CKM is a complex matrix, it can contain sources of CP violation, manifested as complex phases in its entries. It turns out that rotations of the quark fields can reabsorb and make unphysical all complex phases, but one typically called δ. The CKM phase is measured to be [17]

$$\delta = 1.147 \pm 0.026 , \tag{1.29}$$

which is almost maximal. However, this phase is not physical per se, as it can be modified via a field redefinition. The basis-independent quantity that enters physical

processes is the so-called *Jarlskog invariant* [18], J,

$$\mathrm{Im}\left[V_{ij}V_{kl}V_{il}^{*}V_{kj}^{*}\right] \equiv J\sum_{mn}\epsilon_{ikm}\epsilon_{jln}\,. \tag{1.30}$$

For the CKM matrix, its value is given by

$$J = c_{12}c_{23}c_{13}^{2}s_{12}s_{23}s_{13}\sin(\delta) = \left(3.08^{+0.15}_{-0.13}\right)\times 10^{-5} \tag{1.31}$$

However, the situation is slightly more subtle than this. If any of the two up- or down-type quarks have the same masses, it is possible to reabsorb an extra phase from the CKM, thus making δ unphysical and eliminating any trace of CP-violation. A necessary and sufficient condition for CP-violation in the EW sector is given by [18]

$$\text{CP-Violation} \quad\Longleftrightarrow\quad X_{\mathrm{CP}} \equiv \mathrm{Im}\,\mathrm{det}\left[m_u m_u^{\dagger}, m_d m_d^{\dagger}\right] \neq 0. \tag{1.32}$$

If such a commutator vanished, the up- and down-quark mass matrices could be diagonalized simultaneously, making the whole CKM matrix unphysical. Remarkably, one can express such a result in a more transparent form as a function of the Jarlskog invariant

$$X_{\mathrm{CP}} = \Delta m_{tc}^{2}\Delta m_{tu}^{2}\Delta m_{cu}^{2}\Delta m_{bs}^{2}\Delta m_{bd}^{2}\Delta m_{sd}^{2}J\,, \tag{1.33}$$

where $\Delta m_{ij}^{2} \equiv m_i^2 - m_j^2$, which manifests that for CP-violation to be physical, all quarks must have different masses, thus confirming symmetry arguments. In other words, CP-violation effects in flavour blind observables must be proportional to J and quarks mass differences, making the net effects incredibly suppressed despite the large phase.

The Yukawa sector contains 13 new parameters: 9 masses, 3 angles and 1 phase. In total, the SM contains 19 free parameters.

1.1.2. Global and Anomalous Symmetries of the SM

Global symmetries are incredibly powerful tools for understanding physics, especially when calculations are not simple. Searching for global symmetries in the Lagrangian is not always easy, but even identifying approximate ones can greatly help understand physical processes. In fact, if the symmetries are exact, their implications are valid at all orders in perturbation theory. The SM enjoys some accidental global symmetries, which are fundamental to understanding the magnitude of many-

SM processes (e.g. selection rules) without requiring computations. In the following, we will focus on Baryon and Lepton number and their implications.

1.1.2.1. Lepton and Baryon Number

The kinetic terms of the fermions of Eq. (1.11) allow for unitary independent rotations of all left- and right-fermionic fields, corresponding to

$$G_{\text{kinetic}} = \underbrace{U(3)_{Q_L} \times U(3)_{u_R} \times U(3)_{d_R}}_{G_{\text{Q}}} \times \underbrace{U(3)_{L_L} \times U(3)_{e_R}}_{G_{\text{L}}} . \tag{1.34}$$

Both G_Q and G_L are explicitly broken in the Yukawa sector (cfr. Eq. (1.18)) to $U(1)$ transformations. To study exactly which ones survive and how G_{kinetic} is broken, it is convenient to work in the mass basis.

In the leptonic sector, due to the absence of right-handed neutrinos, the group is broken to a $U(1)$ for each flavour

$$G_L \to U(1)_e \times U(1)_\mu \times U(1)_\tau . \tag{1.35}$$

The overall conservation imposed by the $U(1)^3$ of the above equation is referred to in the literature as *Lepton Number* (LN). The global symmetries of Eq. (1.35) imply that LN is conserved overall and per flavour. The consequences of this are very relevant, such as the absence of many kinematically and gauge-allowed processes like $\mu \to e\gamma$ or $\tau \to \mu\gamma$, etc.

In the quark sector, the situation is more involved. The appearance of the CKM matrix induces conversions among different families, which forbids any conservation per flavour as for the leptonic case. The only surviving global symmetry is *Baryon Number* (BN)

$$G_Q \to U(1)_{u,c,t} \equiv U(1)_B . \tag{1.36}$$

This amounts to a global rotation of all up- and down-quarks (left and right) and corresponds to conserving the number of quarks and, consequently, mesons and baryons. One may notice that V_{CKM} can be made unphysical via field redefinition of u_L or d_L if all masses in the up- or down-quarks sector are equal; this is conceptually a more involved version of the CP-violating condition of the CKM matrix presented in Eq. (1.31). This implies that Flavour Violating (FV) processes involving quarks must be proportional to both V_{CKM} and differences or log-ratios of quark masses. As Flavour-Changing Neutral Currents (FCNCs) are realized only at loop-level, one

can estimate the amplitude of a quark flavour-changing process $d_\alpha \to d_\beta$ as

$$\mathcal{M}_{\beta\alpha} \sim \frac{g^2}{16\pi^2} \sum_i (V_{\mathrm{CKM}})_{\alpha i} (V^\dagger_{\mathrm{CKM}})_{i\beta} \times f\left(\frac{m^2_{u,i}}{M^2_W}\right) , \tag{1.37}$$

where $f(x)$ is an amplitude dependent function. If quark masses were the same, the unitarity of the CKM-matrix would reduce the sum to $\delta_{\alpha\beta}$, thus cancelling any FV process. Effectively, as quark masses differences are small compared to M_W and thus of the same order of magnitude (except for the top quark), the unitarity of the CKM-matrix is approximately enforced and suppresses FV besides the 1-loop: this is the celebrated GIM-mechanism [19]. In processes where the top quark contribution is most relevant, the GIM-mechanism is not effective, and contributions can be sizeable (e.g. $b \to s\gamma$ transitions).

If the symmetry is complex enough, zeros or suppressions in the results will almost look like magic!

1.1.2.2. Anomalous Violation of Global Symmetries in the SM

As discussed before, Baryon and Lepton numbers are two global symmetries of the SM Lagrangian. Under BN and LN, the fields are defined to transform as

$$q_{L,R} \to e^{i\alpha_q/3} q_{L,R} \qquad\qquad \ell_{L,R} \to e^{i\alpha_\ell} \ell_{L,R} \,. \tag{1.38}$$

According to Noether's theorem, the classical conserved currents reads

$$\partial_\mu J^\mu_B = \partial_\mu \sum_q \frac{1}{3} \bar{q} \gamma^\mu q = 0, \qquad\qquad \partial_\mu J^\mu_L = \partial_\mu \sum_\ell \bar{\ell} \gamma^\mu \ell = 0. \tag{1.39}$$

A relevant question is whether the two symmetries are valid only in the classical theory at the Lagrangian level or if they survive the quantization procedure and are good symmetries also at the quantum level. It turns out that chiral symmetries, i.e. those symmetries that transform differently left- and right-fermions, are generically not conserved [20]; if that is the case, they are referred to as *anomalous*. Theories with global anomalous symmetries are theoretically consistent and have interesting phenomenological consequences. On the contrary, theories with anomalous gauge symmetries are inconsistent; for example, they convey a different number of degrees of freedom of the associated gauge boson, leading to negative norm states. We will explore the effect of the chiral anomaly in QED in more detail.

Chiral Anomaly in QED The QED Lagrangian reads

$$\mathcal{L}_{\rm QED} = \overline{e_L} i \not{D} e_L + \overline{e_R} i \not{D} e_R - m_e \left(\overline{e_L} e_R + \overline{e_R} e_L \right). \tag{1.40}$$

The current conservation of the global part of the gauge-symmetry enforces the conservation of the electric charge

$$\partial_\mu J^\mu = \partial_\mu \left(\overline{e} \gamma^\mu e \right) = \partial_\mu \left(\overline{e_L} \gamma^\mu e_L + \overline{e_R} \gamma^\mu e_R \right) = 0. \tag{1.41}$$

If the electron was massless, the conserved symmetry would be larger and include independent rotations of left-handed and right-handed electrons

$$e_{L,R} \to e^{i(\alpha + \beta\gamma_5)} e_{L,R} \,. \tag{1.42}$$

The conservation of the axial current in the presence of a massless electron is encoded in

$$\partial_\mu J_5^\mu = \partial_\mu \left(\overline{e} \gamma^\mu \gamma_5 e \right) = 2 i m_e \overline{e} \gamma_5 e \,, \tag{1.43}$$

which vanishes in the limit $m_e \to 0$. This formula is derived at tree-level, i.e. without taking into account the quantization procedure. Let us assume $m_e = 0$ from the beginning so that both the vectorial and axial currents are conserved. If we define

$$i M_5^{\alpha\mu\nu} (2\pi)^4 \delta(p - k_1 - k_2) \equiv \int\!\!\!\int\!\!\!\int d^4x \, d^4y \, d^4z e^{-ipx} e^{ik_1 y} e^{ik_2 z} \left\langle J_5^\alpha(x) J^\mu(y) J^\nu(z) \right\rangle \,, \tag{1.44}$$

the explicit computation reveals that

$$p_\alpha M_5^{\alpha\mu\nu} = \frac{1}{4\pi^2} \epsilon^{\mu\nu\rho\sigma} k_{1\rho} k_{2,\sigma} \neq 0. \tag{1.45}$$

In position-space, the above result translates to

$$\partial_\mu \quad J_5^\mu J^\beta J^\alpha \quad \neq 0, \tag{1.46}$$

which can be matched to operators via

$$\partial_\mu J_5^\mu = -\frac{e^2}{16\pi^2} \epsilon^{\mu\nu\rho\sigma} F_{\mu\nu} F_{\rho\sigma} = -\frac{e^2}{8\pi^2} \widetilde{F}_{\mu\nu} F^{\mu\nu} \,. \tag{1.47}$$

Diagrammatically, $M_5^{\alpha\mu\nu}$ corresponds to the calculation of the triangle diagram of Fig. 1.1. This is the famous Adler-Bell-Jackiw (ABJ) anomaly [21, 22]. This implies that 1-loop corrections spoil the axial symmetry even in the massless limit while preserving the vectorial one. Consequently, it implies that QED with a single Weyl

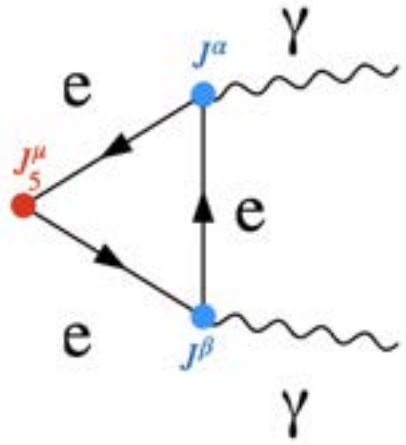

Figure 1.1: Example of triangle diagram in QED contributing to the axial anomaly.

fermion cannot be consistent. In such a case, the only possible transformation is axial, which we know is not preserved, making the gauge symmetry anomalous. As the vectorial or axial nature of the transformation is encoded in the sum and difference of the couplings

$$e_{L,R} \to e^{i\alpha_{L,R}} e_{L,R} = \exp\left[i \left(\frac{\alpha_R + \alpha_L}{2} \right) + i\gamma_5 \left(\frac{\alpha_R - \alpha_L}{2} \right) \right] e_{L,R} \,, \tag{1.48}$$

one can immediately learn that if a fermion is charged under $U(1)_X$ with charges $\alpha_{L,R}$, the contribution to the anomaly must be proportional to the difference of charges

$$\partial_\mu J^\mu_{X,5} \propto (\alpha_L - \alpha_R) . \tag{1.49}$$

In other words, the transformation of the left- and right-handed spinors generates opposite contributions to the anomaly.

Finally, a last comment is in order. The above result can be derived either by explicitly computing the triangle diagram which corresponds to the currents of Eq. (1.56) (perturbative method) or by studying how the path-integral measure changes under the transformation of Eq. (1.38). The latter is a non-perturbative method, i.e. no perturbative expansion in the couplings is required and is known in the literature as *Fujikawa method* [23]. As the two methods give identical results, one can infer that **anomalies are 1-loop exact**. The generalization to non-abelian gauge groups is straightforward: given a gauge group with field-strength F and coupling g, the anomaly contribution reads

$$\partial_\mu J^\mu_5 = -\frac{g^2}{8\pi^2} \operatorname{tr}\left[\widetilde{F}^{\mu\nu} F_{\mu\nu} \right] , \tag{1.50}$$

Diagrammatically, the anomaly remains at 1-loop, but besides the above-mentioned triangle-diagram, it includes square and pentagon diagrams due to the non-abelian nature of the group; they are encoded in $\mathrm{tr}\left[\widetilde{F}^{\mu\nu}F_{\mu\nu}\right]$.

Anomaly Cancellation in the SM As the transformation of the left- and right-spinors of the same Dirac spinor generate opposite contributions to the anomaly, vectorial gauge groups such as QCD, are automatically anomaly-free in the SM. However, Weak and Hypercharge interactions are not vectorial: the former only couples to left-handed fields while the latter couples with different Hypercharge. As proved by Witten [20], an $SU(2)_L$ theory involving only fermion doublets is anomalous only if it contains an odd number of them; this is not the case in the SM as for each flavour there are two weak doublets: a quark and a lepton one. This implies that the only potentially dangerous source of anomaly comes from $U(1)_Y$. All in all, denoted by Y_ψ the Hypercharge of the field $\psi = Q, L, u, d, e$, there are four conditions on the charges to ensure anomaly cancellation

$$U(1)_Y^3 : \qquad 3(2Y_Q^3 - Y_u^3 - Y_d^3) + (2Y_L^3 - Y_e^3) = 0, \tag{1.51}$$

$$U(1)_Y \times SU(2)_L^2 : \qquad 3Y_Q + Y_L = 0, \tag{1.52}$$

$$U(1)_Y \times SU(3)_C^2 : \qquad 2Y_Q - Y_u - Y_d = 0, \tag{1.53}$$

$$U(1)_Y \times \text{gravity}^2 : \qquad 3(2Y_Q - Y_u - Y_d) + (2Y_L - Y_e) = 0. \tag{1.54}$$

One can explicitly verify that the SM hypercharges

$$Y_Q = \frac{1}{6}\,, \qquad Y_u = \frac{2}{3}\,, \qquad Y_d = -\frac{1}{3}, \qquad Y_L = -\frac{1}{2}, \qquad Y_e = -1, \tag{1.55}$$

automatically satisfy all of them and is, therefore, anomaly-free. However, notice that the SM charge assignment is not the unique solution to such equations. This is a remarkable result, as the first generation of fermions charges were established before discovering the charge conditions for anomaly cancellation. Finally, the power of anomaly cancellation goes beyond consistency and allows a deeper understanding of some experimental facts. For example, the condition $3Y_Q + Y_L = 0$ implies that a proton must have exactly equal and opposite charge to the electron, even if a different solution for the hypercharges was chosen.

Anomaly of Baryon and Lepton Number While in the SM the gauge charges of the fields are such that the anomaly cancels in a highly non-trivial way, the same

does not hold for Baryon and Lepton numbers. One finds [24, 23]

$$\partial_\mu J^\mu_B = \partial_\mu J^\mu_L = \frac{N_f}{32\pi^2}\left(-g^2 W^{a,\mu\nu}\widetilde{W}^a_{\mu\nu} + g'^2 B^{\mu\nu}\widetilde{B}_{\mu\nu}\right) \neq 0, \tag{1.56}$$

where N_f is the number of flavours. This implies that neither BN nor LN is conserved in the SM at 1-loop. However, as their violation is identical, the conserved global symmetry is $B - L$. The effects of $B + L$ violation are exponentially suppressed at zero-temperature (e.g. collider) but become relevant at large temperatures, (e.g. during cosmic evolution).

1.2. Open Problems and Puzzles

The SM is an incredibly successful theory. The theory contains 19 free parameters: 3 gauge couplings, 9 fermionic masses, 3 mixing angles, 1 phase in the CKM matrix, 2 parameters in the Higgs sector (the Higgs mass and its vev) and finally, the QCD vacuum angle. Once these parameters are fixed, the theory can predict hundreds of observables across different energy ranges, finding astonishing agreement. An overview of such accomplishment can be seen in Fig. 1.2.

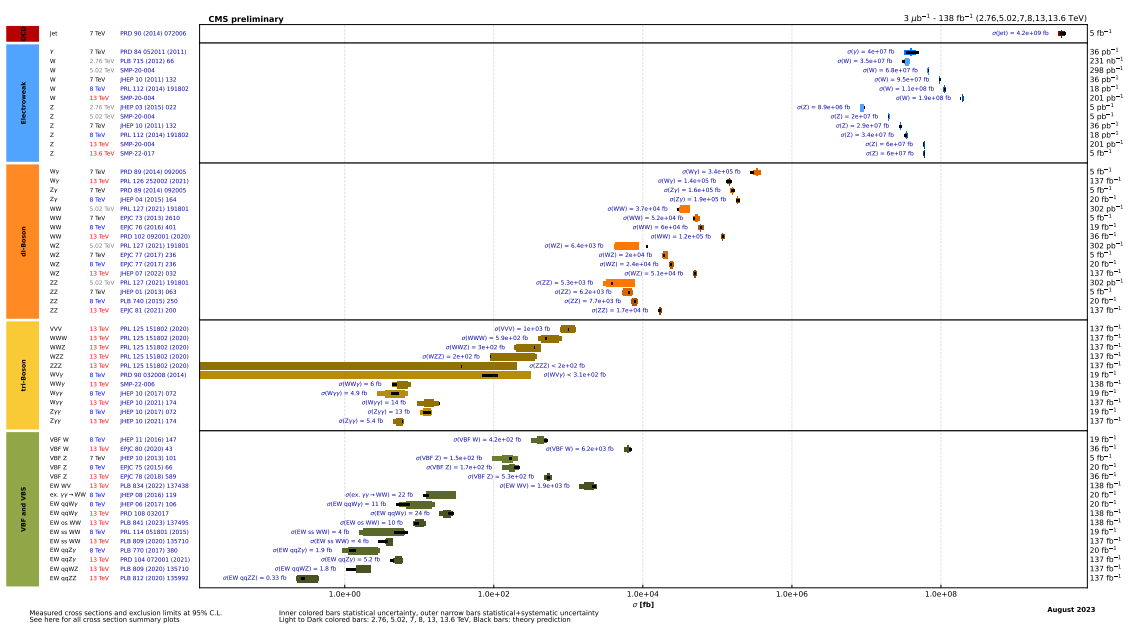

Figure 1.2: Overview of CMS cross-section results [25]. Experimental results (black dots) are in excellent agreement with the theory predictions (coloured area).

The development of the SM has been driven in its last stage by a remarkable joint effort between experiments and theory. While experimental guidance is somewhat obvious when doing science, the latter is less obvious. The mathematical

consistency of the theory played a crucial role in the SM development, which culminated in the prediction of the existence of the Higgs boson (unitarization of gauge bosons scattering). Such precious guidance ended with its discovery and nowadays leads studies in quantum gravity. Even though this precious guide has faded away in high-energy particle physics, some experimental facts may seem *puzzling*. These are not strictly "problems", as the theory makes correct predictions once the input-free parameters are fixed. These puzzles are typically related to the size of input parameters themselves, which show either some hierarchy or require delicate cancellations with other theory parameters to give the correct measured values. Theories able to explain such puzzling numbers are highly non-trivial and are, therefore, a precious guide to BSM model building.

We report here a list of open problems and puzzles of the SM. The separation between the two classifications is very subtle and very bias-dependent. In this Thesis, we adopt the most conservative view:

- **Experimental Problems:** *the theory cannot predict experimental observations once the input free parameters are fixed*; in this category falls the existence of neutrino oscillations and dark matter. These are real objective problems of the SM, as the theory makes wrong predictions about them.[3]
- **Boundary-Initial Conditions Puzzles:** *the theory can predict such phenomena at the price of requiring some fine-tuned initial conditions;* in this category falls the lack of mechanisms to dynamically explain the Baryon asymmetry of the universe (*baryogenesis*) and *cosmic inflation*.
- **Theory Puzzles:** *the theory makes correct predictions once the input free parameters are fixed, but the latter show fine-tuned or hierarchical values*; some notable puzzles of this category are related to the smallness of CP-violation in the QCD sector (*strong-CP puzzle*), the hierarchical structure of fermion masses and mixing (*flavour puzzle*), the (in)stability of the Higgs potential if new mass scales are introduced (*hierarchy puzzle*).

We will briefly review the key aspects of the SM problems in Sec. 1.2.1 and of SM puzzles in Sec. 1.2.2.

1.2.1. SM Problems

In this section, we review two SM problems: two experimental evidences that cannot be explained within the SM once all free parameters of the theory are fixed.

[3] Quantum gravity also represents a problem for the SM, but it occupies a special place. The SM is an effective theory with a cut-off provided by the Planck scale, $M_{Pl} \sim 10^{19}$ GeV. This indicates that at some scale, dynamics must happen, and General Relativity breaks down. We do not discuss it in this thesis.

1.2.1.1. Neutrinos' Oscillation

In the SM, neutrinos are massless due to the absence of a right-handed partner, which forbids the presence of a Yuakwa term compatible with $G_{\rm SM}$. Furthermore, leptons' interactions with gauge bosons and the Higgs are always flavour diagonal (cfr. Eq. (1.24)), thus conserving LN per flavour. This is due to the freedom of rotating ν'_L in the same way as e'_L. This has very strong phenomenological implications. As SM neutrinos are electrically neutral and massless, they can propagate very large distances, retaining their properties. In particular, if an astrophysical source emits a neutrino of a certain flavour, this will propagate almost undisturbed for huge distances, arriving at Earth, where it can be detected. Knowing the production mechanism of the neutrinos at the source, the SM roughly predicts measuring the flux of neutrinos at Earth with the same flavour components as produced at the source. This statement is valid independently of the distance between production and detection. However, this prediction turns out to be wrong. In the late 1960s, experiments such as the Homestake experiment (Ray Davis Jr.) and the Kamiokande experiment in Japan (led by Masatoshi Koshiba) observed a deficit in the number of electron neutrinos arriving from the Sun compared to theoretical predictions, detecting $\sim 1/3$ of the expected flux, compatibly with neutrino flavour oscillations. Later on, further experiments involving atmospheric neutrinos, long-baseline neutrinos, and reactor neutrinos measured all the relevant parameters, as we will briefly discuss in the following section.

The oscillation data are in agreement with the assumption of massive neutrinos. The first idea of neutrino masses and oscillation was proposed in 1957 by B. Pontecorvo, which suggested the possibility of neutrino-antineutrino oscillations in analogy with $K^0 - \overline{K^0}$-oscillations for the quarks [27]. In the year of muon-neutrino discovery, 1962, the first two flavours neutrino mixing model was proposed by Z. Maki, M. Nakagawa and S. Sakata [28]; in 1967 B. Pontecorvo proposed solar neutrino oscillations as a test of neutrino masses [29]. Proper treatment of neutrino oscillation involves a wave-packet approach and has been intensively studied in the literature (see e.g. Ref.s. [30, 31]). However, in the first approximation, the phenomenon is well-captured by the plain-waves approach. Denoted by ν_α the flavour eigenstates and by ν_i the mass eigenstates, they are related by a unitary transformation parameterized by the so-called PMNS-matrix, $U_{\rm PMNS}$ (or U for simplicity in the following), via

$$\nu_\alpha = \sum_{i=1}^{3} (U_{\rm PMNS})_{\alpha i}\, \nu_i \,. \tag{1.57}$$

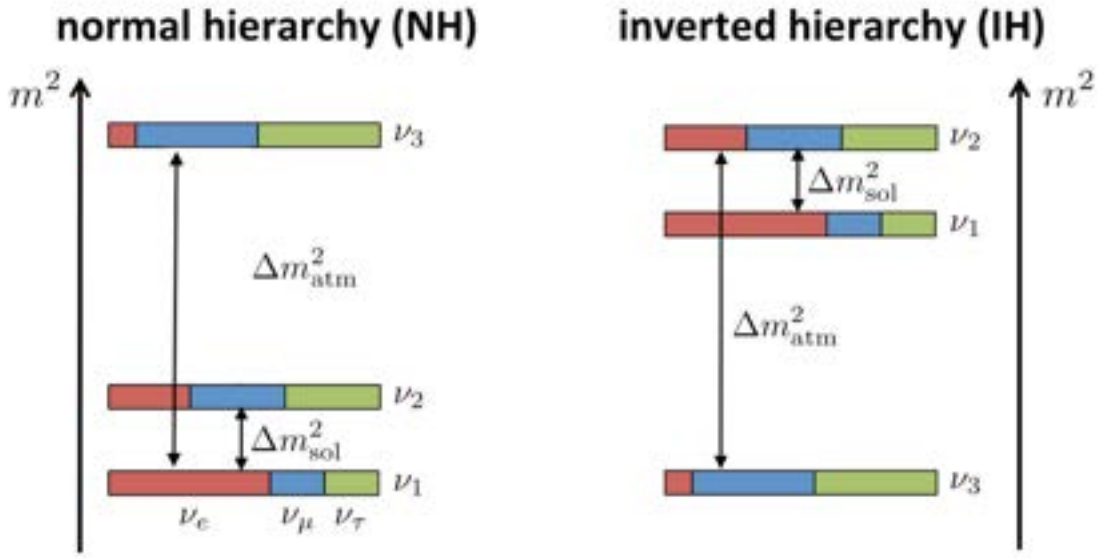

Figure 1.3: Visualisation of possible mass orderings and their mixings: definition of atmospheric mass splitting from Ref. [26]. (Image credit: JUNO).

As for the CKM, the PMNS contains three angles and a complex phase

$$U_{\rm PMNS} = \begin{pmatrix} c_{12}c_{13} & s_{12}c_{13} & s_{13}e^{-i\delta_{\rm CP}} \\ -s_{12}c_{23} - c_{12}s_{23}s_{13}e^{i\delta_{\rm CP}} & c_{12}c_{23} - s_{12}s_{23}s_{13}e^{i\delta_{\rm CP}} & s_{23}c_{13} \\ s_{12}s_{23} - c_{12}c_{23}s_{13}e^{i\delta_{\rm CP}} & -c_{12}s_{23} - s_{12}c_{23}s_{13}e^{i\delta_{\rm CP}} & c_{23}c_{13} \end{pmatrix} \begin{pmatrix} \end{pmatrix} \quad (1.58)$$

As an illustrative example, if one assumes a fixed momentum of the state and ultra-relativistic limit, one obtains the conversion probability to be

$$P_{\nu_\alpha \to \nu_\beta}(t) = |\langle \nu_\beta | e^{iHt} | \nu_\alpha \rangle|^2 = \sum_{i=1}^{3} \left(U_{i\alpha} U^*_{i\beta} e^{iE_i t} \right)^2 \approx \sum_{i,j=1}^{3} U_{i\alpha} U^*_{i\beta} U^*_{j\alpha} U_{j\beta} e^{-i\frac{\Delta m^2_{ij}}{2E}t}{}^2 , \quad (1.59)$$

where

$$\Delta m^2_{ij} \equiv m^2_i - m^2_j \, . \quad (1.60)$$

Thus, neutrino oscillations are sensitive to the PMNS matrix and the mass-squared differences of the neutrinos. The works presented in this Thesis are not sensitive to the precision of such parameters and, therefore, we do not delve into the details of the fitting strategies and different results present in the literature. For definiteness, in the following, we adopt the fitting of the data to three massive neutrino models from the NuFit Collaboration [32, 26] whose most recent results can be seen in

		Normal Ordering (best fit)		Inverted Ordering ($\Delta\chi^2 = 9.1$)	
		bfp $\pm 1\sigma$	3σ range	bfp $\pm 1\sigma$	3σ range
without SK atmospheric data	$\delta_{\rm CP}/^\circ$	197^{+41}_{-25}	$108 \to 404$	286^{+27}_{-32}	$192 \to 360$
	$\frac{\Delta m^2_{21}}{10^{-5}\ {\rm eV}^2}$	$7.41^{+0.21}_{-0.20}$	$6.81 \to 8.03$	$7.41^{+0.21}_{-0.20}$	$6.81 \to 8.03$
	$\frac{\Delta m^2_{3\ell}}{10^{-3}\ {\rm eV}^2}$	$+2.511^{+0.027}_{-0.027}$	$+2.428 \to +2.597$	$-2.498^{+0.032}_{-0.024}$	$-2.581 \to -2.409$
with SK atmospheric data	$\sin^2\theta_{12}$	$0.307^{+0.012}_{-0.011}$	$0.275 \to 0.344$	$0.307^{+0.012}_{-0.011}$	$0.275 \to 0.344$
	$\theta_{12}/^\circ$	$33.67^{+0.73}_{-0.71}$	$31.61 \to 35.94$	$33.67^{+0.73}_{-0.71}$	$31.61 \to 35.94$
	$\sin^2\theta_{23}$	$0.454^{+0.019}_{-0.016}$	$0.411 \to 0.606$	$0.568^{+0.016}_{-0.021}$	$0.412 \to 0.611$
	$\theta_{23}/^\circ$	$42.3^{+1.1}_{-0.9}$	$39.9 \to 51.1$	$48.9^{+0.9}_{-1.2}$	$39.9 \to 51.4$
	$\sin^2\theta_{13}$	$0.02224^{+0.00056}_{-0.00057}$	$0.02047 \to 0.02397$	$0.02222^{+0.00069}_{-0.00057}$	$0.02049 \to 0.02420$
	$\theta_{13}/^\circ$	$8.58^{+0.11}_{-0.11}$	$8.23 \to 8.91$	$8.57^{+0.13}_{-0.11}$	$8.23 \to 8.95$
	$\delta_{\rm CP}/^\circ$	232^{+39}_{-25}	$139 \to 350$	273^{+24}_{-26}	$195 \to 342$
	$\frac{\Delta m^2_{21}}{10^{-5}\ {\rm eV}^2}$	$7.41^{+0.21}_{-0.20}$	$6.81 \to 8.03$	$7.41^{+0.21}_{-0.20}$	$6.81 \to 8.03$
	$\frac{\Delta m^2_{3\ell}}{10^{-3}\ {\rm eV}^2}$	$+2.505^{+0.024}_{-0.026}$	$+2.426 \to +2.586$	$-2.487^{+0.027}_{-0.024}$	$-2.566 \to -2.407$

Figure 1.4: Fitted neutrinos parameters from NuFit Collaboration [26]; $\Delta m^2_{3\ell}$ takes $\ell = 1$ for NO and $\ell = 2$ for IO.

Fig. 1.4. They are in good agreement with the literature [33, 34, 35]. Notice that current data are still compatible with one neutrino being massless. Furthermore, while solar neutrinos are sensitive to the sign of Δm^2_{12}, in the case of atmospheric neutrinos, only its modulus can be measured, thus leaving open two scenarios, named with the degree of mixture with the electron-flavour. The first one, dubbed *normal ordering* (NO), assumes the heaviest neutrino to be the one with the least electronic component and the lightest with the maximal one; the second, dubbed *inverted ordering* (IO), revert the neutrino with the least electronic component to be the lightest, as shown in Fig. 1.3. The fitted PMNS matrix at 3σ lies in the range given by [26]

$$|U^{3\sigma}_{\rm PMNS}| = \begin{pmatrix} 0.803 \to 0.845 & 0.514 \to 0.578 & 0.143 \to 0.155 \\ 0.244 \to 0.498 & 0.502 \to 0.693 & 0.632 \to 0.768 \\ 0.272 \to 0.517 & 0.473 \to 0.672 & 0.623 \to 0.761 \end{pmatrix} , \tag{1.61}$$

which shows large off-diagonal entries if compared to the almost-diagonal CKM. The presence of the PMNS induces rich phenomenology, in full analogy to the CKM. Along with neutrino masses, it breaks the per-family LN to

$$U(1)_e \times U(1)_\mu \times U(1)_\tau \to U(1)_L \,. \tag{1.62}$$

Due to the smallness of neutrino masses, all LN-violating processes (e.g. $\mu^- \to e^-\gamma$)

are extremely suppressed and virtually impossible to detect at the current status of experiments, making neutrino oscillations the only direct probe of neutrino physics.

If this were the end of the story, the problem of neutrino oscillations would be considered closed. The issue relies upon establishing the Lagrangian, which gives rise to massive neutrinos and, thus, neutrino oscillations. The simplest solution follows the SM chiral structure, introducing three right-handed neutrinos with the relative Yukawa coupling to the Higgs and the left-handed Lepton doublet. However, under closer inspection, a right-handed neutrino ν_R would be a singlet under G_{SM}, allowing for another Poincaré invariant and renormalizable operator, the so-called *Majorana mass term*, M_N,

$$-\mathcal{L} \supset \overline{L_L} Y_\nu \widetilde{H} \nu_R + \frac{1}{2} \overline{\nu_R^c} M_N \nu_R \,. \tag{1.63}$$

The presence of a Majorana mass has two main consequences: it introduces extra sources of CP-violation, the so-called *Majorana-phases* in the PMNS matrix, and explicitly violates LN (and thus BN-LN, or in short B-L), thus allowing processes otherwise forbidden in the SM. The presence of Majorana phases can be encoded in the PMNS by adding, in the most general case, two relative phases $\alpha_{1,2}$

$$U_{\text{PMNS}} \to U_{\text{PMNS}} \times \begin{pmatrix} e^{i\alpha_1} & & \\ & e^{i\alpha_2} & \\ & & 1 \end{pmatrix} \tag{1.64}$$

Alongside measuring all the parameters of the PMNS, establishing the Majorana nature of neutrinos is one of the core missions in neutrino physics. Furthermore, this is not the only way of introducing neutrino masses. Could there be more or less than three right-handed neutrinos? May other types of particles be involved and give rise to the same phenomenology? A category of fascinating theoretical models which relies on a large Majorana mass to naturally explain the smallness of neutrino masses will be discussed in Section 2.1.

1.2.1.2. Dark Matter

The existence of Dark Matter (DM) is nowadays a well-established fact. Its existence was first proposed in 1933 by Fritz Zwicky [36]. Studying the Coma Cluster of galaxies, Zwicky observed that galaxies were moving too fast to remain gravitationally bounded given the amount of luminous matter. Zwicky conjectured the existence of some "dark" matter that could solve the problem. More solid evidence for DM was obtained independently in 1970 by K. C. Freeman [37] and V. Rubin

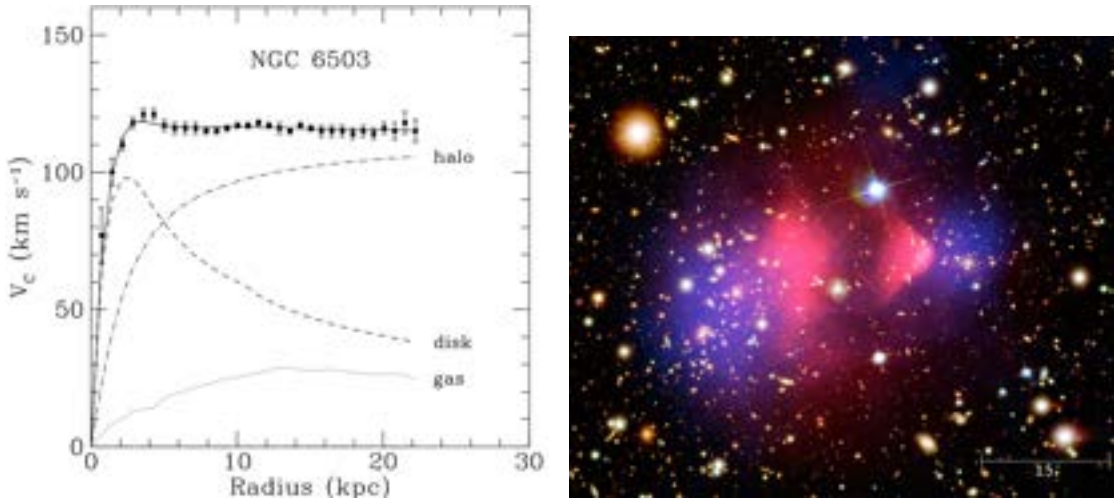

(a) (b)

Figure 1.5: Some experimental pieces of evidence for DM. **Left.** Rotational velocity curve of the galaxy NGC 6503 as a function of the distance from the galactic centre from Ref. [41]. The dotted, dashed and dash-dotted lines are the contributions of gas, disk and dark matter, respectively. **Right.** The bullet cluster: in pink the X-ray emission associated with visible matter, while in purple the computed (dark) matter abundance compatible with the observed gravitational microlensing.

et al. [38], which measured galactic rotational velocities. According to Newtonian gravity, the velocity of the disk as a function of the distance from the galactic centre, r, should decrease for large values as $1/\sqrt{r}$. Contrary to the expectations, they observed that the velocity remained constant, compatible with a halo of non-luminous matter, as exemplified in Fig. 1.5(a). More studies were performed in the following years, confirming these observations and reinforcing the DM hypothesis. Further experimental confirmations of DM come from micro-lensing and the study of anisotropies in the Cosmic Microwave Background (CMB). The former studies distortion of light propagation induced by gravitational fields; the most notable example of DM comes from the bullet cluster [39], shown in Fig. 1.5(b). The most precise measurement of the abundance of DM, assuming the standard cosmological scenario, the so-called ΛCDM, are due to CMB measurements by the Planck mission; its most recent results of 2018 [40] give at 68% C.L.

$$\Omega_B h^2 = 0.02242 \pm 0.00014, \qquad \Omega_{\rm DM} = 0.11933 \pm 0.00091, \tag{1.65}$$

where $\Omega_{B,\rm DM} h^2$ is the density parameter of Baryons and DM, respectively. As can be seen, the DM density parameter is ~ 6 larger than the baryonic one.

Overall, observations suggest DM behaves as an ideal fluid with the equation of state of matter and is "cold", i.e. non-relativistic. From the particle physics

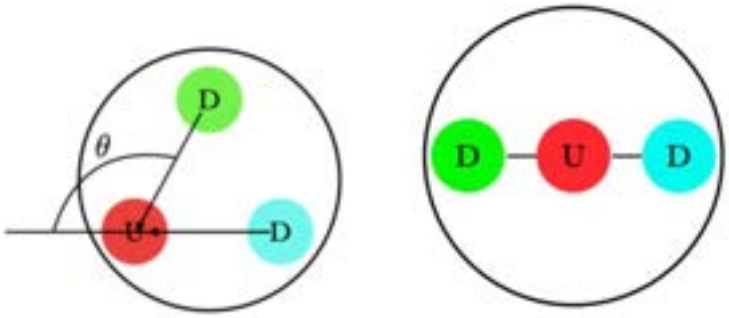

Figure 1.6: Pictorial image of the meaning of $\overline{\theta}$ with respect to the nEDM. Image Credit: Ref. [42].

point-of-view,-DM-is-essentially-electrically-neutral,-collisionless-and-non-dissipating,-properties-that-Baryonic-matter-does-not-possess.-For-a-detailed-review-see-e.g.-Ref.-[17].-

In-the-SM,-neutrinos-are-the-only-neutral-and-stable-particles-that-can-aspire-to-be-DM.-However,-given-their-tiny-mass,-they-are-too-relativistic-to-constitute-the-primary-component-of-DM-and-cannot-thus-solve-the-problem.-

1.2.2. SM Puzzles

The-experimental-evidence-presented-in-the-previous-section-cannot-be-predicted-by-the-SM-and-constitute-a-problem.-We-list-as-"SM-puzzle"-facts-which-do-not-cause-a-problem-on-the-experimental-side-but-appear-to-be-"puzzling"-from-the-purely-theoretical-point-of-view;-they-are-typically-in-contrast-with-some-"simplicity"-and-"naturalness"-criteria.-In-this-section,-we-present-the-most-compelling-ones.-

1.2.2.1. Strong CP Puzzle

The-Strong-CP-Puzzle-involves-the-$G \wedge \widetilde{G}$-term-of-the-of-the-Lagrangian-

$$\mathcal{L}_{\text{Gauge}} \supset \theta_{\text{QCD}} \frac{g_s^2}{32\pi^2} G^{a\mu\nu} \widetilde{G}^a_{\mu\nu} \,, \tag{1.66}$$

and,-more-specifically,-the-size-of-its-coupling.-For-a-complete-review,-see-e.g.-Ref.s.-[42,-43].-The-term-is-particularly-interesting-as-it-explicitly-breaks-CP-in-the-strong-sector.-The-operator-of-Eq.-(1.66)-resembles-anomalous-operators-generated-by-BN-and-LN-in-Eq.-(1.39).-This-is-not-a-coincidence.-One-must-delve-into-how-the-path-integral-measures-change-upon-a-chiral-rotation-of-fermions-(non-perturbative-approach)-to-understand-its-origin-and-connection-to-physical-observables.-Under-a-

global chiral transformation $q \to e^{i\alpha\gamma_5} q$

$$q_L \to e^{-i\alpha} q_L \,, \qquad\qquad q_R \to e^{i\alpha} q_R \,, \tag{1.67}$$

the path integral measure changes

$$\mathcal{D}q\,\mathcal{D}\overline{q} \to \exp\left[-i(2\alpha)\frac{g_s^2}{32\pi^2} G^{a\mu\nu}\widetilde{G}^a_{\mu\nu}\right] \mathcal{D}q\,\mathcal{D}\overline{q}\,, \tag{1.68}$$

which effectively amounts to a contribution in the Lagrangian to $G \wedge \widetilde{G}$

$$\Delta\mathcal{L} = -(2\alpha)\frac{g_s^2}{32\pi^2} G^{a\mu\nu}\widetilde{G}^a_{\mu\nu}\,. \tag{1.69}$$

In the Yukawa sector, one global phase can be removed from $Y_{u,d}$ via a chiral rotation when the fermions are rotated from the gauge to the mass basis. The base-independent (thus physical) phase can be written as

$$\theta_{\rm q} \equiv \arg\det(Y_d Y_u)\,, \tag{1.70}$$

and can be removed from $\sim \overline{q_L} e^{i\theta_{\rm q}} q_R$ by identifying $\alpha = -\theta_{\rm q}/2$. The QCD anomalous operator and its effective coefficient are thus customarily defined in the literature as

$$\overline{\theta} \equiv \theta_{\rm QCD} + \theta_q\,. \tag{1.71}$$

Notice that this term can be made unphysical if any of the quarks are massless by rotating it away from the Lagrangian with the opposite procedure described above.

Experimentally, non-vanishing $\overline{\theta}$ induces a neutron Electric Dipole Moment (EDM), d_n (see Fig. 1.6 for an intuitive meaning of $\overline{\theta}$). Its effective operator in the Lagrangian is defined as

$$\mathcal{L}_{\rm nEDM} = d_n \overline{n}\sigma_{\mu\nu} i\gamma_5 n F^{\mu\nu}\,. \tag{1.72}$$

By employing the chiral Lagrangian (see Sec. 2.2.1.4), it can be shown that 1-loop Feynman diagrams generated by the exchange of pions induce non-vanishing nEDM proportional to

$$d_n \sim e\frac{\overline{\theta}}{16\pi^2 f_\pi^2} \times \left(\frac{m_u m_d}{m_u + m_d}\right) \log\left(\frac{\Lambda^2}{f_\pi^2}\right) \sim 10^{-16} \times \overline{\theta}\, e\,\text{cm}, \tag{1.73}$$

where $\Lambda = 4\pi f_\pi$ is the cut-off of the pion EFT. The current experimental bound on

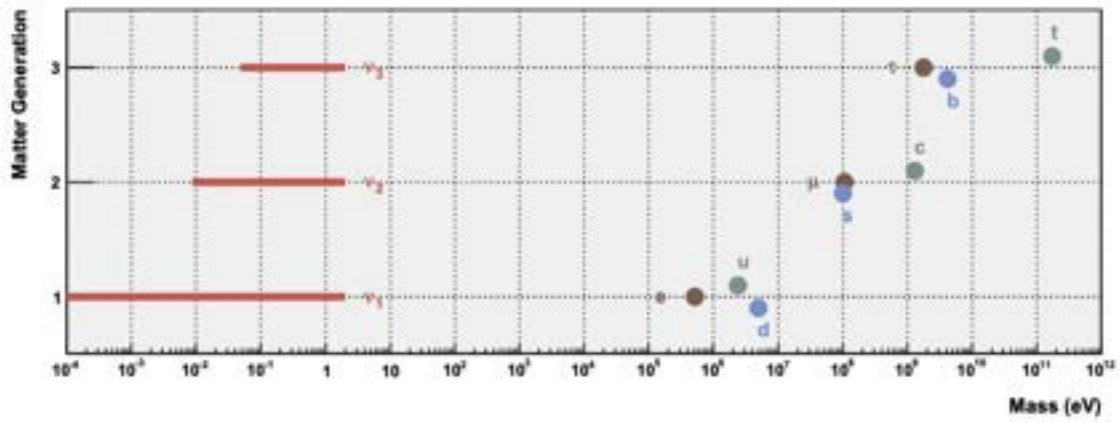

Figure 1.7: Summary of the masses of the fermions in the SM; NO for the neutrinos is used. Image credit: Ref. [51].

the nEDM reads [44]

$$d_n^{\text{exp}} = (0.0 \pm 1.1_{\text{stat}} \pm 0.2_{\text{sys}}) \times 10^{-26}\, e\,\text{cm}, \tag{1.74}$$

which implies

$$\overline{\theta} \lesssim 10^{-10}\,. \tag{1.75}$$

The smallness of such a parameter, which enforces CP-conservation in QCD, constitutes the Strong CP puzzle. A natural way out of such a puzzle would be invoking the up-quark mass to be zero as $d_n \propto m_u$ [45, 46]. However, lattice simulations rule out such a hypothesis [47, 48, 49, 50].

1.2.2.2. Flavour Puzzle

The flavour puzzle is related to the sector of the Lagrangian with the largest number of free parameters, 13, out of a total of 19. There are two puzzling facts. The first one is related to the mass distributions of fermions, which span about 12 orders of magnitude from the top mass $m_t \sim 170$ GeV to neutrino masses $m_\nu \sim 0.1$ eV (see Fig. 1.7). Even if neutrinos were left out, still, there would be about 7 orders of magnitude as $m_e \sim 0.5$ MeV. As all masses in the SM are generated by the Higgs mechanism and are proportional to the Higgs vev, one would naively expect all fermions to live approximately at the Higgs scale, like the top; instead, this is far from being realized.

The second puzzling fact lies in the structure of the mixing of quarks and leptons, i.e. of the CKM and PMNS matrices (cfr. Eqs. (1.28)-(1.28)). While the former shows a very hierarchical structure, which makes it almost diagonal, the latter is very "democratic" with entries compatible with almost maximal mixing.

Altogether, the question that naturally arises is whether there is a UV reason that could fit all these parameters in a smaller set that can predict all this rich structure.

1.2.2.3. Electroweak and Cosmological Constant Hierarchy Puzzles

There are two ways to describe this puzzle. We present both perspectives, starting with the EFT one. Denoted by O_i^n an operator with energy dimension $[O_i^n] = n$, the EFT Lagrangian valid at energies $E \ll \Lambda_{\rm UV}$ can be written as

$$\mathcal{L} = \sum_{n=0}^{\infty} \sum_i \frac{C_{i,n}}{\Lambda_{\rm UV}^{n-4}} \mathcal{O}_i^n \,, \tag{1.76}$$

where $C_{i,n}$ are the so-called Wilson coefficients and $\Lambda_{\rm UV}$ is the energy cut-off of the theory at which NP is expected. The expansion contains three types of operators

- operators with $n > 4$ are suppressed by powers of $\Lambda_{\rm UV}$ and are thus irrelevant for low-energy processes: they are called *irrelevant* operators;
- operators with $n = 4$ are not affected by $\Lambda_{\rm UV}$ and are thus present at all scales: they are called *marginal* operators;
- operators with $n < 4$ are enhanced by powers of $\Lambda_{\rm UV}$, making them the most important at low-energy: they are called *relevant* operators.

This approach suggests that all relevant operators should be enhanced with $\Lambda_{\rm UV}$ powers. There are two such quantities in the SM: the Higgs mass, μ^2, and the cosmological constant, Λ

$$\mathcal{L}_{\rm SM}^{n\leq 2} \supset -\Lambda + \mu^2 H^\dagger H \,. \tag{1.77}$$

The only large energy scale associated with an EFT in the SM is the Planck mass, M_{Pl}, from General Relativity. Therefore, one would expect all dimensionful parameters to be of $\mathcal{O}(M_{Pl})$

$$\Lambda \overset{\rm EFT}{\sim} M_{Pl}^4 \,, \qquad\qquad \mu^2 \overset{\rm EFT}{\sim} M_{Pl}^2 \,. \tag{1.78}$$

However, experimentally one finds $\mu \sim 100$ GeV and $\Lambda \sim 1\,{\rm GeV}/m^3$ and thus

$$\begin{cases} \left(\dfrac{\mu^2}{M_{Pl}^2}\right)^{1/2} \sim \left(\dfrac{10^2\ {\rm GeV}}{10^{19}\ {\rm GeV}}\right) \sim 10^{-17} \,, \\ \left(\dfrac{\Lambda}{M_{Pl}^4}\right)^{1/4} \sim \left(\dfrac{10^{-12}\ {\rm GeV}}{10^{19}\ {\rm GeV}}\right) \sim 10^{-31} \,. \end{cases} \tag{1.79}$$

As can be seen, both quantities are incredibly far away from the expectations, and to be correct, they would need Wilson coefficients of the order of

$$C_{\mu^2} \sim 10^{-34}\,, \qquad\qquad C_\Lambda \sim 10^{-124}\,. \tag{1.80}$$

Such a hierarchy in the Wilson coefficients is not enforced by any known principle or symmetry and constitutes one possible way to see the Hierarchy puzzle: why are the relative Wilson coefficients so small? Is there any dynamics or mechanism that enforces them or makes the previous estimation wrong?

An equivalent point of view comes from calculating quantum corrections to such parameters. Let us consider the SM Higgs mass for simplicity. If new fermions or scalars have masses, M, associated with a large new scale $M \sim \Lambda_{\rm UV}$, the two-point functions of the Higgs receive large corrections. This can happen both at tree- and loop-level. The former can be accomplished by mixing a heavy scalar field, ϕ, with large vev $\langle\phi\rangle \sim \Lambda_{\rm UV}$ to the Higgs via $|\phi|^2|H|^2$. Even if tree-level corrections are absent, by dimensional analysis, loops involving the heavy new particles can spoil the Higgs mass. If NP couples to the Higgs with some coupling $g_{\rm NP}$, the loop-correction can only be proportional to $\Lambda^2_{\rm UV}$ such that in dimensional regularization $d = 4 - 2\epsilon$

$$\delta\mu^2 \sim \frac{g^2_{\rm NP}}{16\pi^2}\Lambda^2_{\rm UV}\left[\text{finite} + \frac{1}{\widetilde{\epsilon}} + \log\left(\frac{\mu_R^2}{\Lambda^2_{\rm UV}}\right)\right] \tag{1.81}$$

where $1/\widetilde{\epsilon} \equiv 1/\epsilon - \gamma_E + \log(4\pi)$ and γ_E is the Euler-Mascheroni constant. The divergent part can be renormalized and will have an impact on the running, the log-contribution can be eliminated by setting the renormalization scale $\mu_R = \Lambda_{\rm UV}$, while the finite part directly modifies the bare parameter. Denoted by μ_0^2 the Higgs bare parameter, the physical Higgs mass would then be

$$\mu^2 = \mu_0^2 + \delta\mu^2\,. \tag{1.82}$$

To set $\mu^2 \sim (100\,\text{GeV})^2$, one needs to enforce a cancellation between the bare parameter and radiative corrections. This implies that the bare parameter is not stable under radiative corrections and is subject to large running effects; this implies that a precise cancellation (fine-tuning) among parameters must be enforced to obtain the experimental result. The result of Eq. (1.82) is qualitatively the same result estimated with the EFT approach in Eq. (1.78) and make manifest the possibility to see the problem either as a large hierarchy of couplings or as a fine-tuning. The hierarchy problem can be seen as an instability problem of the couplings under quantum corrections.

1.2.2.4. Baryogenesis

From experimental observations, it is clear that the observed universe is dominated by matter over anti-matter. After photons decouple at the CMB epoch, this Baryon asymmetry can be defined as

$$\eta \equiv \frac{n_B - n_{\overline{B}}}{n_\gamma}\,, \tag{1.83}$$

where n_X is the number density of particles and

$$n_\gamma = 2\frac{\zeta(3)}{\pi^2}T^3\,. \tag{1.84}$$

According to the latest Planck data [40], it is measured to be

$$\eta = (6.10 \pm 0.40) \times 10^{-10}\,. \tag{1.85}$$

If the universe were perfectly symmetric, one would expect $\eta = 0$. Therefore, the explanation for such asymmetry has to be found either in some fine-tuned initial conditions or in a more stable dynamic mechanism. More precisely, assuming only SM physics, one can estimate that for every 6 millions antiquarks, there should have been 6 millions+1 quarks to survive the sphalerons washout and generate the measured baryon asymmetry [52]. Therefore, searching for a deeper reason for generating η is theoretically appealing. The process of generating an asymmetry between baryons and anti-baryons goes under the name of *Baryogenesis*. Generally, a mechanism that wants to generate (and somewhat preserve) baryon asymmetry must obey three necessary (but not sufficient) conditions; they were first pointed out in 1967 by A. Sakharov [53] and are therefore called *Sakharov condtions*:

(i) BN-violation;
(ii) C- and CP-violation;
(iii) departure from thermal equilibrium.

The first condition is the basic requirement for producing an asymmetry. C—and CP—violations are also necessary as they regulate processes with the production and destruction of quarks and anti-quarks, which will ultimately determine the BN. Finally, if the system remained in thermal equilibrium, all microscopic details of the theory, such as BN, would be washed out, thus spoiling any successful generation of CP.

EW Brayogenesis The SM could in principle possess all requirements to generate the observed BN asymmetry: Baryon number is broken by the EW-anomaly (cfr. Eq. (1.56)), C is maximally violated by Weak interactions and CP by the CKM-phase (cfr. Eq. (1.29)), and finally the departure from thermal equilibrium could be realized by a first-order phase transition when the Higgs gets a vev. This setting is typically called in the literature as *EW-Baryogenesis*. Unfortunately, these conditions fail at the quantitative level. First, given the measured Higgs mass $m_h \sim 125$ GeV, the Higgs transition is not first or second order but a smooth cross-over. Second, despite the large CKM phase, the amount of CP-violation in the SM is too small due to the almost-diagonal structure of the CKM and small quark masses. In fact, as X_{CP} must enter all flavour blind CP-observables, one can estimate a CP-asymmetry parameter at the critical temperature $T_c \sim 100$ GeV to be

$$d_{\rm CP} = \frac{X_{CP}}{T_c^{12}} \sim \frac{(10^9\ {\rm GeV}^{12}) \times 10^{-5}}{10^{24}\ {\rm GeV}^{12}} \sim 10^{-20}\,, \tag{1.86}$$

in overall agreement with the full estimations [54, 55]. Such estimation of CP-violation is too small as $\eta \sim 10^{-2} d_{\rm CP}$ [54].

Baryogenesis via Leptogenesis As we saw, CP-violation in the quark sector is insufficient, and the Higgs does not comply with the requirement for a first-order phase transition. As explained in Section 1.2.1.1, current experimental data points toward massive neutrinos. New Yukawas in the model could feature new sources of CP-violation. If this was the case, the mystery of Baryogenesis could hide in the leptonic sector rather than in the quark one. Any asymmetry in the leptonic sector can be translated to the baryonic one via sphaleron transitions at high temperatures. This is the main idea of *Baryogenesis via Leptogenesis*.[4] As we discussed for the CP-violation of the CKM matrix, the relevant quantity that enters these flavour blind processes is not the CP-violating phase itself but its combination with the sector's mass parameters, making it physical. If only light neutrinos were available, the situation would be even more catastrophic than the one discussed for direct Baryogenesis. The situation is very different if neutrino masses are generated via large Majorana masses. Neutrino models, which feature very large Majorana masses, go generically under the name of *Seesaw models*; their theoretical grounds will be discussed in more detail in Section 2.1. The advantages of large Majorana masses are twofold: on the one side, the Majorana nature of the phase protects it from dilution and makes it dependent solely on the Majorana mass, which can be large; on the other side, large Majorana masses allow for decay processes, which automatically

[4] For a detailed review, see, for example, Ref. [52].

satisfy the out-of-thermal-equilibrium condition once the temperature drops below the Majorana mass scale. All in all, in the simplest Seesaw leptogenesis scenario, one requires Majorana masses to be $M_N \gtrsim 10^9$ GeV [52], which unfortunately makes such scenarios very hard to be directly probed. Nevertheless, today, Baryogenesis via Leptogenesis remains one of the most appealing solutions to the puzzle and further focuses on the neutrino sector.

Chapter 2

New Physics from Heavy and Light Particles

The requirements of Poincaré and gauge invariance of the theory (assuming they remain valid) are perhaps the most precious constraints when considering an extension of the SM. Generic BSM extensions include

(i) extra particles which obey the SM gauge group, e.g. Vector-Like Leptons (VLL);

(ii) dark sectors sterile under $G_{\rm SM}$, which interact with the SM via so-called *portals*.

Portals to the SM can be realized by using new scalars, fermions, or spin-1 bosons. Their simplest realizations are the following:

- *scalar*; given a new scalar Φ, it is always possible to write the interaction

$$\mathcal{L} \supset \frac{\lambda_{H\Phi}}{4} |H|^2 |\Phi|^2 \,. \tag{2.1}$$

  This is the so-called *Higgs portal*;

- *spin-1/2 fermion*: the simplest possibility is to include a right-handed neutrino, N_R, which is singlet under $G_{\rm SM}$. The new fermion can then directly couple to other sectors without any gauge restriction from the SM

$$\mathcal{L} \supset -\overline{L_L} \widetilde{H} Y_\nu N_R + \mathcal{L}_{N_R X} \,. \tag{2.2}$$

  This is the so-called *right-handed neutrino portal*;

- *spin-1 boson*: one can introduce a new gauge group, e.g. $U(1)_X$, with field strength $\mathcal{B}^{\mu\nu}$ and couple it to the SM via mixing

$$\mathcal{L} \supset -\frac{1}{4} B^{\mu\nu} \mathcal{B}_{\mu\nu} \,. \tag{2.3}$$

This is sometimes referred to as the *vector portal*.
In principle, portals that include higher spin new particles such as 3/2, 2, ... are also possible. Such theories, if the new particles are massive, typically show problems of unitarization, which are very hard to solve. For example, theories of massive gravitons (spin-2) can solve this issue and mimic the EFT of GR only by recurring to an infinite tower of spin-2 fields, thus leading to models of extra dimensions. If, instead, the new particles are massless (thus with maximum spin 2), very strong experimental constraints apply and are typically not interesting to phenomenology. All BSM extensions can be composed as a combination of the above portals.

In the following, we will review two classes of NP

1. Heavy-Right handed neutrinos or Heavy Neutral Leptons (HNLs): heavy neutral particles which can be directly related to neutrino masses;
2. Nambu-Goldstone-Bosons (NGBs) and Axion-Like Particles (ALPs): light particles related to multiple contexts of physics.

2.1. Heavy: Seesaw Models and Right-Handed Neutrinos

As commented before, the neutrino oscillation problem in its simplest form can be solved by giving neutrinos a mass. This can be achieved by introducing a mass term in the Yukawa sector in full analogy with the charged leptons

$$-\mathcal{L} \supset \overline{L}\widetilde{H}Y_\nu N_R\,. \tag{2.4}$$

This approach, at present time, does not suffer any experimental inconsistency. However, it would dramatically enhance the Flavour Puzzle as one would need

$$|Y_\nu| \sim \mathcal{O}(10^{-12}), \tag{2.5}$$

which is $\sim 10^7$ smaller than the electron Yukawa.

The above problem can be (partially) mitigated by hypothesising that such hierarchy in Yukawas is generated by some unknown heavy UV-physics at some scale $\Lambda_\nu \gg v$. Assuming the SM gauge group to be valid up to such scale, one can capture model independently new heavy physics within the SM Effective Field Theory (SMEFT) [56, 57, 58]. The SMEFT consists of extending the SM Lagrangian

including all operators of energy dimension > 4 invariant under $G_{\rm SM}$. Explicitly

$$\mathcal{L}_{\rm SMEFT} = \mathcal{L}_{\rm SM} + \sum_i \frac{C_i}{\Lambda_{\rm UV}^{[\mathcal{O}_i]-4}} \mathcal{O}_i \,, \tag{2.6}$$

where $\mathcal{O}_i$ is a $G_{\rm SM}$-invariant operator, $[\mathcal{O}_i] \geq 5$ its energy dimension and $\Lambda_{\rm UV}$ is the UV-energy scale of the unknown heavy physics. Remarkably, at dimension 5 there is a single operator in the SMEFT, the so-called *Weinberg operator*

$$\mathcal{O}_5 = \left(\overline{L_L}\widetilde{H}\right)\left(\widetilde{H}^T L_L^c\right), \tag{2.7}$$

where $L_L^c \equiv (L_L)^c$ is the charge conjugated field[1]

$$\psi^c \equiv C\overline{\psi}^T \,, \tag{2.10}$$

Remarkably, such an operator can provide neutrinos with a mass. When the Higgs gets a vev, one obtains a Majorana mass for the neutrino

$$\mathcal{L} \supset \frac{C_5}{\Lambda_{\rm UV}} \times \frac{1}{2} v^2 \, (\overline{\nu_L}\nu_L^c) \,, \tag{2.11}$$

thus predicting

$$m_\nu = C_5 \frac{v^2}{\Lambda_{\rm UV}} \,. \tag{2.12}$$

The larger the UV scale, the smaller the neutrino mass is predicted to be. Models that generate such a prediction for neutrino masses go in the literature under the name of *seesaw (SS) mechanisms*. The value of $\Lambda_\nu \equiv \Lambda_{\rm UV}$ depends on C_5. Overall, there are two limits

$$\Lambda_\nu \sim \begin{cases} 10^{14} \ \text{GeV}, & C_5 \sim 1, \\ 10^{4} \ \text{GeV}, & C_5 \sim Y_e^2 \sim 10^{-10} \,. \end{cases} \tag{2.13}$$

The first case amounts to fully resolving the flavour puzzle in the neutrino sector; the second relaxes it to the level of the charged leptons. In the following, we will discuss the main typologies of seesaw mechanisms.

[1] For any Dirac spinors ψ and χ, the following useful properties hold

$$\overline{\psi^c}\chi = \overline{\chi^c}\psi \,, \qquad \overline{\psi^c}\gamma_5\chi = \overline{\chi^c}\gamma_5\psi \,, \tag{2.8}$$

$$\overline{\psi^c}\gamma^\mu\chi = -\overline{\chi^c}\gamma^\mu\psi \,, \qquad \overline{\psi^c}\gamma^\mu\gamma_5\chi = \overline{\chi^c}\gamma^\mu\gamma_5\psi \,. \tag{2.9}$$

Type	Spin	Particle	$G_{\rm SM}$
I	1/2	N_R	$(\mathbf{1},\mathbf{1},0)$
II	0	Δ	$(\mathbf{1},\mathbf{3},1)$
III	1/2	Σ_R	$(\mathbf{1},\mathbf{3},0)$

Table 2.1: Exotic particle content of Type-I, -II, -III seesaw mechanisms.

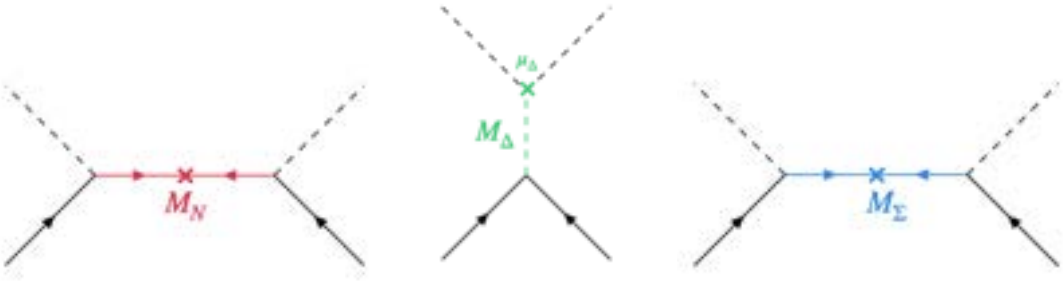

(a) Type-I SS (b) Type-II SS (c) Type-III SS

Figure 2.1: Schematic Feynman diagrams generating neutrino masses for different seesaw mechanisms; new particles lines are coloured.

2.1.1. Traditional Seesaw Mechanisms

Different UV models can lead to the SMEFT prediction of Eq. (2.12). The simplest realizations of the seesaw are usually called *Type-I*, *Type-II* and *Type-III*. The main difference between these models is related to the extra degree(s) of freedom which take(s) care of generating the Weinberg operator. They introduce fermionic singlets (right-handed neutrinos), a scalar triplet and a fermionic triplet, respectively. A summary can be found in Tab. 2.1. The corresponding new terms in the Lagrangian read[2] [3]

$$-\mathcal{L}_{\text{Type-I}} \supset \overline{L_L}\widetilde{H}Y_D N_R + \frac{1}{2}\overline{N_R^c}M_N N_R + \text{h.c.}, \tag{2.14}$$

$$-\mathcal{L}_{\text{Type-II}} \supset \overline{L_L^c}Y_\Delta i\sigma_2\Delta_L L_L + M_\Delta \,\text{Tr}\left[\Delta_L^\dagger\Delta_L\right] + \mu_\Delta\widetilde{H}^\dagger\Delta_L^\dagger H + \text{h.c.}, \tag{2.15}$$

$$-\mathcal{L}_{\text{Type-III}} \supset \sqrt{2}\overline{L_L}Y_\Sigma\Sigma_R\widetilde{H} + \frac{1}{2}\text{Tr}\left[i\sigma_2\overline{\Sigma_R^c}i\sigma_2 M_\Sigma\Sigma_R\right] + \text{h.c.}. \tag{2.16}$$

The mass generation for neutrinos can be diagrammatically seen in Fig. 2.1.

[2] Recall that for a generic matrix $U \in SU(2)$, $Ui\sigma_2 = i\sigma_2 U^*$.

[3] We adopt the convention $\Sigma_R^c \equiv C\overline{\Sigma_R}^T$; in the literature, sometimes the $i\sigma_2$ factors present in the mas term are included in such definition as $\Sigma_R^c \equiv i\sigma_2 C\overline{\Sigma_R}^T i\sigma_2$.

Type-I Seesaw This setup represents Ockham's razor solution regarding particle content. It resembles the SM structure by including right-handed partners for all fermions. For a recent comprehensive review, see e.g. Ref. [59]. In a Type-I seesaw, once the Higgs gets a vev, the neutral mass matrix reads

$$-\mathcal{L} \supset \frac{1}{2}\begin{pmatrix}\overline{\nu_L} & \overline{N_R^c}\end{pmatrix}\begin{pmatrix}0 & m_D\\ m_D^T & M_N\end{pmatrix}\begin{pmatrix}\nu_L^c\\ N_R\end{pmatrix}, \tag{2.17}$$

where $m_D \equiv Y_D v/\sqrt{2}$. If the Majorana mass is large compared to the EW-scale, $\|M_N\| \gg v$, the matrix can be perturbatively block-diagonalized by a unitary rotation of the form

$$\begin{pmatrix}\nu_L\\ N_R^c\end{pmatrix} \to U \begin{pmatrix}\nu_L\\ N_R^c\end{pmatrix}, \qquad U \approx \begin{pmatrix}\mathbf{1} - \frac{1}{2}\Theta\Theta^\dagger & \Theta\\ -\Theta^\dagger & \mathbf{1} - \frac{1}{2}\Theta^\dagger\Theta\end{pmatrix}, \tag{2.18}$$

where we have defined the mixing angle

$$\Theta \equiv m_D M_N^{-1} \tag{2.19}$$

yielding the light-neutrino mass matrix

$$-\mathcal{L} \supset \frac{1}{2}\overline{\nu_L} m_\nu \nu_L^c\,, \qquad m_\nu \approx -\Theta m_D^T = -m_D M_N^{-1} m_D^T\,. \tag{2.20}$$

This is the structure generated by the Weinberg operator in Eq. (2.12), identifying the scales $\Lambda_{\rm UV} \sim \|M_N\|$ and $C_5 \sim |Y_D|^2$. The neutrino mass matrix must then be diagonalized by a second unitary transformation, which corresponds to the PMNS matrix,

$$\nu_L \to U_{\rm PMNS}\nu_L\,, \qquad U_{\rm PMNS}^\dagger m_\nu U_{\rm PMNS} = m_{\nu,\rm diag.}\,. \tag{2.21}$$

Type-II Seesaw The idea of Type-II SS is that the neutrino mass's smallness is induced by the vev of a new scalar field Δ_L. This translates to the problem of generating a very small vev for the new scalar. As it will turn out, this is achieved by SS structure in the scalar potential between the free mass of Δ_L and the Higgs vev. A review can be found in Ref. [60]. The triplet scalar can be decomposed in matrix representation as

$$\Delta_L = \begin{pmatrix}\frac{\Delta^+}{\sqrt{2}} & \Delta^{++}\\ \Delta^0 & -\frac{\Delta^+}{\sqrt{2}}\end{pmatrix}, \tag{2.22}$$

Besides the Higgs, in Type-II also the new scalar gets a vev

$$\langle \Delta_L \rangle = \begin{pmatrix} 0 & 0 \\ \frac{v_\Delta}{\sqrt{2}} & 0 \end{pmatrix} , \tag{2.23}$$

where the vev is related to the triplet mass via[4]

$$v_\Delta \approx \frac{\mu_\Delta v^2}{\sqrt{2} M_\Delta^2} . \tag{2.24}$$

The generated Majorana neutrino mass reads

$$-m_\nu = \sqrt{2} Y_\Delta v_\Delta = Y_\Delta \mu_\Delta \frac{v^2}{M_\Delta^2} . \tag{2.25}$$

Type-III Seesaw The Type-III SS is conceptually identical to Type-I. The neutral components of the triplet play the role of "right-handed neutrino" and generate the SS mass matrix texture of the Type-I. In this case, mixing with SM-charged leptons is also induced. The fermionic triplet can be written as

$$\Sigma_R \equiv \begin{pmatrix} \frac{\Sigma_R^0}{\sqrt{2}} & \Sigma_R^+ \\ \Sigma_R^- & -\frac{\Sigma_R^0}{\sqrt{2}} \end{pmatrix} \qquad i\sigma_2 \Sigma_R^c i\sigma_2 = \begin{pmatrix} \frac{(\Sigma_R^0)^c}{\sqrt{2}} & (\Sigma_R^-)^c \\ (\Sigma_R^+)^c & -\frac{(\Sigma_R^0)^c}{\sqrt{2}} \end{pmatrix} \tag{2.26}$$

The neutral sector of the Lagrangian of Eq. (2.16) reads

$$-\mathcal{L}_{\text{Type-III}} \supset \frac{1}{2} \begin{pmatrix} \overline{\nu_L} & (\Sigma_R^0)^c \end{pmatrix} \begin{pmatrix} 0 & m_\Sigma \\ m_\Sigma^T & M_\Sigma \end{pmatrix} \begin{pmatrix} \nu_L^c \\ \Sigma_R^0 \end{pmatrix} , \tag{2.27}$$

which is the same texture of Type-I SS reported in Eq. (2.17). Phenomenologically, the main difference stems from the charged components of the triplet, which mix with the SM-charged leptons via the mass term

$$-\mathcal{L}_{\text{Type-III}} \supset \sqrt{2} \overline{e_L} m_\Sigma \Sigma_R^- , \tag{2.28}$$

which also induces mixing angles and rich phenomenology in the charged sector. For an overview of its bounds see e.g. Ref. [61].

[4] Notice that we did not consider the impact of other couplings (e.g. quartic coupling between Δ_L) which would affect this expression.

2.1.2. Low-Scale Seesaws

In the different seesaw models presented in the previous section, the smallness of neutrino masses was due to either a very large UV-scale or a TeV-ish scale, but at the price of very small Yukawas. While the former choice could be justified, for instance, in theories of Grand-Unifications (GUTs), the latter worsens the flavour puzzle. Models which attempt to theoretically justify TeV-ish scale SS go under the name of *Low-Scale Seesaws* (LSS). In LSS models, the smallness of neutrino masses is related to the robustness of a global symmetry rather than a large scale. The key observation is that the Majorana neutrino mass of Eq. (2.12) generated by the Weinberg operator breaks Lepton-Number (LN) by two units. As it will be shown, SS and LSS share qualitatively the same formulas but retain very different "natural values" of the parameters.

For simplicity, we consider only two right-handed neutrinos, N_R and S_R. This is the minimal number as their couplings contain enough parameters to correctly reproduce the PMNS matrix and generate two massive neutrinos and a massless one compatible with current oscillation data. Including more right-handed neutrinos can be implemented straightforwardly following the same approach. The neutral leptonic Yukawa sector of the Lagrangian reads

$$-\mathcal{L} \supset \overline{L_L}\widetilde{H}Y_N N_R + \overline{L_L}\widetilde{H}Y_S S_R + \frac{\Lambda}{2}\left[\overline{N_R^c}S_R + \overline{N_R^c}S_R\right] + \frac{1}{2}\left[\mu'\overline{N_R^c}N_R + \mu\overline{S_R^c}S_R\right] + \text{h.c.}\,, \tag{2.29}$$

By combining left- and right-handed neutrinos in a single left-handed field $\chi_L \equiv (\nu_L, N_R^c, S_R^c)^T$, the following mass matrix is generated once the Higgs gets a vev

$$-\mathcal{L} \supset \frac{1}{2}\overline{\chi_L}\mathcal{M}_\chi \chi_L^c\,, \qquad \mathcal{M}_\chi = \begin{pmatrix} 0 & m_N & m_S \\ m_N^T & \mu' & \Lambda \\ m_S^T & \Lambda & \mu \end{pmatrix}, \tag{2.30}$$

where $m_X \equiv Y_X v/\sqrt{2}$. Let us now consider the global LN $U(1)$ symmetry and assign initial charge $\mathcal{C}_{LN}(L_L) = 1$. To have at least one term which respects the symmetry, we can assign in full generality $\mathcal{C}_{LN}(N_R) = 1$: the diagonal Majorana term involving $\overline{N_R^c}N_R$ breaks LN. To preserve the seesaw expansion and have both HNLs, one has to allow the mass term Λ and therefore set $\mathcal{C}_{LN}(S_R) = -1$. All the other terms are explicitly LN-breaking and are consequently assumed to be very small if LN is a robust symmetry of the theory. To make it explicit, we will write ϵm_S, such that $\epsilon,\ \mu,\ \mu' \ll 1$.

The diagonalization procedure of the mass matrix goes in full analogy with the

case of Type-I seesaw (cfr. Eq. (2.20)) identifying

$$m_D = \begin{pmatrix} m_N & m_S \end{pmatrix}, \qquad M_N = \begin{pmatrix} \mu' & \Lambda \\ \Lambda & \mu \end{pmatrix}. \tag{2.31}$$

The mixing angle (cft. (2.19)) now reads

$$\Theta_{\rm LSS} \approx \frac{1}{\Lambda} \times \begin{pmatrix} \epsilon m_S - \mu \dfrac{m_N}{\Lambda} & m_N - \mu' \dfrac{\epsilon m_S}{\Lambda} \end{pmatrix}, \tag{2.32}$$

and the neutrino mass matrix is given by

$$\begin{aligned} -m_{\nu,\rm LSS} &\approx \epsilon \frac{m_N m_S^T + m_S m_N^T}{\Lambda} - \mu \frac{m_N m_N^T}{\Lambda^2} - \epsilon^2 \mu' \frac{m_S m_S^T}{\Lambda^2}, \\ &\approx \epsilon \frac{m_N m_S^T + m_S m_N^T}{\Lambda} - \mu \frac{m_N m_N^T}{\Lambda^2}, \end{aligned} \tag{2.33}$$

where we neglected the last term as it was of order cube in small LN-breaking parameters expansion. A mass matrix that gives rise to the first term of Eq. (2.33) proportional to Λ^{-1} is typically dubbed as *Linear* LSS. A mass matrix that gives rise to the second term of Eq. (2.33) proportional to Λ^{-2} is typically dubbed as *Inverse* LSS.

2.1.3. Matching Seesaw to Neutrino Masses and PMNS Matrix

With only two HNLs, only two neutrinos can acquire a mass. This can be understood by realising that the neutrino mass matrix is built solely from two Yukawas, $Y_{N,S}$. If the Yukawas are not aligned, this restricts the theory to a 2-dimensional vectorial space, implying that only two eigenvectors can be related to non-trivial eigenvalues. All in all, one can decompose the eigenvectors, $u_{1,2,3}$, of m_ν as a linear combination of the Yukawas

$$u_{1,2} = \alpha_{1,2} Y_N + \beta_{1,2} Y_S, \qquad u_3 = \alpha_3 Y_N \times Y_S. \tag{2.34}$$

One can then require normalization of eigenstates and solve exactly for the eigenvalues equation. The exact solution for a generic mass matrix involves some lengthy formulas and can be found in special limits, as shown as in Sec. 3.4.

An explicit example. A clean example of such a procedure can be found in Ref. [62] for the LSS mass matrix of Eq. (2.30) with $\mu = \mu' = 0$. We report below

the case results: the same procedure applies to the more general case $\mu \neq \mu' \neq 0$.

1. We define the direction vectors of the Yukawas and their Hermitian scalar product

$$u \equiv \frac{Y_N}{|Y_N|}\,, \qquad v \equiv \frac{Y_S}{|Y_S|}\,, \qquad u^\dagger v = \langle u|v\rangle \equiv \eta = |\eta| e^{i\theta}\,. \tag{2.35}$$

   The neutrino mass matrix then reads

$$m_\nu = -\frac{|Y_N||\epsilon Y_S|}{\Lambda} \left(uv^T + vu^T\right). \tag{2.36}$$

   The matrix m_ν can be diagonalized by a unitary matrix U (the PMNS) such that $U^\dagger m_\nu U^* = m_{\nu,\mathrm{diag}}$.

2. By exploiting the fact that $U^\dagger m_\nu m_\nu^\dagger U = m_{\nu,\mathrm{diag}} m_{\nu,\mathrm{diag}}^\dagger$, one can translate the problem to finding the eigenvalues of a more convenient hermitian matrix. We can thus write

$$m_\nu m_\nu^\dagger = \left(\frac{|Y_N||\epsilon Y_S|}{\Lambda}\right)^2 \left(uu^\dagger + \eta uv^\dagger + \eta^* vu^\dagger + vv^\dagger\right), \tag{2.37}$$

   where $u^\dagger v \equiv \rho$.

3. As the eigenvalues do not depend on the basis, one can look for a convenient orthonormal basis to write this matrix. For example, one can choose

$$u_1 = u\,, \qquad u_2 = \frac{1}{\sqrt{1-|\eta|^2}}\,(v - \eta u). \tag{2.38}$$

   One can check that $u_i^\dagger u_i = 1$ and $u_1^\dagger u_2 = 0$. This amounts to the replacement

$$u = u_1\,, \qquad v = \eta u_1 + \sqrt{1-|\eta|^2}\,u_2\,. \tag{2.39}$$

4. Let us now assume that the zero eigenvalue is the first one; in such a basis, the matrix reads

$$(m_\nu m_\nu^\dagger)_{u_{1,2}} = \left(\frac{|Y_N||\epsilon Y_S|}{\Lambda}\right)^2 \begin{pmatrix} 0 & 0 & 0 \\ 0 & 1+3|\eta|^2 & 2\eta\sqrt{1-|\eta|^2} \\ 0 & 2\eta^*\sqrt{1-|\eta|^2} & 1-|\eta|^2 \end{pmatrix}, \tag{2.40}$$

   whose eigenvalues can be extracted straightforwardly

$$|m_\pm|^2 = \left(\frac{|Y_N||\epsilon Y_S|}{\Lambda}\right)^2 (1 \pm |\eta|)^2\,. \tag{2.41}$$

One can then fix both $|\eta|$ and $(|Y_N||\epsilon Y_S|/\Lambda)$ by means of the measured neutrino mass splittings.

5. The eigenvectors, $e_{0,\pm}$, can be extracted by explicitly solving the eigenvector equation

$$(m_\nu m_\nu^\dagger)\,|e_i\rangle = m_i^2\,|e_i\rangle\ . \tag{2.42}$$

In this case, they take the simple form

$$e_\pm = \frac{1}{\sqrt{2}\sqrt{1\pm|\eta|}}\left(e^{i\theta/2}u \pm e^{-i\theta/2}v\right), \qquad e_0 = \frac{u\times v}{\sqrt{|u\times v|}}\,, \tag{2.43}$$

thus

$$u = \frac{e^{-i\theta/2}}{\sqrt{2}}\left(\sqrt{1+|\eta|}e_+ + \sqrt{1-|\eta|}e_-\right), \tag{2.44}$$

$$v = \frac{e^{i\theta/2}}{\sqrt{2}}\left(\sqrt{1+|\eta|}e_+ - \sqrt{1-|\eta|}e_-\right). \tag{2.45}$$

6. Finally, the PMNS matrix, U, is made out from the eigenvectors. The ordering of the PMNS entries must be done accordingly to the choice of NO or IO This allows identifying the eigenvectors as the columns of the PMNS, which then allows extracting u and v via Eq. (2.44)-(2.45). The rotation matrix U in general, contains also the Majorana phases, which, in this case, can be encoded in the matching of parameters via

$$U = U_{\rm PMNS}U_{\rm phase} \equiv U_{\rm PMNS}\begin{pmatrix} e^{i\alpha} & & \\ & e^{-i\alpha} & \\ & & 1 \end{pmatrix}. \tag{2.46}$$

For instance, if one assumes ν_1 to be massless (NO), then

$$U = \begin{pmatrix} e_0 & e_- & e_+ \end{pmatrix}. \tag{2.47}$$

For example, one can extract the Y_N Yukawa

$$Y_{N,i} = |Y_N|u_i = \frac{|Y_N|e^{-i\theta/2}}{\sqrt{2}}\left(\sqrt{1+|\eta|}U_{i3} + \sqrt{1-|\eta|}U_{i2}\right), \tag{2.48}$$

and similarly for Y_S.

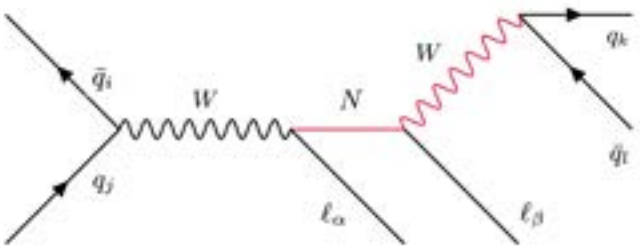

Figure 2.2: Example of HNL production and decay in dilepton and two jets final state searched at collider. The red internal line corresponds to particles produced on-shell. The case of tri-lepton final state amounts to the same diagram with the final W decaying into $W \to \ell\nu$ instead of two jets.

2.1.4. Current Bounds on HNLs

As the HNLs are singlets under $G_{\rm SM}$, their impact on SM physics depends on the mixing with the active left-handed neutrinos parameterized by Θ. Its overall size strongly depends on the type of realization of the seesaw. The presence of heavy right-handed neutrinos has two main imprints on phenomenology. They appear at different orders in Θ and we thus discuss them separately.[5]

2.1.4.1. Collider Direct Searches

At linear order in Θ, the mixing between light neutrinos and HNLs

$$\nu_L \to \nu_L + \Theta N_R^c \,, \tag{2.49}$$

generates coupling of gauge bosons to HNLs

$$-\mathcal{L}_W \supset \frac{g}{\sqrt{2}} \left(\overline{\nu_L} \gamma^\mu e_L \, W_\mu^+ + \text{h.c.}\right) \quad \to \supset \frac{g}{\sqrt{2}} \left(\overline{N_R^c} \gamma^\mu \Theta^\dagger e_L \, W_\mu^+ + \text{h.c.}\right) \tag{2.50}$$

Colliders studies can bound HNLs by studying typical signatures such as same-sign or different flavour charged di- and tri-leptons final states [64, 65, 66, 67, 68]; an example of such topologies is shown in Fig. 2.2. These signatures are among the most promising as the final states are suppressed in the SM. The HNL is produced on-shell (and thus Θ-suppressed) and promptly decays in the detector.

For masses $M_N \geq 200$ GeV, the most constraining bounds on $\Theta_{e,\mu}$ come from CMS [67, 68, 69]; they are shown in Fig. 2.3. While the constraints are relatively strong for $M_N \lesssim 100$ GeV with $|\Theta_{e,\mu}| \lesssim \mathcal{O}(10^{-2})$, they rapidly become weaker as the mass increases and moves to the region where SS models start appearing,

[5] A comprehensive analysis of the low-energy effects of the different types of SS mechanisms can be found in Ref. [63].

with $\Theta_{e,\mu} \lesssim 1$ for $M_N \sim 1$ TeV. For Θ_μ, a search from analyzing Vector Boson Fusion (VBF) has been performed [70], which remarkably extends a relatively mild bound $|\Theta_\mu| \lesssim \mathcal{O}(0.5)$ to very large masses up to $M_N = 25$ TeV where the bound weakens to unity. All in all, the diagram for this process is essentially equivalent to the one of neutrinoless-double-beta-decay; this large range of masses can be achieved as the HNL is never produced on-shell, thus eliminating kinematical suppressions due to lack of energy. Bounds on $|\Theta_\tau|$ are challenging to extract at colliders as taus can decay hadronically, thus making it difficult to separate the signal from the background. The current strongest bounds from collider for $M_N \lesssim 100$ GeV come from the DELPHI Collaboration [72]. For larger masses, the strongest bounds solely come from the most recent results of CMS [69], which analyzes tri-lepton final states. While the constraints on $\Theta_{e,\mu}$ are of the same order of magnitude of those previously found [68], the constraints on Θ_τ are much weaker, $\Theta \lesssim \mathcal{O}(0.7)$. They can be seen in Fig. 2.3.

This kind of search typically assumes the presence of a single HNL and sometimes also of a single mixing angle at a time. The presence of multiple HNLs at the same mass scale (e.g. as in a LSS) can have an impact in extracting the bound on the couplings from the experimental data [73]. The possible constructive or destructive interference of Feynman diagrams can enhance or significantly weaken the amplitude. It depends on the ratio of the HNLs' mass splitting to its width $\Delta M_N/\Gamma_N$: a large(small) ratio amounts to having no(maximal) interference. Its impact in the analysis is highly model-dependent, but general corrections to the bounds are of $\mathcal{O}(1)$. In LNV processes, instead, destructive interference can be as large as cancelling the amplitude due to approximate LN conservation in the Lagrangian, thus considerably weakening the bounds.

All in all, direct searches cannot put stringent bounds on seesaw models mainly due to the difficulty of producing HNLs in the final state, thus leaving large space for $\sim$ TeV HNLs at relatively large mixing angles.

2.1.4.2. Non-Unitarity Constraints

At second order in Θ, HNLs dilute the interactions of light neutrinos to gauge bosons via mixing (cfr. Eqs. (2.18) and (2.21)). This is referred to in the literature as *non-unitarity* effect as light-neutrinos flavour eigenstates, $\nu_{L,\alpha}$, and mass eigenstates, $\nu_{L,i}$, are related by the non-unitary transformation [74, 71]

$$\nu_L \to \left(\mathbf{1} - \frac{1}{2}\Theta\Theta^\dagger\right) U_{\text{PMNS}}\nu_L \,. \tag{2.51}$$

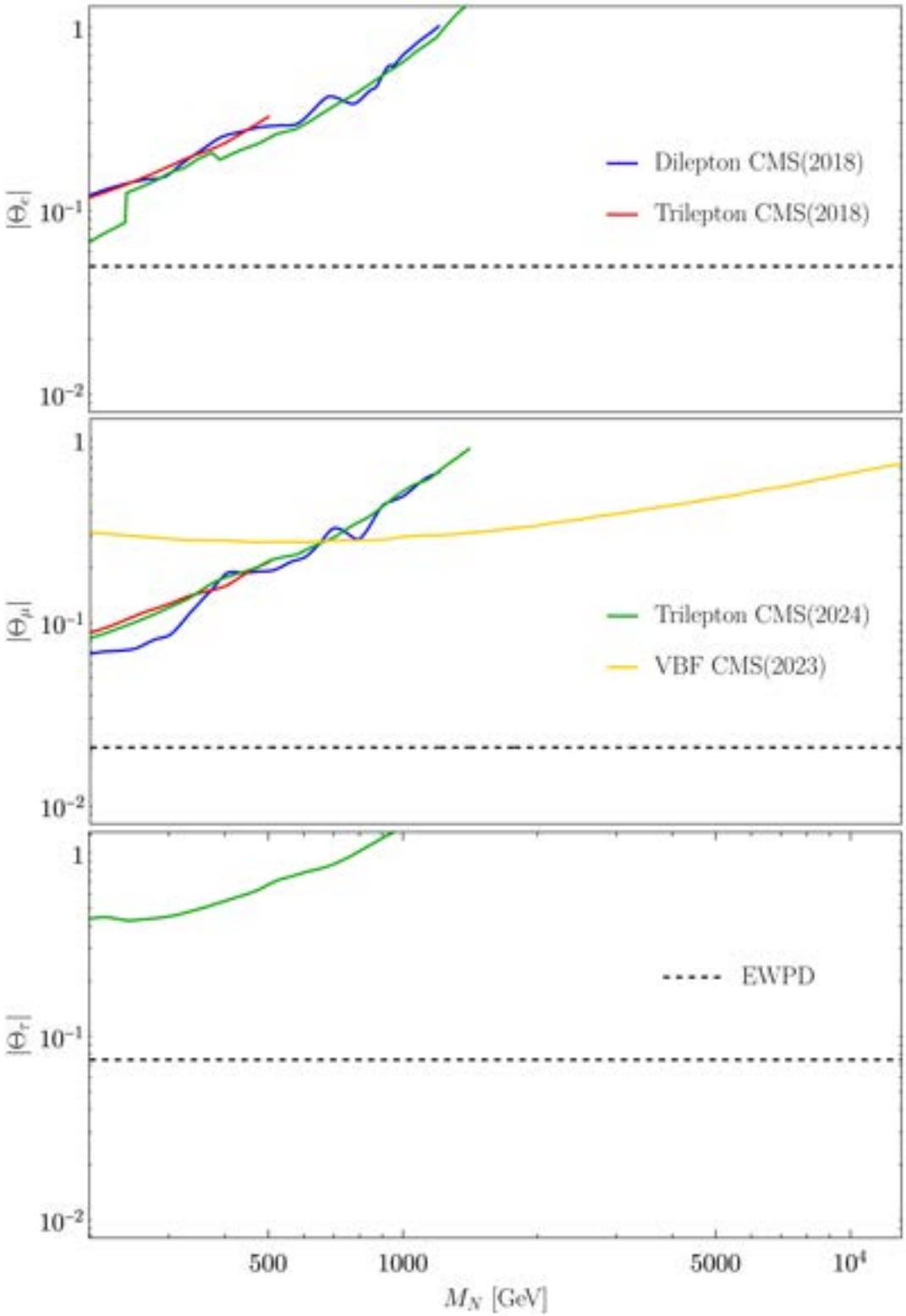

Figure 2.3: Bounds at 95% C.L. on $|\Theta_{e,\mu,\tau}|$ from direct searches with dilepton [67] (blue), tri-leptons [68, 69] (red and green) final states and t-channel VBF [70] (yellow). Indirect bounds from EWPD are shown in black-dashed [71].

It is useful to encode non-unitarity effects via a hermitian matrix, η, defined as [71]

$$\nu_\alpha = \sum_{i=1}^{3} \Big((\mathbf{1} - \eta) U_{\rm PMNS} \big]_{\alpha_i} \nu_i \,, \qquad \eta \equiv \frac{1}{2} \Theta \Theta^\dagger \,. \tag{2.52}$$

The presence of non-unitarity affects several observables, both Flavour-Conserving (FC) and Flavour-Violating (FV). It is important to stress that such effects are indirect and thus do not depend directly on the HNL mass but only the mixing angle, $\Theta(\eta)$. Diagonal entries of η modify predictions of SM processes. Among them, the most notable are

(I) EW-universality decays ratios of mesons (e.g. pions, kaons) or W/Z-decays to charged leptons or hadronic final states,

$$\frac{\Gamma_\alpha}{\Gamma_\beta} \equiv \frac{\Gamma_\alpha}{\Gamma_\beta}_{\rm SM} R^2_{\alpha\beta} \approx \frac{\Gamma_\alpha}{\Gamma_\beta}_{\rm SM} \times (1 - 2\eta_{\alpha\alpha} + 2\eta_{\beta\beta}) , \tag{2.53}$$

such as $R^{\pi,W,K}_{\mu e,\tau\mu}$.

(II) EW observables and decays; the main responsible for such deviations is the induced mismatch between the Fermi constant, G_F and its determination measured via muon decay, G_μ,

$$\Gamma(\mu^- \to e^- \nu_\mu \overline{\nu_e}) \approx \frac{m_\mu^5 G_F^2}{192\pi^3} \times (1 - 2\eta_{ee} - 2\eta_{\mu\mu}) \equiv \frac{m_\mu^5 G_\mu^2}{192\pi^3} \,, \tag{2.54}$$

with consequent redefinition of the Fermi-constant,

$$G_F = G_\mu (1 + \eta_{ee} + \eta_{\mu\mu}) . \tag{2.55}$$

Such a modification propagates to all low-energy EW observables, the most notable being the prediction for M_W.

(III) CKM unitarity tests; violation of CKM unitarity is indirectly induced by affecting processes from CKM parameters are extracted, e.g. superallowed beta decays (V_{ud}) or Kaon decays (V_{us})

$$|V_{ud}^\beta| = (1 + \eta_{\mu\mu}) |V_{ud}| \,, \qquad |V_{us}^{K \to \pi \ell_\alpha \overline{\nu_\alpha}}| = (1 + \eta_{\alpha\alpha}) |V_{us}| \,. \tag{2.56}$$

Non-vanishing off-diagonal entries of η induce processes forbidden or, at best, neutrino-mass suppressed in the SM. Among them, the most notable ones are lepton-

flavour-violating decays with a γ, Higgs [75, 76, 77] and Z-decays [78, 79, 80]

$$\ell \to \ell'\gamma : \begin{cases} \mu^- \to e^-\gamma\,, \\ \tau^- \to e^-\gamma\,, \\ \tau^- \to \mu^-\gamma\,, \end{cases} \qquad h(Z) \to \ell\ell' : \begin{cases} h(Z) \to \mu e\,, \\ h(Z) \to \tau e\,, \\ h(Z) \to \tau\mu\,, \end{cases} \tag{2.57}$$

tri-leptons decays [81], such as $\mu \to eee$, $\tau \to eee$, $\tau \to \mu\mu\mu$, and $\mu \to e$ conversion in nuclei [82, 83, 84]. Besides direct constraints, being η a positive Hermitian matrix, its off-diagonal entries can be indirectly bounded by the Cauchy-Schwarz Inequality (CSI)

$$|\eta_{\alpha\beta}| \leq \sqrt{|\eta_{\alpha\alpha}||\eta_{\beta\beta}|}\,. \tag{2.58}$$

We report here the results from Ref. [71] of the global fit of non-unitarity effects to EW-Precision-Data (EWPD) in a generic SS scenario; at 2σ, the authors find

$$|\Theta_e| < 0.050\,, \qquad |\Theta_\mu| < 0.021\,, \qquad |\Theta_\tau| < 0.075\,. \tag{2.59}$$

Bounds on off-diagonal entries derived by CSI are weaker than those presented above, with the only exception of $\eta_{e\mu}$ from $\mu \to e\gamma$, which reads

$$\sqrt{2\eta_{e\mu}} = \sqrt{|\Theta_e\Theta_\mu|} < 4.9 \times 10^{-3}\,, \qquad \text{at } 95\%\text{ C.L.}\,; \tag{2.60}$$

the bound is about a factor of 10 stronger than the one which could be derived from CSI.

The bounds from non-unitarity can be compared to those stemming from direct searches in Fig. 2.3. All in all, we learn that direct searches are somewhat far from competitive with indirect ones from EWPD and that, as a rule of thumb, current data requires $|\Theta_\ell| \lesssim \mathcal{O}\,(5 \times 10^{-2})$.

2.1.4.3. Type-I or LSS?

A natural question is whether the bounds presented in the previous section can probe either Type-I or Low-Scale SS. In Type-I SS, the Yukawas are assumed to be the same orders of magnitude. Therefore, one would naively expect

$$\|\Theta_{\text{type-I}}\| \sim |Y_D|\frac{v}{\|M_N\|}\,, \qquad \|m_\nu\| \sim |Y_D|^2\frac{v^2}{\|M_N\|}\,, \tag{2.61}$$

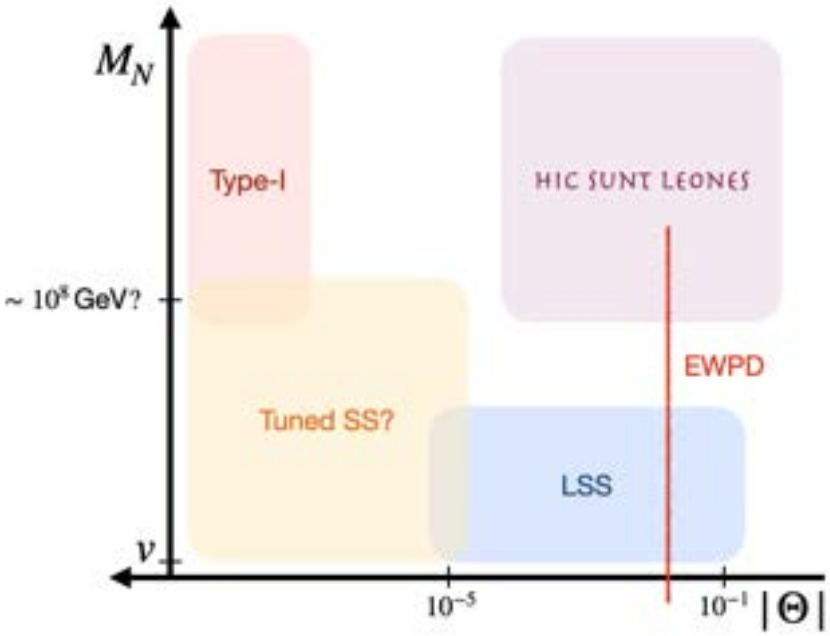

Figure 2.4: Conceptual summary of heavy right-handed neutrinos and $|\Theta|$ in SS models with heavy right-handed neutrinos. The purple area represents a theoretically unfavourable case, as it should contain large mixing associated with very heavy physics, contrary to the decoupling theorem [85].

and thus

$$\|\Theta_{\text{type-I}}\| \sim \sqrt{\frac{\|m_\nu\|}{\|M_N\|}} \leq \mathcal{O}(10^{-5}), \tag{2.62}$$

where in the estimation we took the best possible scenario $\|m_\nu\| \sim 0.1$ eV, $\|M_N\| \sim 200$ GeV. This implies that even in the case of strong tuning of the Yukawa, a Type-I seesaw would be incredibly challenging to test. For the traditional case of realization of Type-I SS with $\|M_N\| \sim 10^{13}$ GeV, direct experimental testability seems not feasible.

The conclusions are sensibly different for a LSS. The light neutrino masses and the mixing angle are not in one-to-one correspondence (cfr. Eqs. (2.33)-(2.32)). The neutrino mass can be made arbitrarily small by demanding greater robustness of LN, i.e. ϵ, $\mu \ll 1$. In this limit the mixing angle reads

$$\Theta_{\text{LSS}} \approx \left(0, \frac{m_N}{\Lambda}\right), \tag{2.63}$$

which can span a much wider range of values. For the construction of a LSS to be consistent, the Yukawa Y_N must not be of the same order as the LN-breaking parameters. This also imposes directly a constraint on the mass scale Λ, which, if too large, would transform the model into a Type-I SS, thus with a loss of consistency in

constructing the model from symmetry arguments. This implies that the relatively large values of $\Theta \leq \mathcal{O}(10^{-5})$ not covered by the Type-I SS are the ideal regime for the LSS.

As both theoretical constructions are a priori well-motivated, agnostic searches for HNLs assuming Θ as effective BSM coupling are justified from a theoretical point of view in all ranges. A schematic summary of this rich landscape of HNLs models can be found in Fig. 2.4.

2.2. Light: Pseudo-Nambu-Goldstone Bosons and Axion-Like Particles

Light feebly interacting BSM particles are phenomenologically very appealing as they could be produced on-shell. They might impact astrophysical processes such as stellar cooling but also appear at colliders as missing energy or with some new signatures if short-lived enough. If one considers NP to appear at some UV scale $\Lambda_{\rm UV}$, one would also expect the mass scale of such new particles to be proportional to $\Lambda_{\rm UV}$; the introduction of such new light degrees of freedom would thus generically require very hierarchical couplings, which are not theoretically appealing. In the following, we discuss a class of models which can naturally accomplish that: pseudo-Nambu-Goldstone-Bosons.

2.2.1. Light Scalars from SSB

Light scalars associated with large-scale dynamics are naturally associated with theories which feature SSB. In this context, they are typically dubbed either *Pseudo-Nambu-Goldstone-Bosons* (pNGBs) [86, 87] or *Axion-Like Particles* (ALPs). Nowadays, the two wordings are synonyms at the practical level, and the difference in wording depends on the physics community that studies them, mainly due to historical reasons.

2.2.1.1. The Goldstone Theorem

The existence of light scalars after SSB of global symmetries is guaranteed by the Nambu-Goldstone Theorem. For completeness, we report an elegant argument of the theorem from Ref. [88]. Let us assume the Lagrangian possesses a global symmetry, with conserved Noether current $J^\mu(x)$

$$\partial_\mu J^\mu = 0, \tag{2.64}$$

and conserved charge Q

$$Q \equiv \int \mathrm{d}^3x\, J^0(x) . \tag{2.65}$$

As the charge is conserved, it commutes with the Hamiltonian

$$[H, Q] = i\partial_t Q = 0 . \tag{2.66}$$

Let us now consider SSB, that is to say, that the vacuum is not invariant under the symmetry of the Lagrangian, or, in other words,

$$Q\,|\Omega\rangle \neq 0 . \tag{2.67}$$

Assuming the vacuum has energy E_0, the state $Q\,|\Omega\rangle$ has the same energy as $|\Omega\rangle$

$$H\left(Q\,|\Omega\rangle\right) = QH\,|\Omega\rangle = E_0\left(Q\,|\Omega\rangle\right) . \tag{2.68}$$

We can construct the state

$$|\pi(\boldsymbol{p})\rangle \propto \int \mathrm{d}^3x e^{-i\boldsymbol{x}\cdot\boldsymbol{p}} J^0(x)|\Omega\rangle \ , \tag{2.69}$$

whose energy on top of the vacuum energy is given by $E = E_\pi(\boldsymbol{p}) + E_0$. For $\boldsymbol{p} \to \boldsymbol{0}$, $|\pi(\boldsymbol{0})\rangle \propto Q\,|\Omega\rangle$ which has energy E_0, implying that $E_\pi(\boldsymbol{0}) \xrightarrow{\boldsymbol{p}\to\boldsymbol{0}} 0$, which satisfies a massless dispersion relation. That is to say, if the Lagrangian possess a symmetry under which the vacuum is not invariant, the low-energy theory contains massless particles, the celebrated so-called NGBs. The definition of the state in Eq. (2.69) requires the presence of a dimensional parameter, f_π, which is typically fixed by requiring

$$\langle\pi(\boldsymbol{p})|J^\mu(x)|\Omega\rangle \equiv ip^\mu f_\pi e^{ip\cdot x} . \tag{2.70}$$

The new scale f_π is associated with the SSB scale and is typically referred to as the NGB's decay constant.

If the symmetry was not exact and explicitly broken in the Lagrangian by a parameter, ϵ, the current would not be conserved

$$\partial_\mu J^\mu \propto \epsilon . \tag{2.71}$$

The NGBs acquire a tiny mass proportional to the breaking parameters; when this happens they are referred to as *pseudo*-NGBs (pNGBs).

2.2.1.2. NGB from Global $U(1)$

The simplest case of NGB stems from SSB of a global $U(1)$. The Lagrangian must thus be invariant under the transformation $\phi \to e^{i\alpha}\phi$, for any α. The SSB can be achieved by the vev of a complex singlet scalar field, ϕ, $\langle|\phi|^2\rangle = f_a^2/2$. The conserved current, according to Noether's theorem, reads

$$J^\mu = i\alpha\left(\phi\partial^\mu\phi^* - \phi^*\partial^\mu\phi\right). \tag{2.72}$$

The GB is contained within the degrees of freedom of ϕ, but the choice of parameterization can hide it. The appropriate choice is given by

$$\phi = \frac{f_a + \rho}{\sqrt{2}} e^{ia/f_a}\,, \qquad J^\mu = \alpha\left(1 + \frac{\rho}{f_a}\right)^2 f_a\partial^\mu a \approx \alpha\, f_a\,\partial^\mu a\,, \tag{2.73}$$

which identifies from Eq. (2.70)

$$|\pi\rangle \equiv |a\rangle\,, \qquad f_\pi \equiv f_a\,. \tag{2.74}$$

The conservation of the current, $\partial_\mu J^\mu = 0$, consistently with the NG theorem, imposes the Klein-Gordon equation of a massless scalar field. Notice that in Eq. (2.73), even though formally the $U(1)$ is broken by the vev of ϕ, the symmetry is still intact and amounts now to a *shift-symmetry* for the field a.

2.2.1.3. SM pNGBs from explicit breaking: Pions

The existence of pNGBs is far more common than NGBs, as the existence of exact accidental global symmetries is highly non-common. The most famous examples of pNGBs in the SM are the pions. Let us consider the first generation of quarks. By grouping left and right quarks in doublets, the kinetic terms

$$\mathcal{L} \supset \overline{Q_L} i\not{\partial} Q_L + \overline{Q_R} i\not{\partial} Q_R\,, \tag{2.75}$$

are invariant under $SU(2)_L \times SU(2)_R$, which transform independently left- and right-handed doublets, respectively[6]

$$Q_L \equiv \begin{pmatrix} u_L \\ d_L \end{pmatrix} \to U_L \begin{pmatrix} u_L \\ d_L \end{pmatrix}, \qquad Q_R \equiv \begin{pmatrix} u_R \\ d_R \end{pmatrix} \to U_R \begin{pmatrix} u_R \\ d_R \end{pmatrix}. \tag{2.76}$$

[6] In reality, the Lagrangian possesses a larger $U(2)_L \times U(2)_R = U(1)_L \times U(1)_R \times SU(2)_L \times SU(2)_R$ symmetry. We will ignore the extra $U(1)_{L,R}$ for the moment and come back on them.

When QCD confines, the quarks bilinear gets non-zero expectation value $\overline{Q}_L Q_R \sim \Lambda^3_{\rm QCD} \neq 0$, thus breaking $SU(2)_L \times SU(2)_R$ to the subgroup which transforms left- and right-handed fields in the same way, the so-called vectorial subgroup $SU(2)_V$. The number of broken generators of $SU(2)$ is three, and the NGB theorem thus predicts the existence of three NGBs: the pions. However, $SU(2)_L \times SU(2)_R$ was not an exact symmetry, to begin with, as quarks are massive. The Yukawa mass term explicitly breaks the symmetry

$$\mathcal{L} \supset -\overline{Q_L} M_q Q_R + \text{h.c.} = -\overline{Q_L} \begin{pmatrix} m_u & 0 \\ 0 & m_d \end{pmatrix} \left(Q_R + \text{h.c.} \right. \tag{2.77}$$

As a consequence, the pions acquire a mass

$$m_\pi^2 \sim \frac{\Lambda^3_{\rm QCD}}{f_\pi^2}(m_u + m_d), \tag{2.78}$$

which vanishes in the limit $m_{u,d} \to 0$, making them the lightest pNGBs of the SM.

2.2.1.4. EFT of pNGBs: Chiral Perturbation Theory (χPT)

The formal derivation of Eq. (2.78) can be achieved by employing Chiral Perturbation Theory (χPT). Generally, χPT is an EFT built to deal with the pNGBs. The ingredients involve solely the global symmetry structure of the theory in the UV, $\mathcal{G}$, and the residual symmetry in the IR, $\mathcal{H}$. χPT then describes the pNGBs derived from the breaking of $\mathcal{G}/\mathcal{H}$. Contrary to the SMEFT, χPT does not organize the expansion in inverse powers of a large scale, rather as counting of derivatives, i.e. in powers of the momentum. In the case of QCD confinement, χPT is extremely important as the symmetry breaking is non perturbative. The pions are described within χPT identifying

$$\mathcal{G} = SU(2)_L \times SU(2)_R\,, \qquad\qquad \mathcal{H} = SU(2)_V\,. \tag{2.79}$$

We will now show how to build the χPT Lagrangian for the pions. The extension of such a tool to different global symmetries follows the same procedure. Similarly to the $U(1)_X$ case, the symmetry breaking transforms $\mathcal{G}$ into a shift for the pNGBs. The $\mathcal{H}$ structure is needed to parametrize the pNGBs correctly. This allows one to consider

$$U \equiv \exp\left[i \frac{\pi^a \sigma^a}{f_\pi} \right] \left(= \exp\left[\begin{pmatrix} i & \pi^0 & \sqrt{2}\pi^- \\ f_\pi & \sqrt{2}\pi^+ & -\pi^0 \end{pmatrix} \right] \right. , \tag{2.80}$$

where we defined $\pi^\pm = (\pi^1 \pm \pi^2)/\sqrt{2}$. Under $SU(2)_L \times SU(2)_R$, we can define the field to transforms as

$$U \to U_L U U_R^\dagger \,. \tag{2.81}$$

Furthermore, as $UU^\dagger = 1$, U must always enter with a derivative. The most general non-redundant Lagrangian that can be built out of invariant operators reads

$$\begin{aligned}\mathcal{L}_\chi = &\frac{f_\pi^2}{4}\,\mathrm{tr}\left[(D^\mu U)^\dagger (D_\mu U)\right] + L_1\,\mathrm{tr}\left[(D^\mu U)^\dagger (D_\mu U)\right]^2 \\ &+ L_2\,\mathrm{tr}\left[(D^\mu U)^\dagger (D_\nu U)\right]\mathrm{tr}\left[(D^\nu U)^\dagger (D_\mu U)\right] + L_3\,\mathrm{tr}\left[(D^\mu U)^\dagger (D_\nu U)\right] + \dots \,.\end{aligned} \tag{2.82}$$

The coefficients L_i as well as the decay constant f_π must be determined experimentally. If this was the end of the story, the pions would be massless. As we know there is an explicit breaking in the UV. This can be taken into account by adding an explicit breaking which must encode the UV one, thus proportional to the quarks masses

$$\mathcal{L}_\chi^{\text{breaking}} = -B\frac{f_\pi^2}{2}\,\mathrm{tr}\left[U M_q^\dagger + M_q U^\dagger\right], \tag{2.83}$$

which reproduces the pion masses of Eq. (2.78) for $B = \Lambda_{\text{QCD}}^3/f_\pi^2$.

2.2.1.5. SM pGB from anomalous breaking: the η'

We know that there are three generations of quarks in nature, so we might expect more pNGBs than the three pions discussed previously. The third quark family has masses larger than Λ_{QCD}, which introduces subtleties in estimating the pGB masses (in fact, it starts becoming meaningless to use this name to begin with given the size of breaking). We will focus on the case with the three lightest quarks, (u, d, s). The discussion follows the same lines as the one for the pions case. The kinetic terms of Eq. (2.75) are invariant under

$$U(3)_L \times U(3)_R = U(1)_L \times U(1)_R \times SU(3)_L \times SU(3)_R \,. \tag{2.84}$$

We discussed previously that QCD-confinement breaks $SU(2)_L \times SU(2)_R \to SU(2)_V$ generating three pions. The breaking of $SU(3)_L \times SU(3)_R \to SU(3)_V$ generates eight pNGBs, which experimentally can be identified with the three pions ($\pi^{0,\pm}$, $m_\pi \sim 140$ MeV), four Kaons ($K^0, \overline{K^0}, K^\pm$, $m_K \sim 500$ MeV) and the Eta (η, $m_\eta \sim 550$ MeV): all these mesons have masses of the same order of magnitude around Λ_{QCD}. The same fate applies to $U(1)_L \times U(1)_R \to U(1)_V$. Following the group-theoretical structure and χPT, one would thus expect, according to the NGB theorem, the presence of another scalar with similar mass, the so-called η'. Such a

particle would need $m_{\eta'} < \sqrt{3} m_{\pi^0}$ [89], but instead the η' is found to have a much larger mass $m'_\eta \sim 1$ GeV. This mismatch was historically called the *missing meson problem*. The reason is that the axial component of $U(1)_L \times U(1)_R$, $U(1)_A$ is anomalous, exactly as for Baryon and Lepton number discussed in Eq. (1.56). This implies that such a symmetry was broken to begin with, meaning that there is an extra contribution to its mass. The estimation of such a term is highly non-trivial and requires lattice simulations.

In the following sections, we will discuss two notable examples of BSM pNGBs which stem from the SSB of a global $U(1)$: the Majoron and the QCD axion.

2.2.2. The Majoron

Traditionally, the Majoron is the NGB associated with the SSB of $U(1)_{\text{B-L}}$ which also dynamically generates the Majorana mass term for right-handed neutrinos, M_N, of Eq. (2.14) [90]. As the individual breaking of BN and LN is non-perturbative, typically, one mentions only LN when studying the Majoron, so we will do so unless required. The simplest realization amounts to including a SM scalar singlet, ϕ. Being a singlet, the Type-I SS Lagrangian admits the term

$$-\mathcal{L} \supset \frac{1}{2} \phi \overline{N_R^c} Y_\phi N_R \,. \tag{2.85}$$

The Majorana mass term $\overline{N_R^c} N_R$ without the singlet is explicitly LN violating and, in such constructions, is omitted, assuming that LN is a robust symmetry. The Lagrangian admits a $U(1)$ symmetry where the scalar field can now reabsorb the will-be Majorana mass term charges

$$\mathcal{C}(L_L) = \mathcal{C}(N_R) = 1, \qquad \mathcal{C}(\phi) = -2. \tag{2.86}$$

If the scalar singlet gets a vev[7]

$$\phi = \frac{f_a + \rho}{\sqrt{2}} e^{ia/f_a} \,, \tag{2.87}$$

a Majorana mass term for the RH neutrinos is generated

$$M_N \equiv \frac{f_a}{\sqrt{2}} Y_\phi \,, \tag{2.88}$$

[7] Sometimes the Majoron filed is denoted with J rather than a. We keep a to highlight the similarity with the other fields presented in the following sections.

thus breaking LN dynamically. Similarly, as previously discussed, the Majoron is the angular part of the singlet, a. The original Majoron was predicted to be massless.

At tree-level the Majoron interacts solely with neutral leptons. The coupling is proportional to their masses, i.e. very suppressed with SM light neutrinos and much larger with HNLs. Interactions with charged fermions are realized at 1-loop [91, 92, 93] and are thus suppressed, allowing the Majoron to escape bounds and giving it a larger parameter space to live in. For example, generically, the coupling of the Majoron to leptons, ℓ_α reads

$$\mathcal{L}_a \supset \frac{ia}{16\pi^2 f_a}\overline{\ell}\left(m_\ell \,\mathrm{Tr}(K_1)\gamma_5 + 2m_\ell K_2 P_L - 2K_2 m_\ell P_R\right)\ell\,, \tag{2.89}$$

where m_ℓ is the diagonal mass matrix of charged leptons, and $K_{1,2}$ are two model-dependent matrices that encode the mixing structure of the HNLs with the light-neutrinos. Detailed examples of such matrices can be found, for example, in Ref. [93].

The interactions with gauge bosons are also generated starting from 1-loop for couplings to ZZ, γZ and WW. Interactions with $\gamma\gamma$ and gg are generated at two-loops. The explicit computation of both one- and two-loop couplings of the Majoron to gauge-bosons can be found, e.g. in Ref. [92]. Majoron couplings to massive gauge bosons, Z and W,

$$\mathcal{L}_a \supset -\frac{1}{4}g_{aZZ}\frac{a}{f_a}Z^{\mu\nu}\widetilde{Z}_{\mu\nu} - \frac{1}{2}g_{aWW}\frac{a}{f_a}W^{+,\mu\nu}\widetilde{W}^{-}_{\mu\nu} - \frac{1}{4}g_{aZ\gamma}\frac{a}{f_a}Z^{\mu\nu}\widetilde{F}_{\mu\nu}\,, \tag{2.90}$$

are not dictated by anomalous contributions [94]. On the contrary, those to vector-like gauge bosons are anomaly-driven. However, as couplings generated by the anomaly are 1-loop exact, and as the Majoron can only couple to them at 2-loops, it is not possible to match the diagrams to $aF\widetilde{F}$ or $aG\widetilde{G}$. Instead one finds the matching to $\Box a F\widetilde{F}$ or $\Box a G\widetilde{G}$ [92]

$$\mathcal{L}_a \supset -\frac{1}{4}g_{a\gamma\gamma}\frac{\Box a}{v^2 f_a}F^{\mu\nu}\widetilde{F}_{\mu\nu} - \frac{1}{4}g_{agg}\frac{\Box a}{v^2 f_a}G^{\mu\nu}\widetilde{G}_{\mu\nu}\,. \tag{2.91}$$

When the Majoron is taken on-shell, this effectively amounts to trading

$$\Box a F\widetilde{F} \to m_a^2 a F\widetilde{F}\,. \tag{2.92}$$

This implies that if the Majoron is light, the coupling is not only 2-loops suppressed but also gets an extra suppression due to its mass, making it incredibly elusive to many astrophysical bounds.

2.2.3. The QCD Axion

In this section, we present the QCD Axion. We first introduce the main idea and then focus on the two most popular realizations.

The QCD axion was proposed in the late 1970s as a possible solution to the Strong-CP puzzle (see Section 1.2.2.1) [95, 96, 97]. There are multiple ways to understand why the QCD-axion solution works and to create a QCD axion, but the main idea is the following: let us consider a real scalar field, a, equipped with a shift-symmetric Lagrangian, that is

$$\mathcal{L}(a) = \mathcal{L}(a + c), \qquad \forall c \in \mathbf{R}\,. \tag{2.93}$$

Let us also assume that such a field possesses a shift-breaking coupling to $G \wedge \widetilde{G}$ such that the Lagrangian contains

$$\mathcal{L} \supset \frac{g_s^2}{32\pi^2}\left(\overline{\theta} + \frac{a}{f_a}\right) G^{a,\mu\nu}\widetilde{G}^a_{\mu\nu}\,. \tag{2.94}$$

A field with such properties suffices to solve the Strong-CP puzzle, as $\overline{\theta}$ can be made unphysical by redefining

$$a \to a - f_a\overline{\theta}\,, \tag{2.95}$$

which does not affect the rest of the Lagrangian as it is shift-invariant by assumption. A particle with such properties is a QCD axion. This explanation hides a very important loophole: gluonic fields induce non-perturbative effects when QCD confines and could generate a potential for a with $\langle a\rangle \neq 0$, thus reintroducing an effective $\theta_{\text{eff.}}$ spoiling the solution. Indeed, QCD generates a potential for the axion, but remarkably, with a minimum in zero $\langle a\rangle = 0$. This somewhat surprising fact is a consequence of the celebrated Vafa-Witten theorem [98, 99]. Let us consider a vector-like theory, such as QCD; the integral measure of fermion is positive, thus allowing the following relation involving the Euclidean action

$$\begin{aligned} e^{-E(\overline{\theta})} &= \int \mathcal{D}\overline{\psi}\mathcal{D}\psi\mathcal{D}A e^{-S+i\overline{\theta}\int G\wedge\widetilde{G}} = \int \mathcal{D}A \det\left((\not{D}+m)\right) e^{-S_{\text{eff.}}+i\overline{\theta}\int G\wedge\widetilde{G}} \\ &\leq \int \mathcal{D}A \det\left((\not{D}+m)\right) \quad e^{-S_{\text{eff.}}+i\overline{\theta}\int G\wedge\widetilde{G}} = \int \mathcal{D}A \det\left((\not{D}+m)\right) \quad e^{-S_{\text{eff.}}} \\ &= e^{-E(0)}\,, \end{aligned} \tag{2.96}$$

that is, the energy is minimized by a theory with $\overline{\theta} = 0$. Conversely, this implies that if $\overline{\theta}$ were dynamical, the SM itself would relax it to zero. This is simply another way of thinking about why the QCD axion works and ensures that the potential

of a after the field redefinition has a minimum in zero. Indeed, by employing the formalism of χPT, one can show explicitly that after QCD-confinement, the operator in Eq. (2.94) generates the following potential for the axion

$$V(a) = -m_\pi^2 f_\pi^2 \sqrt{1 - \frac{4 m_u m_d}{(m_u + m_d)^2} \sin^2\left(\frac{a}{2 f_a}\right)} \Bigg(\tag{2.97}$$

whose minimum lies in $a = 0$.[8] By expanding the potential, one finds its mass to be

$$m_a^2 = \frac{m_u m_d}{(m_u + m_d)^2} \frac{m_\pi^2 f_\pi^2}{f_a^2} \,. \tag{2.98}$$

The larger the axion f_a decay constant, the smaller its mass becomes. The above relation in the log-(m_a, f_a)-plane corresponds to a straight line, the so-called *QCD-axion canonical band*.

2.2.3.1. The KSVZ and DFSZ QCD Axion Models

So far, we have not mentioned any explicit UV model that could give rise to an axion. The main idea put forward already in the late 1970s [95, 96, 97], consists in introducing an abelian global symmetry $U(1)_{\rm PQ}$, the so-called *Peccei-Quinn symmetry*. If one considers the axion to be part of the angular mode of a complex scalar field, $\phi \propto e^{ia/f_a}$, the presence of $U(1)_{\rm PQ}$ automatically enforces shift-symmetric interactions of a in the Lagrangian, as a global transformation amounts to $a \to a + c$. Finally, shift-breaking interactions with $G \wedge \widetilde{G}$ are induced via the chiral anomaly in QCD background, analogously to the case of the η'. In other words, to have a good QCD Axion from a $U(1)_{\rm PQ}$, one must ensure to couple ϕ to coloured states which transform axially under such a symmetry.

The simplest realizations of QCD Axion are most likely the so-called KSVZ and DFSZ models; for a detailed review see e.g. Ref. [43]. Both models introduce a complex singlet whose angular part plays the role of the axion. To generate the $G \wedge \widetilde{G}$ term, the new singlet must couple to coloured states; to achieve that, the KSVZ introduces new coloured fermions, while DFSZ new scalars. We will discuss them separately.

KSVZ QCD Axion The Kim-Shifman-Vainshtein-Zakharov (KSVZ) model [102, 103] extends the SM spectrum by a new complex singlet and heavy vector-like

[8] The method to compute it is to perform a chiral rotation to shift a from $G \wedge \widetilde{G}$ to the quark mass term $M_q \to M_q(a)$; one can then employ χPT and obtain the axion potential directly from Eq. (2.83). For more details see e.g. Ref. [100].

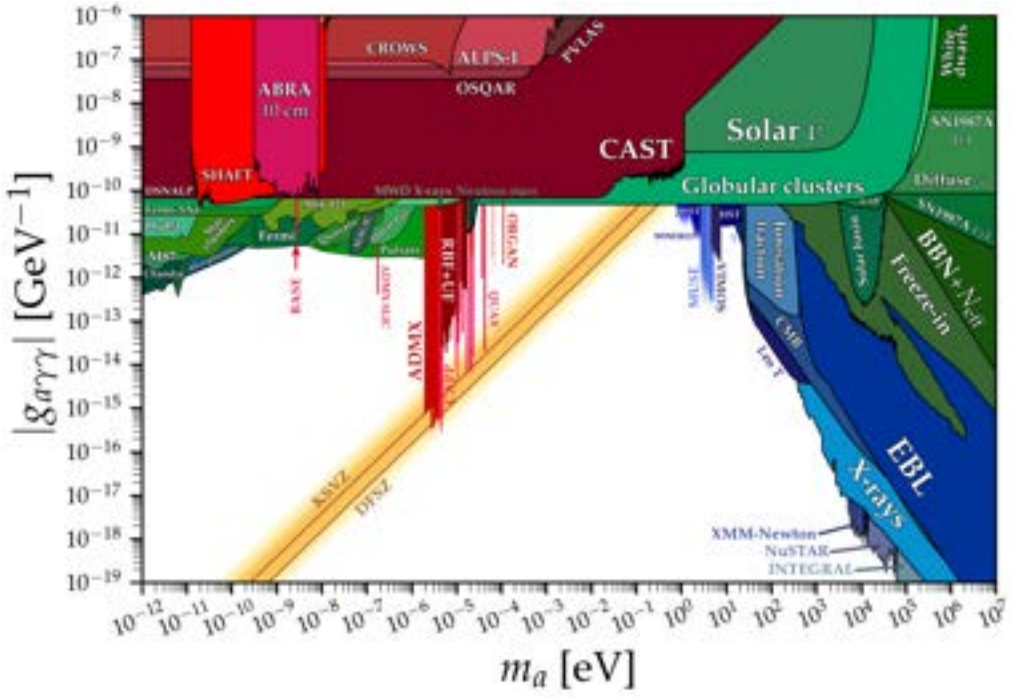

Figure 2.5: Axion (ALP) photon bounds with $\mathcal{L} \supset g_{a\gamma\gamma} a F^{\mu\nu} \widetilde{F}_{\mu\nu}/4$. The QCD axion canonical band is shown in orange. Bounds in green are related to astrophysics and cosmology, blue to DM, and red comprehends various terrestrial experiments. (Image Credit: Ref. [101])

quarks, $\mathcal{Q}_{L,R}$ charged solely under $SU(3)_C$, $\mathcal{Q}_{L,R} = (\mathbf{3}, \mathbf{1}, 0)$. The Lagrangian admits the new operators

$$\mathcal{L}_{\rm KSVZ} = \mathcal{L}_{\rm SM} + \overline{\mathcal{Q}} i \not{D} \mathcal{Q} - y_{\mathcal{Q}} \phi \overline{\mathcal{Q}_L} \mathcal{Q}_R - V(\phi, H), \tag{2.99}$$

where $V(\phi, H)$ is a PQ-preserving potential. The Lagrangian is invariant under the PQ-transformation

$$\phi \to \phi e^{i\alpha}\,, \qquad \mathcal{Q}_R \to \mathcal{Q}_R e^{-i\alpha/2}\,, \qquad \mathcal{Q}_L \to \mathcal{Q}_L e^{+i\alpha/2}\,. \tag{2.100}$$

The symmetry is spontaneously broken by the potential at a scale f_a

$$V(\phi, H) \supset \lambda_\phi |\phi|^2 \left(|\phi|^2 - f_a^2\right)^2\,, \qquad \phi = \frac{f_a + \rho}{\sqrt{2}} e^{ia/f_a}\,. \tag{2.101}$$

The SSB generates masses for the VLL quark and the radial mode, which in the absence of hierarchical couplings, are expected to be found around f_a

$$m_{\mathcal{Q}} = y_{\mathcal{Q}} \frac{f_a}{\sqrt{2}}, \qquad m_\rho^2 = 2\lambda_\phi f_a^2\,. \tag{2.102}$$

As the PQ is exact at the classical level, no tree-level mass for a is generated. The Axion can be rotated away from the $\overline{\mathcal{Q}_L}\mathcal{Q}_R$ term by performing a PQ transformation of $\mathcal{Q}$ as in Eq. (2.100) with $\alpha = a/f_a$, which in turn generates the anomalous term

$$\Delta\mathcal{L}_{\text{KSVZ}} = \frac{a}{f_a}\frac{g_s^2}{32\pi^2}G^{a,\mu\nu}\widetilde{G}^a_{\mu\nu}\,, \tag{2.103}$$

thus realizing the setup described previously (cfr. Section 2.2.3). It is also instructive to follow the fate of the axion coupling with fermions once the rotation is performed. The Axion does not disappear from the Lagrangian, instead, it appears again via the kinetic term of $\mathcal{Q}$

$$\mathcal{L} \supset \overline{\mathcal{Q}}i\not{\partial}\mathcal{Q} \to \overline{\mathcal{Q}}i\not{\partial}\mathcal{Q} + \frac{\partial_\mu a}{2f_a}\left(\overline{\mathcal{Q}}_L\gamma^\mu\mathcal{Q}_L - \overline{\mathcal{Q}}_R\gamma^\mu\mathcal{Q}_R\right), \tag{2.104}$$

which manifests the shift-symmetry of the axion. In this basis, the exponential has been fully reabsorbed in the above dimension-5 operator. The possibility to express the interactions of a with fermions with derivative interactions is the manifestation of the χPT derivative expansion for a $U(1)$ group.

Why not a Majoron? An important observation can be made at this point. One may wonder why we could not simply employ a Majoron to solve the strong-CP problem as it stems from a singlet field ϕ. Performing the appropriate rotation, showing that only derivative interactions appear with fermions, is also possible. However, there is a substantial difference. The 2-loops Feynman diagrams responsible for the Majoron's coupling to gluons match to the operator $\Box a G\widetilde{G}$, not $aG\widetilde{G}$. This has a simple explanation: the anomalous term $G \wedge \widetilde{G}$ is 1-loop exact, therefore it cannot be generated at 2-loops. The interaction $\Box a G\widetilde{G}$ is also shift-preserving, so it cannot reabsorb $\overline{\theta}$. Thus, any scalar that aims to solve the Strong-CP problem must couple directly to coloured fermions.

DFSZ QCD Axion The Dine-Fischler-Srednicki-Zhitnitsky (DSFZ) model [104, 105] is somewhat the counter-part of the KSVZ model. Instead of adding new fermions, besides a complex scalar singlet, the model extends the SM by a second Higgs doublet. We denote the two doublets of the theory as $H_{1,2} = (\mathbf{1}, \mathbf{2}, 1/2)$. The SM Higgs doublet is given by a combination of them. The most generic PQ-preserving potential can be written as

$$V(H_1, H_2, \phi) = \widetilde{V}(H_1, H_2, |\phi|) + H_2^\dagger H_1\left(\mu_{12}\phi + \lambda_{12}\phi^2\right) + \text{h.c.}, \tag{2.105}$$

As before, one assumes the PQ-charge of ϕ to be unity to define the symmetry, $\mathcal{C}(\phi) = 1$. The terms proportional to μ_{12}, λ_{12} cannot appear simultaneously as they would altogether imply an explicit PQ-breaking. Let us, therefore, set for simplicity $\lambda_{12} = 0$. This implies

$$\mathcal{C}(\phi) = 1, \qquad \mathcal{C}(H_2) - \mathcal{C}(H_1) = 1. \tag{2.106}$$

The term μ_{12} induces mixing among the three scalars, such that the axion cannot be identified directly with the angular mode of ϕ, but rather as a combination of ϕ and $H_{1,2}$. Conversely, this implies that both $H_{1,2}$ contain a piece of axion.

Regarding the Yukawa sector, each fermion must also be charged under PQ. Nevertheless, one has to choose the charges to either couple to H_1 or H_2. This freedom leads to four distinct phenomenological models

$$-\mathcal{L}_{\text{Yukawa}} = \overline{Q}_L Y_u \widetilde{H}_1 u_R + \overline{Q}_L Y_d H_{1,2} d_R + \overline{L}_L Y_e H_{1,2} e_R \,, \tag{2.107}$$

where we choose in full generality to fix the doublet of the up sector to be H_1. As the axion is a combination of all three scalars, $H_{1,2}$ indirectly induces direct axion couplings in the Yukawa sector, thus bringing us back to the situation of the KSVZ, but this time with SM quarks. Notice that this implies tree-level coupling with all SM fermions, including leptons; they acquire derivative Axion couplings as in Eq. (2.104). Furthermore, as SM leptons are charged under $U(1)_Y \times SU(2)_L$, chiral rotations induce axion anomalous couplings to gauge bosons. The most notable are the couplings to gluons and photons, defined as

$$\Delta\mathcal{L}_{\text{DFSZ}} \supset \frac{a}{f_a}\frac{N g_s^2}{32\pi^2} G^{a,\mu\nu}\widetilde{G}^a_{\mu\nu} + \frac{a}{f_a}\frac{E e^2}{32\pi^2} F^{\mu\nu}\widetilde{F}_{\mu\nu} \,, \tag{2.108}$$

where E, N are the QCD and electromagnetic anomaly coefficients, respectively; they depend on the specific choice of the model. It is customarily to redefine f_a to keep only the $1/f_a$ dependence in front of the QCD anomaly, $f_a \to N f_a$, such that the Lagrangian is usually written in terms of

$$\Delta\mathcal{L}_{\text{DFSZ}} \supset \frac{a}{f_a}\frac{g_s^2}{32\pi^2} G^{a,\mu\nu}\widetilde{G}^a_{\mu\nu} + \frac{a}{f_a}\frac{e^2}{32\pi^2}\frac{E}{N} F^{\mu\nu}\widetilde{F}_{\mu\nu} \,, \tag{2.109}$$

Such extra coupling to photons can also be generated for the KSVZ model if one assumes $\mathcal{Q}$ to transform under some representation of $U(1)_Y \times SU(2)_L$, beside QCD. Searches for such coupling and relative bunds can be found in Fig. 2.5. As can be seen, the QCD axion band is a straight line in such parameter space.

2.2.3.2. The PQ Quality Problem

One may wonder whether some BSM models could populate the space outside the canonical QCD band. It turns out this is indeed the case, and, in some special constructions, such models can also play the role of QCD axions [106, 107]. In general, pNGBs from $U(1)_{\rm PQ}$ share many properties of a QCD axion and are nowadays therefore referred to as *Axion-Like-Particles* (ALPs) (we will discuss them in the next section). However, typically, their potential (tree-level or loop-generated by the Coleman-Weinberg [108]) is not aligned with the QCD one of the axion, spoiling the position of the minimum and thus not solving the Strong-CP puzzle. The question that naturally arises is how large the potential can be.

To answer the above question, let us consider a potential of the form

$$V = \frac{A}{4}\cos(\omega x + \phi) - c\sqrt{1 - d\sin^2\left(\frac{x}{2}\right)}\,, \tag{2.110}$$

where $c = (m_\pi f_\pi)^2$, $d = 4(m_u m_d)/(m_u + m_d)^2$ and $x = a/f_a$ to match with QCD-axion potential of Eq. (2.97). The strong CP puzzle is solved if the minimum of x respects the experimental condition $x \lesssim 10^{-10}$. One can expand the potential in x and finds the minimum in

$$x_{\rm min.} \approx \frac{A\omega\sin\phi}{cd - A\omega^2\cos\phi} \overset{cd\gg A\omega}{\approx} \frac{A\omega}{cd}\sin\phi\,. \tag{2.111}$$

This implies that for a generic phase ϕ, one should require

$$A^{1/4} \lesssim 10^{-1}\ \text{MeV}, \tag{2.112}$$

as typically $\omega \sim d \sim 1$. Given the natural expectation of $A \sim f_a^4$, the above constraint effectively requires the PQ symmetry to be extremely solid. This is the essence of the so-called *PQ-Quality problem*. In the EFT language, it can be formulated by requiring PQ-violating effects to appear at high order to satisfy the current constraint on $\overline{\theta}$. It turns out that even if one identifies $\Lambda_{\rm UV} = M_{Pl}$ and considers the effective PQ-breaking operator

$$\mathcal{L}_{\rm breaking} \sim \frac{1}{M_{Pl}^{n-4}}\phi^n\,, \tag{2.113}$$

with $\phi \sim f_a e^{ia/f_a}$, one needs to require $n \gtrsim 10$ not to spoil the PQ-solution, thus requiring a more intricate mechanism to protect it [109]. As a rule of thumb, models that violate, even slightly, the PQ cannot solve the Strong-CP puzzle.

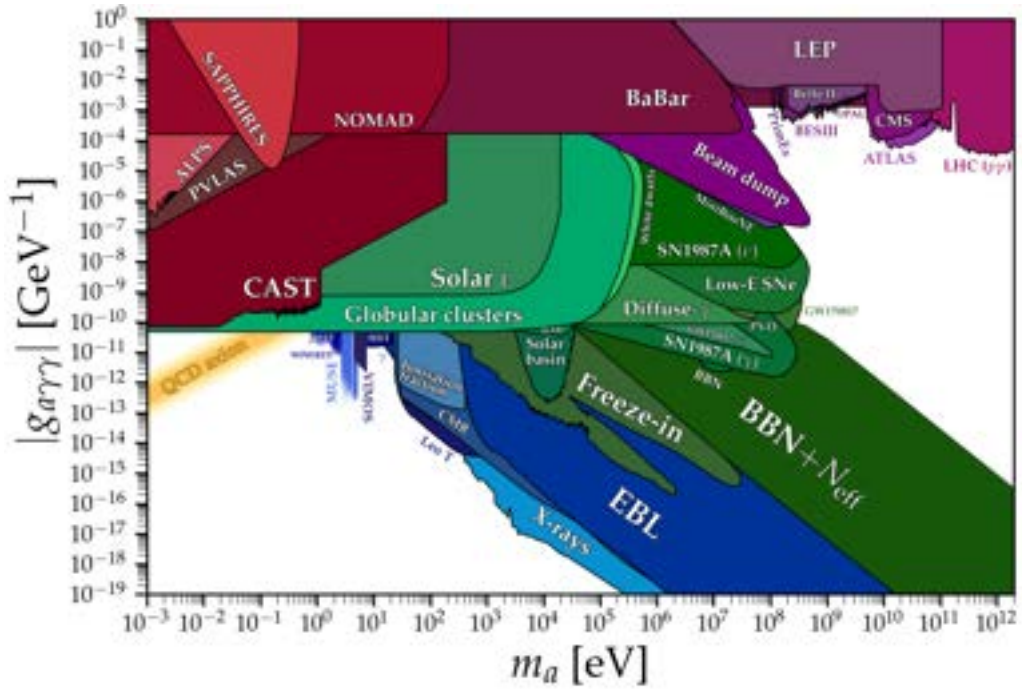

Figure 2.6: ALP photon bounds with $\mathcal{L} \supset g_{a\gamma\gamma} a F^{\mu\nu} \widetilde{F}_{\mu\nu}/4$. Bounds in green are related to astrophysics and cosmology, blue to DM, purple to collider/beam-dump searches, and red comprehends various terrestrial experiments. (Image Credit: Ref. [101])

2.2.4. The ALP EFT

In this section, we describe Axion-Like-Particles (ALPs). An ALP is a real scalar singlet with derivative interactions with fermions and anomalous interactions with gauge bosons. All in all, the ALP EFT [110, 111] describes the effective Lagrangian of a pNGB whose $U(1)$ was broken in the UV either by explicit breaking operators or by anomalies. The ALP Lagrangian shares the same properties as the QCD axion one but with a free mass parameter, which generically implies the impossibility of solving the Strong-CP puzzle. ALPs emerge in very different contexts, e.g. in flavour dynamics [112, 113, 114, 115, 116, 117], neutrino mass generation (Majoron models) [118, 90, 119], composite Higgs models [120, 121, 122], supersymmetry [123] and string theory [124, 125, 126].

2.2.4.1. ALP Lagrangian - Derivative Basis

In its most generic form the ALP Lagrangian, $\mathcal{L}_a$, at dimension-5 reads

$$\mathcal{L}_a = \frac{1}{2}\partial_\mu a \partial^\mu a - \frac{1}{2} m_a^2 a^2 - \frac{\partial_\mu a}{f_a} \sum_\Psi \overline{\Psi'} c'_\Psi \gamma^\mu \Psi' - \frac{1}{4} c_{\widetilde{X}} \frac{a}{f_a} X^{a,\mu\nu} \widetilde{X}^a_{\mu\nu} \,, \tag{2.114}$$

where $\Psi' \in \{Q'_L, L'_L, u'_R, d'_R, e'_R\}$ is a SM fermionic field in the gauge basis, $X \in \{B, W^a, G^a\}$ is a SM gauge field and the Wilson coefficients c'_Ψ are 3×3 Hermitian matrices. If one assumes CP-conserving interactions,[9] as we will do for simplicity, then $c_\psi = c_\psi^T$ implies real fermion couplings. As for the QCD axion, the interactions with fermions are shift-symmetric, while the interactions with gauge bosons are shift-breaking. The derivative structure of the ALP couplings to fermions manifests its structure of pNGB and the SSB from which it stems. After EWSB, the anomalous interactions can be matched to

$$\begin{aligned}\mathcal{L}_a \supset & -\frac{1}{4}c_{a\gamma\gamma}\frac{a}{f_a}F_{\mu\nu}\tilde{F}^{\mu\nu} - \frac{1}{4}c_{a\gamma Z}\frac{a}{f_a}F_{\mu\nu}\tilde{Z}^{\mu\nu} - \frac{1}{4}c_{aZZ}\frac{a}{f_a}Z_{\mu\nu}\tilde{Z}^{\mu\nu} \\ & - \frac{1}{2}c_{aWW}\frac{a}{f_a}W^+_{\mu\nu}\tilde{W}^{-\mu\nu} - \frac{1}{4}c_{agg}\frac{a}{f_a}G^a_{\mu\nu}\tilde{G}^{a\mu\nu}\,.\end{aligned} \tag{2.115}$$

where the matching is given by

$$c_{a\gamma\gamma} \equiv c_w^2 c_{\widetilde{B}} + s_w^2 c_{\widetilde{W}}\,, \quad c_{a\gamma Z} \equiv 2c_s s_w\left(c_{\widetilde{W}} - c_{\widetilde{B}}\right), \quad c_{aZZ} \equiv s_w^2 c_{\widetilde{B}} + c_w^2 c_{\widetilde{W}}\,, \tag{2.116}$$

$$c_{aWW} = c_{\widetilde{W}}\,, \quad c_{agg} = c_{\widetilde{G}}\,, \tag{2.117}$$

where s_w and c_w are the sine and cosine of the Weinberg angle, respectively.

Studies on the impact of 1-loop corrections and running effects on the ALP EFT couplings can be found e.g. in Ref.s [131, 132, 133, 134, 135, 136]

2.2.4.2. ALP Lagrangian - Chirality-Flipping Basis

For phenomenological purposes, it is sometimes convenient to work in the so-called *chirality-flipping* basis. By performing appropriate chiral rotations or using the equation of motion of the fermions and moving to the mass basis, one can write the fermionic part as

$$\mathcal{L}_a^\psi = \frac{ia}{f_a}\sum_{\psi=u,d,e}\sum_{i,j}\left[(m_{\psi_i} - m_{\psi_j})\left(K_\psi^S\right)_{ij}\overline{\psi}_i\,\psi_j + (m_{\psi_i} + m_{\psi_j})\left(K_\psi^P\right)_{ij}\overline{\psi}_i\gamma_5\psi_j\right]\,, \tag{2.118}$$

where m_{ψ_i} denotes the mass of the fermion ψ_i, and the K_ψ matrices defined as combinations of coefficients c'_ψ. In the base in which the down sector masses are diagonal, it follows that

$$K_u^{S,P} \equiv \frac{c_u \pm V_{\rm CKM} c_Q V_{\rm CKM}^\dagger}{2}\,, \qquad K_d^{S,P} \equiv \frac{c_d \pm c_Q}{2}\,, \qquad K_e^{S,P} \equiv \frac{c_e \pm c_L}{2}\,, \tag{2.119}$$

[9] For studies on CP-violating ALPs see e.g. Ref.s [127, 128, 129, 130].

where we have defined

$$\begin{gathered} U_{u_R}^\dagger c'_u U_{u_R} \equiv c_u\,, \qquad U_{d_R}^\dagger c'_d U_{d_R} \equiv c_d\,, \qquad U_{e_R}^\dagger c'_e U_{e_R} \equiv c_e\,, \\ U_{d_L}^\dagger c'_Q U_{d_L} \equiv c_Q\,, \qquad U_{e_L}^\dagger c'_L U_{e_L} \equiv c_L\,. \end{gathered} \tag{2.120}$$

Due to the chiral rotations, the anomalous couplings receive corrections and get redefined, $c_i \to c_i + \Delta c_i$, with

$$\begin{aligned} &\Delta c_{a\gamma\gamma} \equiv c_w^2 K_B + s_w^2 K_W\,, \qquad \Delta c_{a\gamma Z} \equiv 2 c_w s_w \left(K_W - K_B\right), \\ &\Delta c_{aZZ} \equiv s_w^2 K_B + c_w^2 K_W\,, \qquad \Delta c_{a\widetilde{W}} \equiv K_W\,, \qquad \Delta c_{a\widetilde{G}} \equiv K_G\,, \end{aligned} \tag{2.121}$$

where K_X depend on the fermionic ALP couplings, c_Ψ,

$$\begin{aligned} K_B &\equiv \frac{\alpha_{em}}{8\pi c_w^2}\,\mathrm{Tr}\left(\frac{1}{3}c_Q - \frac{8}{3}c_u - \frac{2}{3}c_d + c_L - 2c_e\right), \\ K_W &\equiv \frac{\alpha_{em}}{8\pi s_w^2}\,\mathrm{Tr}\left(3c_Q + c_L\right), \\ K_G &\equiv \frac{\alpha_s}{8\pi}\,\mathrm{Tr}\left(2c_Q - c_u - c_d\right). \end{aligned} \tag{2.122}$$

There are two main consequences from the chirality-flipping interactions of the ALP with fermions of Eq. (2.118):

(i) the coupling of the ALP to fermions is proportional to the fermion masses;

(ii) flavour diagonal couplings to fermions can only be pseudo-scalar (if CP conserving).

Therefore, the heavier the particle, the stronger the effective coupling. This key observation makes a possible ALP-HNL coupling appealing (see Ref. [7]). Finally, couplings to gauge bosons grow with the centre of mass energy of the process.

2.2.4.3. Overview on ALP Constraints

The bounds on ALP couplings strongly depend on the ALP mass itself. A detailed discussion could take an arbitrary number of pages and goes beyond the scope of this introduction; we try instead to give an overview. Astrophysics imposes incredibly strong constraints, which depend on the possibility of producing the ALP on-shell. The qualitative difference can be appreciated from the photon coupling plots of Fig. 2.6. We, therefore, separate the discussion for two macro-ranges with m_a larger/smaller than 100 MeV.

$m_a \lesssim 100$ MeV. Astrophysical constraints strongly bound ALP couplings below $m_a \lesssim 100$ MeV. A detailed description of such bounds is far beyond the scope of

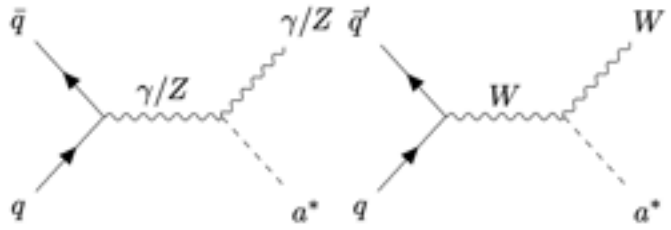

Figure 2.7: Representative set of Feynman diagrams contributing to ALP-production in mono-EW-gauge-boson searches from initial quarks at LHC. Analogous diagrams with gluon's initial and s-channel states can be obtained analogously.

this introduction; a collection of bounds from astrophysics can be found in Ref. [137, 101]. For example, the photon coupling is constrained to be $g_{a\gamma\gamma} \equiv c_{a\gamma\gamma}/f_a \lesssim 10^{-10}$ GeV^{-1}, implying a scale $f_a \gtrsim 10^{10}$ GeV if one assumes $c_{a\gamma\gamma} \sim \mathcal{O}(1)$, as can be seen in Fig. 2.6. The same qualitative features apply to the other coupling, which can couple to particles present in stars, such as electrons and protons/neutrons. Bounds to different flavours of leptons and quarks can be obtained indirectly by loop effects.

$m_a \gtrsim 100$ MeV. In this regime, the constraints on ALP couplings are dominated by collider searches and beam-dump experiments. They can be seen in purple in Fig. 2.6. As a rule of thumb, assuming Wilson coefficients of $\mathcal{O}(1)$, the ALP scale is constrained to be $f_a \gtrsim 1$ TeV. The bound can be made stronger or weaker by a factor of about 10 depending on the specific value of the mass. Given the derivative structure of the ALP to fermions and anomalous couplings, couplings involving light fermions are typically very hard to probe directly. Bounds on such couplings are obtained mainly by considering their 1-loop impact on gauge boson couplings [138, 139, 134, 136]. The coupling of ALPs to gauge bosons is proportional to the process' energy, making it appealing at LHC. The ALP can be produced on-shell via Vector-Boson-Fusion processes and on-shell along with mono-γ, mono-Z, and mono-W emissions. Finally, one can study non-resonant searches [140]. The corresponding diagrams can be seen in Fig. 2.7. Finally, strong bounds can be obtained considering running effects and flavour observables in different facilities [141, 142, 143, 144, 135, 145].

Bibliography

[1] J. Alonso-Gonzalez, A. de Giorgi, L. Merlo, and S. Pokorski, *Searching for BSM physics in Yukawa couplings and flavour symmetries*, JHEP **05** (2022) 041, [arXiv:2109.07490].

[2] A. de Giorgi and S. Vogl, *Warm dark matter from a gravitational freeze-in in extra dimensions*, JHEP **04** (2023) 032, [arXiv:2208.03153].

[3] J. Bonilla, A. de Giorgi, B. Gavela, L. Merlo, and M. Ramos, *The cost of an ALP solution to the neutral B-anomalies*, JHEP **02** (2023) 138, [arXiv:2209.11247].

[4] A. de Giorgi, L. Merlo, and S. Pokorski, *The Low-Scale Seesaw Solution to the M_W and $(g-2)\mu$ Anomalies*, Fortsch. Phys. **71** (2023), no. 4-5 2300020, [arXiv:2211.03797].

[5] J. Bonilla, A. de Giorgi, and M. Ramos, *Neutral B-anomalies from an on-shell scalar exchange*, arXiv:2211.05135.

[6] A. de Giorgi and G. Piazza, *A lesson from $R_{\tau\tau}^{K^{(*)}}$ and $R_{\nu\nu}^{K^{(*)}}$ at Belle II*, Fortsch. Phys. **72** (2024), no. 1 2300200, [arXiv:2211.05595].

[7] A. de Giorgi, L. Merlo, and J.-L. Tastet, *Probing HNL-ALP couplings at colliders*, Fortsch. Phys. **71** (2023), no. 4-5 2300027, [arXiv:2212.11290].

[8] A. de Giorgi, F. Koutroulis, L. Merlo, and S. Pokorski, *Flavour and Higgs physics in Z2-symmetric 2HD models near the decoupling limit*, Nucl. Phys. B **994** (2023) 116323, [arXiv:2304.10560].

[9] A. de Giorgi and S. Vogl, *Gravity-matter sum rules in models with a single extra-dimension*, JHEP **05** (2024) 315, [arXiv:2311.01507].

[10] A. de Giorgi, L. Merlo, X. Ponce Díaz, and S. Rigolin, *The minimal massive Majoron Seesaw Model*, JHEP **03** (2024) 094, [arXiv:2312.13417].

[11] A. de Giorgi, M. F. Zamoro, and L. Merlo, *GeV ALP from TeV Vector-like Leptons*, arXiv:2402.14059.

[12] J. C. Romao and J. P. Silva, *A resource for signs and Feynman diagrams of the Standard Model*, Int. J. Mod. Phys. A **27** (2012) 1230025, [arXiv:1209.6213].

[13] C.-N. Yang and R. L. Mills, *Conservation of Isotopic Spin and Isotopic Gauge Invariance*, Phys. Rev. **96** (1954) 191–195.

[14] F. Englert and R. Brout, *Broken Symmetry and the Mass of Gauge Vector Mesons*, Phys. Rev. Lett. **13** (1964) 321–323.

[15] P. W. Higgs, *Broken Symmetries and the Masses of Gauge Bosons*, Phys. Rev. Lett. **13** (1964) 508–509.

[16] G. S. Guralnik, C. R. Hagen, and T. W. B. Kibble, *Global Conservation Laws and Massless Particles*, Phys. Rev. Lett. **13** (1964) 585–587.

[17] **Particle Data Group** Collaboration, R. L. Workman *et. al.*, *Review of Particle Physics*, PTEP **2022** (2022) 083C01.

[18] C. Jarlskog, *Commutator of the Quark Mass Matrices in the Standard Electroweak Model and a Measure of Maximal CP Nonconservation*, Phys. Rev. Lett. **55** (1985) 1039.

[19] S. L. Glashow, J. Iliopoulos, and L. Maiani, *Weak Interactions with Lepton-Hadron Symmetry*, Phys. Rev. D **2** (1970) 1285–1292.

[20] E. Witten, *An SU(2) Anomaly*, Phys. Lett. B **117** (1982) 324–328.

[21] S. L. Adler, *Axial vector vertex in spinor electrodynamics*, Phys. Rev. **177** (1969) 2426–2438.

[22] J. S. Bell and R. Jackiw, *A PCAC puzzle: $\pi^0 \to \gamma\gamma$ in the σ model*, Nuovo Cim. A **60** (1969) 47–61.

[23] K. Fujikawa, *Path Integral Measure for Gauge Invariant Fermion Theories*, Phys. Rev. Lett. **42** (1979) 1195–1198.

[24] G. 't Hooft, *Symmetry Breaking Through Bell-Jackiw Anomalies*, Phys. Rev. Lett. **37** (1976) 8–11.

[25] C. Collaboration, *Cms standard model summary plots*, 2024.

[26] NuFIT, *Three-neutrino fit based on data available in november 2022*, 2022. http://www.nu-fit.org/?q=node/256 [Accessed: 25/03/2024].

[27] B. Pontecorvo, *Inverse beta processes and nonconservation of lepton charge*, Zh. Eksp. Teor. Fiz. **34** (1957) 247.

[28] Z. Maki, M. Nakagawa, and S. Sakata, *Remarks on the unified model of elementary particles*, Prog. Theor. Phys. **28** (1962) 870–880.

[29] B. Pontecorvo, *Neutrino Experiments and the Problem of Conservation of Leptonic Charge*, Zh. Eksp. Teor. Fiz. **53** (1967) 1717–1725.

[30] E. K. Akhmedov and A. Y. Smirnov, *Paradoxes of neutrino oscillations*, Phys. Atom. Nucl. **72** (2009) 1363–1381, [arXiv:0905.1903].

[31] E. Akhmedov and A. Y. Smirnov, *Damping of neutrino oscillations, decoherence and the lengths of neutrino wave packets*, JHEP **11** (2022) 082, [arXiv:2208.03736].

[32] I. Esteban, M. C. Gonzalez-Garcia, M. Maltoni, T. Schwetz, and A. Zhou, *The fate of hints: updated global analysis of three-flavor neutrino oscillations*, JHEP **09** (2020) 178, [arXiv:2007.14792].

[33] P. F. de Salas, D. V. Forero, C. A. Ternes, M. Tortola, and J. W. F. Valle, *Status of neutrino oscillations 2018: 3σ hint for normal mass ordering and improved CP sensitivity*, Phys. Lett. B **782** (2018) 633–640, [arXiv:1708.01186].

[34] P. F. de Salas, D. V. Forero, S. Gariazzo, P. Martínez-Miravé, O. Mena, C. A. Ternes, M. Tórtola, and J. W. F. Valle, *2020 global reassessment of the neutrino oscillation picture*, JHEP **02** (2021) 071, [arXiv:2006.11237].

[35] F. Capozzi, E. Di Valentino, E. Lisi, A. Marrone, A. Melchiorri, and A. Palazzo, *Unfinished fabric of the three neutrino paradigm*, Phys. Rev. D **104** (2021), no. 8 083031, [arXiv:2107.00532].

[36] H. Andernach and F. Zwicky, *English and spanish translation of zwicky's (1933) the redshift of extragalactic nebulae*, 2017.

[37] K. C. Freeman, *On the disks of spiral and SO Galaxies*, Astrophys. J. **160** (1970) 811.

[38] V. C. Rubin and W. K. Ford, Jr., *Rotation of the Andromeda Nebula from a Spectroscopic Survey of Emission Regions*, Astrophys. J. **159** (1970) 379–403.

[39] D. Clowe, M. Bradac, A. H. Gonzalez, M. Markevitch, S. W. Randall, C. Jones, and D. Zaritsky, *A direct empirical proof of the existence of dark matter*, Astrophys. J. Lett. **648** (2006) L109–L113, [astro-ph/0608407].

[40] **Planck** Collaboration, N. Aghanim *et. al.*, *Planck 2018 results. VI. Cosmological parameters*, Astron. Astrophys. **641** (2020) A6, [arXiv:1807.06209]. [Erratum: Astron.Astrophys. 652, C4 (2021)].

[41] K. G. Begeman, A. H. Broeils, and R. H. Sanders, *Extended rotation curves of spiral galaxies: dark haloes and modified dynamics*, Monthly Notices of the Royal Astronomical Society **249** (1991), no. 3 523–537.

[42] A. Hook, *TASI Lectures on the Strong CP Problem and Axions*, PoS **TASI2018** (2019) 004, [arXiv:1812.02669].

[43] L. Di Luzio, M. Giannotti, E. Nardi, and L. Visinelli, *The landscape of QCD axion models*, Phys. Rept. **870** (2020) 1–117, [arXiv:2003.01100].

[44] C. Abel *et. al.*, *Measurement of the Permanent Electric Dipole Moment of the Neutron*, Phys. Rev. Lett. **124** (2020), no. 8 081803, [arXiv:2001.11966].

[45] A. G. Cohen, D. B. Kaplan, and A. E. Nelson, *Testing m(u)=0 on the lattice*, JHEP **11** (1999) 027, [hep-lat/9909091].

[46] M. Dine, P. Draper, and G. Festuccia, *Instanton Effects in Three Flavor QCD*, Phys. Rev. D **92** (2015), no. 5 054004, [arXiv:1410.8505].

[47] A. Bazavov *et. al.*, *B- and D-meson leptonic decay constants from four-flavor lattice QCD*, Phys. Rev. D **98** (2018), no. 7 074512, [arXiv:1712.09262].

[48] **Fermilab Lattice, MILC, TUMQCD** Collaboration, A. Bazavov *et. al.*, *Up-, down-, strange-, charm-, and bottom-quark masses from four-flavor lattice QCD*, Phys. Rev. D **98** (2018), no. 5 054517, [arXiv:1802.04248].

[49] **Flavour Lattice Averaging Group** Collaboration, S. Aoki *et. al.*, *FLAG Review 2019: Flavour Lattice Averaging Group (FLAG)*, Eur. Phys. J. C **80** (2020), no. 2 113, [arXiv:1902.08191].

[50] C. Alexandrou, J. Finkenrath, L. Funcke, K. Jansen, B. Kostrzewa, F. Pittler, and C. Urbach, *Ruling Out the Massless Up-Quark Solution to the Strong **CP** Problem by Computing the Topological Mass Contribution with Lattice QCD*, Phys. Rev. Lett. **125** (2020), no. 23 232001, [arXiv:2002.07802].

[51] J. J. Gomez-Cadenas, J. Martin-Albo, M. Mezzetto, F. Monrabal, and M. Sorel, *The Search for neutrinoless double beta decay*, Riv. Nuovo Cim. **35** (2012), no. 2 29–98, [arXiv:1109.5515].

[52] S. Davidson, E. Nardi, and Y. Nir, *Leptogenesis*, Phys. Rept. **466** (2008) 105–177, [arXiv:0802.2962].

[53] A. D. Sakharov, *Violation of CP Invariance, C asymmetry, and baryon asymmetry of the universe*, Pisma Zh. Eksp. Teor. Fiz. **5** (1967) 32–35.

[54] M. B. Gavela, P. Hernandez, J. Orloff, and O. Pene, *Standard model CP violation and baryon asymmetry*, Mod. Phys. Lett. A **9** (1994) 795–810, [hep-ph/9312215].

[55] P. Huet and E. Sather, *Electroweak baryogenesis and standard model CP violation*, Phys. Rev. D **51** (1995) 379–394, [hep-ph/9404302].

[56] C. N. Leung, S. T. Love, and S. Rao, *Low-energy manifestations of a new interactions scale: Operator analysis*, Zeitschrift für Physik C Particles and Fields **31** (1986), no. 3 433–437.

[57] W. Buchmüller and D. Wyler, *Effective lagrangian analysis of new interactions and flavour conservation*, Nuclear Physics B **268** (1986), no. 3 621–653.

[58] B. Grzadkowski, M. Iskrzynski, M. Misiak, and J. Rosiek, *Dimension-Six Terms in the Standard Model Lagrangian*, JHEP **10** (2010) 085, [arXiv:1008.4884].

[59] S. Centelles Chuliá, A. Herrero-Brocal, and A. Vicente, *The Type-I Seesaw family*, arXiv:2404.15415.

[60] S. Antusch, O. Fischer, A. Hammad, and C. Scherb, *Low scale type II seesaw: Present constraints and prospects for displaced vertex searches*, JHEP **02** (2019) 157, [arXiv:1811.03476].

[61] C. Biggio, E. Fernandez-Martinez, M. Filaci, J. Hernandez-Garcia, and J. Lopez-Pavon, *Global Bounds on the Type-III Seesaw*, JHEP **05** (2020) 022, [arXiv:1911.11790].

[62] M. B. Gavela, T. Hambye, D. Hernandez, and P. Hernandez, *Minimal Flavour Seesaw Models*, JHEP **09** (2009) 038, [arXiv:0906.1461].

[63] A. Abada, C. Biggio, F. Bonnet, M. B. Gavela, and T. Hambye, *Low energy effects of neutrino masses*, JHEP **12** (2007) 061, [arXiv:0707.4058].

[64] **CMS** Collaboration, V. Khachatryan *et. al.*, *Search for heavy Majorana neutrinos in $\mu^{\pm}\mu^{\pm}$+ jets events in proton-proton collisions at $\sqrt{s}$ = 8 TeV*, Phys. Lett. B **748** (2015) 144–166, [arXiv:1501.05566].

[65] **ATLAS** Collaboration, G. Aad *et. al.*, *Search for heavy Majorana neutrinos with the ATLAS detector in pp collisions at $\sqrt{s} = 8$ TeV*, JHEP **07** (2015) 162, [arXiv:1506.06020].

[66] **CMS** Collaboration, V. Khachatryan *et. al.*, *Search for heavy Majorana neutrinos in ee+ jets and $e\,\mu$+ jets events in proton-proton collisions at $\sqrt{s} = 8$ TeV*, JHEP **04** (2016) 169, [arXiv:1603.02248].

[67] **CMS** Collaboration, A. M. Sirunyan *et. al.*, *Search for heavy Majorana neutrinos in same-sign dilepton channels in proton-proton collisions at $\sqrt{s} = 13$ TeV*, JHEP **01** (2019) 122, [arXiv:1806.10905].

[68] **CMS** Collaboration, A. M. Sirunyan *et. al.*, *Search for heavy neutral leptons in events with three charged leptons in proton-proton collisions at* $\sqrt{s} = 13$ *TeV*, Phys. Rev. Lett. **120** (2018), no. 22 221801, [arXiv:1802.02965].

[69] **CMS** Collaboration, A. Hayrapetyan *et. al.*, *Search for heavy neutral leptons in final states with electrons, muons, and hadronically decaying tau leptons in proton-proton collisions at* $\sqrt{s}$ *=13 TeV*, arXiv:2403.00100.

[70] **CMS** Collaboration, A. Tumasyan *et. al.*, *Probing Heavy Majorana Neutrinos and the Weinberg Operator through Vector Boson Fusion Processes in Proton-Proton Collisions at s=13 TeV*, Phys. Rev. Lett. **131** (2023), no. 1 011803, [arXiv:2206.08956].

[71] E. Fernandez-Martinez, J. Hernandez-Garcia, and J. Lopez-Pavon, *Global constraints on heavy neutrino mixing*, JHEP **08** (2016) 033, [arXiv:1605.08774].

[72] **DELPHI** Collaboration, P. Abreu *et. al.*, *Search for neutral heavy leptons produced in Z decays*, Z. Phys. C **74** (1997) 57–71. [Erratum: Z.Phys.C 75, 580 (1997)].

[73] A. Abada, P. Escribano, X. Marcano, and G. Piazza, *Collider searches for heavy neutral leptons: beyond simplified scenarios*, Eur. Phys. J. C **82** (2022), no. 11 1030, [arXiv:2208.13882].

[74] E. Fernandez-Martinez, M. B. Gavela, J. Lopez-Pavon, and O. Yasuda, *CP-violation from non-unitary leptonic mixing*, Phys. Lett. B **649** (2007) 427–435, [hep-ph/0703098].

[75] **CMS** Collaboration, V. Khachatryan *et. al.*, *Search for Lepton-Flavour-Violating Decays of the Higgs Boson*, Phys. Lett. B **749** (2015) 337–362, [arXiv:1502.07400].

[76] **CMS** Collaboration, A. M. Sirunyan *et. al.*, *Search for lepton-flavor violating decays of the Higgs boson in the* $\mu\tau$ *and* $e\tau$ *final states in proton-proton collisions at* $\sqrt{s} = 13$ *TeV*, Phys. Rev. D **104** (2021), no. 3 032013, [arXiv:2105.03007].

[77] **CMS** Collaboration, A. Hayrapetyan *et. al.*, *Search for the lepton-flavor violating decay of the Higgs boson and additional Higgs bosons in the* $e\mu$ *final state in proton-proton collisions at* $\sqrt{s} = 13$ *TeV*, Phys. Rev. D **108** (2023), no. 7 072004, [arXiv:2305.18106].

[78] **ATLAS** Collaboration, G. Aad *et. al.*, *Search for the lepton flavor violating decay* $Z \to e\mu$ *in pp collisions at* $\sqrt{s}$ *TeV with the ATLAS detector*, Phys. Rev. D **90** (2014), no. 7 072010, [arXiv:1408.5774].

[79] **ATLAS** Collaboration, G. Aad *et. al.*, *Search for charged-lepton-flavour violation in Z-boson decays with the ATLAS detector*, Nature Phys. **17** (2021), no. 7 819–825, [arXiv:2010.02566].

[80] **ATLAS** Collaboration, G. Aad *et. al.*, *Search for the charged-lepton-flavor-violating decay* $Z \to e\mu$ *in pp collisions at* $\sqrt{s} = 13$ *TeV with the ATLAS detector*, Phys. Rev. D **108** (2023) 032015, [arXiv:2204.10783].

[81] K. Hayasaka *et. al.*, *Search for Lepton Flavor Violating Tau Decays into Three Leptons with 719 Million Produced Tau+Tau- Pairs*, Phys. Lett. B **687** (2010) 139–143, [arXiv:1001.3221].

[82] **SINDRUM II** Collaboration, C. Dohmen *et. al.*, *Test of lepton flavor conservation in mu —> e conversion on titanium*, Phys. Lett. B **317** (1993) 631–636.

[83] **SINDRUM II** Collaboration, W. Honecker *et. al.*, *Improved limit on the branching ratio of mu —> e conversion on lead*, Phys. Rev. Lett. **76** (1996) 200–203.

[84] **SINDRUM II** Collaboration, W. H. Bertl *et. al.*, *A Search for muon to electron conversion in muonic gold*, Eur. Phys. J. C **47** (2006) 337–346.

[85] T. Appelquist and J. Carazzone, *Infrared Singularities and Massive Fields*, Phys. Rev. D **11** (1975) 2856.

[86] Y. Nambu, *Quasi-particles and gauge invariance in the theory of superconductivity*, Phys. Rev. **117** (Feb, 1960) 648–663.

[87] J. Goldstone, *Field Theories with Superconductor Solutions*, Nuovo Cim. **19** (1961) 154–164.

[88] M. D. Schwartz, *Quantum Field Theory and the Standard Model*. Cambridge University Press, 2013.

[89] S. Weinberg, *The U(1) Problem*, Phys. Rev. D **11** (1975) 3583–3593.

[90] Y. Chikashige, R. N. Mohapatra, and R. D. Peccei, *Are There Real Goldstone Bosons Associated with Broken Lepton Number?*, Phys. Lett. B **98** (1981) 265–268.

[91] C. Garcia-Cely and J. Heeck, *Neutrino Lines from Majoron Dark Matter*, JHEP **05** (2017) 102, [arXiv:1701.07209].

[92] J. Heeck and H. H. Patel, *Majoron at two loops*, Phys. Rev. D **100** (2019), no. 9 095015, [arXiv:1909.02029].

[93] A. Herrero-Brocal and A. Vicente, *The majoron coupling to charged leptons*, JHEP **01** (2024) 078, [arXiv:2311.10145].

[94] J. Quevillon and C. Smith, *Axions are blind to anomalies*, Eur. Phys. J. C **79** (2019), no. 10 822, [arXiv:1903.12559].

[95] R. D. Peccei and H. R. Quinn, *CP Conservation in the Presence of Instantons*, Phys. Rev. Lett. **38** (1977) 1440–1443.

[96] S. Weinberg, *A New Light Boson?*, Phys. Rev. Lett. **40** (1978) 223–226.

[97] F. Wilczek, *Problem of Strong P and T Invariance in the Presence of Instantons*, Phys. Rev. Lett. **40** (1978) 279–282.

[98] C. Vafa and E. Witten, *Restrictions on Symmetry Breaking in Vector-Like Gauge Theories*, Nucl. Phys. B **234** (1984) 173–188.

[99] C. Vafa and E. Witten, *Parity conservation in quantum chromodynamics*, Phys. Rev. Lett. **53** (Aug, 1984) 535–536.

[100] G. Grilli di Cortona, E. Hardy, J. Pardo Vega, and G. Villadoro, *The QCD axion, precisely*, JHEP **01** (2016) 034, [arXiv:1511.02867].

[101] C. O'Hare, "cajohare/axionlimits: Axionlimits." https://cajohare.github.io/AxionLimits/, July, 2020.

[102] J. E. Kim, *Weak Interaction Singlet and Strong CP Invariance*, Phys. Rev. Lett. **43** (1979) 103.

[103] M. A. Shifman, A. I. Vainshtein, and V. I. Zakharov, *Can Confinement Ensure Natural CP Invariance of Strong Interactions?*, Nucl. Phys. B **166** (1980) 493–506.

[104] A. R. Zhitnitsky, *On Possible Suppression of the Axion Hadron Interactions. (In Russian)*, Sov. J. Nucl. Phys. **31** (1980) 260.

[105] M. Dine, W. Fischler, and M. Srednicki, *A Simple Solution to the Strong CP Problem with a Harmless Axion*, Phys. Lett. B **104** (1981) 199–202.

[106] L. Di Luzio, B. Gavela, P. Quilez, and A. Ringwald, *An even lighter QCD axion*, JHEP **05** (2021) 184, [arXiv:2102.00012].

[107] B. Gavela, P. Quílez, and M. Ramos, *The QCD axion sum rule*, JHEP **04** (2024) 056, [arXiv:2305.15465].

[108] S. R. Coleman and E. J. Weinberg, *Radiative Corrections as the Origin of Spontaneous Symmetry Breaking*, Phys. Rev. D **7** (1973) 1888–1910.

[109] M. Dine, *The Problem of Axion Quality: A Low Energy Effective Action Perspective*, arXiv:2207.01068.

[110] H. Georgi, D. B. Kaplan, and L. Randall, *Manifesting the Invisible Axion at Low-energies*, Phys. Lett. B **169** (1986) 73–78.

[111] K. Choi, K. Kang, and J. E. Kim, *Effects of η' in Low-energy Axion Physics*, Phys. Lett. B **181** (1986) 145–149.

[112] A. Davidson and K. C. Wali, *MINIMAL FLAVOR UNIFICATION VIA MULTIGENERATIONAL PECCEI-QUINN SYMMETRY*, Phys. Rev. Lett. **48** (1982) 11.

[113] F. Wilczek, *Axions and Family Symmetry Breaking*, Phys. Rev. Lett. **49** (1982) 1549–1552.

[114] L. Calibbi, F. Goertz, D. Redigolo, R. Ziegler, and J. Zupan, *Minimal axion model from flavor*, Phys. Rev. D **95** (2017), no. 9 095009, [arXiv:1612.08040].

[115] F. Arias-Aragon and L. Merlo, *The Minimal Flavour Violating Axion*, JHEP **10** (2017) 168, [arXiv:1709.07039]. [Erratum: JHEP 11, 152 (2019)].

[116] F. Arias-Aragón, E. Fernández-Martínez, M. González-López, and L. Merlo, *Dynamical Minimal Flavour Violating inverse seesaw*, JHEP **09** (2022) 210, [arXiv:2204.04672].

[117] L. Di Luzio, A. W. M. Guerrera, X. P. Díaz, and S. Rigolin, *On the IR/UV flavour connection in non-universal axion models*, JHEP **06** (2023) 046, [arXiv:2304.04643].

[118] Y. Chikashige, R. N. Mohapatra, and R. D. Peccei, *Spontaneously Broken Lepton Number and Cosmological Constraints on the Neutrino Mass Spectrum*, Phys. Rev. Lett. **45** (1980) 1926.

[119] G. B. Gelmini and M. Roncadelli, *Left-Handed Neutrino Mass Scale and Spontaneously Broken Lepton Number*, Phys. Lett. B **99** (1981) 411–415.

[120] L. Merlo, F. Pobbe, and S. Rigolin, *The Minimal Axion Minimal Linear σ Model*, Eur. Phys. J. C **78** (2018), no. 5 415, [arXiv:1710.10500]. [Erratum: Eur.Phys.J.C 79, 963 (2019)].

[121] I. Brivio, M. B. Gavela, S. Pascoli, R. del Rey, and S. Saa, *The axion and the Goldstone Higgs*, Chin. J. Phys. **61** (2019) 55–71, [arXiv:1710.07715].

[122] J. Alonso-Gonzalez, J. M. Lizana, V. Martinez-Fernandez, L. Merlo, and S. Pokorski, *Probing effective field theory approach in the CP violating minimal linear σ model*, Eur. Phys. J. C **81** (2021), no. 6 538, [arXiv:2012.03990].

[123] B. Bellazzini, A. Mariotti, D. Redigolo, F. Sala, and J. Serra, *R-axion at colliders*, Phys. Rev. Lett. **119** (2017), no. 14 141804, [arXiv:1702.02152].

[124] E. Witten, *Some Properties of O(32) Superstrings*, Phys. Lett. B **149** (1984) 351–356.

[125] K.-S. Choi, I.-W. Kim, and J. E. Kim, *String compactification, QCD axion and axion-photon-photon coupling*, JHEP **03** (2007) 116, [hep-ph/0612107].

[126] M. Cicoli, M. Goodsell, and A. Ringwald, *The type IIB string axiverse and its low-energy phenomenology*, JHEP **10** (2012) 146, [arXiv:1206.0819].

[127] L. Di Luzio, R. Gröber, and P. Paradisi, *Hunting for CP-violating axionlike particle interactions*, Phys. Rev. D **104** (2021), no. 9 095027, [arXiv:2010.13760].

[128] L. Di Luzio, G. Levati, and P. Paradisi, *The chiral Lagrangian of CP-violating axion-like particles*, JHEP **2024** (2024), no. 02 020, [arXiv:2311.12158].

[129] L. Di Luzio, H. Gisbert, G. Levati, P. Paradisi, and P. Sørensen, *CP-Violating Axions: A Theory Review*, arXiv:2312.17310.

[130] V. Enguita, B. Gavela, B. Grinstein, and P. Quilez, *ALP contribution to the Strong CP problem*, arXiv:2403.12133.

[131] M. Chala, G. Guedes, M. Ramos, and J. Santiago, *Running in the ALPs*, Eur. Phys. J. C **81** (2021), no. 2 181, [arXiv:2012.09017].

[132] M. Bauer, M. Neubert, S. Renner, M. Schnubel, and A. Thamm, *The Low-Energy Effective Theory of Axions and ALPs*, JHEP **04** (2021) 063, [arXiv:2012.12272].

[133] J. Bonilla, I. Brivio, M. B. Gavela, and V. Sanz, *One-loop corrections to ALP couplings*, JHEP **11** (2021) 168, [arXiv:2107.11392].

[134] A. M. Galda, M. Neubert, and S. Renner, *ALP — SMEFT interference*, JHEP **06** (2021) 135, [arXiv:2105.01078].

[135] M. Bauer, M. Neubert, S. Renner, M. Schnubel, and A. Thamm, *Flavor probes of axion-like particles*, JHEP **09** (2022) 056, [arXiv:2110.10698].

[136] J. Bonilla, B. Gavela, and J. Machado-Rodríguez, *Limits on ALP-neutrino couplings from loop-level processes*, Phys. Rev. D **109** (2024), no. 5 055023, [arXiv:2309.15910].

[137] A. Caputo and G. Raffelt, *Astrophysical Axion Bounds: The 2024 Edition*, PoS **COSMICWISPers** (2024) 041, [arXiv:2401.13728].

[138] G. Alonso-Álvarez, M. B. Gavela, and P. Quilez, *Axion couplings to electroweak gauge bosons*, Eur. Phys. J. C **79** (2019), no. 3 223, [arXiv:1811.05466].

[139] F. Ertas and F. Kahlhoefer, *On the interplay between astrophysical and laboratory probes of MeV-scale axion-like particles*, JHEP **07** (2020) 050, [arXiv:2004.01193].

[140] J. Bonilla, I. Brivio, J. Machado-Rodríguez, and J. F. de Trocóniz, *Nonresonant searches for axion-like particles in vector boson scattering processes at the LHC*, JHEP **06** (2022) 113, [arXiv:2202.03450].

[141] E. Izaguirre, T. Lin, and B. Shuve, *Searching for Axionlike Particles in Flavor-Changing Neutral Current Processes*, Phys. Rev. Lett. **118** (2017), no. 11 111802, [arXiv:1611.09355].

[142] M. Bauer, M. Neubert, and A. Thamm, *Collider Probes of Axion-Like Particles*, JHEP **12** (2017) 044, [arXiv:1708.00443].

[143] M. B. Gavela, R. Houtz, P. Quilez, R. Del Rey, and O. Sumensari, *Flavor constraints on electroweak ALP couplings*, Eur. Phys. J. C **79** (2019), no. 5 369, [arXiv:1901.02031].

[144] S. Gori, G. Perez, and K. Tobioka, *KOTO vs. NA62 Dark Scalar Searches*, JHEP **08** (2020) 110, [arXiv:2005.05170].

[145] L. Di Luzio, A. W. M. Guerrera, X. Ponce Díaz, and S. Rigolin, *Axion-Like Particles in Radiative Quarkonia Decays*, arXiv:2402.12454.

Chapter 3

Papers of this Thesis

3.1. A Small Introduction to the Papers

Ariadne's thread of the papers presented in this compendium explores theoretical and phenomenological aspects of ALP-HNLs couplings. This path naturally emerged as one of the research topics during my PhD studies.

The opening work, *The Low-Scale Seesaw Solution to the M_W and $(g-2)_\mu$ Anomalies* (3.2), is purely related to the phenomenology of HNLs. This is a fertile ground for studying BSM as it provides a convincing explanation for the smallness of neutrino masses. The modification of the coupling of the muon to gauge bosons induced by the HNLs affects several observables, which makes it compatible with some pressing old and new experimental anomalies: the $(g-2)_\mu$ and M_W. If taken seriously, the parameter space of the theory has to be greatly reduced, yielding very predictive BSM scenarios.

The work, *GeV ALP from TeV Vector-like Leptons* (3.3), directly builds upon the previous one. If some of the mass-scales of the HNLs are generated dynamically, one naturally obtains an ALP from the model. We then have a meaningful scenario to test the properties of ALPs. The model naturally features an explicit PQ breaking, giving the ALP a preferred and natural range of masses. The ALP coupling to fermions is severely affected by the nature of the explicit breaking of the PQ, making the work a case study of ALPs EFT with explicit shift-symmetry breaking.

The two previous works studied the parameter space of an ALP in an LSS. The radiative ALP mass showed a generic proportionality to $v^2 f_a^2$, which is expected to be a fairly common feature of BSM models with HNLs. One may wonder if a more constrained scenario existed or if some models are special concerning others. The question is explored in *The Minimal Massive Majoron Seesaw Model* (3.4).

Remarkably, only a single model can naturally relate the radiative contribution to the ALP and neutrino masses in a one-to-one correspondence. The peculiar relation between the two identifies a preferred and unique region in the parameter space.

Finally, while all previous work directly looks at UV models and their consequences, one may wonder which conclusions can be drawn from an EFT approach. Given that in SS mechanisms, the HNLs must be "heavy", and the coupling of an ALP to fermions is proportional to their masses, the mutual existence of such particles would be mutually beneficial for their discoveries. The search for a signal-topology at collider which could fulfil this hope is explored in *Probing HNL-ALP Couplings at Colliders* (3.5). Indeed, the unique characteristics of the HNLs allow signals that are greatly suppressed in the pure SM case, allowing to probe down to the SS scenario even in cases in which the mixing was too small. A generalisation of such work to include bounds of other SM couplings is on the edge of completion at the time of writing.

RESEARCH ARTICLE

Fortschritte der Physik Progress of Physics

www.fp-journal.org

The Low-Scale Seesaw Solution to the M_W and $(g-2)_\mu$ Anomalies

Arturo de Giorgi, Luca Merlo, and Stefan Pokorski*

The recent CDF-II measurement of the *W*-boson mass shows a strong tension with the corresponding Standard Model prediction. Once active neutrino masses are explained in the context of the Low-Scale Seesaw mechanisms, this tension can be resolved. We investigate the possibility of explaining the longstanding muon anomalous magnetic moment anomaly within the same frameworks. We present a simplified extension of the Standard Model, accounting only for the second lepton generation, that describes a massive active neutrino and provides a combined solution to these anomalies. The model is renormalisable and introduces in the spectrum, beyond the sterile species of the Low-Scale Seesaw mechanism, only one pair of exotic vector-like leptons, doublets under the electroweak symmetry. We moreover discuss the extension of this model to the realistic three-family case.

1. Introduction

Among the scientific achievements in particle physics of the last century, the formulation of the Standard Model (SM) is one of the most relevant results. Its success culminated with the discovery of the Higgs boson in 2012 at the Large Hadron Collider[1,2] and there has not been evidence of the existence of any other new particle till nowadays.

On the other hand, the SM cannot be considered the ultimate theory of Nature. It is lacking a mechanism for the neutrino mass generation, does not explain the baryon asymmetry of the Universe and the existence of Dark Matter, and leaves aside the gravitational interactions. Moreover, several tensions are present between the SM predictions and the corresponding experimental determinations. One of the latest anomalies is associated with the mass of the W gauge boson, M_W, that has been recently measured by the CDF II collaboration[3] with the best-achieved sensitivity,

$$M_W = 80.4335 \pm 0.0094 \text{ GeV}\,, \tag{1.1}$$

showing a 7σ discrepancy relative to the SM prediction.[1]

Among the numerous proposals to explain such a tension, the class of the so-called Low-Scale Seesaw (SS) mechanisms[4,5] represents a very appealing possibility,[6,7] as it also provides a description for massive neutrinos. In the generic model of this type, two kinds of exotic neutral leptons, N_R and S_R in the following, with opposite lepton numbers, are added to the SM spectrum. The number of the exotic neutral leptons of each type depends on the specific realisation: for example, in Ref. [7], three N_R and three S_R have been considered in the exotic spectrum. In general, for an arbitrary number of N_R and of S_R, it is convenient to adopt a compact notation for all the neutral leptons, SM and exotic, defining a multidimensional vector in the flavour space[1]

$$\chi \equiv (\nu_L,\, N_R^c,\, S_R^c)^T\,, \tag{1.2}$$

where ν_L stands for the neutral component of the EW lepton doublet ℓ_L. The characteristic mass term for the Low-Scale SS setup reads

$$-\mathscr{L}_Y \supset \frac{1}{2}\overline{\chi}\mathcal{M}_\chi\chi^c + \text{h.c.}\,, \tag{1.3}$$

with

$$\mathcal{M}_\chi = \begin{pmatrix} 0 & \frac{v}{\sqrt{2}}Y_N & \epsilon\frac{v}{\sqrt{2}}Y_S \\ \frac{v}{\sqrt{2}}Y_N^T & \mu' & \Lambda \\ \epsilon\frac{v}{\sqrt{2}}Y_S^T & \Lambda^T & \mu \end{pmatrix}, \tag{1.4}$$

where $v = 246$ GeV is the Higgs doublet H vacuum expectation value (VEV), Y_N and Y_S are the Dirac Yukawa matrices that couple

A. de Giorgi, L. Merlo
Departamento de Física Teórica and Instituto de Física Teórica
UAM/CSIC
Universidad Autónoma de Madrid
Cantoblanco, Madrid Spain
E-mail: arturo.degiorgi@uam.es
S. Pokorski
Institute of Theoretical Physics
Faculty of Physics
University of Warsaw
Warsaw Poland

DOI: 10.1002/prop.202300020

[1] The CDF II measurement is by far the most precise one over the nine different determinations. As reported in Ref. [3], neglecting the possible correlations, one could estimate the average among them obtaining $M_W = 80.4242 \pm 0.0087$ GeV, that is only 1σ far from the CDF II result, as expected. For this reason, we will perform our analysis considering the value in Equation (1.1), understanding that the conclusions would remain invariant using instead the average quantity.

ℓ_L to N_R and S_R respectively, while Λ, μ and μ' are matrices in the flavour space of N_R and S_R, and finally ϵ is a real parameter.

If lepton number conservation is taken as an exact symmetry, then the terms corresponding to μ, μ' and ϵ are forbidden in the Lagrangian and then the neutrinos would remain massless. Allowing, however, for an explicit soft violation of the lepton number conservation, that is for non-zero values of the parameters μ, μ' and ϵ (or some of them) and with Λ dominating the other entries, the light neutrino mass matrix at tree-level reads

$$m_\nu \simeq \frac{v^2}{2}\left[\left(Y_N \frac{1}{\Lambda^T}\mu\frac{1}{\Lambda}Y_N^T\right) - \epsilon\left(Y_S\frac{1}{\Lambda}Y_N^T + Y_N\frac{1}{\Lambda^T}Y_S^T\right)\right]. \tag{1.5}$$

Notice that μ' does not contribute to the neutrino masses at this expansion order. Depending on which contribution dominates, a different name is used in the literature to refer to the specific SS mechanism: "Inverse (ISS)"[8–10] if the first term in Equation (1.5) is mainly responsible for the neutrino masses; "Linear (LSS)"[11] otherwise.

In order to reproduce the atmospheric mass splitting $|\Delta m^2_{\rm atm}| \sim 2.5\times10^{-3}$ eV^2,[12] assuming $\Lambda \sim \mathcal{O}$(TeV) and the Yukawa matrices with entries of $\mathcal{O}(1)$, we can estimate the values for μ and ϵ: $\mu \sim$ KeV in the ISS and $\epsilon \sim 10^{-10}$ in the LSS. This is the first interesting feature of these Low-Scale mechanisms: the masses of the light neutrinos are explained through a soft breaking of the lepton number conservation, with small values of the parameters ϵ and/or $\mu^{(\prime)}$, instead of a breaking by the large masses for the sterile species, such as in the traditional Type-I SS mechanism.[13–16] Indeed, the heavy neutral leptons can have masses at the TeV scale, which makes them possibly detectable at colliders. A second relevant aspect is that the Yukawa couplings are sizable and so are the mixings between the sterile species and the active neutrinos. This is particularly interesting due to the significant induced deviation from the unitarity of the PMNS matrix,[17–20] which translates into a tree-level contribution to M_W and allows to solve the CDF II anomaly, as discussed in Refs. [6, 7]. Indeed, any modification of the leptonic charged current implies an additional contribution to the muon β decay, from which the value of the Fermi Constant G_F (defined as the parameter that enters the Fermi Lagrangian) is computed: labelling with G_μ the parameter extracted from the muon lifetime,

$$G_F = G_\mu(1+\Delta_G), \tag{1.6}$$

where Δ_G represents the generic deviation. Its effect appears in the prediction of M_W as

$$M_W = M_Z\sqrt{\frac{1}{2}+\sqrt{\frac{1}{4}-\frac{\pi\,\alpha\,(1-\Delta_G)}{\sqrt{2}\,G_\mu\,M_Z^2(1-\Delta r)}}}, \tag{1.7}$$

where α is the fine-structure constant, M_Z is the mass of the Z gauge boson and Δr accounts for loop corrections. A value of $\Delta_G \sim 5\times10^{-3}$ would solve the tension in M_W.

Other observables are affected by the deviations in the leptonic charged current, such as the invisible Z decay, various meson decays used to extract the values of the CKM matrix elements, and several decay width ratios that test the lepton flavour universality of the SM. As concluded in Ref. [6], the explanation of the CDF II anomaly is consistent with all these observables, but at the price of worsening the so-called Cabibbo Anomaly: the extracted value of the CKM entry V_{ud} after the inclusion of the non-unitarity effects turns out to be larger than its actual value. We will ignore in this paper the Cabibbo anomaly, assuming that a different new physics may be responsible for its explanation.[2]

The main goal of this paper is to propose a possible modification of the Low-Scale SS models in order to solve the longstanding anomaly associated with the muon anomalous magnetic moment, $(g-2)_\mu$. It has been measured by the Muon $g-2$ collaboration at the Brookhaven National Laboratories[22] and more recently at Fermilab,[23] showing a combined 4.2σ tension with the SM result,[24]

$$\delta a_\mu \equiv \frac{(g-2)_\mu^{\rm exp} - (g-2)_\mu^{\rm SM}}{2} = (2.51\pm0.59)\times10^{-9}. \tag{1.8}$$

It has to be mentioned that the BMW lattice collaboration[25] has recently presented a lattice result for the SM contributions to the hadronic vacuum polarization that would soften this tension. After that, other groups[26,27] seem to align with that result. One may then wonder if QCD effects not only explain the $(g-2)_\mu$ anomaly but also the one associated to the M_W determination. However, as discussed in Ref. [28], this is not the case as new physics is necessary to explain both of them simultaneously. Moreover, the lattice results are in tension with the $e^+e^-\to$ hadrons data,[29–32] so the global situation associated to the $(g-2)_\mu$ remains unclear. While waiting for further calculations to establish a clear picture, we will adopt the result in Equation (1.8) for the rest of the paper.

It is well known that no solution to the $(g-2)_\mu$ anomaly can be obtained with only sterile leptons. In several Refs. [33–37], a broad analysis has been performed investigating which exotic fields beyond the SM (BSM) spectrum may play an interesting role in this respect. An approach that received attention in the last two years[38–40] consists of the introduction of vector-like leptons transforming as a doublet of the electroweak (EW) symmetry. Its attractiveness resides in the absence of contributions to the $(g-2)_\mu$ suppressed by only two powers of the mass of the exotic states. The first relevant chirally enhanced term is suppressed by the fourth power of the mass. This represents a scenario where light new physics may be responsible for the $(g-2)_\mu$ anomaly. Notice that this framework requires, beyond the exotic EW doublets, the presence of also leptonic sterile species in order to explain this anomaly.

The question we want to answer in this paper is whether the introduction of additional vector-like lepton EW doublets, discussed in Refs. [33–37], in the Low-Scale SS setups may consistently explain the light active neutrino masses, the CDF II tension in M_W, and the $(g-2)_\mu$ anomaly. This construction would then represent a minimal setup where all the additional fields with respect to the SM spectrum are strictly necessary. With respect to the past literature, we revisit the analysis of the $(g-2)_\mu$, pointing out any difference in signs and factors and investigating new part of the parameter space, while explaining for the first time in this context the lightness of the active neutrinos and the M_W CDF II measurement.

[2] Recently, an updated study by the UTfit collaboration has been published.[21] The results seem to slightly reduce the significance of the Cabibbo anomaly.

Table 1. Transformation properties of the SM leptons ℓ_L and μ_R, the Higgs doublet H, the sterile neutrinos N_R and S_R, and of the leptonic vector-like EW doublet ψ under the gauge EW symmetry and their lepton charges.

	$SU(2)_L$	$U(1)_Y$	$U(1)_L$
ℓ_L	2	$-1/2$	1
μ_R	1	1	1
H	2	$+1/2$	0
N_R	1	1	1
S_R	1	1	-1
ψ_L	2	$-1/2$	1
ψ_R	2	$-1/2$	1

We will first proceed in Section 2 with the formulation of a minimal and simplified one-generation scenario that describes only the muon and the muonic neutrino. This will be realised by introducing only one N_R, one S_R and one pair of vector-like EW doublets of exotic leptons. The model is a renormalisable extension of the Standard Model with all the terms allowed by the Standard Model symmetries present in the Lagrangian. In Section 3, we present the relevant phenomenology, distinguishing between observables that receive contributions at tree-level from those that do at loop-level. These two sections provide a proof of concept of the existence of a framework with massive neutrinos, where the CDF II M_W tension and the $(g-2)_\mu$ anomaly can be simultaneously solved. In Section 4, we comment on possible generalisations to account for the three generations of fermions, discussing the advantages and the disadvantages of each of them. Finally, we will conclude in Section 5.

2. Formulation of the One-Generation Model

This section is devoted to the description and discussion of the simplified model that only treats the second lepton generation. The lepton and scalar sector of the framework is defined in Table 1 together with its transformation properties under the gauge EW symmetry and its lepton charges.

The notation refers to the second lepton generation and therefore ℓ_L stands for the leptonic EW doublet containing the left-handed (LH) muon and muonic neutrino, while μ_R is the right-handed (RH) muon. N_R and S_R are two fermionic EW singlets with opposite lepton charges, while ψ_L and ψ_R constitute a leptonic vector-like EW doublet. Finally, H is the Higgs EW doublet.

The corresponding mass Lagrangian can be written as

$$\begin{aligned}-\mathscr{L}_Y = {} & \overline{\ell_L} H Y_\mu \mu_R + \overline{\ell_L}\widetilde{H} Y_N N_R + \epsilon \overline{\ell_L}\widetilde{H} Y_S S_R \\ & + \frac{1}{2}\mu' \overline{N_R^c} N_R + \frac{1}{2}\mu \overline{S_R^c} S_R + \Lambda \overline{N_R^c} S_R \\ & + Y_R \overline{\psi_L} H \mu_R + Y_V \overline{S_R^c}\widetilde{H}^\dagger \psi_R + Y_V' \overline{\psi_L}\widetilde{H} N_R \\ & + M_\psi \overline{\psi_L}\psi_R + M_L \overline{\ell_L}\psi_R + \text{h.c.}\,,\end{aligned} \tag{2.1}$$

where $\widetilde{H} \equiv i\sigma_2 H^*$, with σ_2 the second Pauli matrix, and all the terms respect the lepton number conservation, except for those proportional to Y_S, μ and μ' which ensure the Low-Scale SS mechanism discussed in the Introduction. Without loss of generality and in order to keep the construction as minimal as possible, we will neglect the μ' term in what follows. It does not intervene in the determination of the neutrino masses at the order considered and, secondly, it is expected to be as small as μ and therefore negligible for the $(g-2)_\mu$ contributions, which is the main topic we want to address.[3]

Once the EW symmetry is spontaneously broken by the Higgs VEV, the mass terms can be compactly rewritten as

$$-\mathscr{L}_Y \supset \frac{1}{2}\overline{\chi}\mathcal{M}_\chi \chi^c + \overline{\zeta_L}\mathcal{M}_\zeta \zeta_R + \text{h.c.}\,, \tag{2.2}$$

where the neutral lepton multiplet χ and the charged one ζ are defined as

$$\chi \equiv (\nu_L,\, N_R^c,\, S_R^c,\, \psi_L^0,\, \psi_R^{0c})^T\,, \qquad \zeta \equiv (\mu,\, \psi^-)^T\,, \tag{2.3}$$

generalising the definition of χ in Equation (1.2) to include the neutral components of ψ. The mass matrices $\mathcal{M}_\chi$ and $\mathcal{M}_\zeta$ are then written as

$$\mathcal{M}_\chi = \begin{pmatrix} 0 & m_N & \epsilon\, m_S & 0 & M_L \\ m_N & 0 & \Lambda & m_{V'} & 0 \\ \epsilon\, m_S & \Lambda & \mu & 0 & m_V \\ 0 & m_{V'} & 0 & 0 & M_\psi \\ M_L & 0 & m_V & M_\psi & 0 \end{pmatrix}, \qquad \mathcal{M}_\zeta = \begin{pmatrix} m_\mu & M_L \\ m_R & M_\psi \end{pmatrix}, \tag{2.4}$$

where we use a shortcut notation for the product of the EW VEV and a Yukawa coupling, such that $m_i \equiv v Y_i/\sqrt{2}$.

Before entering into the details of the (block) diagonalisation of these mass matrices, a few comments are in order. If the only non-vanishing entries would be those with Λ and M_ψ, then $(N_R,\, S_R)$, $(\psi_L^0,\, \psi_R^0)$ and $(\psi_L^-,\, \psi_R^-)$ would be three massive Dirac pairs, while the neutrino and the muon would remain massless. The introduction of M_L does not change this feature: the determinant of the two mass matrices would still be zero and therefore the lightest neutral and charged states would still be massless. However, the presence of M_L induces a redefinition of the mass for the Dirac pairs $(\psi_L^0,\, \psi_R^0)$ and $(\psi_L^-,\, \psi_R^-)$, and more importantly leads to a mixing between the components of the LH fields ℓ_L and ψ_L. As we will see later, this results in the muon and the neutrino being composite states, whose level of compositeness depends on the hierarchy between M_ψ and M_L. Once the terms proportional to the EW VEV and μ are considered, the muon and the neutrino acquire masses. With respect to the traditional Low-Scale SS mechanisms, the introduction of the EW doublet ψ, besides making the neutrino composite, does not modify either the expression for the neutrino mass or that for the mixing between the light active neutrino and the heavy species. We thus expect that the neutrino phenomenology for this model will remain essentially unmodified with respect to the one of the traditional Low-Scale SS mechanisms.

[3] Our model is a renormalisable construction with a Lagrangian that includes all the terms invariant under the SM gauge symmetry. This differs from the setup considered in Ref. [38], where the tree-level muon Yukawa term has been neglected: as a consequence, that framework is not renormalisable and a physical cut-off at about 10^5 GeV has been considered.

Given the interesting physical impact of the presence of M_L, it is illustrative to discuss an intermediate step in the mass matrix diagonalisation, that we will refer to with a tilde in the different quantities. This will be very useful for discussing the phenomenology of the model as the different observables can be written in a compact form in terms of the tilde parameters.

The mass M_L may be large and therefore the diagonalisation procedure would require a large rotation. The fields in the tilde basis, where M_L does not appear in the off-diagonal entries of the mass matrices, read: for the charged leptons

$$\begin{aligned} &\widetilde{\mu}_L \equiv \cos\theta\,\mu_L - \sin\theta\,\psi_L^- && \widetilde{\mu}_R \equiv \mu_R \\ &\widetilde{\psi}_L^- \equiv \sin\theta\,\mu_L + \cos\theta\,\psi_L^- && \widetilde{\psi}_R^- \equiv \psi_R^- \end{aligned} \tag{2.5}$$

and for the neutral leptons

$$\begin{aligned} &\widetilde{\nu}_L \equiv \cos\theta\,\nu_L - \sin\theta\,\psi_L^0 \\ &\widetilde{N}_R \equiv N_R && \widetilde{S}_R \equiv S_R \\ &\widetilde{\psi}_L^0 \equiv \sin\theta\,\nu_L + \cos\theta\,\psi_L^0 && \widetilde{\psi}_R^0 \equiv \psi_R^0\,. \end{aligned} \tag{2.6}$$

As we can see, only the LH components of the two EW doublets are affected by this redefinition while the other fields remain the same. In these expressions, θ is a mixing angle defined as

$$\cos\theta \equiv \frac{M_\psi}{\widetilde{M}_\psi}\,, \quad \sin\theta \equiv \frac{M_L}{\widetilde{M}_\psi}\,, \qquad \text{with} \quad \widetilde{M}_\psi \equiv \sqrt{M_\psi^2 + M_L^2}\,. \tag{2.7}$$

In the case in which M_L and M_ψ are taken of the same order of magnitude then the angle is close to 45°, while once M_L is negligible (dominant) with respect to M_ψ then $\sin\theta \approx 0$ ($\cos\theta \approx 0$). We will further discuss these three cases later in this section.

Finalising the diagonalisation, all the fields are redefined and the light active neutrino gets mass. Denoting by a "hat" the quantities in the mass basis, the charged lepton masses are given by

$$\widehat{m}_\mu = \widetilde{m}_\mu\left[1 - \frac{1}{2}\left(\frac{\widetilde{m}_R}{\widetilde{M}_\psi}\right)^2\right], \qquad \widehat{m}_{\psi^-} = \widetilde{M}_\psi\left[1 + \frac{1}{2}\left(\frac{\widetilde{m}_R}{\widetilde{M}_\psi}\right)^2\right], \tag{2.8}$$

where we used as definitions

$$\widetilde{m}_\mu = m_\mu\cos\theta - m_R\sin\theta\,, \qquad \widetilde{m}_R = m_R\cos\theta + m_\mu\sin\theta\,, \tag{2.9}$$

and we neglected terms that have a relative suppression at least equal to $(v/\widetilde{M}_\psi)^2$ with respect to the expressions of the masses. The corresponding mass eigenstates are defined by

$$\widehat{\zeta}: \begin{cases} \widehat{\mu}_L = \widetilde{\mu}_L\,, & \widehat{\psi}_L^- = \widetilde{\psi}_L^-\,, \\ \widehat{\mu}_R = \widetilde{\mu}_R - \left(\dfrac{\widetilde{m}_R}{\widetilde{M}_\psi}\right)\widetilde{\psi}_R^-\,, & \widehat{\psi}_R^- = \widetilde{\psi}_R^- + \left(\dfrac{\widetilde{m}_R}{\widetilde{M}_\psi}\right)\widetilde{\mu}_R\,, \end{cases} \tag{2.10}$$

where now the neglected terms are more suppressed by only a $v/\widetilde{M}_\psi$ power.

Analogously, for the neutral lepton sector, the final expressions for the masses are

$$\begin{aligned} \widehat{m}_\nu &= \frac{\mu\,\widetilde{m}_N^2}{\Lambda^2} - \frac{2\,\epsilon\,\widetilde{m}_N\,m_S\cos\theta}{\Lambda}\,, \\ \widehat{m}_{N_R} &= \Lambda + \frac{\mu}{2} + \frac{\widetilde{m}_N^2}{2\Lambda} + \frac{1}{4}\left[\frac{(m_V+\widetilde{m}_{V'})^2}{\Lambda-\widetilde{M}_\psi} + \frac{(m_V-\widetilde{m}_{V'})^2}{\Lambda+\widetilde{M}_\psi}\right], \\ \widehat{m}_{S_R} &= \Lambda - \frac{\mu}{2} + \frac{\widetilde{m}_N^2}{2\Lambda} + \frac{1}{4}\left[\frac{(m_V+\widetilde{m}_{V'})^2}{\Lambda-\widetilde{M}_\psi} + \frac{(m_V-\widetilde{m}_{V'})^2}{\Lambda+\widetilde{M}_\psi}\right], \\ \widehat{m}_{\psi^0} &= \widetilde{M}_\psi - \frac{1}{4}\left[\frac{(m_V+\widetilde{m}_{V'})^2}{\Lambda-\widetilde{M}_\psi} - \frac{(m_V-\widetilde{m}_{V'})^2}{\Lambda+\widetilde{M}_\psi}\right], \end{aligned} \tag{2.11}$$

while those for the mass eigenstates read

$$\widehat{\chi}: \begin{cases} \widehat{\nu}_L = \widetilde{\nu}_L - \dfrac{\widetilde{m}_N}{\Lambda}\widetilde{S}_R^c\,, \\ \widehat{N}_R = \dfrac{\widetilde{N}_R + \widetilde{S}_R}{\sqrt{2}} + \dfrac{\widetilde{m}_N}{\sqrt{2}\Lambda}\widetilde{\nu}_L^c + \dfrac{1}{2}\left[\dfrac{m_V+\widetilde{m}_{V'}}{\Lambda-\widetilde{M}_\psi}\dfrac{\widetilde{\psi}_L^{0c}+\widetilde{\psi}_R^0}{\sqrt{2}} - \dfrac{m_V-\widetilde{m}_{V'}}{\Lambda+\widetilde{M}_\psi}\dfrac{\widetilde{\psi}_L^{0c}-\widetilde{\psi}_R^0}{\sqrt{2}}\right], \\ \widehat{S}_R = i\left\{-\dfrac{\widetilde{N}_R - \widetilde{S}_R}{\sqrt{2}} + \dfrac{\widetilde{m}_N}{\sqrt{2}\Lambda}\widetilde{\nu}_L^c - \dfrac{1}{2}\left[\dfrac{m_V-\widetilde{m}_{V'}}{\Lambda+\widetilde{M}_\psi}\dfrac{\widetilde{\psi}_L^{0c}+\widetilde{\psi}_R^0}{\sqrt{2}} - \dfrac{m_V+\widetilde{m}_{V'}}{\Lambda-\widetilde{M}_\psi}\dfrac{\widetilde{\psi}_L^{0c}-\widetilde{\psi}_R^0}{\sqrt{2}}\right]\right\}, \\ \widehat{\psi}_L^0 = \dfrac{\widetilde{\psi}_L^0 + \widetilde{\psi}_R^{0c}}{\sqrt{2}} - \dfrac{1}{2}\left[\dfrac{m_V+\widetilde{m}_{V'}}{\Lambda-\widetilde{M}_\psi}\dfrac{\widetilde{N}_R^c + \widetilde{S}_R^c}{\sqrt{2}} + \dfrac{m_V-\widetilde{m}_{V'}}{\Lambda+\widetilde{M}_\psi}\dfrac{\widetilde{N}_R^c - \widetilde{S}_R^c}{\sqrt{2}}\right], \\ \widehat{\psi}_R^0 = i\left\{-\dfrac{\widetilde{\psi}_L^{0c} - \widetilde{\psi}_R^0}{\sqrt{2}} - \dfrac{1}{2}\left[\dfrac{m_V-\widetilde{m}_{V'}}{\Lambda+\widetilde{M}_\psi}\dfrac{\widetilde{N}_R + \widetilde{S}_R}{\sqrt{2}} + \dfrac{m_V+\widetilde{m}_{V'}}{\Lambda-\widetilde{M}_\psi}\dfrac{\widetilde{N}_R - \widetilde{S}_R}{\sqrt{2}}\right]\right\}, \end{cases} \tag{2.12}$$

where we defined

$$\widetilde{m}_N = m_N \cos\theta - m_{V'} \sin\theta\,, \qquad \widetilde{m}_{V'} = m_{V'} \cos\theta + m_N \sin\theta \tag{2.13}$$

and we neglected higher order terms: some of them follow the same pattern as the charged states, that is $(v/(\Lambda,\, \widetilde{M}_\psi))^2$ for the masses and $v/(\Lambda,\, \widetilde{M}_\psi)$ for the eigenstates; while others are proportional to $(\mu, m_S)/(\Lambda, \widetilde{M}_\psi)$. This holds for all the expressions, except for $\widehat{m}_\nu$, where the terms with μ and m_S are the leading ones. Requiring that the neglected terms are smaller than the 20% of the shown contributions to the masses translates into a lower bound for Λ and $\widetilde{M}_\psi$, such that

$$\Lambda,\, \widetilde{M}_\psi \gtrsim 500\ \text{GeV}\,. \tag{2.14}$$

This consistency constraint will be imposed in the following analysis. Moreover, the "i" in front of the third and fifth lines guarantees that the corresponding expressions for the masses are defined as positive. Special care is required for the active neutrinos: in case the LSS contribution proportional to ϵ dominates, then the mass would turn negative and then we should redefine $\widehat{\nu}_L$ introducing the dependence of an "i" factor. Finally, to match with the literature of the Low-Scale Seesaw, the mixing between active neutrinos and the heavy neutral leptons responsible for their masses, defined as $\widehat{\nu}_L \simeq \widetilde{\nu}_L - \Theta\, \widetilde{S}^c_R$, is given by

$$\Theta = \frac{\widetilde{m}_N}{\Lambda} \tag{2.15}$$

and it will be useful for discussing the direct searches of the heavy states at colliders.

Moreover, it is interesting to consider three different scenarios depending on the hierarchy between M_L and M_ψ:

- $\mathbf{M_L \ll M_\psi}$: in this case, $\sin\theta \sim 0$ and the main contribution to the muon mass is due to the muon Yukawa term Y_μ and the muon field almost coincides with the elementary field μ, such as in the SM.
- $\mathbf{M_L \gg M_\psi}$: this is the opposite case with respect the previous one, where $\cos\theta \sim 0$ and then the main contribution to the muon mass is now the Y_R Yukawa term. Correspondingly, the LH component of the muon field coincides with the exotic field ψ^-_L, while the RH component can be almost identified with the SM μ_R.
- $\mathbf{M_L \sim M_\psi}$: in this intermediate case, the muon mass receives sizable contributions from both Y_μ and Y_R Yukawa terms and the LH component of the muon field is a composite state of μ_L and ψ^-_L.

3. Phenomenology of the One-Generation Model

The presence of the exotic leptons can be tested both with deviations from the SM predictions and with direct searches at colliders. The analysis on indirect signals requires the effective Lagrangian describing the SM lepton couplings with the SM gauge bosons and with one physical Higgs h that reads

$$\begin{aligned}\mathscr{L}_{\rm SM} \supset & -\frac{h}{v}\left[\widetilde{m}_\mu\left(1-\frac{3}{2}\frac{\widetilde{m}_R^2}{\widetilde{M}_\psi^2}\right)\overline{\widehat{\mu}}_L\widehat{\mu}_R\right.\\ & \left.+\left(\frac{\mu\,\widetilde{m}_N^2}{\Lambda^2}-\frac{2\,\epsilon\,\widetilde{m}_N\,m_S\cos\theta}{\Lambda}\right)\overline{\widehat{\nu}}_L\widehat{\nu}^c_L+\text{h.c.}\right]\\ & + e\,\overline{\widehat{\mu}}\,\not{A}\,\widehat{\mu}-\frac{g_L}{\sqrt{2}}\left[\left(1-\frac{\widetilde{m}_N^2}{2\Lambda^2}\right)\overline{\widehat{\nu}}_L\,\not{W}^+\,\widehat{\mu}_L+\text{h.c.}\right]\\ & -\frac{\sqrt{g_L^2+g_Y^2}}{2}\left[\left(1-\frac{\widetilde{m}_N^2}{\Lambda^2}\right)\overline{\widehat{\nu}}_L\,\not{Z}\,\widehat{\nu}_L-\cos 2\theta_W\,\overline{\widehat{\mu}}\,\not{Z}\,\widehat{\mu}\right.\\ & \left.+\left(1-\frac{\widetilde{m}_R^2}{\widetilde{M}_\psi^2}\right)\overline{\widehat{\mu}}_R\,\not{Z}\,\widehat{\mu}_R\right]\,,\end{aligned} \tag{3.1}$$

where $g_{L(Y)}$ is the $SU(2)_L(U(Y))$ gauge-coupling and we neglected the Higgs coupling to the active neutrino as it does not lead to any relevant phenomenology.

It is useful to perform the matching with the phenomenological Lagrangian describing the same interactions,

$$\begin{aligned}\mathscr{L}^{\rm eff.}_{\rm SM} \supset & -\frac{h}{v}\left[m_\mu^{\rm exp}\,\kappa_\mu\,\overline{\widehat{\mu}}\,\widehat{\mu}+i\,m_\mu^{\rm exp}\,\tilde{\kappa}_\mu\,\overline{\widehat{\mu}}\,\gamma_5\,\widehat{\mu}\right]\\ & -\frac{g_L}{\sqrt{2}}\left[(1+\delta g_L^{W\mu})\,\overline{\widehat{\nu}}_L\,\not{W}^+\,\widehat{\mu}_L+\text{h.c.}\right]\\ & -\sqrt{g_L^2+g_Y^2}\left[\sum_{f=\mu,\nu}\left[\left(T_f^3-s^2_{\theta_W}Q_f\right)+\delta g_L^{Zf}\right]\overline{\widehat{f}}_L\,\not{Z}\,f_L\right.\\ & \left.+\left(s^2_{\theta_W}+\delta g_R^{Z\mu}\right)\overline{\widehat{\mu}}_R\,\not{Z}\,\widehat{\mu}_R\right]\,,\end{aligned} \tag{3.2}$$

where $m_\mu^{\rm exp}$ is the experimental value of the muon mass, $T^3_\nu = +1/2$ and $T^3_\mu = -1/2$, while δg are the deviations from the corresponding SM values, and κ_μ and $\tilde{\kappa}_\mu$ represent the deviations from the SM (real and imaginary) values of the muon Yukawa.

Comparing Equations (3.1) and (3.2), we find the following expression of the effective quantities in terms of the parameters of the model:

$$\begin{aligned}&\kappa_\mu = 1-\frac{3}{2}\frac{\widetilde{m}_R^2}{\widetilde{M}_\psi^2}\,, && \tilde{\kappa}_\mu = 0\,,\\ &\delta g_L^{W\mu} = \delta g_L^{Z\nu} = -\frac{\widetilde{m}_N^2}{2\Lambda^2}\,, && \delta g_L^{Z\mu} = 0\,, \qquad \delta g_R^{Z\mu} = -\frac{\widetilde{m}_R^2}{2\widetilde{M}_\psi^2}\,.\end{aligned} \tag{3.3}$$

On the other hand, in order to discuss direct searches at colliders, we need the Lagrangian describing the interactions of the physical Higgs and the SM gauge bosons with one light lepton and one heavy:

$$\mathscr{L}_h \supset -\frac{h}{v}\left\{\widetilde{m}_R\left(1-\frac{\widetilde{m}_R^2-2\widetilde{m}_\mu^2}{2\widetilde{M}_\psi^2}\right)\overline{\widehat{\mu}}_R\widehat{\psi}_L^- + \frac{\widetilde{m}_\mu\widetilde{m}_R}{\widetilde{M}_\psi}\overline{\widehat{\mu}}_L\widehat{\psi}_R^- + \frac{\widetilde{m}_N}{2}\left[1-\frac{\widetilde{m}_N^2}{\Lambda^2}+\frac{m_V\widetilde{m}_{V'}}{\Lambda\widetilde{M}_\psi}-\frac{m_V}{\Lambda}\left(\frac{m_V\Lambda+\widetilde{m}_{V'}\widetilde{M}_\psi}{\Lambda^2-\widetilde{M}_\psi^2}\right)-\frac{1}{2}\left(\frac{m_V\Lambda+\widetilde{m}_{V'}\widetilde{M}_\psi}{\Lambda^2-\widetilde{M}_\psi^2}\right)^2\right]\right.$$
$$\left.\times\left(\overline{\widehat{\nu}_L^c}\frac{\widehat{N}_R^c-i\widehat{S}_R^c}{\sqrt{2}}+\overline{\widehat{\nu}}_L\frac{\widehat{N}_R+i\widehat{S}_R}{\sqrt{2}}\right)-\frac{\widetilde{m}_N}{2}\left[\frac{m_V}{\Lambda}+\frac{m_V\Lambda+\widetilde{m}_{V'}\widetilde{M}_\psi}{\Lambda^2-\widetilde{M}_\psi^2}\right]\left(\overline{\widehat{\nu}_L^c}\frac{\widehat{\psi}_L^0+i\widehat{\psi}_R^{0c}}{\sqrt{2}}+\overline{\widehat{\nu}}_L\frac{\widehat{\psi}_L^{0c}-i\widehat{\psi}_R^0}{\sqrt{2}}\right)\right\}+\text{h.c.} \tag{3.4}$$

$$\mathscr{L}_Z \supset -\frac{\sqrt{g_L^2+g_Y^2}}{2}Z_\mu\left\{\frac{\widetilde{m}_R}{\widetilde{M}_\psi}\overline{\widehat{\mu}}_R\gamma^\mu\widehat{\psi}_R^- + \frac{\widetilde{m}_N}{\Lambda}\overline{\widehat{\nu}}_L\gamma^\mu\frac{\widehat{S}_R^c-i\widehat{N}_R^c}{\sqrt{2}}+\frac{1}{2}\left[\frac{m_V+\widetilde{m}_{V'}}{\Lambda-\widetilde{M}_\psi}-\frac{m_V-\widetilde{m}_{V'}}{\Lambda+\widetilde{M}_\psi}\right]\overline{\widehat{\nu}}_L\gamma^\mu\frac{i\widehat{\psi}_L^0+\widehat{\psi_R^{0c}}}{\sqrt{2}}\right\} \tag{3.5}$$

$$\mathscr{L}_W \supset -\frac{g_L}{\sqrt{2}}W_\mu^-\left\{\frac{\widetilde{m}_N}{\Lambda}\overline{\widehat{\mu}}_L\gamma^\mu\frac{\widehat{N}_R^c+i\widehat{S}_R^c}{\sqrt{2}}-\frac{\widetilde{m}_R}{2\widetilde{M}_\psi}\left[\frac{m_V+\widetilde{m}_{V'}}{\Lambda-\widetilde{M}_\psi}+\frac{m_V-\widetilde{m}_{V'}}{\Lambda+\widetilde{M}_\psi}\right]\overline{\widehat{\mu}}_R\gamma^\mu\frac{\widehat{N}_R+i\widehat{S}_R}{\sqrt{2}}\right.$$
$$\left.-\left[\frac{\widetilde{m}_\mu\widetilde{m}_R}{\widetilde{M}_\psi^2}+\frac{\widetilde{m}_N}{2\widetilde{M}_\psi}\left(\frac{m_V+\widetilde{m}_{V'}}{\Lambda-\widetilde{M}_\psi}+\frac{m_V-\widetilde{m}_{V'}}{\Lambda+\widetilde{M}_\psi}\right)\right]\overline{\widehat{\mu}}_L\gamma^\mu\frac{\widehat{\psi}_L^0-i\widehat{\psi}_R^{0c}}{\sqrt{2}}-\frac{\widetilde{m}_R}{\widetilde{M}_\psi}\overline{\widehat{\mu}}_R\gamma^\mu\frac{\widehat{\psi}_L^{0c}-i\widehat{\psi}_R^0}{\sqrt{2}}\right\}+\text{h.c.}\,. \tag{3.6}$$

We can now proceed with the phenomenological analysis, dividing the discussion between observables receiving contributions at tree level and those at 1-loop level.

3.1. Relevant Phenomenology at Tree-Level

Colliders bounds on Higgs couplings

The precise measurement of the Higgs couplings to fermions became a primordial goal after the Higgs discovery and ATLAS and CMS experiments have reported numerous results. The most recent combinations of different Higgs signal strengths have been recently released in Refs. [41] (ATLAS) and [42] CMS, using data at $\sqrt{s}=13$ TeV. In addition, both collaborations reported in Refs. [43] and [44] the observations of Higgs decays into a pair of opposite-sign muons, in collisions at $\sqrt{s}=13$ TeV. Using these collider data, Ref. [45–47] performed a global fit obtaining a bound on a combination of κ_μ and $\tilde{\kappa}_\mu$,

$$0.36 \lesssim \kappa_\mu^2+\tilde{\kappa}_\mu^2 \lesssim 1.85\,, \tag{3.7}$$

that, given the matching in Equation (3.3), translates into a bound on the ratio $\widetilde{m}_R^2/\widetilde{M}_\psi^2$,

$$0.6 \lesssim \kappa_\mu \lesssim 1.36 \quad\Rightarrow\quad \frac{\widetilde{m}_R^2}{\widetilde{M}_\psi^2} \lesssim 0.27\,. \tag{3.8}$$

EW global fit bounds on Z couplings

A stronger constraint on this parameter ratio can be extracted from the bounds on the deviation of the $Z-\mu$ coupling from its SM prediction: the results of the EW global fit performed in Ref. [48] gives

$$\delta g_L^{Z\mu}=(0.1\pm1.2)\times10^{-3}\,,\qquad \delta g_R^{Z\mu}=(0.0\pm1.4)\times10^{-3}\,, \tag{3.9}$$

that translates at the 2σ level to

$$\frac{\widetilde{m}_R^2}{\widetilde{M}_\psi^2} < 5.6\times10^{-3}\,. \tag{3.10}$$

CDF II M_W Tension

The same EW global fit also gives a bound on $\delta g_L^{W\mu}$, but the input data used do not take into consideration the recent CDF II measurement of the W mass and for this reason, we will proceed with a dedicated discussion in what follows. The modification of the W coupling has an impact on the computation of the muon β decay: assuming that the W coupling with the first generation leptons is as in the SM, the decay rate of $\mu\to e\bar{\nu}\nu$ reads

$$\Gamma_\mu \simeq \frac{m_\mu^{\exp 5}G_F^2}{192\,\pi^3}\left(1-\frac{\widetilde{m}_N^2}{2\Lambda^2}\right)^2 \equiv \frac{m_\mu^{\exp 5}G_\mu^2}{192\,\pi^3}\,, \tag{3.11}$$

where we recall that G_F is the Fermi constant parameter as defined in the Fermi Lagrangian, G_μ is the corresponding experimental determination extracted from the muon lifetime (after correcting for $O(\alpha_{EM})$ radiative effects). The relation between these two quantities is such that

$$G_F \simeq G_\mu\left(1+\frac{\widetilde{m}_N^2}{2\Lambda^2}\right), \tag{3.12}$$

and this implies a modification of the relation between the W boson mass and the experimental determination of G_μ,

$$M_W \simeq M_Z \sqrt{\frac{1}{2} + \sqrt{\frac{1}{4} - \frac{\pi\,\alpha_{\rm em}}{\sqrt{2}\,G_\mu\,M_Z^2\,(1-\Delta r)}\left(1-\frac{\widetilde{m}_N^2}{2\Lambda^2}\right)}}\,, \tag{3.13}$$

in the on-shell scheme, where the tree-level formula for the sine of the Weinberg angle is promoted to the definition of the renormalised quantity:

$$\sin\theta_W \equiv 1 - \frac{M_W^2}{M_Z^2}\,. \tag{3.14}$$

Considering the following numerical values of the input parameters[49]

$$\begin{aligned} m_\mu^{\rm exp} &= 105.6583755(23)\ \text{MeV} \\ \alpha_{\rm em} &= 7.2973525693(11)\times 10^{-3} \\ G_\mu &= 1.1663787(6)\times 10^{-5}\ \text{GeV}^{-2} \\ M_Z &= 91.1876(21)\ \text{GeV} \\ \Delta r &= 0.03657(21)(7)\,, \end{aligned} \tag{3.15}$$

we can extract the range of values necessary to explain the recent CDF II measurement in Equation (1.1): at the 2σ level,

$$\frac{\widetilde{m}_N^2}{\Lambda^2} \in [6.6, 11.8]\times 10^{-3}\,. \tag{3.16}$$

This bound is consistent with the results shown in Refs. [6, 7]. Additional modifications to the W mass appear at the loop level, but they are completely negligible in the considered parameter space and therefore we will neglect them.

Effective N_ν and LFU ratios

A second bound on this combination of parameters can be obtained from the modification of the Z-decay into neutrinos. It is constrained by the experimental determination of the invisible Z decay rate. The analytic expression for the Z decay rate into neutrinos, assuming that only the coupling with the muon neutrino is modified according to Equation (3.1), while those with the electron and tau neutrinos remain as in the SM, reads

$$\Gamma_{Z\text{-inv}} \simeq \frac{G_\mu\,M_Z^3}{12\sqrt{2}\,\pi}\left(3-\frac{\widetilde{m}_N^2}{2\Lambda^2}\right) \equiv \frac{G_\mu\,M_Z^3\,N_\nu}{12\sqrt{2}\,\pi}\,, \tag{3.17}$$

where N_ν is the number of effective active neutrinos. The experimental determination of the latter is $N_\nu^{\rm exp} = 2.9963(74)$[50] and it provides the following bound on the combination of parameters of the model:

$$\frac{\widetilde{m}_N^2}{\Lambda^2} < 3.7\times 10^{-2}\,, \tag{3.18}$$

compatible with the range of values in Equation (3.16) required to explain the new M_W measurement.

Further constraints follow from pion, kaon and also tau decays: the relative branching ratios of the decay of those particles to different lepton flavours are clean observables that test the lepton flavour universality,

$$\mathcal{R}^P_{\mu/e} \equiv \frac{\Gamma\left(P\to\mu\,\overline{\nu_\mu}\right)}{\Gamma\left(P\to e\,\overline{\nu_e}\right)}\,, \qquad \mathcal{R}^\tau_{\mu/e} \equiv \frac{\Gamma\left(\tau\to\mu\,\overline{\nu_\mu}\,\nu_\tau\right)}{\Gamma\left(\tau\to e\,\overline{\nu_e}\,\nu_\tau\right)}\,. \tag{3.19}$$

In all cases, the deviation due to New Physics (NP) reduces to the same combination of parameters as only the muon sector is affected: comparing with the experimental determinations,[51]

$$\begin{aligned} &1-\frac{\widetilde{m}_N^2}{2\Lambda^2}\Big|_\pi = 1.0010(9)\,, \qquad 1-\frac{\widetilde{m}_N^2}{2\Lambda^2}\Big|_K = 0.9978(18)\,, \\ &1-\frac{\widetilde{m}_N^2}{2\Lambda^2}\Big|_\tau = 1.0018(14)\,. \end{aligned} \tag{3.20}$$

The strongest bound on the combination of the model parameter at the 2σ level is

$$\frac{\widetilde{m}_N^2}{\Lambda^2} < 1.6\times 10^{-3}\,, \tag{3.21}$$

slightly in tension with the preferred region to explain the CDF II anomaly. We expect that this tension can be resolved once extending this analysis to the three flavour case, as will be discussed in the next sections.

Direct searches of heavy leptons

The only couplings between heavy and SM fermions which are not suppressed are the ones involving the Higgs and are proportional to $\widetilde{m}_{N,R}$, as can be seen in Equation (3.4). One would therefore expect sizeable contributions to off-shell Higgs-mediated processes. The bounds on such couplings are extremely interesting, but they go beyond the scope of this work and are left for more detailed and dedicated future analysis.

Concerning the couplings with Z and W gauge bosons, we can distinguish two main scenarios: i) $\Lambda < \widetilde{M}_\psi$, such that among the heavy states, the lightest are $\widehat{N}_R$ and $\widehat{S}_R$ (see Equation (2.11)); ii) $\Lambda > \widetilde{M}_\psi$ and the lightest states are $\widehat{\psi}^{0,-}$. In the case i), the direct search strategy falls in the category of the standard Heavy Neutral Lepton (HNL) scenario (see Ref. [52] for a recent summary). The present experimental bounds from CMS apply only for $\widehat{m}_{N_R,S_R} < 1.2$ TeV and they apply to $\widetilde{m}_N^2/\Lambda^2$, that is the combination of parameters that control the mixing between the light and heavy species both in the neutral and in the charged gauge currents: considering the smallest masses that $\widehat{N}_R$ and $\widehat{S}_R$ can take consistently with Equation (2.14), that is $\widehat{m}_{N_R,S_R} \simeq 500$ GeV, the corresponding bound is weaker than the indirect searches listed above and reads

$$\left[\frac{\widetilde{m}_N}{\Lambda}\right]^2 \lesssim 0.1\,. \tag{3.22}$$

Moving to the case ii), the lightest heavy leptons can be both negatively charged or neutral. The present constraints from colliders, and particularly from the L3 experiment, only put a lower bound on the masses of the charged particles that is at $\widehat{m}_{\psi^-} \sim 100$ GeV,[49] weaker than the consistency limit in Equation (2.14). The neutral particles fall in the category discussed above of the HNL and the same bounds apply also here: for the lightest masses allowed by the consistency condition, $\widehat{m}^0_\psi = 500$ GeV, the corresponding constraints on the couplings of Z and W with a light lepton and a heavy neutral $\widehat{\psi}^0$ read

$$\begin{gathered}\frac{1}{4}\left[\frac{m_V+\widetilde{m}_{V'}}{\Lambda-\widetilde{M}_\psi}-\frac{m_V-\widetilde{m}_{V'}}{\Lambda+\widetilde{M}_\psi}\right]^2 \lesssim 0.1\,,\\ \left[\frac{\widetilde{m}_\mu\widetilde{m}_R}{\widetilde{M}^2_\psi}+\frac{\widetilde{m}_N}{2\widetilde{M}_\psi}\left(\frac{m_V+\widetilde{m}_{V'}}{\Lambda-\widetilde{M}_\psi}+\frac{m_V-\widetilde{m}_{V'}}{\Lambda+\widetilde{M}_\psi}\right)\right]^2 \lesssim 0.1\,, \qquad (3.23)\\ \left[\frac{\widetilde{m}_R}{\widetilde{M}_\psi}\right]^2 \lesssim 0.1\,.\end{gathered}$$

The results on the HNL apply under the assumptions of a single flavour analysis and of the specific Dirac/Majorana nature of the considered HNL that could induce a rescaling of the bounds of $1/2$ or $1/\sqrt{2}$ factors. These possible modifications, however, would not alter the relative relevance of these constraints and then we will stick to the bounds in Equation (3.23).

In the diagonalisation procedure, we have required $\Lambda \neq \widetilde{M}_\psi$. In App. A we provide the results in the degenerate limit, showing the consistency of the analysis even in this limit.

Neutrino masses

In this simplified model, only one active neutrino gets mass, while the other two remain massless. We will then arbitrarily choose that its mass corresponds to the square root of the atmospheric mass squared difference, $\widehat{m}_\nu \sim \sqrt{\Delta m^2_{\rm atm}}$.

Given the bounds on $\widetilde{m}_N/\Lambda$ discussed above, and in particular, having identified in Equation (3.16) the range of values to explain the CDF II measurement of M_W, we can now estimate the conditions to obtain the correct value for the active neutrino mass. We find a well-defined correlation between the two parameters breaking explicitly the lepton number,

$$\mu - 15\,\epsilon\, Y_s\, v \cos\theta \approx 6\ \text{eV}\,, \qquad (3.24)$$

obtained taking the central value for $\widetilde{m}_N/\Lambda$ in Equation (3.16) and the central value for $\Delta m^2_{\rm atm}$. It is then possible to extract constraints on each single parameter assuming that the other is vanishing, that at the 2σ level for $\widetilde{m}_N/\Lambda$ and $\Delta m^2_{\rm atm}$ read

$$\begin{cases}\mu \in [4.3,\ 7.5]\ \text{eV} & \text{for } \epsilon = 0\\ \epsilon\, Y_s \in -[1.7,\ 1.3]\times 10^{-12} & \text{for } \mu = 0\,.\end{cases} \qquad (3.25)$$

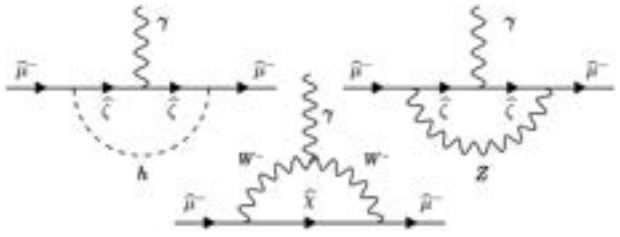

Figure 1. Diagrams contributing to the $g-2$ of the muon at 1-loop in unitary gauge.

3.2. Relevant Phenomenology at 1-Loop-Level

We can move now to the analysis of the loop-level contributions, focusing on muon MDM and on the corrections to the muon mass.

Muon magnetic dipole moment

The leading EW contributions to $(g-2)_\mu$ are those associated with the Feynman diagrams in **Figure 1**, drawn in the mass basis and in the unitary gauge.

As the internal fermion lines may be any of the neutral $\widehat{\chi}$ or charged $\widehat{\zeta}$ leptons defined in Equations (2.10) and (2.12), the total EW contribution then accounts for both the SM EW part $\delta a_\mu^{\rm SM\text{-}EW}$ and the NP one $\delta a_\mu^{\rm NP}$,

$$\delta a_\mu^{\rm EW} \equiv \delta a_\mu^{\rm SM\text{-}EW} + \delta a_\mu^{\rm NP} = \delta a_\mu^h + \delta a_\mu^Z + \delta a_\mu^W\,. \qquad (3.26)$$

Focusing on the NP term, we separately discuss the chirally enhanced and the chirally suppressed contributions: in the latter case, the contribution is suppressed by a muon mass term, besides the one due to the definition of the MDM; in the former, this additional suppression is not present. Notice that, contrary to the naive expectation, we cannot identify the chirally suppressed contributions with only those where the chirality flip is due to the muon Yukawa insertion, as muon mass terms may arise also in the interaction vertices with a scalar or gauge boson. Thus, we may have contributions corresponding to diagrams where the chirality flip occurs due to the heavy mass in the internal lepton propagator, but suppressed by muon mass terms in the vertices: we will consider these contributions as chirally suppressed.

We can qualitatively discuss our expectations, by looking at the couplings of the Lagrangian in Equations (3.4)-(3.6).

Chirally Enhanced (CE) Contributions: The chirality flip has to occur on the internal fermion line so that the total contribution is multiplied by the (heavy) mass of such a fermion. This can only occur in the diagram with the W exchange. There is no vertex $\overline{\widehat{\mu}}_L \not{Z} \widehat{\psi}^-_L$ and therefore no contribution is expected with a Z-loop and the Higgs coupling with the charged fermions $h\overline{\widehat{\mu}}_L\widehat{\psi}^-_R$ is proportional to $\widetilde{m}_\mu \approx \widehat{m}_\mu$; therefore this contribution would be chirally suppressed.

One concludes that there are W-mediated contributions involving $\widehat{N}_R$, $\widehat{S}_R$, $\widehat{\psi}^0_L$ and $\widehat{\psi}^0_R$ exchange, each of them proportional

to

$$\widetilde{m}_N \frac{\widetilde{m}_R}{\widetilde{M}_\psi}\left[\frac{m_V+\widetilde{m}_{V'}}{\Lambda-\widetilde{M}_\psi}+\frac{m_V-\widetilde{m}_{V'}}{\Lambda+\widetilde{M}_\psi}\right] \times\begin{cases}\dfrac{\widehat{m}_{\widehat{\chi}}}{\Lambda} & \text{for } \widehat{N}_R \text{ and } \widehat{S}_R\\ \dfrac{\widehat{m}_{\widehat{\chi}}}{\widetilde{M}_\psi} & \text{for } \widehat{\psi}^0_{L,R}\end{cases} \tag{3.27}$$

As in first approximation $\widehat{m}_{\widehat{N}_R,\widehat{S}_R}\simeq\Lambda$ and $\widehat{m}_{\widehat{\psi}^0_{L,R}}\simeq\widetilde{M}_\psi$ (see Equation (2.11)), the very last ratios are equal to 1 and one is tempted to conclude that the sum of all those contributions would be suppressed by only two powers of the heavy fermion masses. However, this is not the case, as there is an exact cancellation between the contributions of $\widehat{N}_R$ and $\widehat{S}_R$ and the ones of $\widehat{\psi}^0_L$ and $\widehat{\psi}^0_R$. As this feature recently received special attention in Refs. [38–40], we further discuss this aspect here below.

The generic amplitude associated to the W-mediated diagram with an internal neutral lepton $\widehat{\chi}$ with mass $\widehat{m}_{\widehat{\chi}}$ reads

$$i\mathcal{M}_{\widehat{\chi}} = -ig_L^2\int\frac{d^4k}{(2\pi)^4}\left[\overline{u}(p+q)\gamma_\mu\left(c_L^{\widehat{\chi}}P_L+c_R^{\widehat{\chi}}P_R\right)\frac{\not{k}+\widehat{m}_{\chi}}{k^2-\widehat{m}_{\chi}^2+i\epsilon}\right. \left.\times\gamma_\nu\left(c_L^{\widehat{\chi}}P_L+c_R^{\widehat{\chi}}P_R\right)S^{\mu\nu}(k,p,q)u(p)\right], \tag{3.28}$$

where $u(p)$ ($\overline{u}(p+q)$) represents the incoming (outgoing) muon with four-momentum p ($p+q$), $S^{\mu\nu}(k,p,q)$ encodes the W-propagators and the SM interaction of the two Ws with the photon of four-momentum q and $P_{L,R}=(1\mp\gamma_5)/2$ are the chirality projectors. Finally, $c_{L,R}^{\widehat{\chi}}$ [4] are the W-vertices with a muon and the normalisation of the $\widehat{\chi}$ is chosen so that the weak gauge coupling g_L has been factorised out in front of the integral. The CE part of the amplitude $\mathcal{M}_{\widehat{\chi}}^{CE}$ corresponds to the $\widehat{m}_{\widehat{\chi}}$ term in the numerator of the fermion propagator,

$$i\mathcal{M}_{\widehat{\chi}}^{\rm CE} = \widehat{m}_{\chi}c_L^{\widehat{\chi}}c_R^{\widehat{\chi}}\int\frac{d^4k}{(2\pi)^4}\overline{u}(p+q)\gamma_\mu\frac{1}{k^2-\widehat{m}_{\chi}^2+i\epsilon}\gamma_\nu S^{\mu\nu}(k,p,q)u(p)\,, \equiv 2\,i\,\widehat{m}_{\chi}\,c_L^{\widehat{\chi}}\,c_R^{\widehat{\chi}}\,\overline{u}(p+q)\,\mathcal{F}^{\widehat{\chi}}(p,q)\,u(p)\,, \tag{3.29}$$

where the function $\mathcal{F}^{\widehat{\chi}}(p,q)$ is defined so that it encodes the integration over the loop-momentum, the Lorentz structures and some factors. The leading term in the limit of $\widehat{m}_{\chi}\gg v$ reads

$$\mathcal{F}^{\widehat{\chi}}(p,q) = \frac{e}{(16\pi^2)v^2}(\gamma_\alpha\not{q}-q_\alpha)\,\varepsilon^\alpha(q)\,, \tag{3.30}$$

where $\varepsilon^\alpha(q)$ is the polarisation vector of the photon.

The relevant aspect here is the absence of $\widehat{m}_{\chi}$ in the leading term of the function $\mathcal{F}^{\widehat{\chi}}(p,q)$, which guarantees the cancellation mentioned above. Indeed, using the expressions for the couplings $c_{L,R}^{\widehat{\chi}}$ given by Equation (3.6),

$$c_L^{\widehat{N}_R}c_R^{\widehat{N}_R} = c_L^{\widehat{S}_R}c_R^{\widehat{S}_R} = -\frac{\widetilde{m}_N\widetilde{m}_R}{4\,\Lambda\,\widetilde{M}_\psi}\left[\frac{m_V+\widetilde{m}_{V'}}{\Lambda-\widetilde{M}_\psi}+\frac{m_V-\widetilde{m}_{V'}}{\Lambda+\widetilde{M}_\psi}\right], \qquad c_L^{\widehat{\psi}^0_L}c_R^{\widehat{\psi}^0_L} = c_L^{\widehat{\psi}^0_R}c_R^{\widehat{\psi}^0_R} = \frac{\widetilde{m}_N\widetilde{m}_R}{4\,\widetilde{M}_\psi^2}\left[\frac{m_V+\widetilde{m}_{V'}}{\Lambda-\widetilde{M}_\psi}+\frac{m_V-\widetilde{m}_{V'}}{\Lambda+\widetilde{M}_\psi}\right], \tag{3.31}$$

we find that the total CE contribution to the amplitude reads

$$\begin{aligned} i\mathcal{M}^{\rm CE} &= \sum_{\widehat{\chi}=\widehat{N}_R,\widehat{S}_R,\widehat{\psi}^0_L,\widehat{\psi}^0_R} i\mathcal{M}_{\widehat{\chi}}^{\rm CE}\\ &= -i\frac{\widetilde{m}_N\widetilde{m}_R}{2\widetilde{M}_\psi}\left[\frac{m_V+\widetilde{m}_{V'}}{\Lambda-\widetilde{M}_\psi}+\frac{m_V-\widetilde{m}_{V'}}{\Lambda+\widetilde{M}_\psi}\right]\overline{u}(p+q)\\ &\quad\times\left[\frac{\widehat{m}_{N_R}}{\Lambda}\mathcal{F}^{\widehat{N}_R}(p,q)+\frac{\widehat{m}_{S_R}}{\Lambda}\mathcal{F}^{\widehat{S}_R}(p,q)\right.\\ &\quad\left.-\frac{\widehat{m}_{\psi^0_L}}{\widetilde{M}_\psi}\mathcal{F}^{\widehat{\psi}^0_L}(p,q)-\frac{\widehat{m}_{\psi^0_R}}{\widetilde{M}_\psi}\mathcal{F}^{\widehat{\psi}^0_R}(p,q)\right]u(p)\,. \end{aligned} \tag{3.32}$$

Once taking the Leading-Order (LO) expression of the neutral heavy lepton masses as from Equation (2.11),

$$\widehat{m}_{N_R}=\widehat{m}_{S_R}\simeq\Lambda\,, \qquad\qquad \widehat{m}_{\psi^0_{L,R}}\simeq\widetilde{M}_\psi\,, \tag{3.33}$$

the terms in the last line of Equation (3.32) sum up to zero and thus the whole CE amplitude vanishes at LO.

All in all, at 1-loop the CE contribution to $\delta a_\mu^{\rm NP}$ arises only at the Next-to-Leading-Order (NLO) and it is suppressed by four powers of the heavy neutral masses:

$$\delta a_\mu^{\text{CE-1L}} = \frac{3\,m_\mu^{\rm exp}}{4\,\pi^2\,v^2}\frac{M_W^2}{\Lambda\widetilde{M}_\psi}\frac{\widetilde{m}_N\widetilde{m}_R}{\widetilde{M}_\psi}\left(\frac{m_V}{\widetilde{M}_\psi}+\frac{\widetilde{m}_{V'}}{\Lambda}\right)F_0\left(\frac{\Lambda^2}{M_W^2},\frac{\widetilde{M}_\psi^2}{M_W^2}\right) \tag{3.34}$$

where the loop function is defined by

$$F_0(x,y)\equiv\frac{3}{2}-\frac{x\log y-y\log x}{x-y}\,, \tag{3.35}$$

[4] According to the initial Lagrangian, these couplings are assumed to be purely real.

that is negative for $x, y \gg 1$.[5] Notice that Equation (3.34) and the one that will follow are given in terms of the tilde quantities in order to keep the expressions more compact.

It is worth commenting that, although the CE contribution from 2-loop diagrams does not present such a cancellation, it turns out to be smaller than the 20% of $\delta a_\mu^{\text{CE-1L}}$ in the considered parameter space. The dominant 2-loop CE contribution, $\delta a_\mu^{\text{CE-2L}}$, arises from a diagram similar to the one in the bottom in Figure 1 with the addition of a top-bottom-loop from which the photon is emitted, see Ref. [38]. A rough estimation reads

$$\delta a_\mu^{\text{CE-2L}} \approx -\frac{6\, y_t^2\, m_\mu^{\text{exp}}}{(16\pi^2)^2\, v^2}\, \frac{\widetilde{m}_N \widetilde{m}_R}{\widetilde{M}_\psi}\, \frac{\Lambda \widetilde{M}_\psi}{\widetilde{M}_\psi^2 - \Lambda^2} \left(\frac{m_V}{\widetilde{M}_\psi} + \frac{\widetilde{m}_{V'}}{\Lambda} \right) \log \frac{\widetilde{M}_\psi^2}{\Lambda^2}\,, \tag{3.38}$$

where $y_t = 0.81$ is the top quark Yukawa computed at the scale $\Lambda \sim \widetilde{M}_\psi$.

It is to be mentioned that our results agree (with the exception of what is mentioned in footnote) with those presented in the past literature[33–37,40] and in particular Refs. [38–40] focussed on the analysis of the cancellation present in the 1-loop CE contribution.

Chirally Suppressed (CS) Contributions: There are several CS contributions, besides the purely SM ones. We can identify a contribution from the h-mediated diagram, once combining the two vertices in the first line of Equation (3.4). Moreover, a similar contribution arises from the W-mediated diagram with the $\widehat{\psi}^0_{L,R}$ leptons in the loop, considering the vertices in the last two lines of Equation (3.6). In both of them, the chirality flip occurs due to a heavy lepton mass in the fermionic propagator, but the muon mass term is present in the vertex. Additional CS contributions arise again from the W-mediated diagram, but when the chirality flip is due to a muon Yukawa coupling in one of the muon external legs. This occurs due to the terms present in the first and last lines of Equation (3.6), when the same vertex appears twice in the diagram. The complete expression for the 1-loop CS contribution reads

$$\delta a_\mu^{\text{CS-1L}} = \frac{m_\mu^{\text{exp}}}{16\,\pi^2\, v^2} \times \left[-\frac{\widehat{m}_\mu \widetilde{m}_R^2}{\widetilde{M}_\psi^2} + \frac{2 m_\mu^{\text{exp}}}{3} \left(\left(5 + 2\cos 2\theta_W\right) \frac{\widetilde{m}_R^2}{\widetilde{M}_\psi^2} - \frac{3\,\widetilde{m}_N^2}{\Lambda^2} \right) \right], \tag{3.39}$$

where we distinguish the two kind of contributions described above: the one proportional to $m_\mu^{\text{exp}} \widehat{m}_\mu$ comes from the diagrams with the chirality flip due to the heavy lepton masses, while the one with $(m_\mu^{\text{exp}})^2$ from those with the chirality flip in the external muon legs.

If the tree-level contribution to the muon mass is the dominant one, $\widehat{m}_\mu \simeq m_\mu^{\text{exp}}$, it is possible to compute an upper bound for $\delta a_\mu^{\text{CS-1L}}$. Fixing $\widetilde{m}_R^2/\widetilde{M}_\psi^2$ to its maximal value allowed by Equation (3.10) and with $\widetilde{m}_N^2/\Lambda^2$ within the range given in Equation (3.16) for explaining the CFM II result for M_W, we get $|\delta a_\mu^{\text{CS-1L}}| \lesssim 8 \times 10^{-12}$, that is two orders of magnitudes smaller than necessary to explain the $(g-2)_\mu$ anomaly.

The full NP contribution to the $(g-2)_\mu$ is given by the sum of the different terms obtained in the previous paragraphs:

$$\delta a_\mu^{\text{NP}} = \delta a_\mu^{\text{CE-1L}} + \delta a_\mu^{\text{CE-2L}} + \delta a_\mu^{\text{CS-1L}}\,. \tag{3.40}$$

Figure 2 shows the dependence of δa_μ^{NP} on the heavy scales assuming a simplified parameter space with $\Lambda = \widetilde{M}_\psi$ and $\widehat{m}_\mu = m_\mu^{\text{exp}}$. The plots are for the effective couplings Y_V and $\widetilde{Y}_{V'}$, defined as $Y_V = \sqrt{2} m_V/v$ and $\widetilde{Y}_{V'} = \sqrt{2}\widetilde{m}_{V'}/v$, satisfying $Y_V = \widetilde{Y}_{V'} = 0.3$ for the plot on the left and 1 for the one on the right. In each plot, the upper part shows δa_μ^{NP} in red, while the experimental allowed region is depicted in green (yellow) at 1σ level (2σ). In the lower part, we show the ratio of each component, $\delta a_\mu^{\text{CE-1L}}$ in blue, $\delta a_\mu^{\text{CE-2L}}$ in cyan and $\delta a_\mu^{\text{CS-1L}}$ in magenta, to the total contribution δa_μ^{NP} as a function of $\Lambda = \widetilde{M}_\psi$. The width of the curves corresponds to the range of values given in Equation (3.16) within which $\widetilde{m}_N/\Lambda$ can vary. Moreover, in the whole parameter space, the condition in Equation (3.10) for $\widetilde{m}_R^2/\widetilde{M}_\psi^2$ is saturated together with the requirement that $|\widetilde{Y}_N| = \sqrt{2}|\widetilde{m}_N|/v$ and $|\widetilde{Y}_R| = \sqrt{2}|\widetilde{m}_R|/v$ are smaller than 1.

A few conclusions can be made. First of all, we can see that the CS contribution is always subdominant in the considered parameter space, as expected by having fixed $\widehat{m}_\mu = m_\mu^{\text{exp}}$. The CE contribution at two loops becomes relevant, although still subdominant, only for large values of the heavy scales. Moreover, we can identify the ballpark values for $Y_V = \widetilde{Y}_{V'}$ needed to explain the $(g-2)_\mu$ anomaly at the 2σ level: on one hand, $Y_V = \widetilde{Y}_{V'} = 1$ implies that the heavy masses should be as large as 2 TeV; on the other hand, smaller values imply lower heavy scales and the requirement that $\Lambda = \widetilde{M}_\psi \gtrsim 500$ GeV implies that $Y_V = \widetilde{Y}_{V'} \gtrsim 0.07$.

The parameter space can also be investigated after breaking the equality between the two heavy scales and/or the relation $Y_V = \widetilde{Y}_{V'}$. In **Figure 3**, we show δa_μ^{NP} as a function of the ratio $\Lambda/\widetilde{M}_\psi$. In the plot on the left, we fix $Y_V = \widetilde{Y}_{V'} = 0.3$ and we consider three values for $\widetilde{M}_\psi$ that span the same parameter space as the plots in Figure 2: $\widetilde{M}_\psi = 500$ GeV is shown in blue, $\widetilde{M}_\psi = 1000$ GeV in

[5] Our result differ from the one in Ref. [38], that reads:

$$\delta a_\mu^{\text{CE-1L}} = \frac{3\sqrt{2}\, m_\mu^{\text{exp}}}{4\,\pi^2\, v^2}\, \frac{M_W^2}{\Lambda \widetilde{M}_\psi}\, \frac{\widetilde{m}_N \widetilde{m}_R}{\widetilde{M}_\psi} \left(\frac{m_V}{\widetilde{M}_\psi} + \frac{\widetilde{m}_{V'}}{\Lambda} \right) F\left(\frac{\Lambda^2}{M_W^2}, \frac{\widetilde{M}_\psi^2}{M_W^2} \right), \tag{3.36}$$

where the loop function is defined by

$$F(x,y) \equiv \frac{x^3 y \log x}{(y-x)(x-1)^3} + \frac{y^3 x \log y}{(x-y)(y-1)^3} - \frac{xy(3xy - x - y - 1)}{2(x-1)^2(y-1)^2} > 0\,. \tag{3.37}$$

The $\sqrt{2}$ factor follows from the different definition of the value for v. More relevant is the loop-function: $F_0(x,y)$ coincides with the LO expansion of the function $F(x,y)$ for $x, y \gg 1$, besides the global minus sign. Our result is consistent with the analysis in Ref. [53].

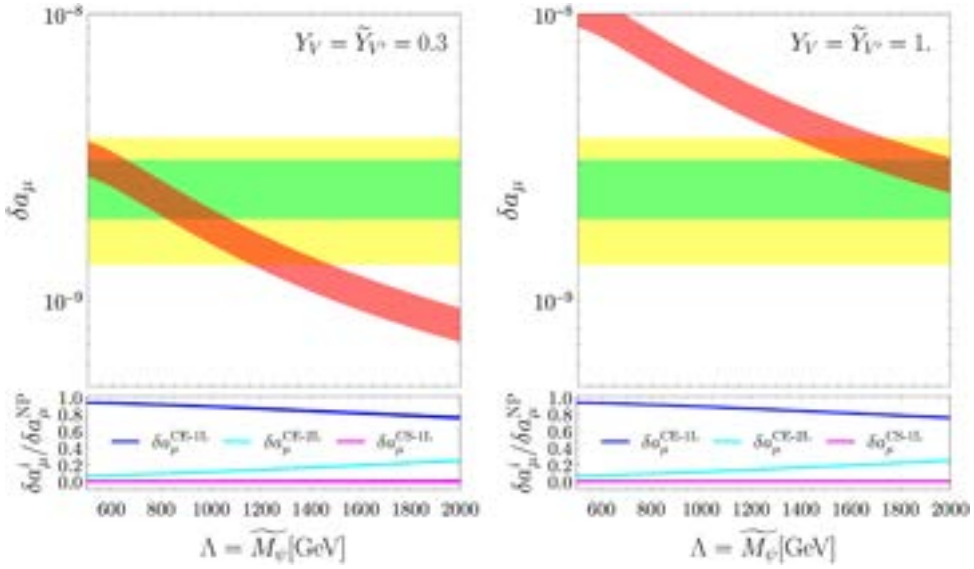

Figure 2. In the upper part of each plot, δa_μ^{NP} (red) is shown as a function of $\Lambda = \widetilde{M}_\psi$. The experimental values at 1σ (2σ) are shown in green (yellow). In the plots, $\widehat{m}_\mu = m_\mu^{exp}$, while $Y_V = \widetilde{Y}_{V'}$ are fixed to 0.3 in the left plot and to 1 in the right one. $\widetilde{m}_N/\Lambda$ can vary according to Equation (3.16), while $\widetilde{m}_R^2/\widetilde{M}_\psi^2$ is taken at its maximum value according to Equation (3.10), together with the requirement that $|\widetilde{Y}_N| \leq 1$ and $|\widetilde{Y}_R| \leq 1$. In the lower part of each plot, the ratios of the different components $\delta a_\mu^{CE\text{-}1L}$ (blue), $\delta a_\mu^{CE\text{-}2L}$ (cyan) and $\delta a_\mu^{CS\text{-}1L}$ (magenta), to the total contribution δa_μ^{NP} are shown.

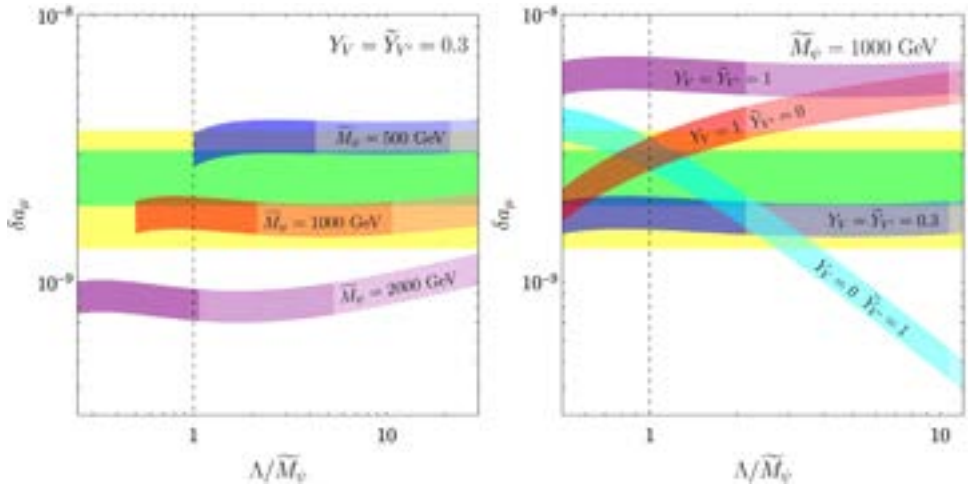

Figure 3. δa_μ^{NP} as a function of the ratio $\Lambda/\widetilde{M}_\psi$, fixing $\widehat{m}_\mu = m_\mu^{exp}$. On the right, $Y_V = \widetilde{Y}_{V'} = 0.3$, with $\widetilde{M}_\psi = 500$ GeV in blue, $\widetilde{M}_\psi = 1000$ GeV in red, $\widetilde{M}_\psi = 2000$ GeV in purple. On the left, $\widetilde{M}_\psi = 1000$ GeV, whith Y_V and $\widetilde{Y}_{V'}$ fixed to different values: $Y_V = \widetilde{Y}_{V'} = 1$ in purple, $Y_V = \widetilde{Y}_{V'} = 0.3$ in blue, $Y_V = 1$ and $\widetilde{Y}_{V'} = 0$ in red, and $Y_V = 0$ and $\widetilde{Y}_{V'} = 1$ in cyan. Within each band, the darkest coloured (intermediate) [lightest] region is for $|\widetilde{Y}_N| < 1$ ($1 < |\widetilde{Y}_N| < 5$) [$|\widetilde{Y}_N| > 5$]. $\widetilde{m}_N/\Lambda$ can vary according to Equation (3.16), while $\widetilde{m}_R^2/\widetilde{M}_\psi^2$ saturates Equation (3.10). The experimentally allowed values at 1σ (2σ) are shown in green (yellow). The dashed vertical line guides the eye for the ratio equal to 1.

red and $\widetilde{M}_\psi = 2000$ GeV in purple. The condition $\Lambda \geq 500$ GeV leads to a sharp cut on the left-hand side of the coloured regions; $\widetilde{m}_N/\Lambda$ can vary according to Equation (3.16) and is responsible for the width of the bands; $\widetilde{m}_R^2/\widetilde{M}_\psi^2$ saturates Equation (3.10); finally, while $\widetilde{Y}_R$ is always smaller than 1 in the whole parameter space, the opacity of the colours indicates the value of $\widetilde{Y}_N$, that is dark (intermediate) [light] for $|\widetilde{Y}_N| < 1$ ($1 < |\widetilde{Y}_N| < 5$) [$|\widetilde{Y}_N| > 5$].

The plot on the right shows complementary information. $\widetilde{M}_\psi$ is fixed to the reference value of 1000 GeV and the different curves show different combinations of Y_V and $\widetilde{Y}_{V'}$: $Y_V = \widetilde{Y}_{V'} = 1$ in purple, $Y_V = \widetilde{Y}_{V'} = 0.3$ in blue, $Y_V = 1$ and $\widetilde{Y}_{V'} = 0$ in red and $Y_V = 0$ and $\widetilde{Y}_{V'} = 1$ in cyan. The same conditions on Λ, $\widetilde{m}_N/\Lambda$, $\widetilde{m}_R^2/\widetilde{M}_\psi^2$, and $\widetilde{Y}_N$ described for the plot on the left apply also here.

The main message following from the two plots is that the parameter space is large and there are many different combinations of parameters for which we can solve the muon MDM anomaly. However, the parameters need to be correlated. This feature and also the role of the constraints following from the simultaneous explanation of the M_W anomaly and precision electroweak fits can be better understood by looking at the qualita-

tive features of the δa_μ contributions. Focussing on the CE ones that are dominant in the considered parameter space, the dependence on the six parameters (Λ, $\widetilde{M}_\psi$, $\widetilde{m}_N$, $\widetilde{m}_R$, m_V, $\widetilde{m}_{V'}$) is to a good approximation a dependence on their three combinations. First of all, for the CE contribution at 1 loop, varying Λ and $\widetilde{M}_\psi$ within [500, 2000] GeV, the function $F_0(x, y)$ appearing in Equation (3.34) spans a very narrow range of value, $-[1.5, 4]$. Taking $F_0(x, y) = -2.5$ in the whole parameter space, the expression in Equation (3.34) reads:

$$\delta a_\mu^{\text{CE-1L}} \simeq -\left(2\times 10^{-3}\ \text{GeV}\right)\left[\frac{\widetilde{m}_N}{\Lambda}\right]\left[\frac{\widetilde{m}_R}{\widetilde{M}_\psi}\right]\frac{1}{\widetilde{M}_\psi}\left(\frac{m_V}{\widetilde{M}_\psi}+\frac{\widetilde{m}_{V'}}{\Lambda}\right), \tag{3.41}$$

where the ratio in the first bracket is constrained by the CDF II measurement of M_W, Equation (3.16), and the ratio in the second bracket is bounded by Equation(3.10). It follows that $\delta a_\mu^{\text{CE-1L}}$ effectively depends on only three parameters, that is $\widetilde{M}_\psi$ and the two ratios $m_V/\widetilde{M}_\psi$ and $\widetilde{m}_{V'}/\Lambda$. We can proceed in a similar way for the CE contribution at 2 loops and we notice that varying Λ and $\widetilde{M}_\psi$ still within [500, 2000] GeV, the combination $\Lambda^2\log(\widetilde{M}_\psi^2/\Lambda^2)/(\widetilde{M}_\psi^2-\Lambda^2)$ spans a very small range of values [0.18, 3]. Fixing it at 1.5, Equation (3.38) reads

$$\delta a_\mu^{\text{CE-2L}} \approx -\left(4\times 10^{-10}\ \text{GeV}^{-1}\right)\left[\frac{\widetilde{m}_N}{\Lambda}\right]\left[\frac{\widetilde{m}_R}{\widetilde{M}_\psi}\right]\widetilde{M}_\psi\left(\frac{m_V}{\widetilde{M}_\psi}+\frac{\widetilde{m}_{V'}}{\Lambda}\right). \tag{3.42}$$

We can use these simplified expressions to easily estimate that $\delta a_\mu^{\text{CE-2L}}$ is always subdominant with respect to $\delta a_\mu^{\text{CE-1L}}$ in the whole considered parameter space $\widetilde{M}_\psi$ vs. Λ. Moreover, taking $\widetilde{m}_N^2/\Lambda^2$ as in Equation (3.16) and $\widetilde{m}_R^2/\widetilde{M}_\psi^2$ at its largest value in Equation (3.10), for fixed values of $\widetilde{M}_\psi$, the region where the experimental measurement for the muon MDM is reproduced reduces to an anti-diagonal straight strip in the parameter space $m_V/\widetilde{M}_\psi$ vs. $\widetilde{m}_{V'}/\Lambda$. Changing the value of $\widetilde{M}_\psi$ simply translates into moving this strip in the plane, maintaining however the slop. This is shown in the plot in **Figure 4**. The two shaded regions represent different values of $\widetilde{M}_\psi$, that is 500 GeV in blue and 2000 GeV in purple, such that δa_μ matches the experimental measurement at 1σ. The intensity of the colours indicate the value of the Yukawa coupling Y_V, which is smaller than 1 for the darkest colour, in the range [1, 5] for the intermediate colour, and larger than 5 for the lightest colour: notice that for $\widetilde{M}_\psi = 500$ GeV and 2000 GeV, $|\widetilde{Y}_N|$ is never larger than 5 in the shown parameter space. The width of the strips corresponds to $\widetilde{m}_N/\Lambda$ varying in the range given by Equation (3.16). Commenting on the signs of $\widetilde{m}_N$ and $\widetilde{m}_R$, the two blue and purple strips correspond to the case with opposite defined signs for the two parameters; instead, if the product $\widetilde{m}_N\,\widetilde{m}_R$ would be positive, then the two coloured strips would appear in the bottom-left part of the plane, symmetric with respect to the origin of the coordinate system.

Notice that, as only an upper bound on $\widetilde{m}_R/\widetilde{M}_\psi$ is provided by the current data, one may consider smaller values of this ratio. This would imply wider regions in the $m_V/\widetilde{M}_\psi$ vs. $\widetilde{m}_{V'}/\Lambda$ parameter space: for fixed values of $\widetilde{M}_\psi$, reducing $|\widetilde{m}_R/\widetilde{M}_\psi|$ translates into larger values for $|Y_V|$ and $|Y_{V'}|$, that can possibly be restricted by the perturbativity requirement on these Yukawa couplings.

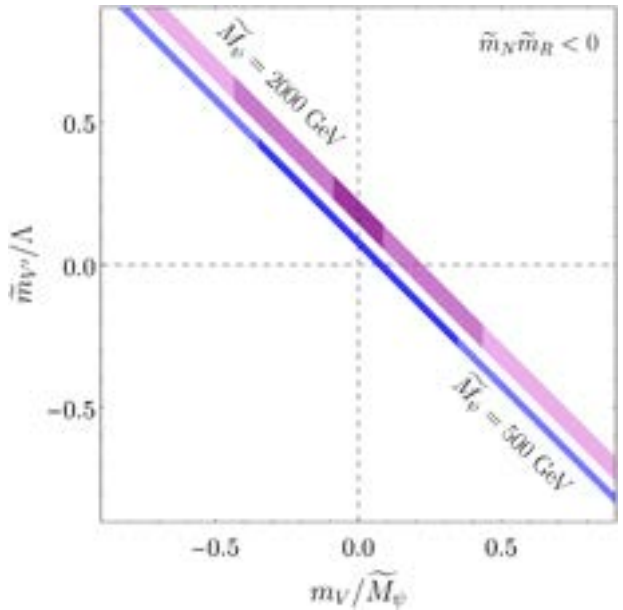

Figure 4. The parameter space $m_V/\widetilde{M}_\psi$ vs. $\widetilde{m}_{V'}/\Lambda$ which gives δa_μ within its 1σ error range, for $\widetilde{m}_N\,\widetilde{m}_R < 0$. The shaded regions correspond to $\widetilde{M}_\psi = 500$ GeV in blue and $\widetilde{M}_\psi = 2000$ GeV in purple. The width of the strips is determined by $\widetilde{m}_N^2/\Lambda^2$ in the range given in Equation (3.16). For the purple band, the darkest (intermediate) [lightest] coloured region is for $|\widetilde{Y}_N| < 1$ ($1 < |\widetilde{Y}_N| < 5$) [$|\widetilde{Y}_N| > 5$], while for the blue one the dark (light) coloured region is for $|\widetilde{Y}_N| < 1$ ($1 < |\widetilde{Y}_N| < 5$) and $|\widetilde{Y}_N|$ is never larger than 5.

If in the future, deviations from the SM model predictions will be found such that a lower bound for $|\widetilde{m}_R/\widetilde{M}_\psi|$ can be fixed, then the correlation between the three (combination of) parameters entering Figure 4 will be uniquely determined. This is possible in this model because $\widetilde{m}_N^2/\Lambda^2$ spans a reduced range of values in order to reproduce the CDF II measurement on M_W.

Muon mass

The diagrams in Figure 1, after removing the photon leg, represent contributions to the muon mass at 1-loop. The absence of the photon, however, has an important consequence: the cancellation present in the CE contribution at 1-loop to δa_μ^{NP} is now absent. Indeed, the muon mass correction reads exactly as Equation (3.28), but with the $\mathcal{S}^{\mu\nu}(k, p)$ function that now encodes only the W-propagator. The amplitude is divergent and dependent on the heavy-fermion mass in the loop. Writing the amplitude as in Equation (3.29), we have to replace the $\mathcal{F}^{\hat{\chi}}(p, q)$ function by a new one $\mathcal{G}^{\hat{\chi}}(p)$ that reads

$$\mathcal{G}^{\hat{\chi}}(p) = -\frac{1}{(16\pi^2)}\frac{\widehat{m}_\chi^2}{v^2}\left[1+\log\left(\frac{\mu_{\text{Ren}}^2}{\widehat{m}_\chi^2}\right)\right], \tag{3.43}$$

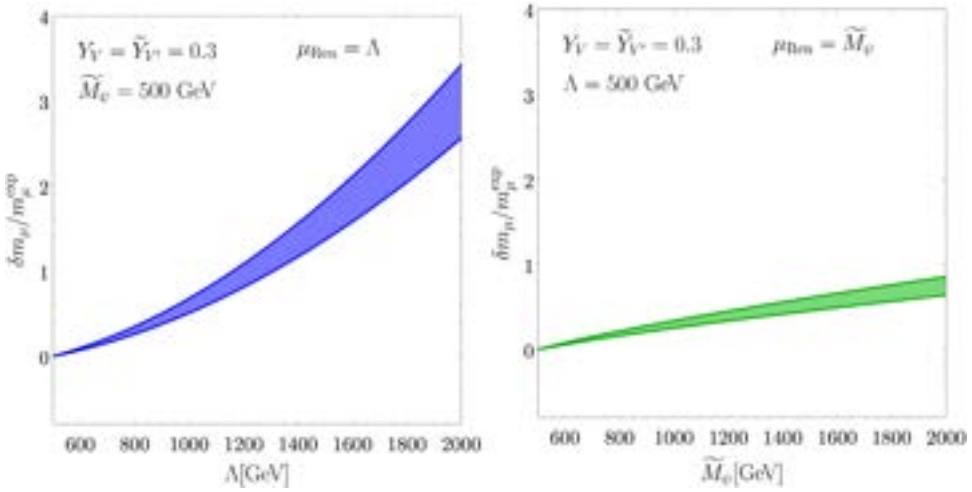

Figure 5. Dependence of δm_μ on Λ ($\widetilde{M}_\psi$) on the left (right), fixing $\widetilde{M}_\psi = 500$ GeV ($\Lambda = 500$ GeV) and the running scale $\mu_{\rm Ren} = \Lambda$ ($\mu_{\rm Ren} = \widetilde{M}_\psi$). Y_V and $\widetilde{Y}_{V'}$ have been taken both equal to 0.3. The width of the bands corresponds to $\widetilde{m}_N^2/\Lambda^2$ within the range in Equation (3.16). $\widetilde{m}_R^2/\widetilde{M}_\psi^2$ has been fixed to the largest value in Equation (3.10) and $\widetilde{m}_N \widetilde{m}_R < 0$.

valid in the limit of $\widehat{m}_\chi \gg v$, where $\mu_{\rm Ren}$ stands for the renormalisation scale in the $\overline{MS}$ scheme. [6]

Summing up all the terms as in Equation (3.32), no cancellation, in general, can take place due to the presence of the mass dependence and the log in the $\mathcal{G}^{\hat{\chi}}(p)$ functions. The final result for the dominant 1-loop contribution at the LO to the muon mass reads

$$\delta m_\mu = -\frac{\widetilde{m}_N \widetilde{m}_R \Lambda}{8\pi^2 v^2}\left(\frac{m_V}{\widetilde{M}_\psi} + \frac{\widetilde{m}_{V'}}{\Lambda}\right) \times \left[1 + \frac{1}{\widetilde{M}_\psi^2 - \Lambda^2}\left(\widetilde{M}_\psi^2 \log\frac{\mu_{\rm Ren}^2}{\widetilde{M}_\psi^2} - \Lambda^2 \log\frac{\mu_{\rm Ren}^2}{\Lambda^2}\right)\right], \quad (3.44)$$

The left plots in **Figure 5** estimates the dependence of $\delta m_\mu / m_\mu^{\rm exp}$ on Λ having fixed $\widetilde{M}_\psi = 500$ GeV and the running scale such that $\mu_{\rm Ren} = \Lambda$. In the right plot, the role of Λ and $\widetilde{M}_\psi$ are interchanged. As we can see, for the considered simplified choice of the parameters, $|\delta m_\mu|$ increases and, for $\widetilde{M}_\psi = 500$ GeV, it can be even larger than the experimental value of the muon mass, at larger values of the masses of the heavy leptons. Choosing $\mu_{\rm Ren}$ to coincide with the largest scale among $\widetilde{M}_\psi$ and Λ reduces the impact of the higher loop-level contributions.

Interestingly, in the limit $\mu_{\rm Ren} = \widetilde{M}_\psi = \Lambda$, the term in the squared brackets vanishes at leading order: Equation (3.43) trivially shows that the log-dependent term is identically zero as far as the renormalisation scale coincides with the mass of the exotic fermion; however, even the constant term does not lead to any contributions at leading order once $\widetilde{M}_\psi = \Lambda$ and the reason can be understood repeating the analysis done for the muon $g-2$ in Equations (3.29)-(3.33), substituting $\mathcal{F}^{\hat{\chi}}(p,q)$ with $\mathcal{G}^{\hat{\chi}}(p)$. This can be more explicitly appreciated considering the gauge boson couplings to fermions in the limit $\widetilde{M}_\psi = \Lambda$, reported in App. A: at the expansion order considered, the singlet and the doublet exotic fields couples to the elementary muon fields exactly in the same way, except for a global sign.

We can simplify the expression in Equation (3.44) in the same line as we did for the muon MDM: varying Λ and $\widetilde{M}_\psi$ within [500, 2000] GeV and taking the renormalisation scale equal to the largest among Λ and $\widetilde{M}_\psi$, we get

$$\delta m_\mu \simeq -[0, 0.7] \times \left[\frac{\widetilde{m}_N}{\Lambda}\right]\left[\frac{\widetilde{m}_R}{\widetilde{M}_\psi}\right]\widetilde{M}_\psi\left(\frac{m_V}{\widetilde{M}_\psi} + \frac{\widetilde{m}_{V'}}{\Lambda}\right). \quad (3.45)$$

Given the similarity of the expressions for the CE contributions of the δa_μ and δm_μ, it is useful to combine δm_μ and $\delta a_\mu^{\rm CE}$ in a single formula, using the exact expressions in Equations (3.34), (3.38) and (3.44), we get

$$\frac{\delta a_\mu^{\text{CE-1L}}}{\delta m_\mu} = -\frac{6\, m_\mu^{\rm exp} M_W^2}{\Lambda^2 \widetilde{M}_\psi^2} F_0\left(\frac{\Lambda^2}{M_W^2}, \frac{\widetilde{M}_\psi^2}{M_W^2}\right) \times \left[1 + \frac{1}{\widetilde{M}_\psi^2 - \Lambda^2}\left(\widetilde{M}_\psi^2 \log\frac{\mu_{\rm Ren}^2}{\widetilde{M}_\psi^2} - \Lambda^2 \log\frac{\mu_{\rm Ren}^2}{\Lambda^2}\right)\right]^{-1}$$

$$\frac{\delta a_\mu^{\text{CE-2L}}}{\delta m_\mu} = \frac{3\, y_t^2}{16\pi^2}\frac{m_\mu^{\rm exp}}{\widetilde{M}_\psi^2 - \Lambda^2}\log\frac{\widetilde{M}_\psi^2}{\Lambda^2} \times \left[1 + \frac{1}{\widetilde{M}_\psi^2 - \Lambda^2}\left(\widetilde{M}_\psi^2 \log\frac{\mu_{\rm Ren}^2}{\widetilde{M}_\psi^2} - \Lambda^2 \log\frac{\mu_{\rm Ren}^2}{\Lambda^2}\right)\right]^{-1}, \quad (3.46)$$

that hold whenever $\delta m_\mu \neq 0$. When instead δm_μ vanishes, that is whenever $\mu_{\rm Ren} = \widetilde{M}_\psi = \Lambda$, there is no correlation between these two quantities and δa_μ can fit the corresponding experimental

[6] As our model is renormalisable, $\mu_{\rm Ren}$ is the renormalisation scale. On the contrary, $\mu_{\rm Ren}$ represents the physical cut-off in Ref. [38].

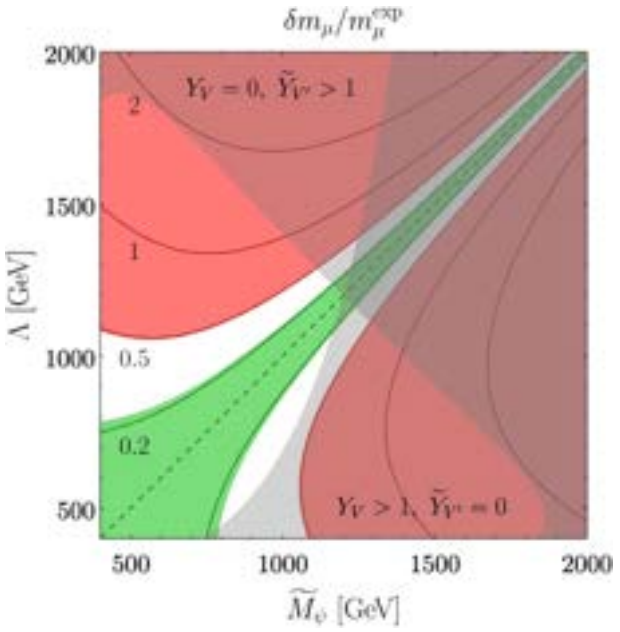

Figure 6. $\delta m_\mu/m_\mu^{\rm exp}$ in the parameter space of $\widetilde{M}_\psi$ *vs.* Λ. The black curves represent the value of the ratio $\delta m_\mu/m_\mu^{\rm exp}$, with the dashed one referring to the case when it is vanishing. In the whole parameter space, δa_μ coincides with the corresponding experimental central value. The green region is when the loop-level contribution to the muon mass is smaller than the tree-level one by the 30%, while the white one is when it is larger than the 30% but still smaller than the tree-level one. Finally, the red region, instead, is when the loop-level contribution is larger than the tree-level one. The two grey regions provide an intuition of when $|Y_V|$ and $|\widetilde{Y}_{V'}|$ get larger than 1, but still smaller than 5.

value although no quantum correction to the muon mass is present at 1-loop and at LO.

Figure 6 illustrates the parameter space of $\widetilde{M}_\psi$ *vs.* Λ when δa_μ coincides with the corresponding experimental central value, with the black curves showing the values of the ratio $\delta m_\mu/m_\mu^{\rm exp}$. The plot has been obtained using the complete expressions in Equations (3.34), (3.38) and (3.44), fixing the renormalisation scale $\mu_{\rm Ren}$ equal to the largest among Λ and $\widetilde{M}_\psi$. The colours describe the relationship between the tree-level and the loop-level contributions to the muon mass: the loop contribution is larger than the tree-level one in the red area, while it is smaller than the 50% (30%) of the tree-level one in the white (green) one. To draw these conditions, in each point of the parameter space, the value of the tree-level contribution is fixed by the requirement that

$$\widehat{m}_\mu = m_\mu^{(2\ \rm TeV)} - \delta m_\mu\,, \tag{3.47}$$

where $m_\mu^{(2\ \rm TeV)} = 103.62$ MeV is the value of the muon mass at 2 TeV, obtained performing the RG running from the M_Z scale up to 2 TeV within the SM (see Ref. [54] for the values at the scale M_Z and for example Ref. [55] for the RG running within the SM). In grey, we indicate the regions where $1 < |Y_V| < 5$ with $\widetilde{Y}_{V'} = 0$, or $1 < |\widetilde{Y}_{V'}| < 5$ with $Y_V = 0$.

All in all, in the whole considered parameter space, the correct value of the muon $(g-2)$ is achieved without the necessity of an unnaturally large cancellation between tree- and loop-level contributions to the muon mass.

4. Discussion on the Three-Generation Extension

This section discusses the main features of considering the three generations of leptons as in the SM.

A very economical solution in terms of number of both fields and parameters would still consider the NP part of the spectrum as in the one-generation model considered in the previous sections. Not introducing any additional symmetry, the couplings between exotic and the SM fields are in general promoted to vectors and matrices in the flavour space: in particular, Y_e would be a 3×3 matrix, while Y_N, Y_S, Y_R and M_L would be tridimensional vectors. The attractive aspect of this setup is the possibility to correctly describe the pattern of lepton masses and mixings: as first shown in Ref. [56], with only one N_R and one S_R, it is possible to uniquely determine the structure of the Dirac Yukawa vectors in order to describe the PMNS mixing matrix and a neutrino spectrum (with both mass ordering) with the lightest neutrino being massless. As now also the electron couplings would be modified, the LFU ratios, which impose strong bounds in the one-generation model, would simply lead to the condition that electron and muon couplings to the W gauge boson should be very similar to each other. The solution to explain the CDF II measurement of M_W would be in the same ballpark as in the one-generation model – actually, it would change by a factor 2.

Regarding the computations for the MDMs, no relevant change is expected, as indeed the cancellation in the CE contribution at LO would still occur and therefore the associated phenomenology discussed in the one-generation model would still hold.

The main drawback of this simple and elegant scenario is the presence of flavour-changing neutral currents. The exotic fermions would be flavour blind and therefore the same diagrams that contribute to the lepton MDM would also contribute to the radiative lepton decay, with the same dependence on the parameters – the cancellation occurring in the 1L-CE contributions would also occur for this flavour changing processes. The net result is that $\mu \to e\gamma$ would completely exclude the parameter space interesting for the δa_μ solution.

A second possibility is that the NP part of the spectrum is extended so that there are three replicas of the fields considered in the one-generation construction. In this scenario the number of parameters would be largely increased as most of the parameters appearing in Equation (2.1) would be promoted to be 3×3 matrices in the flavour space. The expectation is that all the observables may be fitted but at the price of a very weak predictive power.

The latter possibility is certainly not economical in terms of number of fields and parameters. A radical improvement in predictivity can be obtained e.g. by implementing the family lepton number as a good symmetry of the Lagrangian, broken by the Majorana terms that may also be responsible for introducing the lepton mixings. Each exotic generation would then interact only with one SM lepton generation and the Lagrangian in Equation (2.1) would simply be repeated three times. Each sector would have its own parameters and therefore the possibility of correlations between observables involving different flavours is strongly unlikely. The bottom line is that the three sectors could then be

treated independently. A less radical but very interesting possibility is to extend the horizontal symmetries invoked to explain the pattern of fermion masses and mixings to the NP part of the spectrum. Thus, there exist a variety of potential generalisations to three generations to explore.

5. Concluding Remarks

The new measurement of the W gauge boson mass from the CDF II collaboration, if confirmed, is still another indication of physics beyond the Standard Model. It is an intriguing possibility to explain this deviation in frameworks that describe massive light active neutrinos: this is the case of the Low-Scale Seesaw constructions where the sterile lepton species may live at the TeV scale and then possibly be produced and detected at colliders. Even more fascinating would be to explain within the same framework a long-standing anomaly typically associated with low-energy physics, that is the tension between the theoretical prediction and the experimental determination of the muon anomalous magnetic moment. In this paper, we provide a proof of concept that such a construction can indeed be realised.

We focus on a renormalisable one-generation scenario, extending the Standard Model spectrum with two additional sterile species and one pair of vector-like lepton $SU(2)_L$-doublets that interact only with the muon and the muonic neutrino. We have studied the parameter space of the model pointing out that we can solve the M_W and $(g-2)_\mu$ anomalies at the 2σ level together with reproducing the light active neutrino mass scale, without any relevant fine-tuning. This is achieved for exotic lepton masses in the range [0.5, 2] TeV, smaller than the scale naively expected in the effective field theory description. This is due to an accidental cancellation occurring between different contributions at 1-loop to the $(g-2)_\mu$. This cancellation has been discussed in the lepton flavour basis in Refs. [38–40], with the aim of understanding if an underlying explanation would be present. We have analysed it instead in the lepton mass basis and we concluded that it simply follows from the peculiarity of the couplings of the muon with the exotic states – see Equation (3.31): this is the direct consequence of the chosen spectrum and of the Standard Model gauge symmetry invariance. With respect to the past literature, besides the analysis of the $(g-2)_\mu$ discussed above, focusing in a different part of the parameter space, we explain for the first time in this context the lightness of the active neutrinos and the new measurement from the CDF II collaboration of the M_W mass.

We have also discussed the possible extensions to the three-generation case. The minimal scenario, without any additional new fields in the spectrum beyond the ones already considered, preserves the positive features of the one-generation construction and avoids the strong bounds from the observed lepton flavour universality (see the ratios in Equation (3.19)). However, as the exotic fields are flavour-blind, radiative lepton decays rule it out. A realistic three-generation model requires an extension of the exotic spectrum. An interesting possibility to explore is to impose a flavour symmetry on the spectrum so that the predictivity of such models is preserved. The appeal of such frameworks would also be associated with the future direct searches of new physics at colliders, where the exotic leptons may be produced and detected, confirming or ruling them out.

Appendix A: Degenerate Heavy Fermions

In the limit $\Lambda \approx \widetilde{M}_\psi$ the heavy fermions are almost degenerate. In such case, many of the couplings presented in the main discussion seem to suffer from a divergence of the type $(\Lambda - \widetilde{M}_\psi)^{-1}$. Such divergence is an artifact and the corresponding case must be treated separately to cure it. In such section, we show how the interaction Lagrangian of Equations (3.4), (3.5), and (3.6) looks like in such limit. Such results must be used whenever $v/|\Lambda - \widetilde{M}_\psi| \gtrsim 1$.

As this assumption has consequences only on the neutral sector, we will focus on it. The masses are now given by

$$\begin{aligned}
\widehat{m}_\nu &= \frac{\mu\,\widetilde{m}_N^2}{\Lambda^2} - \frac{2\,\epsilon\,\widetilde{m}_N\,m_S\cos\theta}{\Lambda}\,,\\
\widehat{m}_{N_R} &= \Lambda + \frac{m_V + \widetilde{m}_{V'}}{2}\,,\\
\widehat{m}_{S_R} &= \Lambda - \frac{m_V + \widetilde{m}_{V'}}{2}\,,\\
\widehat{m}_{\psi_L^0} &= \Lambda - \frac{m_V + \widetilde{m}_{V'}}{2}\,,\\
\widehat{m}_{\psi_R^0} &= \Lambda + \frac{m_V + \widetilde{m}_{V'}}{2}\,,
\end{aligned} \tag{A.1}$$

where we have shown the leading and next-to-leading order for each mass. As can be seen, the splitting between the masses increases and now depends on m_V and $\widetilde{m}_{V'}$.

Again, as this phenomenology arises only in the neutral sector, we will omit interactions among two charged fields. The mixing degenerate Lagrangian then reads

$$\mathscr{L}_h^{\rm deg} \supset -\frac{h}{v}\left\{-\frac{\widetilde{m}_N}{2}\,\overline{\widehat{\nu}_L}\,\frac{\widehat{N}_R + i\widehat{S}_R - \widehat{\psi}_L^{0c} - i\widehat{\psi}_R^0}{2} + \text{h.c.}\right\}, \tag{A.2}$$

$$\mathscr{L}_Z^{\rm deg} \supset -\frac{\sqrt{g_L^2+g_Y^2}}{2}\,Z_\mu\left\{-\frac{\widetilde{m}_N}{\Lambda}\,\overline{\widehat{\nu}_L}\gamma^\mu\,\frac{\widehat{N}_R^c + i\widehat{S}_R^c - \widehat{\psi}_L^0 - i\widehat{\psi_R^{0c}}}{2} + \text{h.c.}\right\}, \tag{A.3}$$

$$\begin{aligned}
\mathscr{L}_W^{\rm deg} \supset -\frac{g_L}{\sqrt{2}}\,W_\mu^-\Bigg\{&-\frac{\widetilde{m}_N}{\Lambda}\,\overline{\mu_L}\gamma^\mu\,\frac{\widehat{N}_R^c + i\widehat{S}_R^c - \widehat{\psi}_L^0 - i\widehat{\psi}_R^{0c}}{2}\\
&+\frac{\widetilde{m}_R}{\Lambda}\,\overline{\widehat{\mu}_R}\gamma^\mu\,\frac{\widehat{N}_R - i\widehat{S}_R + \widehat{\psi}_L^{0c} - i\widehat{\psi}_R^0}{2}\Bigg\},
\end{aligned} \tag{A.4}$$

where we have written only the leading-order terms for each coupling.

Acknowledgements

The authors are grateful to E. Fernández-Martínez, F. Feruglio, G. Guedes, K. Harigaya and D.M. Straub for useful discussions. A.d.G. and L.M. thanks the Institute of Theoretical Physics and the Faculty of Physics of the University of Warsaw for hospitality during the development of this project. S.P. thanks the Institute of Theoretical Physics of the

Universidad Autónoma de Madrid for hospitality during the development of this project. A.d.G. and L.M. acknowledge partial financial support by the Spanish Research Agency (Agencia Estatal de Investigación) through the grant IFT Centro de Excelencia Severo Ochoa No CEX2020-001007-S and by the grant PID2019-108892RB-I00 funded by MCIN/AEI/10.13039/501100011033, by the European Union's Horizon 2020 research and innovation programme under the Marie Skłodowska-Curie grant agreement No 860881-HIDDeN. The research of S.P. has received partial financial support by the Polish Science Centre (NCN), grant DEC-2016/23/G/ST2/04301

Conflict Of Interest

The authors have declared no conflict of interest.

Data Availability Statement

Data sharing is not applicable to this article as no new data were created or analyzed in this study.

Keywords

hep, g-2, Neutrinos, W-Boson, Seesaw

Received: January 23, 2023
Revised: January 23, 2023

[1] ATLAS Collaboration, G. Aad, et al., *Phys. Lett. B* **2012**, *716*, 1. [arXiv:1207.7214].
[2] CMS Collaboration, S. Chatrchyan, et al., *Phys. Lett. B* **2012**, *716*, 30. [arXiv:1207.7235].
[3] CDF Collaboration, T. Aaltonen, et al., *Science* **2022**, *376*, 170.
[4] J. Kersten, A. Y. Smirnov, *Phys. Rev. D* **2007**, *76*, 073005. [arXiv:0705.3221].
[5] A. Abada, C. Biggio, F. Bonnet, M. B. Gavela, T. Hambye, *JHEP* **2007**, *12*, 061. [arXiv:0707.4058].
[6] M. Blennow, P. Coloma, E. Fernandez-Martinez, M. Gonzalez-Lopez, *Phys. Rev. D* **2022**, *106*, 073005. [arXiv:2204.04559].
[7] F. Arias-Aragon, E. Fernandez-Martinez, M. Gonzalez-Lopez, L. Merlo, *JHEP* **2022**, *09*, 210. [arXiv:2204.04672].
[8] D. Wyler, L. Wolfenstein, Massless Neutrinos in Left-Right Symmetric Models, *Nucl. Phys. B* **1983**, *218*, 205.
[9] R. N. Mohapatra, J. W. F. Valle, *Phys. Rev. D* **1986**, *34*, 1642.
[10] J. Bernabeu, A. Santamaria, J. Vidal, A. Mendez, J. W. F. Valle, *Phys. Lett. B* **1987**, *187*, 303.
[11] M. Malinsky, J. C. Romao, J. W. F. Valle, *Phys. Rev. Lett.* **2005**, *95*, 161801. [arXiv:hep-ph/0506296].
[12] I. Esteban, M. C. Gonzalez-Garcia, M. Maltoni, T. Schwetz, A. Zhou, *JHEP* **2020**, *09*, 178. [arXiv:2007.14792].
[13] P. Minkowski, *Phys. Lett. B* **1977**, *67*, 421.
[14] M. Gell-Mann, P. Ramond, R. Slansky, *Conf. Proc. C* **1979**, *790927*, 315. [arXiv:1306.4669].
[15] T. Yanagida, Horizontal gauge symmetry and masses of neutrinos, *C.P.C* **1979**, *7902131*, 95.
[16] R. N. Mohapatra, G. Senjanovic, *Phys. Rev. Lett.* **1980**, *44*, 912.
[17] P. Langacker, D. London, *Phys. Rev. D* **1988**, *38*, 886.
[18] S. Antusch, C. Biggio, E. Fernandez-Martinez, M. B. Gavela, J. Lopez-Pavon, *JHEP* **2006**, *10*, 084. [arXiv:hep-ph/0607020].
[19] S. Antusch, O. Fischer, *JHEP* **2014**, *10*, 094. [arXiv:1407.6607].
[20] E. Fernandez-Martinez, J. Hernandez-Garcia, J. Lopez-Pavon, *JHEP* **2016**, *08*, 033. [arXiv:1605.08774].
[21] UTfit Collaboration, M. Bona, et al., *New UTfit Analysis of the Unitarity Triangle in the Cabibbo-Kobayashi-Maskawa scheme*, [arXiv:2212.03894].
[22] Muon {\it g}-2 Collaboration, G. W. Bennett, et al., *Phys. Rev. D* **2006**, *73*, 072003. [hep-ex/0602035].
[23] Muon {\it g}-2 Collaboration, B. Abi, et al., *Phys. Rev. Lett.* **2021**, *126*, 141801. [arXiv:2104.03281].
[24] T. Aoyama, et al., *Phys. Rept.* **2020**, *887*, 1. [arXiv:2006.04822].
[25] S. Borsanyi, et al., *Nature* **2021**, *593*, 51. [arXiv:2002.12347].
[26] M. Ce, et al., *Window observable for the hadronic vacuum polarization contribution to the muon $g-2$ from lattice QCD*, [arXiv:2206.06582].
[27] C. Alexandrou, et al., *Lattice Calculation of the Short and Intermediate Time-Distance Hadronic Vacuum Polarization Contributions to the Muon Magnetic Moment Using Twisted-Mass Fermions*, [arXiv:2206.15084].
[28] P. Athron, A. Fowlie, C.-T. Lu, L. Wu, Y. Wu, B. Zhu, The W boson Mass and Muon $g-2$: Hadronic Uncertainties or New Physics?, [arXiv:2204.03996].
[29] A. Crivellin, M. Hoferichter, C. A. Manzari, M. Montull, *Phys. Rev. Lett.* **2020**, *125*, 091801. [arXiv:2003.04886].
[30] A. Keshavarzi, W. J. Marciano, M. Passera, A. Sirlin, *Phys. Rev. D* **2020**, *102*, 033002. [arXiv:2006.12666].
[31] B. Malaescu, M. Schott, *Eur. Phys. J. C* **2021**, *81*, 46. [arXiv:2008.08107].
[32] G. Colangelo, M. Hoferichter, P. Stoffer, *Phys. Lett. B* **2021**, *814*, 136073. [arXiv:2010.07943].
[33] K. Kannike, M. Raidal, D. M. Straub, A. Strumia, *JHEP* **2012**, *02*, 106. [arXiv:1111.2551]. [Erratum: JHEP 2012, 10, 136].
[34] R. Dermisek, A. Raval, *Phys. Rev. D* **2013**, *88*, 013017. [arXiv:1305.3522].
[35] G. Arcadi, L. Calibbi, M. Fedele, F. Mescia, *Phys. Rev. Lett.* **2021**, *127*, 061802, [arXiv:2104.03228].
[36] C.-T. Lu, R. Ramos, Y.-L. S. Tsai, *JHEP* **2021**, *08*, 073. [arXiv:2104.04503].
[37] G. Guedes, P. Olgoso, *JHEP* **2022**, *09*, 181. [arXiv:2205.04480].
[38] N. Arkani-Hamed, K. Harigaya, *JHEP* **2021**, *09*, 025. [arXiv:2106.01373].
[39] N. Craig, I. G. Garcia, A. Vainshtein, Z. Zhang, *JHEP* **2022**, *05*, 079. [arXiv:2112.05770].
[40] L. Delle Rose, B. von Harling, A. Pomarol, *JHEP* **2022**, *05*, 120. [arXiv:2201.10572].
[41] ATLAS Collaboration, G. Aad, et al., *Phys. Rev. D* **2020**, *101*, 012002, [arXiv:1909.02845].
[42] CMS Collaboration, A. M. Sirunyan, et al., *Eur. Phys. J. C* **2019**, *79*, 421. [arXiv:1809.10733].
[43] ATLAS Collaboration, G. Aad, et al., *Phys. Lett. B* **2021**, *812*, 135980. [arXiv:2007.07830].
[44] CMS Collaboration, A. M. Sirunyan, et al., *JHEP* **2021**, *01*, 148. [arXiv:2009.04363].
[45] J. Alonso-Gonzalez, A. de Giorgi, L. Merlo, S. Pokorski, *JHEP* **2022**, *05*, 041. [arXiv:2109.07490].
[46] H. Bahl, E. Fuchs, S. Heinemeyer, J. Katzy, M. Menen, K. Peters, M. Saimpert, G. Weiglein, *Eur. Phys. J. C* **2022**, *82*, 604. [arXiv:2202.11753].
[47] J. Brod, J. M. Cornell, D. Skodras, E. Stamou, *JHEP* **2022**, *08*, 294. [arXiv:2203.03736].
[48] V. Breso-Pla, A. Falkowski, M. Gonzalez-Alonso, *JHEP* **2021**, *08*, 021. [arXiv:2103.12074].
[49] Particle Data Group Collaboration, R. L. Workman, *PTEP* **2022**, *2022*, 083C01.
[50] P. Janot, S. Jadach, *Phys. Lett. B* **2020**, *803*, 135319. [arXiv:1912.02067].

[51] D. Bryman, V. Cirigliano, A. Crivellin, G. Inguglia, *Testing Lepton Flavor Universality with Pion, Kaon, Tau, and Beta Decays*, [arXiv:2111.05338].
[52] A. M. Abdullahi, et al., The Present and Future Status of Heavy Neutral Leptons. in *2022 Snowmass Summer Study*, **2022**, *3*. [arXiv:2203.08039].
[53] A. Freitas, J. Lykken, S. Kell, S. Westhoff, *JHEP* **2014**, *05*, 145. [arXiv:1402.7065]. [Erratum: JHEP 2014, 09, 155].
[54] G.-y. Huang, S. Zhou, *Phys. Rev. D* **2021**, *103*, 016010, [arXiv:2009.04851].
[55] H. Arason, D. J. Castano, B. Keszthelyi, S. Mikaelian, E. J. Piard, P. Ramond, B. D. Wright, *Phys. Rev. D* **1992**, *46*, 3945.
[56] M. B. Gavela, T. Hambye, D. Hernandez, P. Hernandez, *JHEP* **2009**, *09*, 038. [arXiv:0906.1461].

IFT-UAM/CSIC-23-17

GeV ALP from TeV Vector-like Leptons

Arturo de Giorgi [*], **Marta Fuentes Zamoro** [†], and **Luca Merlo** [‡],

Departamento de Física Teórica and Instituto de Física Teórica UAM/CSIC, Universidad Autónoma de Madrid, Cantoblanco, 28049, Madrid, Spain

Abstract

The generation of a mass for an axion-like-particle is a long-standing open issue. We propose a model where a GeV mass for this pseudo-scalar particle is predicted in a large portion of the parameter space due to the presence of explicit Peccei-Quinn symmetry-breaking terms in an exotic leptonic sector. The latter provides a solution to the muon $g-2$ anomaly, within the framework of the Linear Seesaw neutrino mechanism. The spectrum is extended by a complex scalar singlet only transforming under the Peccei-Quinn symmetry, which generates the axion-like-particle. Its couplings with fermions can continuously span over many orders of magnitude, which constitutes a specific feature of this model in contrast to generic ultraviolet constructions.

[*] arturo.degiorgi@uam.es
[†] marta.zamoro@uam.es
[‡] luca.merlo@uam.es

Contents

1 Introduction

Axions and the more general axion-like-particles (ALPs) are undergoing a revival of interest in these last years. The axion solution to the Strong CP problem consists in the possibility of redefining away the so-called QCD-θ parameter and, in the original formulations of the late 1970s [1–3], is associated to a global Abelian symmetry - the Peccei-Quinn (PQ) $U(1)_{\rm PQ}$, whose spontaneous breaking gives rise to a Goldstone boson (GB), dubbed as axion, a. For this solution to work, the PQ symmetry should be anomalous with QCD and, as a result, a non-perturbative mass m_a for the axion is generated, being inversely proportional to its decay constant f_a, such that $m_a\, f_a \sim 0.01$ GeV^2. For almost four decades, QCD axion models [1–7] were restricted to a very tiny strip in the m_a *vs.* f_a parameter space. However, very much recently [8–17], it has been shown that the relation between m_a and f_a can be relaxed, while still solving the Strong CP problem. This represents a turning point in axion physics, providing strong support towards collider searches for not-so-light pseudo-scalars, commonly referred to as ALPs.

The definition of an ALP in the literature is not unique and here we will consider it as a pseudo-scalar with (dominant) derivative couplings, whose mass is not necessarily associated with any non-perturbative QCD effect. According to the new theoretical results mentioned above, it may or may not be associated with a solution to the Strong CP problem. In the literature, there are many examples of ALPs: associated to flavour dynamics [18–23] or neutrino mass generation [24–26]; appearing in composite Higgs models [27–30], supersymmetric contexts [31] or in string theories [32–36]; even as Dark Matter

candidates [37–42], or playing a role in cosmological observables [43–54]. Given the existence of so many different contexts in which an ALP arises, part of the community committed itself to the development of an Effective Field Theory (EFT) description encoding the generic ALP features. Following the seminal work in Ref. [55], several studies appeared defining the ALP effective Lagrangian [56–65] in order to investigate possible signals at low-energy facilities [66–76] and colliders [58, 77–95].

In contrast to the QCD axion, whose mass is generated through non-perturbative effects, the ALP mass is typically taken as a free parameter. Only a few studies are present discussing the possible origin of the ALP mass and only identifying the ALP as the Majoron [24–26], that is the Goldstone boson arising from the spontaneous breaking of the Lepton number (LN). Such a mass may be originated by the explicit breaking of the LN, either via Planck-suppressed operators [96, 97] or within specific frameworks that deal with the active neutrino mass generation mechanism [98–101]. Very recently, Ref. [101] discussed the possibility of giving the Majoron a mass in the range $m_a \subset [1,\ 10^5]$ keV in a specific Type-I Seesaw context, but at the price of a relatively large f_a scale, $f_a \subset [10^8,\ 10^{12}]$ GeV. This is obtained under the assumption of only one source of LN explicit breaking responsible at the same time for the active neutrino masses and the Majoron mass.

In this paper, we present a framework where an ALP, not being a Majoron, acquires a mass in a very small range of values around $\mathcal{O}(1-10)$ GeV for $f_a \in [0.5,\ 100]$ TeV (prior to considering other phenomenological constraints). Interestingly, the relatively smallness of the ALP decay constant f_a opens up the possibility of a direct search of this exotic state at colliders and flavour facilities. One difference with respect to the context described in Ref. [101] is the presence of an exotic vector-like lepton field transforming as a doublet of $SU(2)_L$ gauge symmetry, owing an explicit PQ symmetry breaking coupling. Although similar results may be obtained with exotic fields transforming under other representations of the electroweak (EW) symmetry, the setup under consideration with an exotic doublet has been recently shown to be extremely appealing, being able to explain the long-standing anomaly in the muon anomalous magnetic moment [102–106]. The $(g-2)_\mu$ is currently at the centre of controversies due to contrasting results in its theoretical prediction with different methods (more on this in Sect. 3). Despite this, it offers a challenging benchmark for phenomenology and model-building.

Refs. [107–109] entered into details of a very specific feature of the framework with an additional exotic vector-like lepton field: the dominant (chirally enhanced) contribution to the $(g-2)_\mu$ at 1−loop arises suppressed by the fourth power of the exotic masses, instead of their square as generically expected. More recently, Ref. [110] explored the possibility of merging the solution to the $(g-2)_\mu$ anomaly with the description of active neutrino masses within the same context, through the Low-Scale Seesaw mechanism [111, 112]. Finally, it is important to note that the non-unitarity of the PMNS matrix induced in this setup leads to possible deviations of the mass of the W gauge boson [22, 113], as also discussed in Ref. [110] with respect to the recent CDF II result [114].

Along the lines of Refs. [107–110], we will consider a simplified one-generation scenario involving only the second lepton generation, adding to the fermion spectrum two right-handed (RH) lepton singlets and a vector-like sibling of the SM lepton EW doublet. We will refer to all the neutral exotic states as Heavy Neutral Leptons (HNLs). From this

point of view, it serves as a proof of concept of how a realistic three-generation model could work. Furthermore, besides the SM gauge symmetries, the LN assignments allow to accommodate the Linear Seesaw (LSS) mechanism [115] and the Lagrangian is made invariant under a PQ symmetry by means of a singlet complex scalar, only transforming under the $U(1)_{\rm PQ}$, whose spontaneous breaking gives rise to the ALP. The exotic fields have an interaction term that explicitly breaks the PQ symmetry, leading to a mass for the ALP induced at 1-loop, but that does respect the LN at any radiative order. Indeed, the charge assignments under the Abelian symmetries are such that the LN remains exact after the spontaneous and explicit PQ breaking: LN gets only broken explicitly by the traditional terms of the LSS mechanism. On the other hand, for the charged sector, the muon does not have any tree-level mass contribution, being the SM Yukawa interaction forbidden by the PQ symmetry. The muon receives a mass only at 1-loop and is mediated by the exotic leptons.

The combination of the exotic neutral singlets and lepton doublet leads to the specific suppressed contributions to the $(g-2)_\mu$ already mentioned above, while, on the contrary, neither the ALP nor the radial component of the PQ scalar field contribute to it. A correlation between the contributions to the muon mass and those to the $(g-2)_\mu$ follows, as already pointed out in Ref. [107]. On the other hand, the ALP as well as the HNLs may give signals at colliders and flavour facilities, although a three-generation model would be necessary for a consistent analysis.

As an additional specific feature of the construction presented in this paper, the ALP-muon coupling spans continuously over various orders of magnitude, from $\ll \mathcal{O}(1)/f_a$ to $\mathcal{O}(1)/f_a$. This occurrence is unusual because the naive estimate for the ALP-muon coupling in a given model is typically either $\ll \mathcal{O}(1)/f_a$ or $\mathcal{O}(1)/f_a$, but it cannot continuously vary across different orders of magnitude. Our model serves as a proof-of-concept for the existence of models exhibiting this particular feature.

The structure of the paper can be read out in the table of Contents.

2 The model description

The specific spectrum considered includes the scalar and gauge sector of the SM and its second-generation leptons, assuming that the other fermions are present and with the SM interactions. This guarantees the gauge anomaly cancellation and the consistency of the theory while introducing modifications to the muon and the muonic neutrino, whose phenomenology will be discussed. Besides the left-handed (LH) EW lepton doublet $\ell_L \equiv (\nu_{\mu L},\, \mu_L)^T$ and the right-handed (RH) muon singlet, μ_R, two RH neutrinos, N_R and S_R, and a vector-like EW lepton doublet, ψ, are introduced. So far, this is the same spectrum considered in Refs. [107–110]. However, we further extend the particle content by adding, on top of the SM Higgs H, a complex scalar field ϕ, singlet under the SM gauge symmetries.

The whole Lagrangian of the model can be divided into three pieces: the canonical kinetic terms of all the fields, the scalar potential and the mass Lagrangian. The latter is the focus of this section and determines the relevant phenomenology to discuss in this paper, but a few comments on the potential are in order. At the renormalisable level, we can distinguish between pure SM couplings, pure ϕ ones and mixed interactions. The

first two are responsible for the spontaneous breaking of the EW and PQ symmetries, while the last one is a source of dangerous contributions to the pure Higgs terms. Indeed, once the scalar singlet gets a vacuum expectation value (VEV), the mixed interaction $\lambda_{H\phi} H^\dagger H \phi^* \phi$ corrects the squared Higgs term. This contribution can be suppressed only with a small coupling $\lambda_{H\phi}$. On the other side, the Higgs parameters receive loop corrections not only from the SM fields but also from the new exotic fermions that, being the heaviest, will provide the largest contributions. This is nothing more than the well-known Higgs Hierarchy problem that we will not attempt to solve, simply assuming that the Higgs and the ϕ scalars develop VEVs at the EW scale $v = 246$ GeV and at $f_a > v$, respectively. In the unitary gauge,

$$H = \frac{v+h}{\sqrt{2}} \begin{pmatrix} 0 \\ 1 \end{pmatrix}, \qquad \phi = \frac{f_a + \rho_a}{\sqrt{2}} e^{ia/f_a}, \tag{2.1}$$

where h is the physical Higgs, ρ_a the radial component of the singlet ϕ, and a its angular component to be identified with the ALP. Notice that f_a represents here both the VEV of ϕ and the ALP decay constant, guaranteeing canonical kinetic terms for the ALP.

Besides the smallness of the mixed quartic coupling, we will further assume that the pure ϕ scalar potential is such that the radial component ρ_a achieves a mass sufficiently larger than f_a to disentangle it from the low-energy Lagrangian and neglect its impact at low-energies. We will comment, however, on how it would affect the main aspects of our phenomenological analysis, showing that it would not have any relevant impact on the $(g-2)_\mu$, even if relatively light.

Regarding the part of the Lagrangian responsible for giving masses to the second SM lepton generation and the exotic leptons, we will assume the following expression

$$\begin{aligned} -\mathscr{L}_Y = \; & Y_N \overline{\ell_L} \widetilde{H} N_R + Y_R \overline{\psi_L} H \mu_R + \\ & + \delta_{x,0} \Lambda \overline{N_R^c} S_R + \delta_{|x|,1} \alpha_N \phi^{(*)} \overline{N_R^c} S_R + \delta_{y,0} M_\psi \overline{\psi_L} \psi_R + \delta_{|y|,1} \alpha_\psi \phi^{(*)} \overline{\psi_L} \psi_R + \\ & + Y_V \overline{S_R^c} \widetilde{H}^\dagger \psi_R + Y_{V'} \overline{\psi_L} \widetilde{H} N_R + \epsilon Y_S \overline{\ell_L} \widetilde{H} S_R + \text{h.c.}, \end{aligned} \tag{2.2}$$

where $\widetilde{H} \equiv i\sigma_2 H$, being σ_2 the second Pauli matrix, and $\delta_{i,j}$ is the Kronecker delta. The quantities Y_N, Y_R, Y_V, $Y_{V'}$, Y_S, α_N and α_ψ are dimensionless parameters and Λ and M_ψ are instead masses. On the other hand, x and y are variables that can only acquire three values, either 0 or ± 1, distinguishing in this way different realisations. For example, the two terms containing the bilinear $\overline{N_R^c} S_R$ cannot be present simultaneously: the idea is that for symmetry reasons this bilinear appears proportional either to the scale Λ or to the product $\alpha_N \phi$ or $\alpha_N \phi^*$, corresponding respectively to $x = 0,\, 1,\, -1$. Similarly for y and the $\overline{\psi_L} \psi_R$-term. Finally, ϵ is a small parameter and is responsible for the active neutrino mass *à la* LSS mechanism.

The Lagrangian described above, neglecting the last line of Eq. (2.2), shows the following symmetries,

$$\Big[SU(2)_L \times U(1)_Y \Big]_{\text{gauge}} \times \Big[U(1)_{\text{LN}} \times U(1)_{\text{PQ}} \Big]_{\text{global}}, \tag{2.3}$$

and the transformation properties of the fields are listed in Tab. 1. Notice that the invariance under the PQ symmetry implies that only two terms in the second line of Eq. (2.2) are allowed, depending on the explicit charges of the fields: one among the terms proportional to x, and one among those proportional to y.

	$SU(2)_L$	$U(1)_Y$	$U(1)_L$	$U(1)_{\rm PQ}$
ℓ_L	**2**	$-1/2$	1	n_{N_R}
μ_R	1	-1	1	n_{ψ_L}
H	**2**	$1/2$	0	0
N_R	1	0	1	n_{N_R}
S_R	1	0	-1	n_{S_R}
ψ_L	**2**	$-1/2$	1	n_{ψ_L}
ψ_R	**2**	$-1/2$	1	n_{ψ_R}
ϕ	1	0	0	n_ϕ

Table 1: *Transformation properties of the SM leptons ℓ_L and μ_R, the Higgs doublet H, the HNLs N_R and S_R, the vector-like EW lepton doublet ψ and the scalar ϕ under $SU(2)_L \times U(1)_Y \times U(1)_{LN} \times U(1)_{PQ}$. The PQ charges of ℓ_L and μ_R have been written in terms of the others according to the first line of the Lagrangian in Eq. (2.2).*

The PQ charges of S_R and ψ_R are not arbitrary but can be written in terms of the other charges after fixing the values of the variables x, and y:

$$\begin{cases} x = 0 \implies n_{S_R} = -n_{N_R} \\ x = 1 \implies n_{S_R} = -n_{N_R} - n_\phi \\ x = -1 \implies n_{S_R} = -n_{N_R} + n_\phi \\ \hline y = 0 \implies n_{\psi_R} = n_{\psi_L} \\ y = 1 \implies n_{\psi_R} = n_{\psi_L} - n_\phi \\ y = -1 \implies n_{\psi_R} = n_{\psi_L} + n_\phi \end{cases} \tag{2.4}$$

The different combinations of possible values for n_{S_R} and n_{ψ_R} give rise to nine different models, that however do not lead to nine distinct phenomenologies. In particular, one of the realisations matches the one discussed in Ref. [110], that is the option with $x = 0 = y$, corresponding to the case with the scalar ϕ not coupling to any fermion. In this case, the interactions proportional to Y_V and $Y_{V'}$ have to be allowed in the Lagrangian to solve the $(g-2)_\mu$ anomaly, and this leads to $n_{N_R} = n_{\psi_R}$. As a result, the two Abelian symmetries coincide and the only explicit breaking is the one associated with ϵY_S that provides a mass to the active neutrino. In the end, the ALP would not couple to any particle and therefore it would be secluded in a dark sector, without taking part in the visible phenomenology. Notice that in this case the traditional tree-level muon Yukawa can be written in the Lagrangian as well as a tree-level mixing between the SM lepton doublet and the exotic one, that is $M_L \overline{\ell_L} \psi_R$. These tree-level terms have been considered in Ref. [110], where the impact of the arbitrary large-scale M_L has been studied.

Focusing instead on the cases where the scalar singlet, with PQ charge $n_\phi \neq 0$, does couple to the leptons, we can identify four models with distinct phenomenological features, differing only in the type of terms in the second line of Eq. (2.2). All in all, we can characterise them in terms of the PQ charges of n_{S_R} and n_{ψ_R}.

Model A: The values of the variables are $(x, y) = (\pm 1, 0)$, such that $n_{\psi_R} = n_{\psi_L}$ and there are two possible choices for the PQ charge assignment of S_R, $n_{S_R} = -n_{N_R} \mp n_\phi$, corresponding to the following Lagrangian,

$$\begin{aligned} -\mathscr{L}_Y^{\mathrm{A}} = \; & Y_N \overline{\ell_L} \widetilde{H} N_R + Y_R \overline{\psi_L} H \mu_R + \alpha_N \phi^{(*)} \overline{N_R^c} S_R + M_\psi \overline{\psi_L} \psi_R + \\ & + Y_V \overline{S_R^c} \widetilde{H}^\dagger \psi_R + Y_V' \overline{\psi_L} \widetilde{H} N_R + \epsilon Y_S \overline{\ell_L} \widetilde{H} S_R + \text{h.c.}\,. \end{aligned} \tag{2.5}$$

Model B: The values of the variables are $(x, y) = (0, \pm 1)$, corresponding to $n_{S_R} = -n_{N_R}$ and two alternatives are possible for the PQ charge assignment of ψ_R, $n_{\psi_R} = n_{\psi_L} \mp n_\phi$. The resulting Lagrangian reads

$$\begin{aligned} -\mathscr{L}_Y^{\mathrm{B}} = \; & Y_N \overline{\ell_L} \widetilde{H} N_R + Y_R \overline{\psi_L} H \mu_R + \Lambda \overline{N_R^c} S_R + \alpha_\psi \phi^{(*)} \overline{\psi_L} \psi_R + \\ & + Y_V \overline{S_R^c} \widetilde{H}^\dagger \psi_R + Y_V' \overline{\psi_L} \widetilde{H} N_R + \epsilon Y_S \overline{\ell_L} \widetilde{H} S_R + \text{h.c.}\,. \end{aligned} \tag{2.6}$$

Model C: The values of the variables are $(x, y) = (1, 1)$ or $(x, y) = (-1, -1)$, such that there are no direct masses, but instead Yukawa-like interactions with the insertion of either only ϕ in the two terms or only ϕ^*. The associate Lagrangian is given by

$$\begin{aligned} -\mathscr{L}_Y^{\mathrm{C}} = \; & Y_N \overline{\ell_L} \widetilde{H} N_R + Y_R \overline{\psi_L} H \mu_R + \alpha_N \phi^{(*)} \overline{N_R^c} S_R + \alpha_\psi \phi^{(*)} \overline{\psi_L} \psi_R + \\ & + Y_V \overline{S_R^c} \widetilde{H}^\dagger \psi_R + Y_V' \overline{\psi_L} \widetilde{H} N_R + \epsilon Y_S \overline{\ell_L} \widetilde{H} S_R + \text{h.c.}\,. \end{aligned} \tag{2.7}$$

Model D: This realisation is very similar to the previous one, but with either $(x, y) = (1, -1)$ or $(x, y) = (-1, 1)$, corresponding to Yukawa-like terms obtained inserting ϕ and ϕ^*, such that both of them are simultaneously present in the Lagrangian. The Lagrangian associated to $(x, y) = (1, -1)$ is then

$$\begin{aligned} -\mathscr{L}_Y^{\mathrm{D}} = \; & Y_N \overline{\ell_L} \widetilde{H} N_R + Y_R \overline{\psi_L} H \mu_R + \alpha_N \phi \overline{N_R^c} S_R + \alpha_\psi \phi^* \overline{\psi_L} \psi_R + \\ & + Y_V \overline{S_R^c} \widetilde{H}^\dagger \psi_R + Y_V' \overline{\psi_L} \widetilde{H} N_R + \epsilon Y_S \overline{\ell_L} \widetilde{H} S_R + \text{h.c.}\,, \end{aligned} \tag{2.8}$$

while the one associated to $(x, y) = (-1, 1)$ is obtained simply interchanging ϕ with ϕ^*. We will see that this difference with respect to Model C has a deep impact on the corresponding phenomenology.

While we determined the symmetries and the Abelian charge assignments looking only at the terms in the first line of the Lagrangian densities above, we still have to discuss the impact of the terms proportional to Y_V, $Y_{V'}$ and Y_S. The first two are trivially invariant under LN, while the last one represents an explicit LN breaking. We thus expect a mass for the active neutrino proportional to ϵY_S.[1]

[1] Alternatively, one could keep a more general approach, without fixing the LN charges equal to ± 1. Doing so, it would turn out that a neutrino mass is originated only if the terms proportional to Y_N and ϵY_S are both non-vanishing.

On the other hand, the terms proportional to Y_V, $Y_{V'}$ and Y_S represent possible sources of explicit PQ symmetry breaking, depending on the specific choice of the PQ charges. It is interesting to further investigate the conditions that lead to this breaking as they would directly tell whether a mass for the ALP is expected or not without performing any explicit computation. We can use the technique of the spurions to make these terms formally PQ invariant: it consists in promoting Y_V, $Y_{V'}$ and Y_S to non-dynamical fields with transformation properties under $U(1)_{\rm PQ}$, such that

$$n_{Y_V} = -n_{\psi_R} - n_{S_R}\,, \qquad n_{Y_{V'}} = n_{\psi_L} - n_{N_R}\,, \qquad n_{Y_S} = n_{N_R} - n_{S_R}\,. \tag{2.9}$$

For each model, *if there is a PQ charge assignment such that* $n_{Y_V}, n_{Y_{V'}}, n_{Y_S} = 0$*, then the corresponding term is not explicitly breaking* $U(1)_{PQ}$. This is easy to compute considering the conditions on n_{S_R} and n_{ψ_R} that characterise each construction. We find:

$$\begin{cases} \text{Model A:} \implies & n_{Y_V} = -n_{Y_{V'}} \pm n_\phi & n_{Y_S} = 2n_{N_R} \pm n_\phi \\ \text{Model B:} \implies & n_{Y_V} = -n_{Y_{V'}} \pm n_\phi & n_{Y_S} = 2n_{N_R} \\ \text{Model C:} \implies & n_{Y_V} = -n_{Y_{V'}} \pm 2n_\phi & n_{Y_S} = 2n_{N_R} \pm n_\phi \\ \text{Model D:} \implies & n_{Y_V} = -n_{Y_{V'}} & n_{Y_S} = 2n_{N_R} \pm n_\phi\,, \end{cases} \tag{2.10}$$

where the signs in front of n_ϕ are not arbitrary and correspond to the specific Lagrangian densities in Eqs. (2.5)–(2.8).

First of all, for Models A, C and D, there is the possibility to fix $n_{N_R} = \mp n_\phi/2 \neq 0$ and then $n_{Y_S} = 0$. For Model B, this same result can also be achieved, but for $n_{N_R} = 0 = n_{S_R}$. As a result, for all the models, the term proportional to Y_S never explicitly breaks the PQ symmetry and therefore it does not lead to any contribution to the ALP mass.

The discussion on n_{Y_V} and $n_{Y_{V'}}$ is slightly more involved. Starting for simplicity with Model D, choosing $n_{\psi_L} = n_{N_R}$ then $n_{Y_V} = 0 = n_{Y_{V'}}$ and thus there is no source at all of PQ explicit breaking and the ALP would remain exactly massless at any loop order.
For Models A, B, and C, we have to distinguish between having both Y_V and $Y_{V'}$ different from zero and when one and only one of the two is vanishing. In the latter case, it is always possible to find a PQ charge assignment such that the spurion charge of the surviving term is zero: it follows that the only would-be-PQ explicit breaking term actually preserves the symmetry and thus the ALP remains massless. On the contrary, when $Y_V \neq 0 \neq Y_{V'}$, it is never possible to have $n_{Y_V} = 0 = n_{Y_{V'}}$ at the same time and therefore the ALP would acquire a mass. This condition implies that a massive ALP only arises if $n_{\psi_R} \neq -n_{S_R}$ and $n_{\psi_L} \neq n_{N_R}$.

All in all, we may expect a massive ALP only in Models A, B and C, whose mass is necessarily proportional to the product of the two parameters $Y_V\, Y_{V'}$ *and the two mass scales of the HNLs, i.e.*

$$m_a^2 \propto Y_V Y_{V'} \Lambda M_\psi\,, \tag{2.11}$$

where Λ and M_ψ can be dynamically generated, i.e. $\Lambda = \alpha_N f_a/\sqrt{2}$ and $M_\psi = \alpha_\psi f_a/\sqrt{2}$.

2.1 Lepton mass Lagrangian

Before moving to the determination of the ALP mass and interactions, we discuss the lepton masses following a very similar notation to Ref. [110]. Once the Higgs and the scalar singlet, always present in the four considered models, get a VEV, the mass Lagrangian for the neutral and charged sectors reads

$$-\mathscr{L}_Y \supset \frac{1}{2}\overline{\chi}\mathcal{M}_\chi\chi^c + \overline{\zeta_L}\mathcal{M}_\zeta\zeta_R + \text{h.c.}\,, \tag{2.12}$$

where we defined the neutral lepton multiplet χ and the charged one ζ as

$$\chi \equiv (\nu_L, N_R^c, S_R^c, \psi_L^0, \psi_R^{0\,c})^T, \qquad \zeta \equiv (\mu, \psi^-)^T\,, \tag{2.13}$$

and the charge conjugation operation is defined by $N_R^c \equiv \mathcal{C}\overline{N_R}^T$ with $\mathcal{C}$ being the charge conjugation matrix. The mass matrices $\mathcal{M}_\chi$ and $\mathcal{M}_\zeta$ read

$$\mathcal{M}_\chi = \begin{pmatrix} 0 & m_N & \epsilon m_S & 0 & 0 \\ m_N & 0 & \Lambda & m_{V'} & 0 \\ \epsilon m_S & \Lambda & 0 & 0 & m_V \\ 0 & m_{V'} & 0 & 0 & M_\psi \\ 0 & 0 & m_V & M_\psi & 0 \end{pmatrix}, \quad \mathcal{M}_\zeta = \begin{pmatrix} 0 & 0 \\ m_R & M_\psi \end{pmatrix}, \tag{2.14}$$

where $m_X \equiv Y_X v/\sqrt{2}$ and, with an abuse of notation, M_ψ stands either for the direct Lagrangian mass M_ψ in model A or for $\alpha_\psi f_a/\sqrt{2}$ in models B, C, and D, and similarly for Λ in the corresponding models.

The neutral mass matrix $\mathcal{M}_\chi$ is very similar to the one in Ref. [110]: they coincide in the limit of vanishing M_L and μ terms, that are the direct mass term $M_L\overline{\ell_L}\psi_R$ already discussed previously and the traditional explicit Lepton number breaking term usually associated to the Inverse Seesaw mechanism, $\mu\overline{S_R^c}S_R$. The mass eigenvalues and eigenvectors can simply be taken from that reference fixing $M_L = 0$ and $\mu = 0$:

$$\begin{aligned} \widehat{m}_\nu &= -\frac{2\,\epsilon\, m_N\, m_S}{\Lambda}\,, \\ \widehat{m}_{N_R} &= \Lambda + \frac{m_N^2}{2\Lambda} + \frac{1}{4}\left[\frac{(m_V + m_{V'})^2}{\Lambda - M_\psi} + \frac{(m_V - m_{V'})^2}{\Lambda + M_\psi}\right], \\ \widehat{m}_{S_R} &= \Lambda + \frac{m_N^2}{2\Lambda} + \frac{1}{4}\left[\frac{(m_V + m_{V'})^2}{\Lambda - M_\psi} + \frac{(m_V - m_{V'})^2}{\Lambda + M_\psi}\right], \\ \widehat{m}_{\psi^0} &= M_\psi - \frac{1}{4}\left[\frac{(m_V + m_{V'})^2}{\Lambda - M_\psi} - \frac{(m_V - m_{V'})^2}{\Lambda + M_\psi}\right], \end{aligned} \tag{2.15}$$

and

$$\widehat{\chi}: \begin{cases} \widehat{\nu}_L = \nu_L - \dfrac{m_N}{\Lambda} S_R^c \,, \\ \widehat{N}_R = \dfrac{N_R + S_R}{\sqrt{2}} + \dfrac{m_N}{\sqrt{2}\Lambda}\nu_L^c + \dfrac{1}{2}\left[\dfrac{m_V + m_{V'}}{\Lambda - M_\psi}\dfrac{\psi_L^{0c} + \psi_R^0}{\sqrt{2}} - \dfrac{m_V - m_{V'}}{\Lambda + M_\psi}\dfrac{\psi_L^{0c} - \psi_R^0}{\sqrt{2}}\right] , \\ \widehat{S}_R = i\left\{-\dfrac{N_R - S_R}{\sqrt{2}} + \dfrac{m_N}{\sqrt{2}\Lambda}\nu_L^c - \dfrac{1}{2}\left[\dfrac{m_V - m_{V'}}{\Lambda + M_\psi}\dfrac{\psi_L^{0c} + \psi_R^0}{\sqrt{2}} - \dfrac{m_V + m_{V'}}{\Lambda - M_\psi}\dfrac{\psi_L^{0c} - \psi_R^0}{\sqrt{2}}\right]\right\} , \\ \widehat{\psi}_L^0 = \dfrac{\psi_L^0 + \psi_R^{0c}}{\sqrt{2}} - \dfrac{1}{2}\left[\dfrac{m_V + m_{V'}}{\Lambda - M_\psi}\dfrac{N_R^c + S_R^c}{\sqrt{2}} + \dfrac{m_V - m_{V'}}{\Lambda + M_\psi}\dfrac{N_R^c - S_R^c}{\sqrt{2}}\right] , \\ \widehat{\psi}_R^0 = i\left\{-\dfrac{\psi_L^{0c} - \psi_R^0}{\sqrt{2}} - \dfrac{1}{2}\left[\dfrac{m_V - m_{V'}}{\Lambda + M_\psi}\dfrac{N_R + S_R}{\sqrt{2}} + \dfrac{m_V + m_{V'}}{\Lambda - M_\psi}\dfrac{N_R - S_R}{\sqrt{2}}\right]\right\} , \end{cases} \tag{2.16}$$

In the previous expressions, we neglected subleading terms that are proportional to $(\epsilon m_S)/(\Lambda, M_\psi)$ and to $(v/(\Lambda,\, M_\psi))^2$ for the masses and to $v/(\Lambda,\, M_\psi)$ for the eigenstates. In the numerical analysis, we will exclude the parameter space where these terms are larger than the 20% of the shown expressions.

The charged sector presents a completely different texture as both entries in the first row of $\mathcal{M}_\zeta$ are vanishing. The diagonalisation of the mass matrix leads to the following eigenvalues

$$\widehat{m}_\mu = 0, \qquad \widehat{m}_{\psi^-} = \sqrt{M_\psi^2 + m_R^2} \approx M_\psi\left[1 + \frac{1}{2}\left(\frac{m_R}{M_\psi}\right)^2\right] , \tag{2.17}$$

where terms that have a relative suppression higher than $(v/(\Lambda, M_\psi))^2$ have been neglected. Interestingly, only a rotation of the right-handed fields is needed, so that the mass eigenstates at tree-level read

$$\widehat{\zeta}: \begin{cases} \widehat{\mu}_L = \mu_L \,, & \widehat{\mu}_R = \dfrac{M_\psi}{\sqrt{M_\psi^2 + m_R^2}}\mu_R - \dfrac{m_R}{\sqrt{M_\psi^2 + m_R^2}}\psi_R^- \,, \\ \widehat{\psi_L^-} = \psi_L^- \,, & \widehat{\psi_R^-} = \dfrac{m_R}{\sqrt{M_\psi^2 + m_R^2}}\mu_R + \dfrac{M_\psi}{\sqrt{M_\psi^2 + m_R^2}}\psi_R^- \,, \end{cases} \tag{2.18}$$

The muon mass is vanishing at tree-level, but we do expect radiative contributions as the global symmetry protecting the muon mass term is explicitly broken. Loop computations have been performed with the help of the MATHEMATICA packages PACKAGE-X and FEYNCALC [116, 117]. The direct computation of the 1-loop diagrams in the $\overline{\text{MS}}$-scheme contributing to the muon bilinear $\overline{\mu}_L\mu_R$ gives

$$\delta m_\mu = -\frac{m_N\, m_R\, \Lambda}{8\,\pi^2\, v^2}\left(\frac{m_V}{M_\psi} + \frac{m_{V'}}{\Lambda}\right)\left[1 + \frac{1}{M_\psi^2 - \Lambda^2}\left(M_\psi^2 \log\frac{\mu_{\rm R}^2}{M_\psi^2} - \Lambda^2 \log\frac{\mu_{\rm R}^2}{\Lambda^2}\right)\right] , \tag{2.19}$$

where we neglected $\mathcal{O}(\Lambda^{-2}, M_\psi^{-2})$ corrections. As Λ and M_ψ are of the same orders of magnitude, we do not expect significant dependence on the renormalisation point and thus we can fix $\mu_{\rm R} = \max\{\Lambda,\, M_\psi\}$.

This is not, however, the end of the story. Radiative contributions are also present in the other entries of the charged lepton mass matrix and in the kinetic terms, inducing 1-loop mixing of the μ and ψ^- self energies

$$\Sigma(\not{p}) \equiv \begin{pmatrix} (1+\Sigma^{p,\mu\mu})\not{p} - \delta m_\mu & \Sigma^{p,\mu\psi}\not{p} - (\delta m_R^\dagger P_L + \delta M_L P_R) \\ \Sigma^{p,\psi\mu}\not{p} - (\delta M_L^\dagger P_L + \delta m_R P_R) & (1+\Sigma^{p,\psi\psi})\not{p} - (M_\psi + \delta M_\psi) \end{pmatrix} , \tag{2.20}$$

where

$$\Sigma^{p,ij} \equiv \Sigma_L^{p,ij} P_L + \Sigma_R^{p,ij} P_R \, , \tag{2.21}$$

and $\delta m_{\mu,R}$, $\delta M_{\psi,L}$ are the $\not{p}$-dependent and independent contributions of the self-energies, respectively. Such a matrix can be diagonalised by a non-unitary rotation and the poles of its inverse identify the pole-masses of the μ and ψ^- fields. The mixing between the left-handed leptons reads

$$\begin{cases} \widehat{\mu}_L = \mu_L \left(1 + \dfrac{\Sigma_L^{p,\mu\mu}}{2}\right) + \psi_L^- \left(-\dfrac{\delta M_L}{M_\psi} + \Sigma_L^{p,\mu\psi}\right) , \\ \widehat{\psi}_L^- = \dfrac{\delta M_L}{M_\psi}\mu_L + \psi_L^- \left(1 + \dfrac{\Sigma_L^{p,\psi\psi}}{2}\right) , \end{cases} \tag{2.22}$$

where we neglected $\mathcal{O}(1/M_\psi^2)$ and $\mathcal{O}(2\text{-loops})$ corrections. We can deduce that the renormalisation of the kinetic terms, proportional to $\Sigma^{p,\mu\mu}$, would lead to only subleading effects to the muon mass term and therefore can be neglected. The muon pole-mass at 1-loop is then simply given by

$$\widehat{m}_\mu = \delta m_\mu \tag{2.23}$$

as defined in Eq. (2.19). Notice that for $\Lambda = M_\psi$, the expression in the squared bracket of Eq. (2.19) is vanishing and the 2-loop computation would be necessary. Moreover, whenever $\Lambda \approx M_\psi$, a realistic value for the muon mass would require large values for the Yukawa couplings to compensate for the partial cancellation of the terms in the squared bracket. All in all, the muon mass prediction is delicate whenever $\Lambda \approx M_\psi$. We will come back to this aspect in the phenomenological analysis.

To conclude, the second eigenvalue also receives radiative corrections, both proportional to δM_L and Σ_L^p. However, these corrections are very much suppressed with respect to the leading tree-level contribution and we will neglect them in the numerical analysis that follows. We only report the result for δM_L as it will enter the ALP couplings: in the $\overline{\text{MS}}$-scheme, it reads

$$\delta M_L = \frac{m_N m_V \Lambda}{8\pi^2 v^2} \left[1 + \log\left(\frac{\mu_R^2}{\Lambda^2}\right)\right] . \tag{2.24}$$

As for δm_μ, in the numerical analysis we will fix $\mu_{\text{R}} = \max\{\Lambda, M_\psi\}$.

2.2 ALP Lagrangian

In this section, we analyse the ALP Lagrangian and the interactions of the ALP, in particular with SM fields. We will mainly work in the so-called *chirality-flipping* basis,

that is the one obtained from the Lagrangian in Eq. (2.2) once the scalar field ϕ gets a VEV, as in Eq. (2.1). Once necessary, we will move to the so-called *derivative-* or *chirality-preserving* basis, easily obtained by redefining the fermionic fields to rotate away the ALP from as many terms of the Yukawa sector as possible. Applying these transformations to the fermionic kinetic terms, derivative couplings between the ALP and fermion bilinears are generated.

The common chirality-flipping Lagrangian, at LO in the f_a-expansion, takes the form

$$\begin{aligned}\mathscr{L}_a =&\frac{1}{2}\partial_\mu a\partial^\mu a - \frac{1}{2}m_a^2 a^2 - \frac{ia}{f_a}\sum_{ij}\left(\overline{\Psi_i}(c^L_{a\Psi_i\Psi_j}P_L + c^R_{a\Psi_i\Psi_j}P_R)\Psi_j\right) + \\ &- \frac{1}{4}g_{a\gamma\gamma}aF^{\mu\nu}\widetilde{F}_{\mu\nu} - \frac{1}{4}g_{aZZ}aZ^{\mu\nu}\widetilde{Z}_{\mu\nu} - \frac{1}{4}g_{a\gamma Z}aF^{\mu\nu}\widetilde{Z}_{\mu\nu} - \frac{1}{2}g_{aWW}aW^{+\mu\nu}\widetilde{W}^-_{\mu\nu}\,,\end{aligned} \tag{2.25}$$

where Ψ can be any of the fermionic fields of the theory.

In the following, we first focus on the ALP-mass and then we will discuss its relevant interactions for the phenomenological analysis

2.2.1 The ALP mass

As discussed in Sec. 2, the PQ explicit breaking generates a radiative mass for the ALP after SSB. Given an interaction of a multiplet of Dirac fermions of the type

$$\mathscr{L}_Y \supset -\overline{\chi_L}\mathcal{M}_\chi\chi_R\,, \tag{2.26}$$

the exact expression of the 1-loop ALP potential can be obtained through the Coleman-Weinberg (CW) potential [118] [2], that in the $\overline{\text{MS}}$-scheme reads

$$V_{\text{CW}} = -\frac{1}{32\pi^2}\left\{\text{Tr}\left[\left(\mathcal{M}_\chi\mathcal{M}_\chi^\dagger\right)^2\log\left(\frac{\mathcal{M}_\chi\mathcal{M}_\chi^\dagger}{\mu_R^2}\right)\right] - \frac{3}{2}\text{Tr}\left[\left(\mathcal{M}_\chi\mathcal{M}_\chi^\dagger\right)^2\right]\right\}\,, \tag{2.27}$$

with $\mathcal{M}_\chi$ is a 5×5 Yukawa interaction matrix which depends, besides the Higgs, on ϕ. Notice that only the contribution from the neutral lepton sector is relevant as the charged one does not involve any PQ breaking term; the same applies for the gauge and scalar sectors. While the exact computation of the radiative ALP mass can be found in App. B, we report here a simplified calculation which reproduces correctly the result at LO when expanding in inverse powers of Λ and M_ψ.

Through symmetry arguments discussed in Sect. 2, we already concluded that the ALP mass must be proportional to the product of four quantities, see Eq. (2.11): the two Yukawa couplings Y_V and $Y_{V'}$ and the two HNL mass scales, Λ and M_ψ, that can be either Lagrangian masses or dynamically generated, thus proportional to f_a. In particular, no LN-violating parameter is expected to contribute at LO and therefore we can set them to zero to simplify the computations. In this limit, we can build a Dirac pair out of the heavy neutral states defining $T \equiv N_R + S_R^c$. As a result, the relevant interactions of the Lagrangian of Eq. (2.2) read

$$-\mathscr{L}_Y \supset \Lambda\overline{T_L}T_R + M_\psi\overline{\psi_L}\psi_R + Y_V\overline{T_L}\widetilde{H}^\dagger\psi_R + Y_{V'}\overline{\psi_L}\widetilde{H}T_R + \text{h.c.}\,, \tag{2.28}$$

[2] Notice that a factor of 1/2 is included as Weyl fermions are employed.

corresponding to the interaction matrix

$$-\mathscr{L}_Y \supset \begin{pmatrix} \overline{T_L} & \overline{\psi_L} \end{pmatrix} \begin{pmatrix} \Lambda & m_V \\ m_{V'} & M_\psi \end{pmatrix} \begin{pmatrix} T_R \\ \psi_R \end{pmatrix} . \tag{2.29}$$

The cases in which the heavy lepton masses are generated dynamically via $\phi^{(*)}$ can be obtained by mapping $\Lambda \to e^{i\,\mathrm{sgn}(x)a/f_a}\Lambda$ and $M_\psi \to e^{i\,\mathrm{sgn}(y)a/f_a}M_\psi$, where the parameters (x, y) interpolate between models A, B, C and D.

The eigenvalues of such 2×2 matrix can be computed easily, and the CW, in the limit of large masses of the heavy fermions, gives the ALP mass in the $\overline{\text{MS}}$-scheme

$$\begin{aligned} f_a^2 m_a^2 = \frac{(\overline{\delta}_{x,1} + \overline{\delta}_{y,1})^2}{4\pi^2} \left(\frac{m_V m_{V'} \Lambda M_\psi}{M_\psi^2 - \Lambda^2} \right) \Bigg[& \frac{(M_\psi^2 + \Lambda^2)}{2} \log\left(\frac{M_\psi^2}{\Lambda^2}\right) \\ & + (M_\psi^2 - \Lambda^2) \left(\log\left(\frac{M_\psi \Lambda}{\mu_R^2}\right) - 1 \right) \Bigg] , \end{aligned} \tag{2.30}$$

neglecting terms $\mathcal{O}(\Lambda^0, M_\psi^0)$, where we defined a Kronecker-delta with sign

$$\overline{\delta}_{x,1} \equiv \mathrm{sgn}(x)\delta_{|x|,1} , \qquad \overline{\delta}_{y,1} \equiv \mathrm{sgn}(y)\delta_{|y|,1} . \tag{2.31}$$

Performing the explicit computation of the different 1-loop diagrams with a single heavy lepton exchange, the ALP mass can be decomposed as the sum of two contributions [101]

$$f_a^2\, m_a^2 = f_a^2 \left(m_{a,\psi}^2 + m_{a,N/S}^2 \right) , \tag{2.32}$$

where

$$\begin{aligned} f_a^2\, m_{a,\psi}^2 &= \frac{(\overline{\delta}_{x,1} + \overline{\delta}_{y,1})^2}{4\pi^2} \left(\frac{m_V m_{V'} \Lambda M_\psi}{M_\psi^2 - \Lambda^2} \right) \times M_\psi^2 \left[\log\left(\frac{M_\psi^2}{\mu_R^2}\right) - 1 \right] , \\ f_a^2\, m_{a,N/S}^2 &= -\frac{(\overline{\delta}_{x,1} + \overline{\delta}_{y,1})^2}{4\pi^2} \left(\frac{m_V m_{V'} \Lambda M_\psi}{M_\psi^2 - \Lambda^2} \right) \times \Lambda^2 \left[\log\left(\frac{\Lambda^2}{\mu_R^2}\right) - 1 \right] , \end{aligned} \tag{2.33}$$

and gives the same result as the CW approach.

This LO expression for the ALP mass vanishes for $M_\psi = \Lambda$ and the NLO contributions should be considered. In this specific limit, the value of the ALP mass reads

$$f_a^2\, m_a^2 = (\overline{\delta}_{x,1} + \overline{\delta}_{y,1})^2 \frac{m_V m_{V'} \left(2m_{V'}^2 + 3m_N^2 - 2m_{V'} m_V + 2m_V^2\right)}{24\pi^2} \tag{2.34}$$

where only terms of order $\mathcal{O}(\Lambda^{-1})$ have been considered. The complete expression will be considered in the numerical analysis.

It is interesting to notice that the Yukawa couplings cannot take arbitrary signs, but the ALP potential dynamically fixes the product $Y_V \times Y_{V'} > 0$ (analogue to Ref. [101]) to ensure a positive ALP mass.

The dependence of m_a on Λ and M_ψ can be seen in Fig. 1 for model A regardless of the presence of ϕ or ϕ^* in the Lagrangian: indeed $m_a^2 \propto (\overline{\delta}_{x,1})^2$. The same behaviour is also

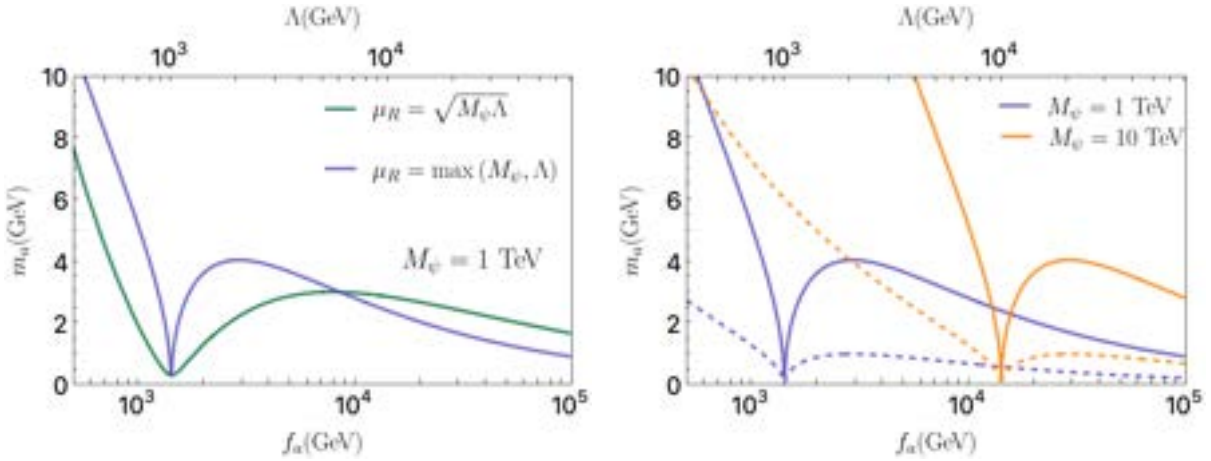

(a) (b)

Figure 1: *ALP mass in $\overline{MS}$-scheme as a function of Λ and f_a for model A. Λ and f_a are related via $\Lambda = \alpha_N f_a/\sqrt{2}$. For convenience, $\alpha_N = 1$. As a reference value, $Y_N = 0.1$.* ***Left:*** *Dependence on the renormalisation scale of the ALP mass. $Y_V = Y_{V'} = 0.4$. The green line indicates $\mu_R = \sqrt{M_\psi \Lambda}$, while the blue represents $\mu_R = \max(M_\psi, \Lambda)$. The minimum corresponds to the point where $\Lambda = M_\psi$.* ***Right:*** *ALP mass as a function of f_a and Λ for different values of M_ψ. $Y_V = Y_{V'} = 0.4$ (0.1) for the continuous (dashed) line.*

obtained for model B at LO as the roles of M_ψ and Λ can be interchanged in Eq. (2.30), that is $m_a^2 \propto (\overline{\delta}_{y,1})^2$. On the other hand, the mass dependence on f_a for model C is different and is discussed in Fig. 2.

Fig. 1(a) shows the dependence of the ALP mass on the renormalisation scale, very much typical of the situation where more than one heavy scale is present: the green line corresponds to $\mu_R = \sqrt{M_\psi \Lambda}$ that estimates an average mass scale between M_ψ and Λ; in the blue line instead μ_R is taken to be the largest scale among M_ψ and Λ. Both lines have a local minimum corresponding to $M_\psi = \Lambda$, where the LO contribution vanishes. The discontinuity of the derivative of the blue line is simply due to the change of value for μ_R: up to $\Lambda = 1$ TeV we have $\mu_R = M_\psi$, while above that value $\mu_R = \Lambda$. In Fig. 1(b), we fix $\mu_R = \max(M_\psi, \Lambda)$, but vary the value of M_ψ and of $Y_V = Y_{V'}$ to show the dependence of the ALP mass on these parameters. Increasing the value of M_ψ we obtain a larger ALP mass, but at the price of a hierarchy between Λ and M_ψ. On the other hand, lowering the value of the two Yukawa couplings from $Y_V = Y_{V'} = 0.4$ to 0.1 suppresses the result of the ALP mass, as we expect from the expression analysis. In both plots, α_N is taken to be equal to 1 for simplicity, and thus Λ is smaller than f_a just by a $\sqrt{2}$ factor: a stronger hierarchy between these two scales is achievable for $\alpha_N < 1$, although values $\alpha_N \ll 1$ are not expected from a symmetry invariance point of view. The value of Y_N is fixed at 0.1, although larger values are viable for larger f_a. As we will discuss in the next section, these values are consistent with other experimental bounds.

Fig. 2 illustrates the prediction for m_a in model C, where the dependence is different as both M_ψ and Λ are obtained via the SSB of the $U(1)_{PQ}$. In particular, for $\alpha_N/\alpha_\psi = 1$ the two masses coincide, $M_\psi = \Lambda$, and thus the LO contribution to the ALP mass vanishes

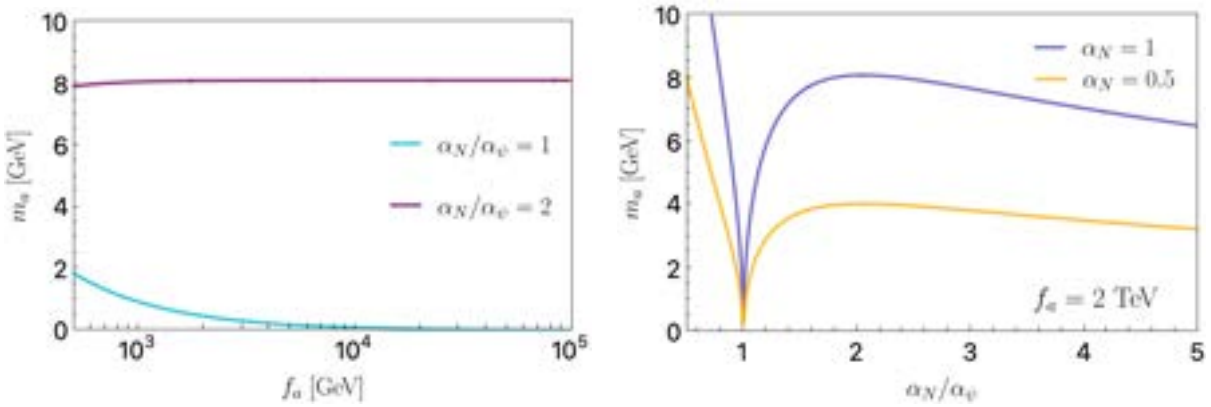

(a) (b)

Figure 2: *ALP mass at NLO (see Eq. (B.11)) in $\overline{MS}$-scheme for model C. In both cases, $Y_V = Y_{V'} = 0.4$.* ***Left:*** *Dependence on the scale f_a for two different values of the ratio α_N/α_ψ. The cyan (purple) line corresponds to the case in which $\alpha_N/\alpha_\psi = 1\,(2)$. In both cases, $\alpha_N = 1$. $Y_N = 0.1$ is taken as a reference value.* ***Right:*** *ALP mass as a function of the ratio α_N/α_ψ for two values of $\alpha_N = 0.5, 1$, which represent the orange and blue lines, respectively. f_a has been fixed to 2 TeV.*

and the expression in Eq. (2.34) holds. This case is shown in Fig. 2(a), where the cyan line illustrates the m_a dependence on f_a. On the other hand, $\alpha_N/\alpha_\psi \neq 1$, the dependence on f_a completely disappears:

$$m_a^2 = \frac{\alpha_\psi^2}{\pi^2}\left(\frac{m_V m_{V'}\frac{\alpha_N}{\alpha_\psi}}{1-\frac{\alpha_N^2}{\alpha_\psi^2}}\right)\left[\left(1+\frac{\alpha_N^2}{\alpha_\psi^2}\right)\log\left(\frac{\alpha_\psi}{\alpha_N}\right)+\left(1-\frac{\alpha_N^2}{\alpha_\psi^2}\right)\left(\log\left(\frac{\alpha_\psi\alpha_N}{\max(\alpha_\psi,\alpha_N)}\right)-1\right)\right], \tag{2.35}$$

taking as renormalisation scale $\mu_R = \max(\alpha_\psi,\, \alpha_N) f_a/\sqrt{2}$. The independence of m_a from f_a can be seen in Fig. 2(a), where the horizontal purple line corresponds to $\alpha_N/\alpha_\psi = 2$. The small deviation for small f_a values is due to the NLO contribution to m_a (see Eq. (B.11)). The Yukawa Y_N is fixed at 0.1, consistently with the previous plots in Fig. 1. Finally, the dependence of m_a on the ratio α_N/α_ψ is shown in Fig. 2(b), for two different values of $\alpha_N = 0.5,\, 1$.

All in all, the ALP in these models receives contributions of $\mathcal{O}$(GeV), which allows it to escape the stringent astrophysical constraint.

2.2.2 ALP interactions

Let us focus now on the interactions of the ALP. A comprehensive list of all tree-level interactions in the mass basis at LO can be found in App. A. Besides the coupling to gauge bosons, the decay $a \to \mu^+\mu^-$ is kinematically viable since the ALP-mass is of $\mathcal{O}$(GeV) and a coupling with muons, $a\overline{\mu_L}\mu_R$, could generate strong bounds on the parameter space of the model. We consider them separately in the following.

ALP-Gauge Bosons Interactions: The couplings with gauge bosons are generated at 1-loop via the anomalous triangle diagram of the ψ^-. A non-vanishing result requires chiral PQ-charge assignments for ψ_L^- and ψ_R^-, which is always achieved in our models if M_ψ is generated via SSB, that is in models B, C, and D. By explicit computation, the couplings to on-shell gauge bosons are found to be

$$g_{a\gamma\gamma} = \overline{\delta}_{y,1}\frac{\alpha_{\rm em}}{\pi f_a}\,, \qquad g_{aZZ} = \overline{\delta}_{y,1}\frac{\alpha_{\rm em}}{6\pi f_a s^2_{2\theta_W}}\left(c_{4\theta_W}+7\right)\,, \qquad g_{aWW} = \overline{\delta}_{y,1}\frac{\alpha_{\rm em}}{2\pi f_a s^2_{\theta_W}}\,, \tag{2.36}$$

where θ_W is the Weinberg angle and $s_X[c_X] \equiv \sin[\cos](X)$. The coupling $g_{aZ\gamma}$ is found to be zero at LO in the expansion.

ALP-Muons Interactions: As there are no direct terms in the interaction basis that couple ϕ to SM fields, they can only be generated by mixing when rotating to the mass basis. However, such contributions do not arise in any of the considered models. This can be first understood by looking at the diagonalisation of the charged mass matrix: as only a RH fields' rotation is required (cfr. Eq. (2.18)), and as the ALP couples only to ψ^- in the interaction basis, there is no possibility to generate a coupling of the form $a\overline{\widehat{\mu}_L}\widehat{\mu}_R$ at any order at tree-level, leaving at best

$$\mathscr{L}_a \supset i\frac{a}{f_a}\left(\overline{\delta}_{y,1} m_R \overline{\widehat{\psi}_L^-}\widehat{\mu}_R\right) + \text{h.c.}\,. \tag{2.37}$$

The situation changes when considering the loop-level contributions. There are two possible contributions to the coupling $a\overline{\widehat{\mu}_L}\widehat{\mu}_R$, namely indirectly induced via 1-loop mixing of $\mu - \psi$ (cfr. Eq. (2.20)) from the interaction of Eq. (2.37), or direct via triangle diagrams, as exemplified in Fig. 3.

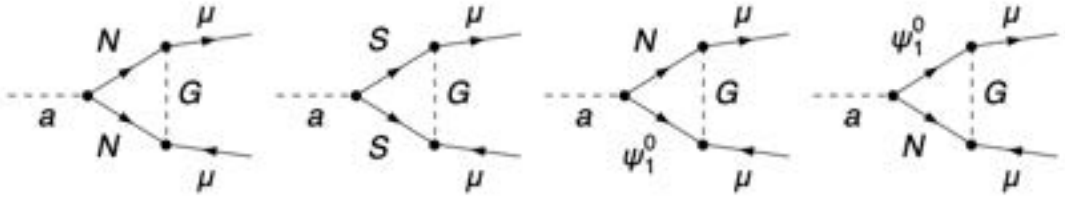

Figure 3: *Illustrative set of triangle diagrams that contribute at 1-loop to* $a \to \mu^+\mu^-$. N, S, ψ_1^0 *are Majorana fermions defined in App. A.*

The total contribution stemming from the triangle diagrams, $iV_{a\mu\mu}$, in the $\overline{\rm MS}$-scheme reads

$$\begin{aligned} iV_{a\mu\mu}(P_R - P_L) = i\frac{m_N m_R m_V}{8\pi^2 f_a v^2}\left(\frac{\Lambda}{M_\psi}\right) \times \frac{P_R - P_L}{\left(M_\psi^2 - \Lambda^2\right)} \times \\ \times \left[M_\psi^2(\overline{\delta}_{x,1}+\overline{\delta}_{y,1})\log\left(\frac{\mu_{\rm R}^2}{M_\psi^2}\right) - \log\left(\frac{\mu_{\rm R}^2}{\Lambda^2}\right)\left(\overline{\delta}_{x,1}\Lambda^2 + \overline{\delta}_{y,1}M_\psi^2\right) + \overline{\delta}_{x,1}\left(M_\psi^2 - \Lambda^2\right)\right]\,, \end{aligned} \tag{2.38}$$

where $P_{R,L} = (1 \pm \gamma_5)/2$ are the right(left)-chirality projectors. Including the mixing between μ and ψ^- from Eq. (2.37), the total ALP-muons coupling as defined in Eq. (2.22) is given by

$$\begin{aligned} c^R_{a\mu\mu} = -c^L_{a\mu\mu} &= \left(m_R \frac{\delta M_L}{M_\psi} + V_{a\mu\mu} \right) , \\ &= \left(\overline{\delta}_{x,1} + \overline{\delta}_{y,1}\right) \frac{m_N\, m_R\, m_V}{8\,\pi^2\, v^2} \left(\frac{\Lambda}{M_\psi}\right) \left[1 + \frac{1}{M^2_\psi - \Lambda^2} \left(M^2_\psi \log \frac{\mu^2_{\rm R}}{M^2_\psi} - \Lambda^2 \log \frac{\mu^2_{\rm R}}{\Lambda^2} \right) \right] , \\ &= \left(\overline{\delta}_{x,1} + \overline{\delta}_{y,1}\right) \times \delta m_\mu \Big|_{m_{V'}=0} , \end{aligned} \tag{2.39}$$

where with $\delta m_\mu \Big|_{m_{V'}=0}$ we refer to the muon mass obtained in Eq. (2.19) and computed for $m_{V'} = 0$. In an exact PQ-symmetric model, the ALP-muon coupling would be proportional to the pole-mass of the muon; in our case, this is not exactly the case as the symmetry is explicitly broken by the simultaneous presence of Y_V and $Y_{V'}$. We further investigate this aspect in App. C.

3 Phenomenological analysis

In this section, we examine the relevant phenomenology to constrain the couplings and predict the masses of the heavy fermions and the ALP. A scheme of the observables we discuss and the couplings they constrain can be seen in Fig. 4.

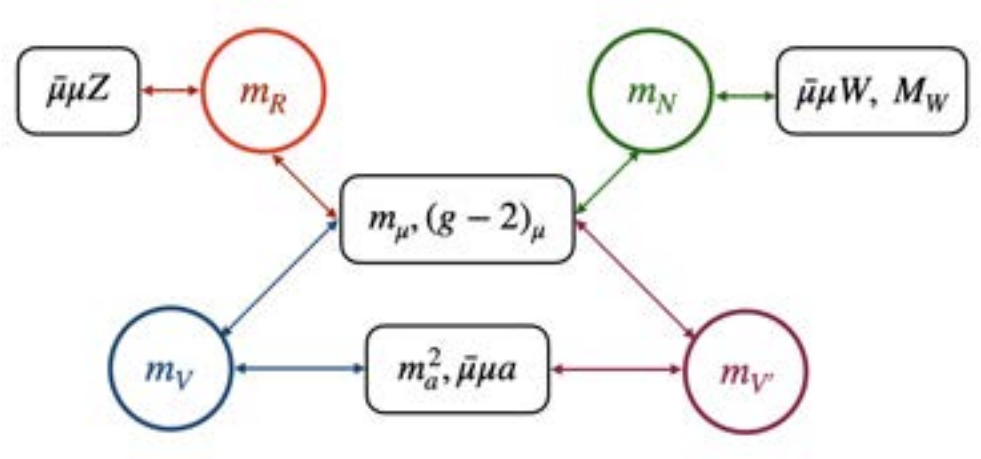

Figure 4: *Couplings and connections to the relevant observables.*

The input parameters used for the numerical analysis are [119]:

$$\begin{aligned} m_\mu^{\rm exp} &= 105.6583755(23)\ \text{MeV} \\ \alpha_{\rm em} &= 7.2973525693(11) \times 10^{-3} \\ G_\mu &= 1.1663788(6) \times 10^{-5}\ \text{GeV}^{-2} \\ M_Z &= 91.1876(21)\ \text{GeV} \end{aligned} \tag{3.1}$$

We will not discuss the phenomenology of model D in what follows, as we are only interested in the models where the ALP is massive.

3.1 Relevant bounds

m_N/Λ: This combination of parameters is constrained by a series of observables. The first one is the determination of the W-gauge boson mass. The most recent and precise value of M_W was obtained by the ATLAS collaboration [120], $M_W = 80.360(16)$ GeV [3]. The modification of the coupling of the W-boson with muons induces a modification in the muon decay $\mu \to e\overline{\nu}\nu$. The measurement of the muon lifetime allows for the most precise measurement of the Fermi constant. The modified decay width of the muon reads

$$\Gamma_\mu \simeq \frac{(m_\mu^{\rm exp})^5 G_F^2}{192\,\pi^3}\left(1-\frac{\widetilde{m}_N^2}{2\Lambda^2}\right)^2 \equiv \frac{(m_\mu^{\rm exp})^5 G_\mu^2}{192\,\pi^3}\,, \tag{3.2}$$

where G_F is the Fermi constant as defined in the Fermi Lagrangian and G_μ is its experimental determination extracted from the muon lifetime such that

$$G_F \simeq G_\mu\left(1+\frac{\widetilde{m}_N^2}{2\Lambda^2}\right)\,. \tag{3.3}$$

As the most precise determination of the M_W takes as input parameters $\alpha_{\rm em}$, M_Z and G_μ, the prediction for the M_W gets shifted

$$M_W \simeq M_Z\sqrt{\frac{1}{2}+\sqrt{\frac{1}{4}-\frac{\pi\,\alpha_{\rm em}}{\sqrt{2}\,G_\mu\,M_Z^2\,(1-\Delta r)}\left(1-\frac{\widetilde{m}_N^2}{2\Lambda^2}\right)}}\,, \tag{3.4}$$

where $\Delta r = 0.03657(21)(7)$ takes into account radiative electromagnetic corrections and the on-shell scheme has been used, thus fixing the Weinberg angle to be

$$\sin\theta_W \equiv 1-\frac{M_W^2}{M_Z^2}\,. \tag{3.5}$$

Considering the latest ATLAS measurement [120] of M_W we thus obtain the following upper bound on m_N

$$\left(\frac{m_N}{\Lambda}\right)^2 \leq 4.0\times 10^{-3}\,. \tag{3.6}$$

This same combination can be constrained by the invisible Z-decay rate and from Lepton Flavour Universality violating processes. However, as discussed in Ref. [110], once extending this setup to more realistic models with three generations, these constraints get relaxed and the most relevant remains the one in Eq. (3.6).

Other bounds on this combination arise from direct searches of HNLs at colliders. As shown in Ref. [110], the present corresponding bounds are two orders of magnitude weaker than the one from the M_W determination.

[3] In April 2022 the CDF collaboration reported the most precise measurement value of M_W [114], $M_W^{\rm CDF\ II} = 80.433(9)$ GeV. Such a measurement is in tension with previous determinations with significance of 7.0σ and is nowadays subject of controversy within the experimental community to establish its accuracy. Its impact in the analysis of the HNLs contributions has been studied in Ref. [110]. In the following, waiting for the matter to be settled, we will adopt a more conservative approach and use the most precise value M_W compatible with the world average pre-CDF II measurement.

$\boldsymbol{m_R/M_\psi}$**:** The coupling Y_R modifies the coupling strength of the Z-boson to right-handed muons. Its deviation can be constrained by EW-fit data and at 2σ reads [110]

$$\left(\frac{m_R}{M_\psi}\right)^2 \leq 5.6 \cdot 10^{-3} \,. \tag{3.7}$$

As discussed in Ref. [110], this bound is much stronger than the one we can extract on the same quantity from collider searches on both Higgs couplings and direct searches on HNLs, which are two orders of magnitude weaker than Eq. (3.7).

3.2 Contributions to the $(g-2)_\mu$

In the model we consider, both the muon mass and anomalous magnetic moment are generated at 1-loop. Once focussing on the HNL contributions, they must receive contributions that are proportional to the same couplings, as the only difference in their Feynman diagrams relies on including or not the external photon leg,

$$\delta m_\mu \propto \delta a_\mu \propto Y_N Y_R Y_{V,V'} \,. \tag{3.8}$$

The latest and most precise measurement of the $(g-2)_\mu$ comes from the Muon g-2 Collaboration [121]

$$a_\mu \equiv \frac{g_\mu - 2}{2} = 116592059(22) \times 10^{-11} \,, \tag{3.9}$$

yielding, according to the Muon $g-2$ Theory Initiative [122], a discrepancy with respect to the SM prediction of

$$\delta a_\mu^{\rm exp} \equiv a_\mu^{\rm exp} - a_\mu^{\rm SM} = (2.49 \pm 0.49) \times 10^{-9} \,, \tag{3.10}$$

corresponding to a significance of 5.1σ. Some comments regarding the above result are in order as it is currently subject to several controversies. The main source of uncertainty to the SM prediction, $a_\mu^{\rm SM}$, comes from non-perturbative contributions of hadronic-vacuum polarization (HVP). The Muon $g-2$ Theory Initiative [122] prediction has been performed by extracting such contribution from low-energy $e^+e^- \to$ hadrons cross sections employing the so-called *dispersive* method. In April 2021 the BMW collaboration first reported a lattice result with the first sub-percent error in the estimation of the HVP [123], making lattice results competitive with dispersive uncertainties for the first time. Such a result is in tension by $\sim 2\sigma$ with dispersive results and relaxes the $\delta a_\mu^{\rm exp}$ significance to 1.7σ. Other collaborations afterwards independently managed to achieve similar precision in computing partial contributions to HVP, being able to partially counter-check the BMW result. While the so-called *short-distance* lattice contribution to HVP seems to agree with the dispersive method [124] (see e.g. Ref. [125]), the so-called *intermediate-distance* lattice contribution [126–128] was found to be larger than the result based on the dispersive method with $\sim 4\sigma$ tension, thus supporting the full BMW result. Finally, in February 2023 the CDM-3 collaboration released a new measurement of the cross-section $e^+e^- \to \pi^+\pi^-$ [129], obtaining a dispersive partial contribution to HVP significantly larger than all previous estimations with significance $\gtrsim 3\sigma$, thus decreasing $\delta a_\mu^{\rm exp}$ discrepancy to 2.4σ.

However, at present, this measurement remains a stand-alone and therefore requires further investigations.

The situation is therefore extremely controversial and far from being settled. We nevertheless take the discrepancy of Eq. (3.10) as input for the analysis. If in the future the solution to such a dispute was found to bring the SM prediction in agreement with the experimental result, the $(g-2)_\mu$ would serve as one of the strongest bounds on the model here studied.

In the SM, all contributions to a_μ are suppressed by two powers of $m_\mu^{\rm exp}$. The first one is unavoidable and comes from the definition of the magnetic dipole operator,

$$\frac{1}{2m_\mu^{\rm exp}}\overline{\mu_L}\sigma^{\mu\nu}\mu_R F_{\mu\nu}\,. \tag{3.11}$$

The second is peculiar to the SM and is due to the chiral structure of the operator and hence is typically dubbed as "chirally suppressed" (CS). In fact, the SM possesses approximate chiral symmetry per lepton generation broken explicitly solely by the Yukawa interactions which guarantees the presence of the muon mass suppression to a_μ at each order in perturbation theory [4].

Generic BSM constructions typically face the same suppression and therefore, once attempting to solve the mentioned tension, the scale of NP is relatively low, often severely constrained by other experiments. The same is not true in models where the new fields introduce extra breaking of the chiral symmetry and are hence dubbed "chirally enhanced" (CE). In practice, one needs a series of interactions that bridge between LH and RH components of the muon field. Such models have been systematically classified in Refs. [102–106] at LO.

In our model, such CE contribution to a_μ is present only at 1-loop and mediated by HNLs, as the muon mass is also generated at 1-loop. Assuming Λ, $M_\psi \gg v$, based on power counting, one would naively expect the LO contribution to be

$$\delta a_\mu^{\rm naive} \propto \frac{Y_N Y_R Y_{V,V'}}{16\pi^2}\frac{m_\mu^{\rm exp} v}{\Lambda M_\psi} + \mathcal{O}\left(\frac{1}{(M_\psi\Lambda)^2}\right)\,, \tag{3.12}$$

thus requiring the NP scale to be at $\mathcal{O}(10)$ TeV. Remarkably, an accidental cancellation unique to this model cancels this contribution, and the first non-vanishing term reads

$$\delta a_\mu = \frac{3\,m_\mu^{\rm exp}}{4\,\pi^2\,v^2}\frac{M_W^2}{\Lambda M_\psi}\frac{m_N m_R}{M_\psi}\left(\frac{m_V}{M_\psi}+\frac{m_{V'}}{\Lambda}\right)F_0\left(\frac{\Lambda^2}{M_W^2},\frac{M_\psi^2}{M_W^2}\right)\,, \tag{3.13}$$

where the loop function is defined by

$$F_0(x,y) \equiv \frac{3}{2} - \frac{x\log y - y\log x}{x-y}\,. \tag{3.14}$$

This allows to lower the NP scale down to $\mathcal{O}(1)$ TeV. Such a feature was first pointed out for its phenomenological significance in Ref. [107] and further studied in detail in Refs. [108–110].

[4] The chiral symmetry receives extra breaking sources in the presence of non-vanishing neutrino masses, which are nevertheless completely negligible at this level of precision.

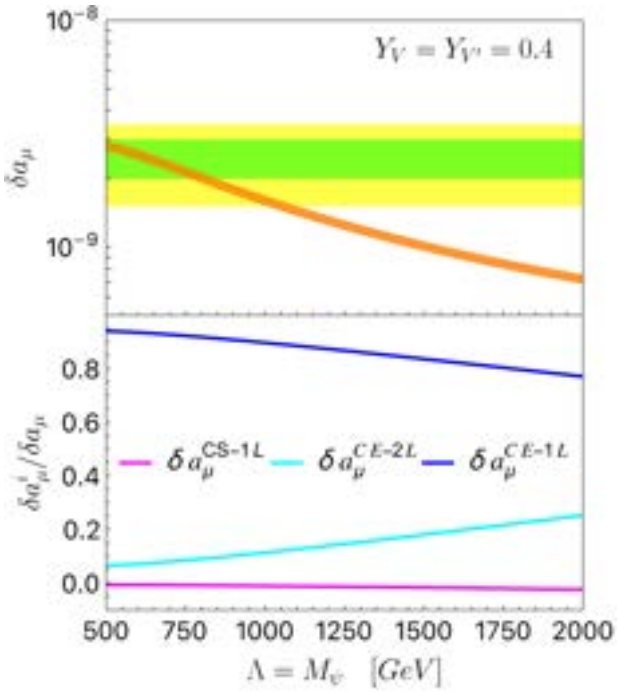

Figure 5: *Illustrative example of δa_μ as a function of $\Lambda = M_\psi$ for $Y_V = Y_{V'} = 0.4$. m_N/Λ and m_R/M_ψ are taken to saturate the bounds of Eqs. (3.6), (3.7), respectively.* ***Above:*** *δa_μ (orange) and the experimental value at 1σ (2σ) in green (yellow).* ***Below:*** *ratios of the different components $\delta a_\mu^{CS\text{-}1L}$ (magenta), $\delta a_\mu^{CE\text{-}2L}$ (cyan) and $\delta a_\mu^{CE\text{-}1L}$ (blue) to the total contribution δa_μ.*

An illustrative example of the possible NP contribution to a_μ is shown in Fig. 5, where we also report the relative contributions of the 2-loops CE-contributions [107] (CE2) and the 1-loop CS-contribution (CS1) [110]. As it can be seen, the CS1 is negligible, while the CE2 can account at most for $\mathcal{O}(20\%)$ and only for larger masses. Therefore we keep, for simplicity, only the CE contribution at 1-loop.

The $(g-2)_\mu$ may receive further contributions from the ALP in all models, but in model A, it appears at NLO and is chirally suppressed. This can be understood by noticing that the corresponding 1-loop Feynman diagram needs necessarily to contain twice the coupling in Eq. (2.37), with the ALP and the $\widetilde{\psi}_L^-$ running into the loop, and thus the chirality flip needs to be in the muon external leg. Naively, we thus expect

$$\delta a_\mu^{\text{naive}} \propto \frac{(m_\mu^{\text{exp}})^2 m_R^2}{\alpha_\psi^2 f_a^4} \,. \tag{3.15}$$

The explicit computation confirms this estimation and reads

$$\delta a_\mu^a = \frac{\delta_{|y|,1}}{96\pi^2} \frac{(m_\mu^{\text{exp}})^2 m_R^2}{f_a^2 M_\psi^2} \,, \tag{3.16}$$

expressed in terms of the physical mass scale M_ψ. With this result, we can neglect the ALP contribution, as we did for the HNL CS1 and CE2 contributions.

Similarly, the radial component ρ also contributes to δa_μ. Given that its couplings are very similar to the ones of the ALP, its contribution owns the same properties of Eq. (3.16) and reads

$$\delta a_\mu^\rho = \frac{\delta_{|y|,1}}{96\pi^2}\frac{(m_\mu^{\rm exp})^2 m_R^2}{f_a^2 m_\rho^2} \times \frac{2+3x_{\rho\psi}\left(1+\log x_{\rho\psi}^2\right)-6x_{\rho\psi}^2+x_{\rho\psi}^3}{(1-x_{\rho\psi})^4} \tag{3.17}$$

where $x_{\rho\psi} \equiv M_\psi^2/m_\rho^2$. This contribution is also negligible with respect to the one in Eq. (3.13).

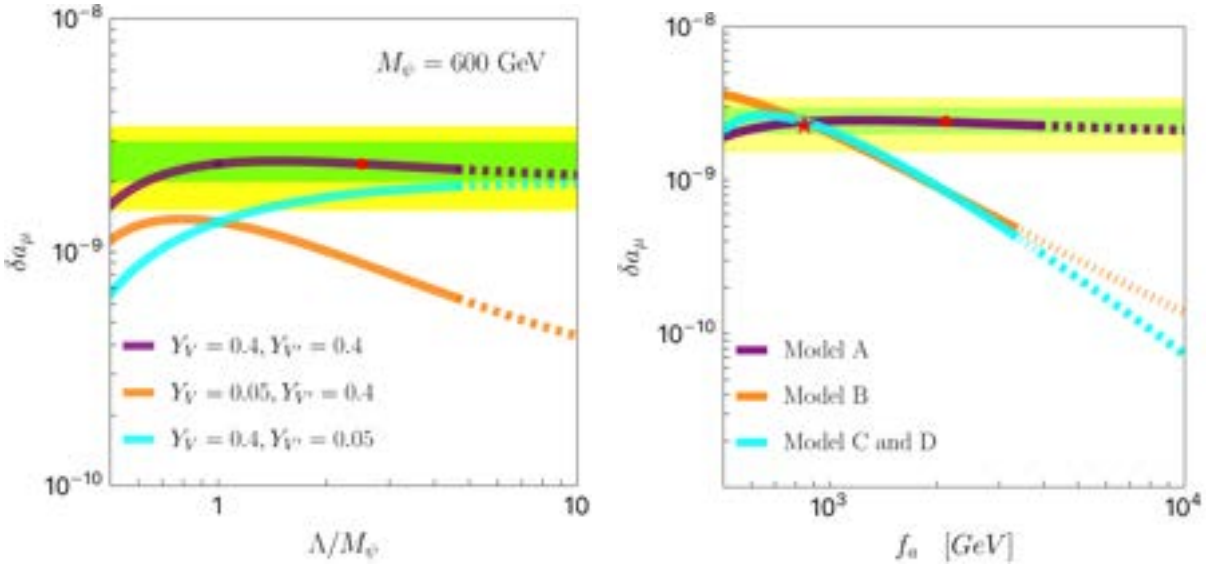

Figure 6: *Dependence of δa_μ on the model parameters. δa_μ^{exp} values at 1σ (2σ) are shown in green (yellow).* ***Left:*** *δa_μ as a function of Λ/M_ψ with $M_\psi = 600$ GeV for $Y_V = Y_{V'} = 0.4$ (purple), $Y_V = 0.05, Y_{V'} = 0.4$ (orange) and $Y_V = 0.4, Y_{V'} = 0.05$ (cyan), for any model. m_N/Λ and m_R/M_ψ saturate Eqs. (3.6) and (3.7), respectively. The solid (dashed) lines represent the values of δa_μ for $|Y_N| \leq 1$ ($1 < |Y_N| \leq 5$). The red dot is a benchmark point of coordinates $(\Lambda, M_\psi) = (1500, 600)$ GeV.* ***Right:*** *δa_μ as a function of the PQ-scale f_a with $Y_V = Y_{V'} = 0.4$ for different models: A (purple), B (orange) and C and D (cyan). For simplicity, $\alpha_{N,\psi}$ have been set to 1 according to each model and the remaining free mass, when present, is fixed to 600 GeV. When the masses are dynamically generated, $\Lambda(M_\psi) = f_a/\sqrt{2}$. The solid (dashed) lines represent the values of δa_μ for $|Y_{N,R}| \leq 1$ ($1 < |Y_{N,R}| \leq 5$). The red dot (star) is a benchmark point of coordinates $(\Lambda, M_\psi) = (1500, 600)$ GeV for model A (B).*

All in all, the relevant expression for δa_μ is the one given in Eq. (3.13). Fig. 6 shows the dependence of δa_μ on the model parameters and the type of model realisation.

We first fix $M_\psi = 600$ GeV and explore what happens for $Y_V \neq Y_{V'}$ (see Fig. 6(a)). Such a value of M_ψ is chosen so that the anomaly can be solved for some parameter space. Although for some higher values of Λ/M_ψ, the case of $Y_V = 0.4, Y_{V'} = 0.05$ can solve the

anomaly at the 2σ level, in general, a contribution from both Y_V and $Y_{V'}$ ought to be present. Notice that the case with $Y_V = 0.05$ does not allow to reach the 2σ level solution. The red benchmark point is determined by the ratio $\Lambda/M_\psi = 2.5$, and slight variations in Λ and M_ψ would cause it to shift very slightly to nearby positions on the plot.

On the other hand, the ratio Λ/M_ψ is not completely free and depends on the specific model considered, with the exception of models C and D which have the same prediction. In the plot on Fig. 6(b), we are interested in seeing the contribution to the $(g-2)_\mu$ in the different models. Model A is the one that solves the anomaly at 1σ for the full parameter range studied. Model B, C and D only solve it for very low values of f_a. This plot is obtained fixing for simplicity $\alpha_{N,\psi} = 1$ when the two scales Λ and/or M_ψ are dynamically generated, while Λ, $M_\psi = 600$ GeV otherwise, and setting $Y_V = Y_{V'} = 0.4$. Choosing higher (lower) values of $Y_{V,V'}$ (not necessarily respecting the equality between both terms), the corresponding line of each model gets shifted towards higher (lower) values of δa_μ.

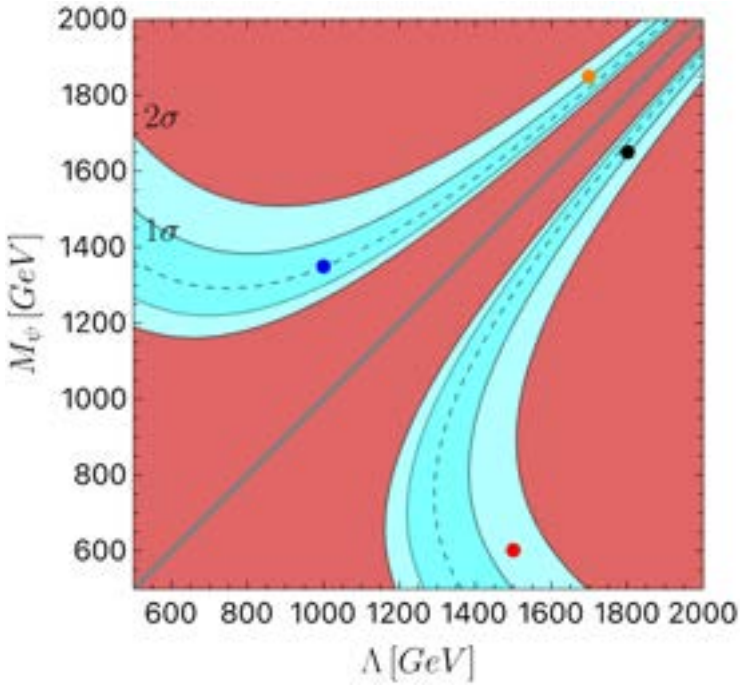

Figure 7: *Regions of the parameter space Λ vs. M_ψ to solve the $(g-2)_\mu$ tension for $\delta m_\mu/m_\mu^{exp} = 1$. The dark (light) cyan area corresponds to the parameter space in which δa_μ is 1σ (2σ) of the experimental central value. The red area represents the rest of the values. The benchmark points chosen are $(\Lambda, M_\psi) = (1500, 600)$ GeV (Red), $(1000, 1350)$ GeV (Blue), $(1700, 1850)$ GeV (Orange) and $(1800, 1650)$ GeV (Black). The grey oblique line shows where qualitatively muon mass vanishes and $Y_{V,V'}$ are thus too large.*

Given the similarity of the expression for the muon mass in Eq. (2.19) and the one for the δa_μ in Eq. (3.13), we can study the correlation between the two observables. For all

the models, the ratio of the two expressions reads

$$\frac{\delta a_\mu}{\widehat{m}_\mu} = -\frac{6\, m_\mu^{\rm exp}\, M_W^2}{\Lambda^2 M_\psi^2} F_0\left(\frac{\Lambda^2}{M_W^2}, \frac{M_\psi^2}{M_W^2}\right)\left[1 + \frac{1}{M_\psi^2 - \Lambda^2}\left(M_\psi^2 \log\frac{\mu_{\rm R}^2}{M_\psi^2} - \Lambda^2 \log\frac{\mu_{\rm R}^2}{\Lambda^2}\right)\right]^{-1} . \tag{3.18}$$

It is interesting to study the dependence of δa_μ on the parameter space $(\Lambda,\, M_\psi)$ once the muon mass agrees with its experimental determination. We show the results of this analysis in Fig. 7, where we simply take $\widehat{m}_\mu = m_\mu^{\rm exp}$ at its central value, given the high precision of the experimental determination. The dark (light) cyan area corresponds to the parameter space in which δa_μ is 1σ (2σ) of the experimental central value. The central grey line corresponds to points where the muon mass is exactly vanishing at 1-loop: for these points, the correlations in Eq. (3.18) are not meaningful. The same applies to the points located near the grey line: in this case, the values of the Yukawa couplings may enter the non-perturbative regime. We will be back on this aspect in the next section.

Although the expression in Eq. (3.18) is independent of the Yukawa couplings Y_N, Y_R, Y_V and $Y_{V'}$, any point in the plot in Fig. 7 corresponds to specific values of the Yukawas: this follows from the condition $\widehat{m}_\mu = m_\mu^{\rm exp}$. We selected four benchmark points corresponding to the coloured circles in the plot, with the red circle corresponding to the red circle in Fig. 6(b). The values of the four benchmark points are reported in Tab. 2: notice that the Yukawa couplings are not uniquely determined, but there is a flat direction between Y_V and $Y_{V'}$.

	(Λ, M_ψ) [GeV]	Y_N	Y_R	$\lvert Y_V + Y_{V'} M_\psi/\Lambda\rvert$
Red	$(1500, 600)$	0.55	0.26	0.42
Blue	$(1000, 1350)$	0.36	0.58	2.26
Orange	$(1700, 1850)$	0.62	0.80	2.58
Black	$(1800, 1650)$	0.66	0.71	2.23

Table 2: *Summary of the values of the parameters for the different benchmark points shown in Figs. 6 and 7. The values of Y_N and Y_R saturate the bounds in Eqs. (3.6) and (3.7).*

3.3 ALP constraints

The ALP Lagrangian in Eq. (2.25) describes ALP couplings with gauge bosons and with muons that can be tested experimentally. Recall that bounds on ALP-gauge boson couplings can be placed only when $\delta_{y,1} = 1$, while ALP-muons ones can be constrained only when $\overline{\delta}_{x,1} + \overline{\delta}_{y,1} \neq 0$ and $Y_V \neq 0$.

The ALP-photon coupling has been deeply studied and its parameter space is constrained by results coming from detector studies [79, 131–142], as well as astrophysical searches [143–145] and cosmology [146]. A summary plot with all the applicable bounds can be seen in Fig. 8, for models B and C where $\delta_{y,1} \neq 0$. Such a parameter space cannot be studied for model A as the ALP-photon coupling is vanishing. The light orange (cyan) regions correspond to the parameter space for model B (C) when $Y_{V,V'} \subset [0.05, 0.4]$ and $\alpha_{N,\psi} \subset [0.5, 1.25]$. Moreover, in model B $\Lambda = 1500$ GeV, and by choosing higher (lower)

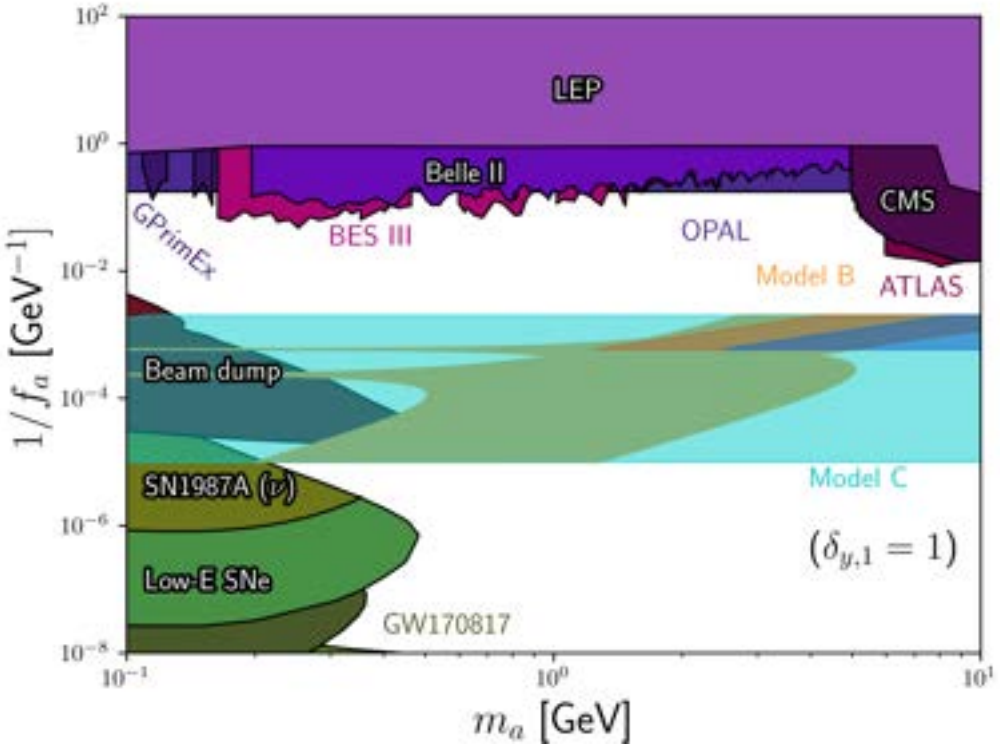

Figure 8: *Photon-ALP coupling as a function of m_a. Adapted from Ref. [130]. The light orange (cyan) region corresponds to the parameter space for model B (C) when $Y_{V,V'} \subset [0.05, 0.4]$ and $\alpha_{N,\psi} \subset [0.5, 1.25]$. In model B, $\Lambda = 1500$ GeV. The darker orange (blue) region, instead, to the benchmark point for model B (C), defined by $\Lambda = 1500$, $M_\psi = 600$ GeV and the Yukawas $Y_{V,V'} \subset [0.05, 0.4]$, while $\alpha_{N,\psi} > 0.5$.*

values the light orange bands displace to the right (left). Additionally, for both models, for larger (smaller) values of $Y_{V,V'}$, the bands of both model B and C displace to the right (left). The dark orange (blue) band represents the parameter space for the benchmark point present in Figs. 6 and 7, defined by $\Lambda = 1500$ GeV and $M_\psi = 600$ GeV for model B (C). The darker orange (blue) region is completely contained in the light orange (cyan) one, as expected. The bounds reported in this plot have been considered assuming the most constraining case with the ALP decaying only into photons, that is $\mathrm{Br}(a \to \gamma\gamma) = 1$. As we can see, the regions of the parameters space of the models (cyan and orange in the plot) are essentially unconstrained from these bounds, and switching on different decay channels simultaneously would only weaken these constraints. Studies on non-resonant vector boson scattering [92] constrain the ALP couplings to SM gauge bosons, g_{aWW}, g_{aZZ}, leading to

$$|g_{aWW}| \leq 3.0\,\mathrm{TeV}^{-1}, \qquad |g_{aZZ}| \leq 2.8\,\mathrm{TeV}^{-1}, \tag{3.19}$$

which results in an upper limit for f_a

$$|f_{a_{WW}}| \geq 1.7\,\mathrm{GeV}, \qquad |f_{a_{ZZ}}| \geq 1.3\,\mathrm{GeV}, \tag{3.20}$$

for masses of $\mathcal{O}(1)$ GeV and models B and C. Also in this case, the bounds have been obtained in the most constraining case, that is assuming that the ALP can have only one viable decay channel at a time. Despite this, these limits are extremely weak.

Finally, it is also possible to place an upper limit on the coupling to muons, Eq. (2.39). A shortcut to translate the existing bounds taken from Ref. [70] into our case consists in matching Eq. (2.39) with the ALP-muon couplings written in the derivative basis: the effective Lagrangian contains the terms

$$\mathscr{L}_{\partial a} \supset \frac{\partial_\mu a}{f_a}\left(c_{\ell_L}\overline{\ell_L}\gamma^\mu\ell_L + c_{\mu_R}\overline{\mu_R}\gamma^\mu\mu_R\right) , \tag{3.21}$$

and the matching consists in

$$g_{a\mu\mu} \equiv \frac{c_{\mu_R} - c_{\ell_L}}{f_a} = \frac{c^R_{a\mu\mu}}{f_a\,\delta m_\mu} = \frac{(\bar{\delta}_{x,1} + \bar{\delta}_{y,1})}{f_a} \times \left(\frac{Y_V}{Y_V + \left(\frac{M_\psi}{\Lambda}\right) Y_{V'}}\right) . \tag{3.22}$$

This result deserves some additional comments. In any UV model, the tree-level couplings c_{ℓ_L} and c_{μ_R} of the ALP derivative Lagrangian $\mathscr{L}_{\partial a}$ coincide with the PQ charges of the lepton fields. Although these charges can be taken to be arbitrary small rational numbers, it is very common that c_{ℓ_L}, $c_{\mu_R} \sim \mathcal{O}(1)$, thus their difference is also expected to be $\mathcal{O}(1)$, unless the PQ charge assignment is vectorial and in this case, the difference vanishes. As a result, as far as the PQ symmetry is not broken explicitly, the naive estimation for the ALP-muon coupling is $g_{a\mu\mu} \sim \mathcal{O}(1)/f_a$, strongly correlated with the couplings with gauge bosons. There are two caveats in this discussion:

(i) with the tree-level ALP-fermion coupling vanishing, the loop contribution is dominant and spoils the $\sim \mathcal{O}(1)/f_a$ dependence;

(ii) with composite fermions, their mixing with other particles with different PQ charges can induce corrections to the ALP-fermion coupling. The latter thus shows a dependence on the mixing parameter that can drastically alter the $\sim \mathcal{O}(1)/f_a$ relation.

However, in both cases, the naive expectation for the ALP-fermion coupling inherited from such contributions can only be $\ll \mathcal{O}(1)/f_a$: in (i) this is due to the loop suppression itself; while in (ii) because the mixing of SM fermions with BSM particles is strongly constrained to be small due to EW-measurements at LHC (cfr. Eq.s (3.6)-(3.7)). Instead, in our case, *the ALP-fermion coupling $g_{a\mu\mu}$ spans continuously over various orders of magnitudes, from $\ll \mathcal{O}(1)/f_a$ to $\mathcal{O}(1)/f_a$, providing a proof-of-concept for the existence of models with this peculiar feature.* This is due to the PQ explicit breaking and effectively removes the direct correlation with f_a decay constant. Given the nature of this breaking, this result is highly model-dependent and cannot be captured in a generic model-independent effective analysis, where instead the ALP-fermion couplings are completely agnostic and should be taken $\mathcal{O}(1)/f_a$, according to the t'Hooft naturalness principle.

In Fig. 9 the relation of the ALP coupling to muons to Λ, M_ψ (α_N, α_ψ) for model A (C) is shown. The results for model B are the same as for model A. Two values of Y_V has been used, namely, $Y_V = 0.1\,(0.5)$ for the left (right) plots. The grey band stands for

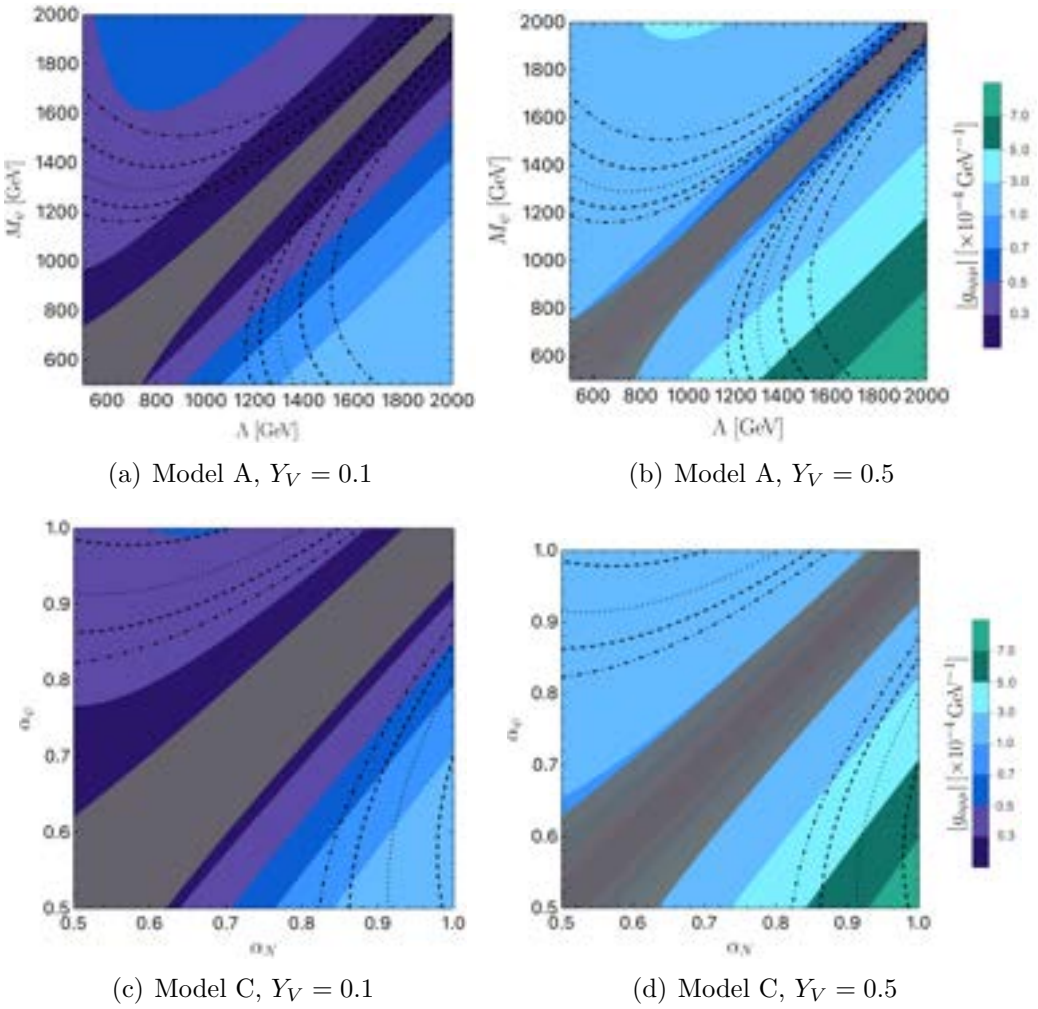

(a) Model A, $Y_V = 0.1$

(b) Model A, $Y_V = 0.5$

(c) Model C, $Y_V = 0.1$

(d) Model C, $Y_V = 0.5$

Figure 9: *Coupling of the ALP to muons, $g_{a\mu\mu}$, in relation to the $(g-2)_\mu$ and the mass of the muon. Coupling values are represented by the different colours in the legend. The parameters are fixed such that $\delta m_\mu = m_\mu^{exp}$ in all the parameter space. The dotted(dashed)[dot-dashed] lines show where the central $(1\sigma)[2\sigma]$ value of $(g-2)_\mu$ can be reproduced. The grey shaded region stands for the area in which $|Y_{V'}| > 5$.* ***Upper row:*** *The left (right) plot represents the ALP coupling to muons in the case of model A for values of $Y_V = 0.1\,(0.5)$. In both cases, $\alpha_N = 1$.* ***Lower row:*** *ALP coupling to muons as a function of $\alpha_{N/\psi}$ for model C and $f_a = 2$ TeV. In the left (right) plot $Y_V = 0.1\,(0.5)$.*

the area in which $|Y_{V'}| > 5$, thus breaking perturbativity. In all four plots, the bounds coming from the EW interaction (Eqs. (3.6) and (3.7)) do not lead to $Y_{N,R}$ outside of the perturbativity regime. Additionally, the information on the muon mass and the $(g-2)_\mu$ is placed. Another interesting aspect is that, for model C, the values of $\alpha_{N,\psi}$ that lead to vanishing ALP mass at LO are not allowed. When comparing with the existing literature, we can extract a conservative bound on this coupling from Ref. [70] (see Fig. 28):

$$\left|g_{a\mu\mu}^{\max}\right| = 0.01 \text{ GeV}^{-1} \tag{3.23}$$

valid in the region $m_a \subset [0.1, 10]$ GeV. This bound comes from detector searches, specifically from BaBar, where a search for a dark photon in e^+e^- collisions was performed [147].

As we can see, this bound is respected in Fig. 9. Stricter bounds could be obtained if the running effects on the coupling of the ALP to the muons were considered. However, this would require a more complex treatment of the theory involving all three generations, which is outside the scope of this work.

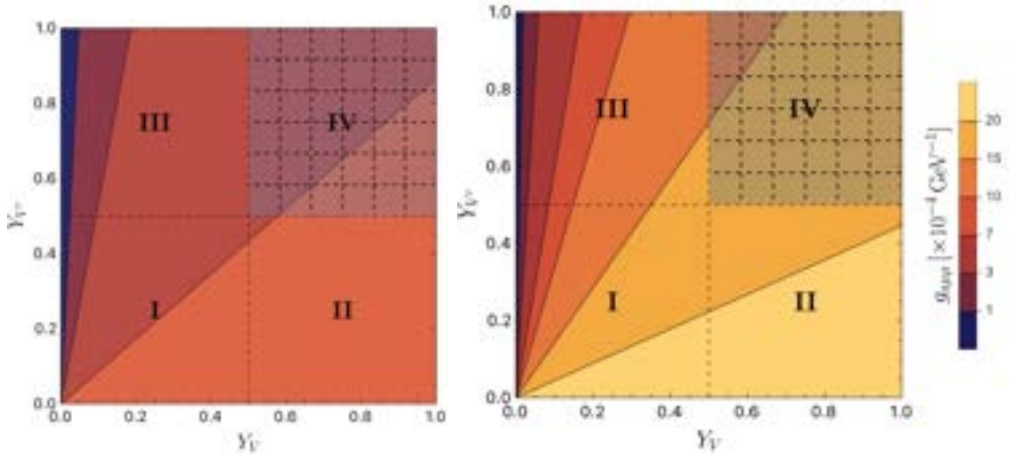

(a) $\alpha_N = 1$ (b) $\alpha_\psi = 1$

Figure 10: *Coupling $g_{a\mu\mu}$ as a function of Y_V, $Y_{V'}$ for model C. The mass scales are taken as $(\Lambda, M_\psi) = (1.5, 0.6)$ TeV. The colours refer to the values of $g_{a\mu\mu}$. The parameters are fixed such that $\delta m_\mu = m_\mu^{exp}$ in all the parameter space.*

It is also interesting to study the behaviour of the ALP-muon coupling as a function of Y_V and $Y_{V'}$. In Fig. 10, we take for definiteness model C and fix $(\Lambda, M_\psi) = (1.5,\ 0.6)$ TeV, that is the red benchmark point in Figs. 6 and 7, for which the $(g-2)_\mu$ tension is solved and the muon mass coincides with its experimental central value. In this case, the $\alpha_{\psi,N}$ parameters are correlated by $\alpha_\psi = \alpha_N\, M_\psi/\Lambda$. The plot in Fig. 10(a) is obtained by fixing for simplicity $\alpha_N = 1$, while in the plot in Fig. 10(b) $\alpha_\psi = 1$. The colours represent the value of the $g_{a\mu\mu}$ coupling: smaller values are in blue while larger values are in yellow, as reported in the side legend. For a given point in this parameter space, the values of the $g_{a\mu\mu}$ coupling in model C are larger than in models A and B by a factor 2, due to the $(\overline{\delta}_{x,1} + \overline{\delta}_{y,1})$ factor. As we can see in no case the upper bound of 0.01 GeV^{-1} is reached.

Besides showing the distribution of the ALP-muon coupling values in this parameter space, we can comment on the patterns of symmetry breaking. As shown in Eq. (2.10), the two Yukawa couplings Y_V and $Y_{V'}$, when promoted to spurions, have different PQ charges that cannot be both simultaneously vanishing for models A, B and C. When the fermion PQ charges are such that $n_{Y_{V'}} = 0$, then the only explicit PQ breaking term is the one associated with Y_V: we thus expect that $Y_V/Y_{V'} \ll 1$, corresponding to the top-left region of the plots, labelled as region III. Instead when $n_V = 0$, it is the other way around, the term with $Y_{V'}$ is the one breaking the symmetry and thus we expect $Y_{V'}/Y_V \ll 1$: it corresponds to the bottom-right region, the II one; when both charges are different from

zero, the corresponding terms are soft PQ breaking, and $Y_{V'} \sim Y_V \ll 1$, that is the bottom-left region, the I one. The only side of both plots that is not theoretically viable is the top-right, region IV, where both Yukawa couplings are relatively large: in this case, both of them should be allowed by the symmetry according to the t'Hooft naturalness principle, but this is inconsistent with the spurion charge analysis.

4 Conclusions

In contrast to gauge symmetries, our knowledge of global symmetries is very much limited. Within the SM, the combination of Baryon and Lepton numbers $B-L$ is conserved at all quantum orders and, experimentally, the lack of proton decay signals suggests that any violation of the Baryon number, if it occurs at all, is by an exceedingly small amount. For the Lepton number, the situation is different, as indeed the Majorana neutrino option is a key ingredient of many Seesaw realisations. Besides this, the Peccei-Quinn solution to the Strong CP problem involves a spontaneously broken Abelian global symmetry, that needs also to be explicitly broken to equip the axion with a mass. The QCD-axion is essentially a pseudo-Goldstone boson that addresses the Strong CP problem. When it does not fulfil this role, it is often referred to as an ALP.

In contrast with the QCD-axion case, no universal mechanism to give an ALP a mass has been identified. In this paper, we present a context where a GeV-mass is originated for an ALP decay constant in the range $f_a \subset [0.5, 100]$ TeV. This is obtained by introducing an additional scalar singlet under the SM gauge symmetries and two lepton $SU(2)_L$-singlets and one vector-like lepton $SU(2)_L$-doublet. This result is novel in the literature, as typically this kind of study is associated with Majorons and the scale f_a is various orders of magnitude larger. We identified three different models, labelled as A, B and C in the main text, where we address different problems: we provide a mass for the ALP and a realistic mass scale for the active neutrinos, solving at the same time the long-standing tension in the anomalous magnetic moment of the muon. Despite being currently subject to strong controversies, the $(g-2)_\mu$ offers a valuable benchmark for BSM phenomenology. If such an anomaly were to fade away, the $(g-2)_\mu$ would become one of the strongest constraints on the model here presented: the ALP phenomenology would quantitatively be different, but qualitatively remains unchanged and thus retains its value.

The peculiar aspect of these models is that the tree-level mass of the muon is forbidden by the global symmetries and it is only generated at 1-loop. In this way, both the muon mass and the δa_μ have a very similar dependence on the Lagrangian parameters, both receiving a LO contribution at 1-loop, chirally enhanced due to the presence of the HNLs in the Feynman diagram. We end up with TeV-scale HNLs that may be tested in the future phase of LHC or next-generation colliders. On the other hand, they also participate in the Seesaw mechanism to give realistic masses and mixings to the active neutrinos, via a Linear Seesaw realisation. Besides that, the simultaneous presence of the lepton singlets and doublet allows to give a GeV-mass to the ALP, which we studied both via the CW potential and explicit loop-computations.

We can summarise the results on the ALP mass and the $(g-2)_\mu$ tension in Fig. 11. Each plot shows the variation of the ALP mass in the Λ $vs.$ M_ψ parameter space, that is the

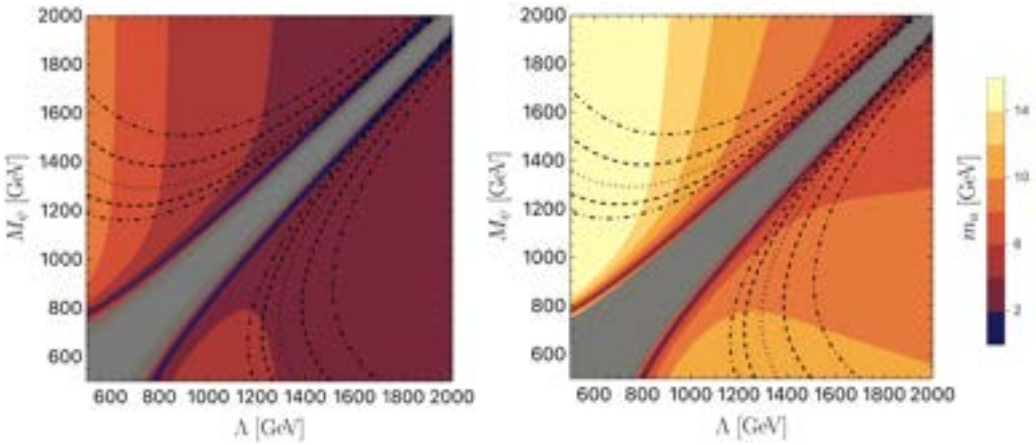

(a) Model A, $Y_V = 0.1$ (b) Model A, $Y_V = 0.5$

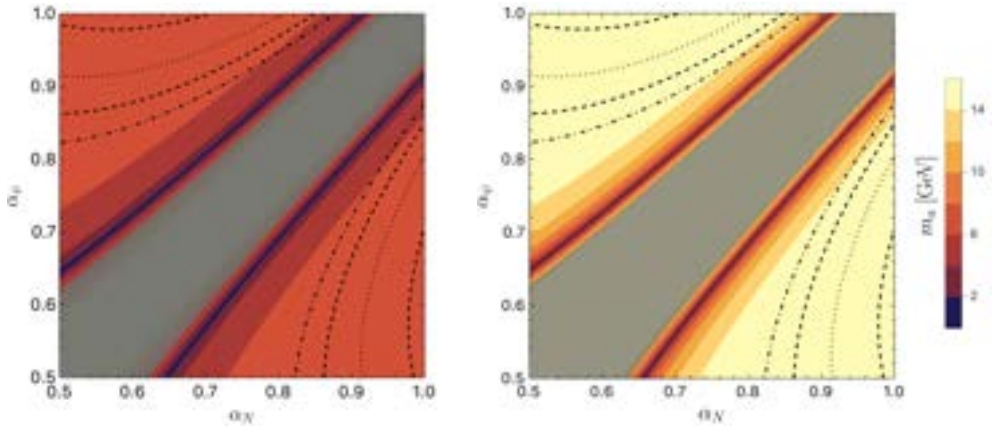

(c) Model C, $Y_V = 0.1$ (d) Model C, $Y_V = 0.5$

Figure 11: *ALP mass in relation to the* $(g-2)_\mu$ *and the mass of the muon. ALP mass values (in GeV) are represented by the different colours in the legend. The dotted line points to the values that explain the experimental muon mass and the central value of the* $(g-2)_\mu$*. The regions between dashed (dot-dashed) lines explain the experimental muon mass when the* $(g-2)_\mu$ *is taken to be at* 1σ (2σ) *from its central experimental value. The grey shaded region stands for the area in which* $|Y_{V'}| > 5$*.* ***Upper row:*** *The left (right) plot represents the ALP mass in the case of model A for values of* $Y_V = 0.1\,(0.5)$*. In both cases,* $\alpha_N = 1$*.* ***Lower row:*** *ALP mass as a function of* α_N/ψ *for model C and* $f_a = 2$ *TeV. In the left (right) plot* $Y_V = 0.1\,(0.5)$*.*

HNLs mass scales, overimposing the regions of the δa_μ solution. The plots on the first row pertain to model A, whereas those for model B can be derived from these plots by reflecting them along the diagonal. The ones in the second row, instead, refer to model C. The plots in the first (second) column have been obtained by fixing $Y_V = 0.1$ ($Y_V = 0.5$). The allowed parameter space, where the active neutrino mass scale is correctly of $\mathcal{O}(0.1)$ eV, the $(g-2)_\mu$ anomaly is solved and the bounds from EW precision observables and collider direct searches of heavy neutral leptons are satisfied, is pretty large, pinpointing to values

for the HNLs masses that cannot be smaller than 1.2 TeV. Accordingly, the predicted ALP masses are about $\sim 1 - 15$ GeV, depending on the value of Y_V. The diagonal grey region for $M_\psi \approx \Lambda$ is theoretically excluded as the muon mass contribution at 1-loop gets highly suppressed unless the Yukawas compensate acquiring large values, thus entering the non-perturbative regime: the thickness of the grey region is determined by the condition $|Y_{V'}| > 5$.

As a specific feature of this model, the ALP-muon coupling spans continuously over various orders of magnitudes, from $\ll \mathcal{O}(1)/f_a$ to $\mathcal{O}(1)/f_a$. This renders our construction a proof-of-concept for the existence of models exhibiting this highly unusual feature: indeed, one would naively expect that the ALP-fermion coupling cannot fluctuate across different orders of magnitude.

Moreover, the ALP-HNLs coupling is fundamental in this construction to obtain the results illustrated above and can be additionally tested at colliders. This type of analysis at present and future Hadron colliders requires the ALP-couplings with quarks or gluons [91]. Instead, a leptophilic ALP could be tested with a dedicated analysis at future leptonic colliders [148].

Acknowledgements

The authors would like to express their gratitude to Stefan Pokorski for his valuable contributions during the initial stages of the project. LM thanks the Department of Physics of the University of California San Diego for hospitality during the development of this project. AdG thanks the University of Heidelberg for its hospitality during the development of this project. The authors acknowledge partial financial support by the European Union's Horizon 2020 research and innovation programme under the Marie Skłodowska-Curie grant agreements No 860881-HIDDeN and 101086085-ASYMMETRY, by the Spanish Research Agency (Agencia Estatal de Investigación) through the grant IFT Centro de Excelencia Severo Ochoa No CEX2020-001007-S and by the grants PID2019-108892RB-I00 and PID2022-137127NB-I00 funded by MCIN/AEI/ 10.13039/501100011033. The work of AdG is supported by the European Union's Horizon 2020 Marie Skłodowska-Curie grant agreement No 860881-HIDDeN. The work of MFZ is supported by the Spanish MIU through the National Program FPU (grant number FPU22/03625). This article is based upon work from COST Action COSMIC WISPers CA21106, supported by COST (European Cooperation in Science and Technology).

A Lagrangian in the mass basis

In this Appendix, we provide the tree-level Lagrangian of Eq. (2.2) in the mass basis, in a generic gauge. We list all interactions with relative corrections of $\mathcal{O}(\Lambda^{-1}, M_\psi^{-1})$. As a reference, we adopt the sign conventions of Ref. [149].

The notation for the Higgs doublet components after the EW symmetry breaking reads

$$H = \begin{pmatrix} G^+ \\ \dfrac{v+h+iG_Z}{\sqrt{2}} \end{pmatrix}, \qquad \widetilde{H} = \begin{pmatrix} \dfrac{v+h-iG_Z}{\sqrt{2}} \\ -G^- \end{pmatrix}, \tag{A.1}$$

where $G^- \equiv (G^+)^*$ are the Goldstone bosons and h the physical Higgs particle. For the neutral fermions, we use the Majorana spinors defined as

$$\psi_{1,2} \equiv \psi^0_{L,R} + (\psi^0_{L,R})^c\,, \qquad N \equiv N_R + N_R^c\,, \qquad S \equiv S_R + S_R^c\,, \qquad \nu \equiv \nu_L + \nu_L^c\,. \tag{A.2}$$

For later convenience, we define the quantities

$$\begin{gathered} s_N \equiv \frac{m_N + \epsilon m_S}{\sqrt{2}}\,, \quad d_N \equiv \frac{m_N - \epsilon m_S}{\sqrt{2}}\,, \quad s_V \equiv \frac{m_V + m_{V'}}{2}\,, \quad d_V \equiv \frac{m_V - m_{V'}}{2}\,, \\ r_+ \equiv \frac{1}{2}\frac{m_V + m_{V'}}{M_\psi - \Lambda} = \frac{s_V}{M_\psi - \Lambda}\,, \quad r_- \equiv \frac{1}{2}\frac{m_V - m_{V'}}{M_\psi + \Lambda} = \frac{d_V}{M_\psi + \Lambda}\,. \end{gathered} \tag{A.3}$$

After the tree-level mass diagonalization procedure, the photon-fermion interactions are exactly SM-like,

$$\mathscr{L}_A = e\left(\overline{\widehat{\mu}}\not{A}\widehat{\mu} + \overline{\widehat{\psi}^-}\not{A}\widehat{\psi}^-\right), \tag{A.4}$$

while the other interactions can be found in Tabs. 3, 4, 5, 6, 7, 8.

$-\left(\frac{h}{v}\right)\times P_R$	$\widehat{\mu}$	$\widehat{\psi}^-$	$\widehat{\nu}$	$\widehat{N}$	$\widehat{S}$	$\widehat{\psi}_1$	$\widehat{\psi}_2$
$\overline{\widehat{\mu}}$	0	0	0	0	0	0	0
$\overline{\widehat{\psi}^-}$	m_R	$\frac{m_R^2}{M_\psi}$	0	0	0	0	0
$\overline{\widehat{\nu}}$	0	0	$-2\epsilon\frac{m_N m_S}{\Lambda}$	s_N	id_N	$(s_N r_+ - d_N r_-)$ $-\frac{s_N s_V + d_N d_V}{\Lambda}$	$i(s_N r_- - d_N r_+)$ $+i\frac{s_N d_V + d_N s_V}{\Lambda}$
$\overline{\widehat{N}}$	0	0	0	$\frac{s_N^2}{\Lambda}+\Lambda(r_+^2+r_-^2)$ $-M_\psi(r_+^2-r_-^2)$	0	s_V	$-id_V$
$\overline{\widehat{S}}$	0	0	0	0	$\frac{d_N^2}{\Lambda}+\Lambda(r_+^2+r_-^2)$ $-M_\psi(r_+^2-r_-^2)$	$-id_V$	$-s_V$
$\overline{\widehat{\psi}_1}$	0	0	0	0	0	$s_V r_+ + d_V r_-$	0
$\overline{\widehat{\psi}_2}$	0	0	0	0	0	0	$s_V r_+ + d_V r_-$

Table 3: h interactions. All interactions should be multiplied by $-h/v$ and include P_R within the fermionic bilinear. The hermitian conjugate is not included.

32

$-\frac{M_Z}{v}Z_\mu\times\gamma^\mu$	$\widehat{\mu}$	$\widehat{\psi}^-$	$\widehat{\nu}$	$\widehat{N}$	$\widehat{S}$	$\widehat{\psi}_1$	$\widehat{\psi}_2$
$\overline{\widehat{\mu}}$	$-c_{2\theta_W}P_L+[1-c_{2\theta_W}]P_R$	$\frac{m_R}{M_\psi}P_R$	0	0	0	0	0
$\overline{\widehat{\psi}^-}$	$\frac{m_R}{M_\psi}P_R$	$-c_{2\theta_W}$	0	0	0	0	0
$\overline{\widehat{\nu}}$	0	0	P_L	$\frac{s_N}{\Lambda}P_L$	$i\frac{d_N}{\Lambda}P_L$	0	0
$\overline{\widehat{N}}$	0	0	$\frac{s_N}{\Lambda}P_L$	0	0	$-r_-P_L$	ir_+P_L
$\overline{\widehat{S}}$	0	0	$-i\frac{d_N}{\Lambda}P_L$	0	0	ir_+P_L	r_-P_L
$\overline{\widehat{\psi}_1}$	0	0	0	$-r_-P_L$	$-ir_+P_L$	0	$-iP_L$
$\overline{\widehat{\psi}_2}$	0	0	0	$-ir_+P_L$	r_-P_L	iP_L	0

Table 4: Z^μ interactions. All interactions should be multiplied by $-M_Z\,Z_\mu/v$ and should include a γ^μ inserted to the left of the projectors. The hermitian conjugate is included.

$i\frac{G_Z}{v}\times P_R$	$\widehat{\mu}$	$\widehat{\psi}^-$	$\widehat{\nu}$	$\widehat{N}$	$\widehat{S}$	$\widehat{\psi}_1$	$\widehat{\psi}_2$
$\overline{\widehat{\mu}}$	0	0	0	0	0	0	0
$\overline{\widehat{\psi}^-}$	$-m_R$	$-\frac{m_R^2}{M_\psi}$	0	0	0	0	0
$\overline{\widehat{\nu}}$	0	0	$-2\epsilon\frac{m_N m_S}{\Lambda}$	s_N	id_N	$\sqrt{2}m_S(r_+ + r_-)$ $+\frac{M_\psi}{\Lambda}(s_N r_- + d_N r_+)$	$i\sqrt{2}m_S(r_+ + r_-)$ $-i\frac{M_\psi}{\Lambda}(s_N r_+ + d_N r_-)$
$\overline{\widehat{N}}$	0	0	0	$\frac{s_N^2}{\Lambda} + 2\Lambda r_+ r_-$	0	$-d_V$	is_V
$\overline{\widehat{S}}$	0	0	0	0	$\frac{d_N^2}{\Lambda} + 2\Lambda r_+ r_-$	is_V	d_V
$\overline{\widehat{\psi}_1}$	0	0	0	0	0	$-2M_\psi r_+ r_-$	0
$\overline{\widehat{\psi}_2}$	0	0	0	0	0	0	$-2M_\psi r_+ r_-$

Table 5: G_Z interactions. Each term has to be multiplied by $i\,G_Z/v$ and must include a P_R within the fermionic bilinears. The hermitian conjugate is not included.

$-\frac{\sqrt{2}M_W W_\mu^-}{v}$	$\widehat{\mu}$	$\widehat{\psi}^-$	$\widehat{\nu}$	$\widehat{N}$	$\widehat{S}$	$\widehat{\psi}_1$	$\widehat{\psi}_2$
$\overline{\widehat{\mu}}$	0	0	P_L	$\frac{s_N}{\Lambda}P_L$	$i\frac{d_N}{\Lambda}P_L$	$-\frac{m_R}{\sqrt{2}M_\psi}P_R$	$i\frac{m_R}{\sqrt{2}M_\psi}P_R$
$\overline{\widehat{\psi}^-}$	0	0	0	$-\frac{r_+ + r_-}{\sqrt{2}}P_L - \frac{r_+ - r_-}{\sqrt{2}}P_R$	$-i\frac{r_+ + r_-}{\sqrt{2}}P_L - i\frac{r_+ - r_-}{\sqrt{2}}P_R$	$\frac{1}{\sqrt{2}}$	$\frac{-i}{\sqrt{2}}$
$\overline{\widehat{\nu}}$	0	0	0	0	0	0	0
$\overline{\widehat{N}}$	0	0	0	0	0	0	0
$\overline{\widehat{S}}$	0	0	0	0	0	0	0
$\overline{\widehat{\psi}_1}$	0	0	0	0	0	0	0
$\overline{\widehat{\psi}_2}$	0	0	0	0	0	0	0

Table 6: W_μ^- interactions. Each term must be multiplied by $-\sqrt{2}M_W\,W_\mu^-/v$ and must include a γ^μ at the left of the projectors in the fermionic bilinear.

$-\left(\frac{\sqrt{2}G^-}{v}\right)$	$\widehat{\mu}$	$\widehat{\psi}^-$	$\widehat{\nu}$	$\widehat{N}$	$\widehat{S}$	$\widehat{\psi}_1$	$\widehat{\psi}_2$
$\overline{\widehat{\mu}}$	0	0	$\left[2\epsilon\frac{m_N m_S}{\Lambda}\right] P_R$	$\left[-\frac{m_R}{\sqrt{2}}\frac{\Lambda}{M_\psi}(r_+ - r_-)\right] P_L$ $+\left[-s_N\right] P_R$	$\left[-i\frac{m_R}{\sqrt{2}}\frac{\Lambda}{M_\psi}(r_+ - r_-)\right] P_L$ $+\left[-id_N\right] P_R$	$\left[\frac{m_R}{\sqrt{2}}\right] P_L$ $+\left[d_N r_- - s_N r_+\right] P_R$	$\left[-i\frac{m_R}{\sqrt{2}}\right] P_L$ $+\left[i(d_N r_+ - s_N r_-)\right] P_R$
$\overline{\widehat{\psi}^-}$	0	0	$\left[\frac{m_N m_V}{\Lambda}\right] P_L$ $+\left[\epsilon\frac{m_S m_{V'}}{\Lambda}\right] P_R$	$\left[-\frac{m_V}{\sqrt{2}}\right] P_L$ $+\left[-\frac{m_{V'}}{\sqrt{2}}\right] P_R$	$\left[-i\frac{m_V}{\sqrt{2}}\right] P_L$ $+\left[-i\frac{m_{V'}}{\sqrt{2}}\right] P_R$	$\left[-\frac{m_V}{\sqrt{2}}(r_+ + r_-) + \frac{m_R^2}{\sqrt{2}M_\psi}\right] P_L$ $+\left[-\frac{m_{V'}}{\sqrt{2}}(r_+ - r_-)\right] P_R$	$\left[i\frac{m_V}{\sqrt{2}}(r_+ + r_-) - i\frac{m_R^2}{\sqrt{2}M_\psi}\right] P_L$ $+\left[i\frac{m_{V'}}{\sqrt{2}}(r_+ - r_-)\right] P_R$
$\overline{\widehat{\nu}}$	0	0	0	0	0	0	0
$\overline{\widehat{N}}$	0	0	0	0	0	0	0
$\overline{\widehat{S}}$	0	0	0	0	0	0	0
$\overline{\widehat{\psi}_1}$	0	0	0	0	0	0	0
$\overline{\widehat{\psi}_2}$	0	0	0	0	0	0	0

Table 7: G^- interactions. Each term has to be multiplied by $-\sqrt{2}G^-/v$. The projectors $P_{L,R}$ must be included within the fermionic bilinears.

$-\frac{\sqrt{2}}{f_a}\phi^{(*)} \times P_R$	$\widehat{\mu}$	$\widehat{\psi}^-$	$\widehat{\nu}$	$\widehat{N}$	$\widehat{S}$	$\widehat{\psi}_1$	$\widehat{\psi}_2$
$\overline{\widehat{\mu}}$	0	0	0	0	0	0	0
$\overline{\widehat{\psi}^-}$	$-\delta_{\lvert y\rvert,1} m_R$	$\delta_{\lvert y\rvert,1} M_\psi$	0	0	0	0	0
$\overline{\widehat{\nu}}$	0	0	0	$-\delta_{\lvert x\rvert,1} s_N$	$-i\delta_{\lvert x\rvert,1} d_N$	0	0
$\overline{\widehat{N}}$	0	0	0	$\delta_{\lvert x\rvert,1}\frac{\Lambda}{2}$	0	$(\delta_{\lvert x\rvert,1}\Lambda - \delta_{\lvert y\rvert,1} M_\psi) r_+$	$i(\delta_{\lvert x\rvert,1}\Lambda + \delta_{\lvert y\rvert,1} M_\psi) r_-$
$\overline{\widehat{S}}$	0	0	0	0	$\delta_{\lvert x\rvert,1}\frac{\Lambda}{2}$	$i(\delta_{\lvert x\rvert,1}\Lambda + \delta_{\lvert y\rvert,1} M_\psi) r_-$	$-(\delta_{\lvert x\rvert,1}\Lambda - \delta_{\lvert y\rvert,1} M_\psi) r_+$
$\overline{\widehat{\psi}_1}$	0	0	0	0	0	$\delta_{\lvert y\rvert,1}\frac{M_\psi}{2}$	0
$\overline{\widehat{\psi}_2}$	0	0	0	0	0	0	$\delta_{\lvert y\rvert,1}\frac{M_\psi}{2}$

Table 8: ϕ interactions. Each term has to be multiplied by $-\sqrt{2}\phi^{(*)}/f_a$. P_R must be inserted in all fermionic bilinears. The choice of ϕ or ϕ^* depends on the model and should be placed in front of the corresponding $\delta_{|x|,1}$ or $\delta_{|y|,1}$. The hermitian conjugate is not included.

B ALP mass full result

The ALP potential can be obtained using the Coleman-Weinberg potential [118] which for Weyl fermions in dimensional regularization $d = 4 - 2\varepsilon$ reads

$$V_{\rm CW} = -\frac{1}{2}\cdot\frac{1}{16\pi^2}\left\{\mathrm{Tr}\left[\left(M_\chi M_\chi^\dagger\right)^2\log\left(\frac{M_\chi M_\chi^\dagger}{\mu_R^2}\right)\right] - \mathrm{Tr}\left[\left(M_\chi M_\chi^\dagger\right)^2\right]\left(\frac{3}{2}+\frac{1}{\widetilde{\varepsilon}}\right)\right\} \tag{B.1}$$

where $\mathcal{M}_\chi$ is the 5×5 neutral mass matrix of Eq. (2.14), μ_R the renormalization scale, and

$$\frac{1}{\widetilde{\varepsilon}} \equiv \frac{1}{\varepsilon} - \gamma_E + \log(4\pi)\,, \tag{B.2}$$

where γ_E is the Euler-Mascheroni constant. The charged mass matrix does not contribute to the ALP potential. By exploiting the properties of the trace, the above expression can be written in terms of the eigenvalues, $\{\lambda_i\}_{i=1}^5$, of $\mathcal{M}_\chi\mathcal{M}_\chi^\dagger$

$$V_{\rm CW} = -\frac{1}{2}\cdot\frac{1}{16\pi^2}\sum_{i=1}^{5}\left\{\lambda_i^2\log\left(\frac{\lambda_i^2}{\mu_R^2}\right) - \lambda_i^2\left(\frac{3}{2}+\frac{1}{\widetilde{\varepsilon}}\right)\right\}. \tag{B.3}$$

We can further simplify the problem. One eigenvalue can be safely neglected due to its smallness as it should be of order of the neutrino mass. Furthermore, the remaining four eigenvalues are equal two to two (cfr. Eq. (2.15)), reducing the problem to the computation of only two eigenvalues here called $\lambda_{1,2}$. They can be conveniently extracted from the traces of $\mathcal{M}_\chi\mathcal{M}_\chi^\dagger$

$$\mathrm{Tr}\left(\mathcal{M}_\chi\mathcal{M}_\chi^\dagger\right) \approx 2(\lambda_1+\lambda_2)\,, \qquad \mathrm{Tr}(\mathcal{M}_\chi\mathcal{M}_\chi^\dagger)^2 \approx 2(\lambda_1^2+\lambda_2^2)\,, \tag{B.4}$$

yielding

$$\lambda_{1,2} \approx \frac{\mathrm{Tr}\left(\mathcal{M}_\chi\mathcal{M}_\chi^\dagger\right) \pm \sqrt{4\mathrm{Tr}\left(\mathcal{M}_\chi\mathcal{M}_\chi^\dagger\right)^2 - \left(\mathrm{Tr}\mathcal{M}_\chi\mathcal{M}_\chi^\dagger\right)^2}}{4}\,. \tag{B.5}$$

Finally, the mass of the ALP can be obtained via

$$m_a^2 \equiv \left.\frac{\partial^2 V_{\rm CW}}{\partial a^2}\right|_{a=0}\,. \tag{B.6}$$

We now turn to the computation of the potential for the four models studied in this paper. The associated mass matrices for each model are

Model A:
$$\mathcal{M}_{\chi,A} = \begin{pmatrix} 0 & m_N & m_S & 0 & 0 \\ m_N & 0 & \alpha_N\phi^{(*)} & m_V' & 0 \\ m_S & \alpha_N\phi^{(*)} & 0 & 0 & m_V \\ 0 & m_V' & 0 & 0 & M_\psi \\ 0 & 0 & m_V & M_\psi & 0 \end{pmatrix}, \tag{B.7}$$

Model B:
$$\mathcal{M}_{\chi,B} = \begin{pmatrix} 0 & m_N & m_S & 0 & 0 \\ m_N & 0 & \Lambda & m_V' & 0 \\ m_S & \Lambda & 0 & 0 & m_V \\ 0 & m_V' & 0 & 0 & \alpha_\psi\phi^{(*)} \\ 0 & 0 & m_V & \alpha_\psi\phi^{(*)} & 0 \end{pmatrix}, \tag{B.8}$$

$$\textbf{Model C:} \qquad \mathcal{M}_{\chi,C} = \begin{pmatrix} 0 & m_N & m_S & 0 & 0 \\ m_N & 0 & \alpha_N\phi^{(*)} & m'_V & 0 \\ m_S & \alpha_N\phi^{(*)} & 0 & 0 & m_V \\ 0 & m'_V & 0 & 0 & \alpha_\psi\phi^{(*)} \\ 0 & 0 & m_V & \alpha_\psi\phi^{(*)} & 0 \end{pmatrix}, \tag{B.9}$$

$$\textbf{Model D:} \qquad \mathcal{M}_{\chi,D} = \begin{pmatrix} 0 & m_N & m_S & 0 & 0 \\ m_N & 0 & \alpha_N\phi & m'_V & 0 \\ m_S & \alpha_N\phi & 0 & 0 & m_V \\ 0 & m'_V & 0 & 0 & \alpha_\psi\phi^* \\ 0 & 0 & m_V & \alpha_\psi\phi^* & 0 \end{pmatrix}. \tag{B.10}$$

Notice that in model A, B and C $\alpha_{N/\psi}$ can be proportional to either ϕ or ϕ^*, while model D is characterised by having $\alpha_N\phi$, $\alpha_\psi\phi^*$ or $\alpha_N\phi^*$, $\alpha_\psi\phi$.

By explicit computation one finds

$$\begin{aligned} V_{\rm CW} &\supset a^2(\overline{\delta}_{x,1}+\overline{\delta}_{y,1})^2\frac{m_{V'}m_V\Lambda M_\psi}{8\pi^2 f_a^2}\left\{\frac{1}{2}\left[\frac{c}{d}\log\left(\frac{c+d}{c-d}\right)+\log\left(\frac{c^2-d^2}{\mu_R^4}\right)\right]-1-\frac{1}{\widetilde{\varepsilon}}\right\}, \\ m_a^2 &= (\overline{\delta}_{x,1}+\overline{\delta}_{y,1})^2\frac{m_{V'}m_V\Lambda M_\psi}{4\pi^2 f_a^2}\left\{\frac{1}{2}\left[\frac{c}{d}\log\left(\frac{c+d}{c-d}\right)+\log\left(\frac{c^2-d^2}{\mu_R^4}\right)\right]-1-\frac{1}{\widetilde{\varepsilon}}\right\}, \\ c &= \frac{1}{2}\left(m_N^2+m_V^2+m_{V'}^2+\Lambda^2+M_\psi^2\right), \\ d &= \sqrt{c^2-m_N^2\left(m_V^2+M_\psi^2\right)-m_{V'}^2m_V^2-\Lambda^2M_\psi^2+2m_Vm_{V'}\Lambda M_\psi}\,, \end{aligned} \tag{B.11}$$

where $(\overline{\delta}_{x,1},\overline{\delta}_{y,1})$ are two parameters that interpolate among all models and follow the convention established in the main text. Taking the limit of large Λ, M_ψ, leads to the LO expression of Eq. (2.30).

C Details on the ALP coupling to muons

In this Appendix, we further investigate the result of the ALP-muon coupling obtained in Eq. (2.39). This result might at first sight look obscure as it comes from a combination of tree-level mixing and loop results. We show here how from symmetry arguments the situation is more transparent and how the result can be obtained solely from them.

As can be noticed from Eq. (2.39), the LO ALP coupling to on-shell muons is zero if

$$c^R_{a\mu\mu} = -c^L_{a\mu\mu} = 0 \qquad \Leftrightarrow \qquad Y_V = 0 \vee \overline{\delta}_{x,1} = -\overline{\delta}_{y,1}\,, \tag{C.1}$$

and otherwise closely resembles the 1-loop muon mass. Such features, which might seem peculiar at first glance, can be understood on more general grounds. To appreciate it, let us first consider the Lagrangian to be PQ-invariant, and let us assume that, still in the interaction-basis, we rotate away the ALP from the Yukawa sector via the rotation

$$\Psi \to e^{i\chi_\Psi\frac{a}{f_a}}\Psi\,, \tag{C.2}$$

being χ_Ψ the PQ-charge of the generic fermion Ψ. As the symmetry is assumed to be exact, the ALP Lagrangian will only contain interactions of the form

$$\mathscr{L}_a \supset -\frac{\partial_\mu a}{f_a}\left(\chi_{\mu_L}\overline{\mu_L}\gamma^\mu\mu_L + \chi_{\mu_R}\overline{\mu_R}\gamma^\mu\mu_R + \chi_{\psi_L^-}\overline{\psi_L^-}\gamma^\mu\psi_L^- + \chi_{\psi_R^-}\overline{\psi_R^-}\gamma^\mu\psi_R^-\right). \tag{C.3}$$

To go to the mass basis, at tree-level, we just need to rotate the right-handed fields (cfr. (2.18)). We are interested in the coupling of the ALP to muons in the chirality-flipping basis. When considering on-shell fermions, one can move from the derivative- to the chirality-flipping basis integrating by parts and applying the equations of motion of the fermions. Using such a procedure, the couplings of the ALP to fermions are found to be proportional to their masses (see e.g. Ref. [73]). As in our case the mass of the muon is generated at 1-loop, all 1-loop contributions to the derivative couplings of Eq. (C.3) formally become 2-loops when moving to the chirality-flipping basis, and thus must be neglected accordingly to the approximation we took throughout the paper. All in all, this implies that at 1-loop it is sufficient to consider only the tree-level mixing of the fields, yielding

$$\mathscr{L}_a \supset -\frac{\partial_\mu a}{f_a}\left[\chi_{\mu_L}\overline{\widehat{\mu}}\gamma^\mu\widehat{\mu} + \left((\chi_{\mu_R}-\chi_{\mu_L}) - (\chi_{\mu_R}-\chi_{\psi_R})\left(\frac{m_R^2}{M_\psi^2}\frac{1}{1+m_R^2/M_\psi^2}\right)\right)\overline{\widehat{\mu}_R}\gamma^\mu\widehat{\mu}_R\right]. \tag{C.4}$$

The first term vanishes when applying the equations of motion, while the second generates the term

$$\mathscr{L}_a \supset \frac{a}{f_a}\left[(\chi_{\mu_R}-\chi_{\mu_L}) - (\chi_{\mu_R}-\chi_{\psi_R})\left(\frac{m_R^2}{M_\psi^2}\frac{1}{1+m_R^2/M_\psi^2}\right)\right]\underbrace{\widehat{m}_\mu}_{=\delta m_\mu}\overline{\widehat{\mu}}i\gamma_5\widehat{\mu}\,. \tag{C.5}$$

This result, valid assuming an exact PQ-symmetry, has two main consequences:

1. the coupling of the muon to the ALP must be proportional to its mass weighted by the PQ-charges;
2. the coupling at LO vanishes if $\chi_{\mu_L} = \chi_{\mu_R}$, i.e. if the rotation is vectorial, and is not zero but suppressed by an extra m_R^2/M_ψ^2 if and only if $\chi_{\mu_L} \neq \chi_{\mu_R}$.

Let us now examine the result of Eq. (2.39) under such considerations. In our case, the PQ-symmetry is not exact, so we have to take some extra care. As we learnt from the computation of m_a^2, the PQ is restored if $Y_V = 0$, $Y_{V'} = 0$, or in model D independently of $Y_{V,V'}$. Let us examine the different cases separately to check the correctness of the consistency of the computation.

$\mathbf{Y_V = 0}$. In this case, one can see that $\chi_{\mu_L} = \chi_{\mu_R}$ is a possible charge assignment in all the models, meaning that we expect no ALP-muon coupling at LO. This is consistent with the explicit computation of Eq. (2.39).

$Y_{V'} = 0$. In this case, the coupling computed in Eq. (2.39) is exactly proportional to the muon mass. The charges in the different models are given in Tab. 9. The case of model D is discussed in the next section, as it is independent of $Y_{V'}$ being zero or not. As it can be seen from the charges, we always find that $\overline{\delta}_{x,1} + \overline{\delta}_{y,1} = (\chi_{\mu_R} - \chi_{\mu_L})$, confirming the matching between explicit loop calculation and the expected result of Eq. (C.5).

Model	χ_{μ_L}	χ_{μ_R}	χ_{ψ_R}	$\overline{\delta}_{x,1}$	$\overline{\delta}_{y,1}$
A	$-1/2$	$1/2$	$1/2$	1	0
B	0	-1	0	0	-1
C	$-1/2$	$3/2$	$1/2$	1	1
D	$-1/2$	$-1/2$	$1/2$	1	-1

Table 9: *PQ-charges of the fields in the case $Y_{V'} = 0$ for the different models.*

Model D. In this case, one finds that $\chi_{\mu_L} = \chi_{\mu_R} = -1/2$, and so the LO coupling is zero. Almost magically, in this case $\overline{\delta}_{x,1} = -\overline{\delta}_{y,1}$, setting to zero the explicitly computed 1-loop ALP-muon coupling.

Despite the PQ being explicitly broken, one can still artificially match the result to the standard ALP EFT in the derivative basis

$$\mathscr{L}_a^{\text{EFT}} \supset \frac{\partial_\mu a}{f_a} \left(c_{\ell_L} \overline{\ell_L} \gamma^\mu \ell_L + c_{\mu_R} \overline{\mu_R} \gamma^\mu \mu_R \right) , \tag{C.6}$$

by imposing

$$\frac{c_{\mu_R} - c_{\ell_L}}{f_a} = \frac{c^R_{a\mu\mu}}{f_a\, \delta m_\mu} = \frac{(\overline{\delta}_{x_1} + \overline{\delta}_{y,1})}{f_a} \times \left(\frac{Y_V}{Y_V + \left(\frac{M_\psi}{\Lambda}\right) Y_{V'}} \right) . \tag{C.7}$$

The only parameters that appear in this result are the same ones that appear also in the computation of m_a^2; this is no coincidence as they are the only ones responsible for the (in)exactness of the PQ-symmetry. If the PQ-symmetry was exact the coupling would only depend on the PQ-charges of the muon; in the case of broken PQ it just retains a proportionality to them, allowing for arbitrarily small values of $c_{\ell_L} - c_{\mu_R}$ depending on $Y_{V,V'}$, Λ, M_ψ. This fact seems trivial from the starting point of the ALP EFT where the Wilson coefficients do not necessarily play the role of PQ-charges and can thus pick any values, but it is highly non-trivial from the point of view of the UV theory. Interestingly, this coupling can be made arbitrarily small by taking $Y_V \to 0$ and still reproducing the correct muon mass via $Y_{V'}$.

Remarkably, notice that the structure of the deviation of the result from the exact-PQ one reported in Eq. (3.22) can be obtained by combining all the previous considerations without the need of actually computing any loops. As the symmetry breaking is realized by the simultaneous presence of four parameters, $Y_{V,V'}$, Λ, M_ψ, one can parameterize the coupling of the ALP to muons as

$$\mathscr{L}_a \supset \frac{a}{f_a} \overline{\widehat{\mu}_L} i\gamma_5 \widehat{\mu}_R \times m_\mu^{\text{exp}} \times \left(\frac{M_\psi(\alpha_1 Y_V + \alpha_2 Y_{V'}) + \Lambda(\beta_1 Y_V + \beta_2 Y_{V'})}{M_\psi(\gamma_1 Y_V + \gamma_2 Y_{V'}) + \Lambda(\delta_1 Y_V + \delta_2 Y_{V'})} \right) , \tag{C.8}$$

where $\alpha_{1,2}$, $\beta_{1,2}$, $\gamma_{1,2}$, $\delta_{1,2}$ are some unknown parameters that should be determined by the computation. By imposing the correction either to vanish or to be exactly 1 when the symmetry is restored, depending on the charges of the fields, we can fix many of the constants. For example, when $Y_V = 0$ we require the PQ-breaking correction to vanish as the PQ is vectorial for the muons at LO, meaning that $M_\psi \alpha_2 = -\Lambda\beta_2$. Applying all conditions, it yields

$$\mathscr{L}_a \supset \frac{a}{f_a}\overline{\widehat{\mu}_L} i\gamma_5 \widehat{\mu}_R \times m_\mu^{\text{exp}} \times \left(\frac{Y_V}{Y_V + \left(\frac{\gamma_2}{\delta_1}\right)\left(\frac{M_\psi}{\Lambda}\right) Y_{V'}} \right) . \tag{C.9}$$

Such an expression correctly reproduces the result of the explicit computation of Eq. (3.22) up to a numerical coefficient that cannot be determined solely by symmetry arguments.

References

[1] R. D. Peccei and H. R. Quinn, *CP Conservation in the Presence of Instantons*, Phys. Rev. Lett. **38** (1977) 1440–1443.

[2] S. Weinberg, *A New Light Boson?*, Phys. Rev. Lett. **40** (1978) 223–226.

[3] F. Wilczek, *Problem of Strong P and T Invariance in the Presence of Instantons*, Phys. Rev. Lett. **40** (1978) 279–282.

[4] A. R. Zhitnitsky, *On Possible Suppression of the Axion Hadron Interactions. (In Russian)*, Sov. J. Nucl. Phys. **31** (1980) 260.

[5] M. Dine, W. Fischler, and M. Srednicki, *A Simple Solution to the Strong CP Problem with a Harmless Axion*, Phys. Lett. B **104** (1981) 199–202.

[6] J. E. Kim, *Weak Interaction Singlet and Strong CP Invariance*, Phys. Rev. Lett. **43** (1979) 103.

[7] M. A. Shifman, A. I. Vainshtein, and V. I. Zakharov, *Can Confinement Ensure Natural CP Invariance of Strong Interactions?*, Nucl. Phys. B **166** (1980) 493–506.

[8] L. Di Luzio, F. Mescia, and E. Nardi, *Redefining the Axion Window*, Phys. Rev. Lett. **118** (2017), no. 3 031801, [arXiv:1610.07593].

[9] L. Di Luzio, F. Mescia, and E. Nardi, *Window for preferred axion models*, Phys. Rev. D **96** (2017), no. 7 075003, [arXiv:1705.05370].

[10] M. K. Gaillard, M. B. Gavela, R. Houtz, P. Quilez, and R. Del Rey, *Color unified dynamical axion*, Eur. Phys. J. C **78** (2018), no. 11 972, [arXiv:1805.06465].

[11] A. Hook, S. Kumar, Z. Liu, and R. Sundrum, *High Quality QCD Axion and the LHC*, Phys. Rev. Lett. **124** (2020), no. 22 221801, [arXiv:1911.12364].

[12] L. Di Luzio, M. Giannotti, E. Nardi, and L. Visinelli, *The landscape of QCD axion models*, Phys. Rept. **870** (2020) 1–117, [arXiv:2003.01100].

[13] L. Di Luzio, R. Gröber, and P. Paradisi, *Hunting for CP-violating axionlike particle interactions*, Phys. Rev. D **104** (2021), no. 9 095027, [arXiv:2010.13760].

[14] L. Di Luzio, B. Gavela, P. Quilez, and A. Ringwald, *An even lighter QCD axion*, JHEP **05** (2021) 184, [arXiv:2102.00012].

[15] L. Di Luzio, B. Gavela, P. Quilez, and A. Ringwald, *Dark matter from an even lighter QCD axion: trapped misalignment*, JCAP **10** (2021) 001, [arXiv:2102.01082].

[16] B. Gavela, P. Quílez, and M. Ramos, *Multiple QCD axion*, arXiv:2305.15465.

[17] P. Cox, T. Gherghetta, and A. Paul, *A common origin for the QCD axion and sterile neutrinos from SU(5) strong dynamics*, JHEP **12** (2023) 180, [arXiv:2310.08557].

[18] F. Wilczek, *Axions and Family Symmetry Breaking*, Phys. Rev. Lett. **49** (1982) 1549–1552.

[19] Y. Ema, K. Hamaguchi, T. Moroi, and K. Nakayama, *Flaxion: a minimal extension to solve puzzles in the standard model*, JHEP **01** (2017) 096, [arXiv:1612.05492].

[20] L. Calibbi, F. Goertz, D. Redigolo, R. Ziegler, and J. Zupan, *Minimal axion model from flavor*, Phys. Rev. D **95** (2017), no. 9 095009, [arXiv:1612.08040].

[21] F. Arias-Aragon and L. Merlo, *The Minimal Flavour Violating Axion*, JHEP **10** (2017) 168, [arXiv:1709.07039]. [Erratum: JHEP 11, 152 (2019)].

[22] F. Arias-Aragón, E. Fernández-Martínez, M. González-López, and L. Merlo, *Dynamical Minimal Flavour Violating inverse seesaw*, JHEP **09** (2022) 210, [arXiv:2204.04672].

[23] L. Di Luzio, A. W. M. Guerrera, X. P. Díaz, and S. Rigolin, *On the IR/UV flavour connection in non-universal axion models*, JHEP **06** (2023) 046, [arXiv:2304.04643].

[24] Y. Chikashige, R. N. Mohapatra, and R. D. Peccei, *Spontaneously Broken Lepton Number and Cosmological Constraints on the Neutrino Mass Spectrum*, Phys. Rev. Lett. **45** (1980) 1926.

[25] Y. Chikashige, R. N. Mohapatra, and R. D. Peccei, *Are There Real Goldstone Bosons Associated with Broken Lepton Number?*, Phys. Lett. B **98** (1981) 265–268.

[26] G. B. Gelmini and M. Roncadelli, *Left-Handed Neutrino Mass Scale and Spontaneously Broken Lepton Number*, Phys. Lett. B **99** (1981) 411–415.

[27] L. Merlo, F. Pobbe, and S. Rigolin, *The Minimal Axion Minimal Linear σ Model*, Eur. Phys. J. C **78** (2018), no. 5 415, [arXiv:1710.10500]. [Erratum: Eur.Phys.J.C 79, 963 (2019)].

[28] I. Brivio, M. B. Gavela, S. Pascoli, R. del Rey, and S. Saa, *The axion and the Goldstone Higgs*, Chin. J. Phys. **61** (2019) 55–71, [arXiv:1710.07715].

[29] J. Alonso-González, L. Merlo, F. Pobbe, S. Rigolin, and O. Sumensari, *Testable axion-like particles in the minimal linear σ model*, Nucl. Phys. B **950** (2020) 114839, [arXiv:1807.08643].

[30] J. Alonso-Gonzalez, J. M. Lizana, V. Martinez-Fernandez, L. Merlo, and S. Pokorski, *Probing effective field theory approach in the CP violating minimal linear σ model*, Eur. Phys. J. C **81** (2021), no. 6 538, [arXiv:2012.03990].

[31] B. Bellazzini, A. Mariotti, D. Redigolo, F. Sala, and J. Serra, *R-axion at colliders*, Phys. Rev. Lett. **119** (2017), no. 14 141804, [arXiv:1702.02152].

[32] E. Witten, *Some Properties of O(32) Superstrings*, Phys. Lett. B **149** (1984) 351–356.

[33] K.-S. Choi, I.-W. Kim, and J. E. Kim, *String compactification, QCD axion and axion-photon-photon coupling*, JHEP **03** (2007) 116, [hep-ph/0612107].

[34] P. Svrcek and E. Witten, *Axions In String Theory*, JHEP **06** (2006) 051, [hep-th/0605206].

[35] A. Arvanitaki, S. Dimopoulos, S. Dubovsky, N. Kaloper, and J. March-Russell, *String Axiverse*, Phys. Rev. D **81** (2010) 123530, [arXiv:0905.4720].

[36] M. Cicoli, M. Goodsell, and A. Ringwald, *The type IIB string axiverse and its low-energy phenomenology*, JHEP **10** (2012) 146, [arXiv:1206.0819].

[37] G. Gelmini, D. N. Schramm, and J. W. F. Valle, *Majorons: A Simultaneous Solution to the Large and Small Scale Dark Matter Problems*, Phys. Lett. B **146** (1984) 311–317.

[38] V. Berezinsky and J. W. F. Valle, *The KeV majoron as a dark matter particle*, Phys. Lett. B **318** (1993) 360–366, [hep-ph/9309214].

[39] M. Lattanzi and J. W. F. Valle, *Decaying warm dark matter and neutrino masses*, Phys. Rev. Lett. **99** (2007) 121301, [arXiv:0705.2406].

[40] F. Bazzocchi, M. Lattanzi, S. Riemer-Sørensen, and J. W. F. Valle, *X-ray photons from late-decaying majoron dark matter*, JCAP **08** (2008) 013, [arXiv:0805.2372].

[41] M. Lattanzi, S. Riemer-Sorensen, M. Tortola, and J. W. F. Valle, *Updated CMB and x- and γ-ray constraints on Majoron dark matter*, Phys. Rev. D **88** (2013), no. 6 063528, [arXiv:1303.4685].

[42] F. S. Queiroz and K. Sinha, *The Poker Face of the Majoron Dark Matter Model: LUX to keV Line*, Phys. Lett. B **735** (2014) 69–74, [arXiv:1404.1400].

[43] R. Z. Ferreira and A. Notari, *Observable Windows for the QCD Axion Through the Number of Relativistic Species*, Phys. Rev. Lett. **120** (2018), no. 19 191301, [arXiv:1801.06090].

[44] F. D'Eramo, R. Z. Ferreira, A. Notari, and J. L. Bernal, *Hot Axions and the H_0 tension*, JCAP **11** (2018) 014, [arXiv:1808.07430].

[45] M. Escudero and S. J. Witte, *A CMB search for the neutrino mass mechanism and its relation to the Hubble tension*, Eur. Phys. J. C **80** (2020), no. 4 294, [arXiv:1909.04044].

[46] F. Arias-Aragón, F. D'eramo, R. Z. Ferreira, L. Merlo, and A. Notari, *Cosmic Imprints of XENON1T Axions*, JCAP **11** (2020) 025, [arXiv:2007.06579].

[47] F. Arias-Aragon, E. Fernandez-Martinez, M. Gonzalez-Lopez, and L. Merlo, *Neutrino Masses and Hubble Tension via a Majoron in MFV*, Eur. Phys. J. C **81** (2021), no. 1 28, [arXiv:2009.01848].

[48] F. Arias-Aragón, F. D'Eramo, R. Z. Ferreira, L. Merlo, and A. Notari, *Production of Thermal Axions across the ElectroWeak Phase Transition*, JCAP **03** (2021) 090, [arXiv:2012.04736].

[49] R. Z. Ferreira, A. Notari, and F. Rompineve, *Dine-Fischler-Srednicki-Zhitnitsky axion in the CMB*, Phys. Rev. D **103** (2021), no. 6 063524, [arXiv:2012.06566].

[50] M. Escudero and S. J. Witte, *The hubble tension as a hint of leptogenesis and neutrino mass generation*, Eur. Phys. J. C **81** (2021), no. 6 515, [arXiv:2103.03249].

[51] T. Araki, K. Asai, K. Honda, R. Kasuya, J. Sato, T. Shimomura, and M. J. S. Yang, *Resolving the Hubble tension in a U(1)$_{L_\mu - L_\tau}$ model with the Majoron*, PTEP **2021** (2021), no. 10 103B05, [arXiv:2103.07167].

[52] F. D'Eramo, F. Hajkarim, and S. Yun, *Thermal Axion Production at Low Temperatures: A Smooth Treatment of the QCD Phase Transition*, Phys. Rev. Lett. **128** (2022), no. 15 152001, [arXiv:2108.04259].

[53] F. D'Eramo, F. Hajkarim, and S. Yun, *Thermal QCD Axions across Thresholds*, JHEP **10** (2021) 224, [arXiv:2108.05371].

[54] F. D'Eramo, E. Di Valentino, W. Giarè, F. Hajkarim, A. Melchiorri, O. Mena, F. Renzi, and S. Yun, *Cosmological bound on the QCD axion mass, redux*, JCAP **09** (2022) 022, [arXiv:2205.07849].

[55] H. Georgi, D. B. Kaplan, and L. Randall, *Manifesting the Invisible Axion at Low-energies*, Phys. Lett. B **169** (1986) 73–78.

[56] K. Choi, K. Kang, and J. E. Kim, *Effects of η' in Low-energy Axion Physics*, Phys. Lett. B **181** (1986) 145–149.

[57] A. Salvio, A. Strumia, and W. Xue, *Thermal axion production*, JCAP **01** (2014) 011, [arXiv:1310.6982].

[58] I. Brivio, M. B. Gavela, L. Merlo, K. Mimasu, J. M. No, R. del Rey, and V. Sanz, *ALPs Effective Field Theory and Collider Signatures*, Eur. Phys. J. C **77** (2017), no. 8 572, [arXiv:1701.05379].

[59] G. Alonso-Álvarez, M. B. Gavela, and P. Quilez, *Axion couplings to electroweak gauge bosons*, Eur. Phys. J. C **79** (2019), no. 3 223, [arXiv:1811.05466].

[60] M. B. Gavela, R. Houtz, P. Quilez, R. Del Rey, and O. Sumensari, *Flavor constraints on electroweak ALP couplings*, Eur. Phys. J. C **79** (2019), no. 5 369, [arXiv:1901.02031].

[61] M. Chala, G. Guedes, M. Ramos, and J. Santiago, *Running in the ALPs*, Eur. Phys. J. C **81** (2021), no. 2 181, [arXiv:2012.09017].

[62] J. Bonilla, I. Brivio, M. B. Gavela, and V. Sanz, *One-loop corrections to ALP couplings*, JHEP **11** (2021) 168, [arXiv:2107.11392].

[63] M. Bauer, M. Neubert, S. Renner, M. Schnubel, and A. Thamm, *Consistent Treatment of Axions in the Weak Chiral Lagrangian*, Phys. Rev. Lett. **127** (2021), no. 8 081803, [arXiv:2102.13112].

[64] F. Arias-Aragón and C. Smith, *Leptoquarks, axions and the unification of B, L, and Peccei-Quinn symmetries*, Phys. Rev. D **106** (2022), no. 5 055034, [arXiv:2206.09810].

[65] F. Arias-Aragón, J. Quevillon, and C. Smith, *Axion-like ALPs*, arXiv:2211.04489.

[66] E. Izaguirre, T. Lin, and B. Shuve, *Searching for Axionlike Particles in Flavor-Changing Neutral Current Processes*, Phys. Rev. Lett. **118** (2017), no. 11 111802, [arXiv:1611.09355].

[67] L. Merlo, F. Pobbe, S. Rigolin, and O. Sumensari, *Revisiting the production of ALPs at B-factories*, JHEP **06** (2019) 091, [arXiv:1905.03259].

[68] M. Bauer, M. Neubert, S. Renner, M. Schnubel, and A. Thamm, *Axionlike Particles, Lepton-Flavor Violation, and a New Explanation of a_μ and a_e*, Phys. Rev. Lett. **124** (2020), no. 21 211803, [arXiv:1908.00008].

[69] M. Bauer, M. Neubert, S. Renner, M. Schnubel, and A. Thamm, *The Low-Energy Effective Theory of Axions and ALPs*, JHEP **04** (2021) 063, [arXiv:2012.12272].

[70] M. Bauer, M. Neubert, S. Renner, M. Schnubel, and A. Thamm, *Flavor probes of axion-like particles*, JHEP **09** (2022) 056, [arXiv:2110.10698].

[71] A. W. M. Guerrera and S. Rigolin, *Revisiting $K \to \pi a$ decays*, Eur. Phys. J. C **82** (2022), no. 3 192, [arXiv:2106.05910].

[72] J. A. Gallo, A. W. M. Guerrera, S. Peñaranda, and S. Rigolin, *Leptonic meson decays into invisible ALP*, Nucl. Phys. B **979** (2022) 115791, [arXiv:2111.02536].

[73] J. Bonilla, A. de Giorgi, B. Gavela, L. Merlo, and M. Ramos, *The cost of an ALP solution to the neutral B-anomalies*, arXiv:2209.11247.

[74] J. Bonilla, A. de Giorgi, and M. Ramos, *Neutral B-anomalies from an on-shell scalar exchange*, arXiv:2211.05135.

[75] A. de Giorgi and G. Piazza, *A lesson from $R_{\tau\tau}^{K^{(*)}}$ and $R_{\nu\nu}^{K^{(*)}}$ at Belle II*, arXiv:2211.05595.

[76] A. W. M. Guerrera and S. Rigolin, *ALP production in weak mesonic decays*, arXiv:2211.08343.

[77] J. Jaeckel, M. Jankowiak, and M. Spannowsky, *LHC probes the hidden sector*, Phys. Dark Univ. **2** (2013) 111–117, [arXiv:1212.3620].

[78] K. Mimasu and V. Sanz, *ALPs at Colliders*, JHEP **06** (2015) 173, [arXiv:1409.4792].

[79] J. Jaeckel and M. Spannowsky, *Probing MeV to 90 GeV axion-like particles with LEP and LHC*, Phys. Lett. B **753** (2016) 482–487, [arXiv:1509.00476].

[80] A. Alves, A. G. Dias, and K. Sinha, *Diphotons at the Z-pole in Models of the 750 GeV Resonance Decaying to Axion-Like Particles*, JHEP **08** (2016) 060, [arXiv:1606.06375].

[81] S. Knapen, T. Lin, H. K. Lou, and T. Melia, *Searching for Axionlike Particles with Ultraperipheral Heavy-Ion Collisions*, Phys. Rev. Lett. **118** (2017), no. 17 171801, [arXiv:1607.06083].

[82] M. Bauer, M. Neubert, and A. Thamm, *LHC as an Axion Factory: Probing an Axion Explanation for $(g-2)_\mu$ with Exotic Higgs Decays*, Phys. Rev. Lett. **119** (2017), no. 3 031802, [arXiv:1704.08207].

[83] A. Mariotti, D. Redigolo, F. Sala, and K. Tobioka, *New LHC bound on low-mass diphoton resonances*, Phys. Lett. B **783** (2018) 13–18, [arXiv:1710.01743].

[84] M. Bauer, M. Neubert, and A. Thamm, *Collider Probes of Axion-Like Particles*, JHEP **12** (2017) 044, [arXiv:1708.00443].

[85] C. Baldenegro, S. Fichet, G. von Gersdorff, and C. Royon, *Searching for axion-like particles with proton tagging at the LHC*, JHEP **06** (2018) 131, [arXiv:1803.10835].

[86] N. Craig, A. Hook, and S. Kasko, *The Photophobic ALP*, JHEP **09** (2018) 028, [arXiv:1805.06538].

[87] M. Bauer, M. Heiles, M. Neubert, and A. Thamm, *Axion-Like Particles at Future Colliders*, Eur. Phys. J. C **79** (2019), no. 1 74, [arXiv:1808.10323].

[88] M. B. Gavela, J. M. No, V. Sanz, and J. F. de Trocóniz, *Nonresonant Searches for Axionlike Particles at the LHC*, Phys. Rev. Lett. **124** (2020), no. 5 051802, [arXiv:1905.12953].

[89] G. Haghighat, D. Haji Raissi, and M. Mohammadi Najafabadi, *New collider searches for axionlike particles coupling to gluons*, Phys. Rev. D **102** (2020), no. 11 115010, [arXiv:2006.05302].

[90] D. Wang, L. Wu, J. M. Yang, and M. Zhang, *Photon-jet events as a probe of axionlike particles at the LHC*, Phys. Rev. D **104** (2021), no. 9 095016, [arXiv:2102.01532].

[91] A. de Giorgi, L. Merlo, and J.-L. Tastet, *Probing HNL-ALP couplings at colliders*, Fortsch. Phys. **71** (2023), no. 4-5 2300027, [arXiv:2212.11290].

[92] J. Bonilla, I. Brivio, J. Machado-Rodríguez, and J. F. de Trocóniz, *Nonresonant searches for axion-like particles in vector boson scattering processes at the LHC*, JHEP **06** (2022) 113, [arXiv:2202.03450].

[93] F. A. Ghebretinsaea, Z. S. Wang, and K. Wang, *Probing axion-like particles coupling to gluons at the LHC*, JHEP **07** (2022) 070, [arXiv:2203.01734].

[94] V. E. Vileta, B. Gavela, R. Houtz, and P. Quilez, *Discrete Goldstone bosons*, Phys. Rev. D **107** (2023), no. 3 035009, [arXiv:2205.09131].

[95] L. Di Luzio, A. W. M. Guerrera, X. Ponce Díaz, and S. Rigolin, *Axion-Like Particles in Radiative Quarkonia Decays*, arXiv:2402.12454.

[96] E. K. Akhmedov, Z. G. Berezhiani, R. N. Mohapatra, and G. Senjanovic, *Planck scale effects on the majoron*, Phys. Lett. B **299** (1993) 90–93, [hep-ph/9209285].

[97] I. Z. Rothstein, K. S. Babu, and D. Seckel, *Planck scale symmetry breaking and majoron physics*, Nucl. Phys. B **403** (1993) 725–748, [hep-ph/9301213].

[98] R. N. Mohapatra and G. Senjanovic, *The Superlight Axion and Neutrino Masses*, Z. Phys. C **17** (1983) 53–56.

[99] P.-H. Gu, E. Ma, and U. Sarkar, *Pseudo-Majoron as Dark Matter*, Phys. Lett. B **690** (2010) 145–148, [arXiv:1004.1919].

[100] M. Frigerio, T. Hambye, and E. Masso, *Sub-GeV dark matter as pseudo-Goldstone from the seesaw scale*, Phys. Rev. X **1** (2011) 021026, [arXiv:1107.4564].

[101] A. de Giorgi, L. Merlo, X. Ponce Díaz, and S. Rigolin, *The Minimal Massive Majoron Seesaw Model*, arXiv:2312.13417.

[102] K. Kannike, M. Raidal, D. M. Straub, and A. Strumia, *Anthropic solution to the magnetic muon anomaly: the charged see-saw*, JHEP **02** (2012) 106, [arXiv:1111.2551]. [Erratum: JHEP 10, 136 (2012)].

[103] R. Dermisek and A. Raval, *Explanation of the Muon g-2 Anomaly with Vectorlike Leptons and its Implications for Higgs Decays*, Phys. Rev. D **88** (2013) 013017, [arXiv:1305.3522].

[104] G. Arcadi, L. Calibbi, M. Fedele, and F. Mescia, *Muon $g-2$ and B-anomalies from Dark Matter*, Phys. Rev. Lett. **127** (2021), no. 6 061802, [arXiv:2104.03228].

[105] C.-T. Lu, R. Ramos, and Y.-L. S. Tsai, *Shedding light on dark matter with recent muon $(g-2)$ and Higgs exotic decay measurements*, JHEP **08** (2021) 073, [arXiv:2104.04503].

[106] G. Guedes and P. Olgoso, *A bridge to new physics: proposing new – and reviving old – explanations of a_μ*, JHEP **09** (2022) 181, [arXiv:2205.04480].

[107] N. Arkani-Hamed and K. Harigaya, *Naturalness and the muon magnetic moment*, JHEP **09** (2021) 025, [arXiv:2106.01373].

[108] N. Craig, I. G. Garcia, A. Vainshtein, and Z. Zhang, *Magic zeroes and hidden symmetries*, JHEP **05** (2022) 079, [arXiv:2112.05770].

[109] L. Delle Rose, B. von Harling, and A. Pomarol, *Wilson coefficients and natural zeros from the on-shell viewpoint*, JHEP **05** (2022) 120, [arXiv:2201.10572].

[110] A. de Giorgi, L. Merlo, and S. Pokorski, *The Low-Scale Seesaw Solution to the M_W and $(g-2)_\mu$ Anomalies*, Fortsch. Phys. **71** (2023), no. 4-5 2300020, [arXiv:2211.03797].

[111] J. Kersten and A. Y. Smirnov, *Right-Handed Neutrinos at CERN LHC and the Mechanism of Neutrino Mass Generation*, Phys. Rev. D **76** (2007) 073005, [arXiv:0705.3221].

[112] A. Abada, C. Biggio, F. Bonnet, M. B. Gavela, and T. Hambye, *Low energy effects of neutrino masses*, JHEP **12** (2007) 061, [arXiv:0707.4058].

[113] M. Blennow, P. Coloma, E. Fernández-Martínez, and M. González-López, *Right-handed neutrinos and the CDF II anomaly*, Phys. Rev. D **106** (2022), no. 7 073005, [arXiv:2204.04559].

[114] **CDF** Collaboration, T. Aaltonen *et. al.*, *High-precision measurement of the W boson mass with the CDF II detector*, Science **376** (2022), no. 6589 170–176.

[115] M. Malinsky, J. C. Romao, and J. W. F. Valle, *Novel supersymmetric SO(10) seesaw mechanism*, Phys. Rev. Lett. **95** (2005) 161801, [hep-ph/0506296].

[116] H. H. Patel, *Package-X 2.0: A Mathematica package for the analytic calculation of one-loop integrals*, Comput. Phys. Commun. **218** (2017) 66–70, [arXiv:1612.00009].

[117] V. Shtabovenko, R. Mertig, and F. Orellana, *FeynCalc 9.3: New features and improvements*, Comput. Phys. Commun. **256** (2020) 107478, [arXiv:2001.04407].

[118] S. R. Coleman and E. J. Weinberg, *Radiative Corrections as the Origin of Spontaneous Symmetry Breaking*, Phys. Rev. D **7** (1973) 1888–1910.

[119] **Particle Data Group** Collaboration, R. L. Workman and Others, *Review of Particle Physics*, PTEP **2022** (2022) 083C01.

[120] **ATLAS** Collaboration, *Improved W boson Mass Measurement using 7 TeV Proton-Proton Collisions with the ATLAS Detector*, .

[121] **Muon g-2** Collaboration, D. P. Aguillard *et. al.*, *Measurement of the Positive Muon Anomalous Magnetic Moment to 0.20 ppm*, Phys. Rev. Lett. **131** (2023), no. 16 161802, [arXiv:2308.06230].

[122] T. Aoyama *et. al.*, *The anomalous magnetic moment of the muon in the Standard Model*, Phys. Rept. **887** (2020) 1–166, [arXiv:2006.04822].

[123] S. Borsanyi *et. al.*, *Leading hadronic contribution to the muon magnetic moment from lattice QCD*, Nature **593** (2021), no. 7857 51–55, [arXiv:2002.12347].

[124] G. Colangelo, A. X. El-Khadra, M. Hoferichter, A. Keshavarzi, C. Lehner, P. Stoffer, and T. Teubner, *Data-driven evaluations of Euclidean windows to scrutinize hadronic vacuum polarization*, Phys. Lett. B **833** (2022) 137313, [arXiv:2205.12963].

[125] S. Kuberski, M. Cè, G. von Hippel, H. B. Meyer, K. Ottnad, A. Risch, and H. Wittig, *Hadronic vacuum polarization in the muon $g-2$: The short-distance contribution from lattice QCD*, arXiv:2401.11895.

[126] **Extended Twisted Mass** Collaboration, C. Alexandrou *et. al.*, *Lattice calculation of the short and intermediate time-distance hadronic vacuum polarization contributions to the muon magnetic moment using twisted-mass fermions*, Phys. Rev. D **107** (2023), no. 7 074506, [arXiv:2206.15084].

[127] M. Cè *et. al.*, *Window observable for the hadronic vacuum polarization contribution to the muon g-2 from lattice QCD*, Phys. Rev. D **106** (2022), no. 11 114502, [arXiv:2206.06582].

[128] **RBC, UKQCD** Collaboration, T. Blum *et. al.*, *Update of Euclidean windows of the hadronic vacuum polarization*, Phys. Rev. D **108** (2023), no. 5 054507, [arXiv:2301.08696].

[129] **CMD-3** Collaboration, F. V. Ignatov *et. al.*, *Measurement of the $e^+e^- \to \pi^+\pi^-$ cross section from threshold to 1.2 GeV with the CMD-3 detector*, arXiv:2302.08834.

[130] C. O'Hare, "cajohare/axionlimits: Axionlimits." https://cajohare.github.io/AxionLimits/, July, 2020.

[131] **ATLAS** Collaboration, G. Aad *et. al.*, *Measurement of light-by-light scattering and search for axion-like particles with 2.2 nb^{-1} of Pb+Pb data with the ATLAS detector*, JHEP **03** (2021) 243, [arXiv:2008.05355]. [Erratum: JHEP 11, 050 (2021)].

[132] M. J. Dolan, T. Ferber, C. Hearty, F. Kahlhoefer, and K. Schmidt-Hoberg, *Revised constraints and Belle II sensitivity for visible and invisible axion-like particles*, JHEP **12** (2017) 094, [arXiv:1709.00009]. [Erratum: JHEP 03, 190 (2021)].

[133] **CHARM** Collaboration, F. Bergsma *et. al.*, *Search for Axion Like Particle Production in 400-GeV Proton - Copper Interactions*, Phys. Lett. B **157** (1985) 458–462.

[134] E. M. Riordan *et. al.*, *A Search for Short Lived Axions in an Electron Beam Dump Experiment*, Phys. Rev. Lett. **59** (1987) 755.

[135] J. Blumlein *et. al.*, *Limits on neutral light scalar and pseudoscalar particles in a proton beam dump experiment*, Z. Phys. C **51** (1991) 341–350.

[136] **NA64** Collaboration, D. Banerjee *et. al.*, *Search for Axionlike and Scalar Particles with the NA64 Experiment*, Phys. Rev. Lett. **125** (2020), no. 8 081801, [arXiv:2005.02710].

[137] **Belle-II** Collaboration, F. Abudinén *et. al.*, *Search for Axion-Like Particles produced in e^+e^- collisions at Belle II*, Phys. Rev. Lett. **125** (2020), no. 16 161806, [arXiv:2007.13071].

[138] **BESIII** Collaboration, M. Ablikim *et. al.*, *Search for an axion-like particle in J/ψ radiative decays*, arXiv:2211.12699.

[139] **CMS** Collaboration, A. M. Sirunyan *et. al.*, *Evidence for light-by-light scattering and searches for axion-like particles in ultraperipheral PbPb collisions at $\sqrt{s_{\mathrm{NN}}} = 5.02$ TeV*, Phys. Lett. B **797** (2019) 134826, [arXiv:1810.04602].

[140] **PrimEx** Collaboration, I. Larin *et. al.*, *A New Measurement of the π^0 Radiative Decay Width*, Phys. Rev. Lett. **106** (2011) 162303, [arXiv:1009.1681].

[141] D. Aloni, C. Fanelli, Y. Soreq, and M. Williams, *Photoproduction of Axionlike Particles*, Phys. Rev. Lett. **123** (2019), no. 7 071801, [arXiv:1903.03586].

[142] J. B. Dent, B. Dutta, D. Kim, S. Liao, R. Mahapatra, K. Sinha, and A. Thompson, *New Directions for Axion Searches via Scattering at Reactor Neutrino Experiments*, Phys. Rev. Lett. **124** (2020), no. 21 211804, [arXiv:1912.05733].

[143] G. Lucente, P. Carenza, T. Fischer, M. Giannotti, and A. Mirizzi, *Heavy axion-like particles and core-collapse supernovae: constraints and impact on the explosion mechanism*, JCAP **12** (2020) 008, [arXiv:2008.04918].

[144] A. Caputo, G. Raffelt, and E. Vitagliano, *Muonic boson limits: Supernova redux*, Phys. Rev. D **105** (2022), no. 3 035022, [arXiv:2109.03244].

[145] A. Caputo, H.-T. Janka, G. Raffelt, and E. Vitagliano, *Low-Energy Supernovae Severely Constrain Radiative Particle Decays*, Phys. Rev. Lett. **128** (2022), no. 22 221103, [arXiv:2201.09890].

[146] P. F. Depta, M. Hufnagel, and K. Schmidt-Hoberg, *Robust cosmological constraints on axion-like particles*, JCAP **05** (2020) 009, [arXiv:2002.08370].

[147] **BaBar** Collaboration, J. P. Lees *et. al.*, *Search for a Dark Photon in e^+e^- Collisions at BaBar*, Phys. Rev. Lett. **113** (2014), no. 20 201801, [arXiv:1406.2980].

[148] A. de Giorgi, M. Burgos-Marcos, L. Merlo, and J.-L. Tastet. *To appear.*

[149] J. C. Romao and J. P. Silva, *A resource for signs and Feynman diagrams of the Standard Model*, Int. J. Mod. Phys. A **27** (2012) 1230025, [arXiv:1209.6213].

Published for SISSA by Springer

Received: *January 11, 2024*
Revised: *February 22, 2024*
Accepted: *February 23, 2024*
Published: *March 15, 2024*

The minimal massive Majoron Seesaw Model

Arturo de Giorgi,[a,b] **Luca Merlo**,[a] **Xavier Ponce Díaz**[c] **and Stefano Rigolin**[c]

[a] *Departamento de Física Teórica and Instituto de Física Teórica UAM/CSIC, Universidad Autónoma de Madrid, Cantoblanco, 28049, Madrid, Spain*
[b] *Department of Physics & Laboratory for Particle Physics and Cosmology, Harvard University, Cambridge, MA 02138, U.S.A.*
[c] *Dipartamento di Fisica e Astronomia "G. Galilei" and Istituto Nazionale Fisica Nucleare, Sezione di Padova, Università degli Studi di Padova, I-35131 Padova, Italy*

E-mail: arturo.degiorgi@uam.es, luca.merlo@uam.es, xavier.poncediaz@pd.infn.it, stefano.rigolin@pd.infn.it

Abstract: A convincing explanation of the smallness of neutrino masses is represented by the Type-I Seesaw mechanism, where the two measured neutrino mass differences can be generated by introducing at least two right-handed neutrinos. In an ultraviolet complete model, it is possible to dynamically generate the heavy Majorana scale through the spontaneous symmetry breaking of a global Abelian symmetry and the most economical realisation consists in coupling the two exotic neutral leptons to a singlet complex scalar field. The associated Goldstone boson is often dubbed as Majoron, which may achieve a non-vanishing mass by means of a small term that explicitly breaks the Abelian symmetry. In a generic model, the neutrino and Majoron mass generation mechanisms are completely uncorrelated. In this paper, instead, we reduce the landscape of possible models proposing a unique, minimal and predictive framework in which these two types of masses are strictly tied and arise from the same source. Bounds from various terrestrial and astrophysical experiments are discussed.

Keywords: Axions and ALPs, Sterile or Heavy Neutrinos, New Light Particles, Models for Dark Matter

ArXiv ePrint: 2312.13417

https://doi.org/10.1007/JHEP03(2024)094

JHEP03(2024)094

Contents

1 Introduction

The heterogeneity of the particle masses in the Standard Model (SM) and Beyond (BSM) is one of the big unknowns of modern high-energy physics. No explanation for the large hierarchy of masses and mixings is present within the SM and, at the time being, no convincing evidence of a specific flavour symmetric BSM construction has emerged. In addition, contrary to the SM original ansatz, active neutrinos do have non-vanishing masses and two main frameworks can be introduced to provide them with a mass: Dirac *vs.* Majorana. If neutrinos are Dirac fermions, similarly to all the other SM fermions, a right-handed (RH) companion for each flavour is introduced in the spectrum and, preserving the Lepton Number (LN) at tree level, they acquire masses through the ElectroWeak (EW) Spontaneous Symmetry Breaking (SSB) mechanism, proportionally to the Higgs vacuum expectation value (vev), $v_{\rm EW}$. This implies, however, that the corresponding Yukawa couplings are tremendously small, deeply worsening the SM flavour puzzle. Conversely, if neutrinos are Majorana fermions, their mass could be associated with the breaking of the LN at a not-well-identified high-energy scale, providing a "natural" explanation for their lightness through the well-known Seesaw (SS) mechanism [1–4].

An intriguing possibility is that the LN breaking, eventually leading to active neutrino masses at low energy, is a manifestation of high-scale dynamics. Indeed, the Majorana masses can be dynamically generated from the SSB of a global U(1) symmetry at a scale

JHEP03(2024)094

$f_a \gg v_{\rm EW}$. Consistently, a Goldstone boson, dubbed as Majoron [5–7], arises in this context and the U(1) symmetry may be identified with the Peccei-Quinn symmetry associated with the traditional QCD axion framework [8–14]. Indeed, in its original formulation, the Majoron model has exactly the same ingredients of the KSVZ invisible axion, i.e. a complex scalar field singlet under the SM symmetry and extra exotic heavy fermionic degrees of freedom. The main difference is, of course, the fact that in the Majoron framework, the new exotic fermions are singlets under the SM gauge group, and therefore the Majoron cannot be evoked for solving the strong CP problem. Subsequent works have introduced the Majoron in the context of the Type-II SS [15–17], radiative neutrino models [18, 19], its role as a possible dark matter candidate [20–25] and more recently its impact in cosmology has been highlighted [26–31], including the possibility that the Majoron may represent a viable solution to the Hubble tension [32–35].

Differently to what happens for the QCD axion, where the $\mathrm{U}(1)_{\rm PQ}$ is explicitly broken by non-perturbative QCD effects thus providing a tiny mass to the axion, the Majoron does not come with an embedded explicit source of symmetry breaking. The mechanism that gives mass to the Majoron has been debated since its formulation [5–7]. In refs. [36, 37], for example, it is shown that Planck-suppressed operators explicitly break any global U(1) symmetry, including LN embedded in a continuous Abelian group. Other mechanisms instead involve the active neutrino mass generation mechanism, which includes a LN breaking, in order to equip the Majoron with a mass [38–40]. In particular, ref. [40] shows that, in the context of the Type-I seesaw mechanism, a minimal number of terms in the neutral lepton mass matrix is necessary in order to build a massive Majoron model.

In this paper we will extend the results in the literature, introducing a realistic and minimal Seesaw construction where LN and PQ are eventually identified and the Majoron mass is strictly linked to the active neutrino masses. The starting point of our analysis is the minimal Type-I SS, where the SM fermion spectrum is enlarged by only two RH neutrinos, also called Heavy Neutral Leptons (HNLs), that are singlets under the whole SM group. In this construction, therefore, at most two active neutrinos can become massive, while the lightest one remains massless. It is possible, then, to embed a dynamical $\mathrm{U}(1)_{\rm PQ}$ SSB mechanism, the Majoron being the associated Goldstone boson. We will work on this setup by adopting the following "minimality" requirements:

i) only renormalisable interactions are considered in the Lagrangian densities;

ii) only one large (Majorana) scale is present, and associated with the SSB of the $\mathrm{U}(1)_{\rm PQ}$ symmetry, i.e. only one complex scalar field couples to the RH neutrinos;

iii) only one (small) explicit $\mathrm{U}(1)_{\rm PQ}$-violating term is introduced.

We will show that satisfying these three conditions will lead to a unique and predictive model where the active neutrino masses and the Majoron mass are deeply connected, i.e. the explicit symmetry-violating term is the necessary and sufficient ingredient to simultaneously provide a mass to the active neutrinos and the Majoron.

The paper is structured as follows. In section 2, we briefly review the generation of active neutrino masses in different SS realisations with only two RH neutrinos, first with

JHEP03(2024)094

the traditional type-I and then in section 2.1 the low-scale SS. In section 2.2, we explicitly derive the active neutrino mass matrix including one-loop contributions induced by a heavy but non-degenerate pair of HNLs. Section 3 describes the minimal massive Majoron Seesaw (mmM) model. We explicitly extend the SM Lagrangian by specific couplings between the HNLs and a complex scalar field, ϕ, singlet under the SM group, but endowed with a $\mathrm{U}(1)_{\mathrm{PQ}}$ symmetry. Once this scalar acquires a vev, f_a, the PQ gets spontaneously broken giving rise to the Majoron. In section 3.1, we analyse different classes of ultraviolet (UV) embeddings that can be constructed with one complex scalar and two RH neutrinos. In section 3.2 we identify the mmM model that respects the three minimality conditions i)-iii). Then, we determine the parameter space in which higher-order contributions to the neutrino mass matrix do not spoil perturbativity, and therefore a realistic active neutrino spectrum and PMNS mixing can be predicted.

Section 4 represents the core of this paper, containing the one-loop derivation of the Majoron mass. A preliminary calculation is shown for a simplified model in section 4.1, both in the chirality flipping and chirality preserving basis for the Majoron, and then in section 4.2 the Majoron mass in the mmM model is derived, in the chirality preserving basis where the calculations are greatly simplified. Finally, in section 5, we discuss the possible phenomenology of this Majoron and compare it with the present bounds under the context of general ALP and Dark Matter searches. This work is completed with three appendices: appendix A deals with the diagonalisation of neutrino mass matrix and Majoron interactions; appendix B describes the HNL interactions with the Majoron and SM gauge and Higgs bosons; and finally, the one-loop Coleman-Weinberg (CW) potential [41] is derived in appendix C, as a crosscheck of the diagrammatic calculation performed in section 4.

2 Seesaws with two HNLs

The Type-I SS mechanism [1–4] provides a natural explanation of the smallness of the active neutrino masses by introducing RH neutrinos. To be able to explain the two neutrino oscillation mass differences at least two HNLs, singlets under the whole SM group, have to be introduced. Therefore, at most two active neutrinos can become massive while the lightest one remains massless. In a compact notation, the SM and exotic neutral lepton fields can be grouped in a left-handed lepton multiplet denoted as,

$$\chi_L \equiv (\nu_L,\, N_R^c,\, S_R^c)^T\,, \tag{2.1}$$

where $\nu_L \equiv (\nu_L^e, \nu_L^\mu, \nu_L^\tau)$ are the SM neutrinos and N_R and S_R are the two HNLs, whose conjugates are defined as $\psi_R^c = \mathcal{C}\overline{\psi}_R^T$, where $\mathcal{C}$ is the charge conjugation matrix.

In this scenario, the most general (renormalizable) Lagrangian describing the neutral lepton interactions reads:

$$\begin{aligned} -\mathscr{L}_{\mathrm{LN}} = \;& \overline{L_L}\,\widetilde{H}\,Y_N\,N_R + \overline{L_L}\,\widetilde{H}\,Y_S\,S_R + \\ & + \frac{1}{2}\Big[\Lambda_{NN}\,\overline{N_R^c}\,N_R + \Lambda_{SS}\,\overline{S_R^c}\,S_R + \Lambda_{NS}\,(\overline{N_R^c}\,S_R + \overline{S_R^c}\,N_R)\Big] + \mathrm{h.c.}\,. \end{aligned} \tag{2.2}$$

where L_L is the EW lepton doublet, triplet in flavour space, and H is the Higgs EW doublet, with $\widetilde{H} \equiv i\sigma_2 H^*$. $Y_{N,S}$ are two generic three-dimensional vectors describing the Dirac-type Yukawa interactions with the Higgs, while Λ_{NN}, Λ_{SS} and Λ_{NS} are three one-dimensional parameters.

JHEP03(2024)094

After EW SSB, with the Higgs developing a vev $v_{\rm EW} = 246\,\text{GeV}$, the following neutral lepton mass matrix is generated

$$-\mathscr{L}_{\nu\text{M}} \supset \frac{1}{2}\,\overline{\chi}_L\,\mathcal{M}_\chi\,\chi_L^c \qquad \text{with} \qquad \mathcal{M}_\chi = \begin{pmatrix} 0 & m_N & m_S \\ m_N^T & \Lambda_{NN} & \Lambda_{NS} \\ m_S^T & \Lambda_{NS} & \Lambda_{SS} \end{pmatrix} \equiv \begin{pmatrix} 0 & \widehat{m} \\ \widehat{m}^T & \widehat{\Lambda} \end{pmatrix}, \tag{2.3}$$

where the Dirac mass terms are defined as $m_{N,S} \equiv Y_{N,S}\,v_{\rm EW}/\sqrt{2}$. Sometimes it will be useful to use the compact notation $\widehat{m}$ and $\widehat{\Lambda}$ for indicating the 3×2 and 2×2 Dirac and Majorana mass terms. For example, diagonalising $\mathcal{M}_\chi$, a mass term for the active neutrinos appears and the corresponding mass matrix is given by

$$m_\nu^{\text{Type-I}} \simeq -\widehat{m}\,\widehat{\Lambda}^{-1}\widehat{m}^T\,. \tag{2.4}$$

The values of the Dirac and Majorana masses are fixed in order to reproduce the active neutrino masses and the PMNS mixings. Assuming no large hierarchies within the entries of the Dirac Yukawas, $(\widehat{m})_{ij} = \mathcal{O}(v_{\rm EW})$, in order to reproduce the neutrino mass squared differences, one is forced to take the overall scale of the Majorana mass matrix as $\texttt{Tr}\,\widehat{\Lambda} \sim 10^{14} - 10^{15}\,\text{GeV}$. The latter is approximately the mass of the HNLs, after the diagonalisation of $\mathcal{M}_\chi$, and therefore it is practically impossible to observe any effect of the HNLs at present/future colliders or flavour factories.

In the original construction of the Type-I SS mechanism, all the leptons have the same transformation properties under LN and customarily $L(L_L) = 1 = L(N_R) = L(S_R)$ is chosen. It follows that the Dirac terms in eq. (2.2) are LN invariant, while the Majorana mass terms violate LN by two units. A useful exercise consists of interpreting the Dirac Yukawas and the Majorana masses as spurion fields, that is non-dynamical fields that may own transformation properties, in this specific case, only under LN. Hence, one can formally implement LN invariance of the whole Lagrangian, assigning specific charges to the spurions: whenever a spurion charge is different from zero, the corresponding term would violate LN. Applying this spurionic description to the Lagrangian in eq. (2.2), one obtains $L(\widehat{m}) = 0$ and $L(\widehat{\Lambda}) = -2$, confirming that the Majorana terms violate LN. Moreover, we obtain that the active neutrino mass matrix also violates LN as $L(m_\nu^{\text{Type-I}}) = 2$, as expected.

Going beyond the original setup, modifying the LN charge assignments would change the previous conclusions, without necessarily affecting the physical observables. For example, if we fix $L(L_L) = 1$ and $L(N_R) = L(S_R) = n \neq 1$, the Dirac terms would now violate the LN as indeed $L(\widehat{m}) = 1 - n$, while the Majorana ones may or may not violate it, depending on the explicit value of n, being $L(\widehat{\Lambda}) = -2n$. However, the active neutrino mass matrix still violates LN by the same quantity as in the traditional case, $L(m_\nu^{\text{Type-I}}) = 2$, for any value of n.

This simple exercise points out the following:

- There are several LN charge assignments that lead to the same physics.
- The LN conserving or violating status of a Lagrangian term can only be assessed with respect to a specific choice of the charges. Moreover, we can conclude that LN conservation can only occur if there is a charge assignment such that all the LN spurions, $\widehat{m}$ and $\widehat{\Lambda}$ in this case, have vanishing charges.

JHEP03(2024)094

- The active neutrino masses necessarily depend on (a combination of) the spurions that, in any charge assignment, have a non-zero charge: this is to say that LN is broken by the simultaneous presence of these spurions, as otherwise, if any of them vanishes, the active neutrinos would remain massless. For the Type-I SS case, as there exist charge assignments such that both $\widehat{m}$ and $\widehat{\Lambda}$ are explicitly LN violating implies that both quantities have to appear in the definition of $m_\nu^{\text{Type-I}}$, confirming the result of the explicit computation and that both of them should be non-vanishing to assure massive active neutrinos. However, in more complicated setups with respect to the Type-I SS, it may occur that LN-violating spurions appear only in loop-level contributions to the active neutrino masses. Indeed, a broken symmetry does not necessarily imply that its effects are manifest in observables described with tree-level Feynman diagrams.

We will use and adapt this reasoning in the next sections, where we will go through other popular SS mechanisms, and show that the very last condition helps identify the genuine LN-violating spurions.

2.1 The low-scale Seesaw models

A popular modification of the canonical Type-I Seesaw is the class of constructions that undergo the name of low-scale Seesaw (LSSS) mechanisms [42–45], also known as "LN protected" SS mechanisms. In this kind of scenarios, the two HNLs have different non-vanishing LN charge assignments. For example, assuming $L(L_L) = L(N_R) = -L(S_R) = 1$ leads to the following LN conserving Lagrangian:

$$-\mathscr{L}_{\text{LN}} = \overline{L_L}\,\widetilde{H}\,Y_N\,N_R + \frac{\Lambda_{NS}}{2}\left(\overline{N_R^c}\,S_R + \overline{S_R^c}\,N_R\right) + \text{h.c.} \tag{2.5}$$

while (a combination of) additional terms, explicitly violating the LN symmetry, have to be added to generate the desired light active neutrino spectrum: in all generality,

$$-\mathscr{L}_{\epsilon\text{LN}} = \overline{L_L}\,\widetilde{H}\,\epsilon Y_S\,S_R + \frac{\epsilon\Lambda_{NN}}{2}\,\overline{N_R^c}\,N_R + \frac{\epsilon\Lambda_{SS}}{2}\,\overline{S_R^c}\,S_R + \text{h.c.}\,. \tag{2.6}$$

By the physical assumption of an approximate LN symmetry, the three parameters $\epsilon Y_S, \epsilon\Lambda_{NN}$ and $\epsilon\Lambda_{SS}$ are naturally small compared to the LN preserving ones appearing in eq. (2.5).

In the broken EW phase, one obtains the following neutrino mass matrix

$$-\mathscr{L}_{\nu\text{M}}^{\text{LSSS}} \supset \frac{1}{2}\,\overline{\chi}_L \mathcal{M}_\chi^{\text{LSSS}} \chi_L^c \qquad \text{with} \qquad \mathcal{M}_\chi^{\text{LSSS}} = \begin{pmatrix} 0 & m_N & \epsilon m_S \\ m_N^T & \mu' & \Lambda_{NS} \\ \epsilon m_S^T & \Lambda_{NS} & \mu \end{pmatrix}, \tag{2.7}$$

with the obvious definitions of the Dirac mass terms, inherited from the Lagrangian densities in eq. (2.5) and (2.6), and where $\mu' = \epsilon\Lambda_{NN}$ and $\mu = \epsilon\Lambda_{SS}$ have been used to make contact with the notation often used in the literature. Adopting the spurion description, with the chosen charge assignment, the parameters of the LN violating terms should be promoted to spurions with non-vanishing charges, $L(\epsilon m_S, \mu', \mu) = (+2, -2, +2)$, while the quantities m_N and Λ_{NS} do not acquire any charge.

JHEP03(2024)094

After the EW SSB, at leading order in the $\mu^{(\prime)}/\Lambda_{NS}$ and $\epsilon m_S/\Lambda_{NS}$ expansion, the active neutrinos mass matrix is given by

$$m_\nu^{\rm LSSS} \simeq -\mu\,\frac{m_N m_N^T}{\Lambda_{NS}^2} - \epsilon\frac{m_S\,m_N^T + m_N\,m_S^T}{\Lambda_{NS}}\,. \tag{2.8}$$

Having introduced only two exotic HNLs, this implies again that the lightest active neutrino remains massless. The other two neutrinos acquire masses that are functions of ϵm_S and μ, but not of μ' that does not play any role at leading order.

The advantage of this class of LSSS models is that having introduced "naturally" small terms, i.e. $\epsilon m_s \ll m_N$ and $\mu \ll \Lambda_{NS}$, one can explain the active neutrino masses by introducing a much lighter Majorana scale. To reproduce the observed neutrino mass spectrum it is sufficient to fix $\epsilon m_S(\mu) \sim 10(1000)\,\text{eV}$ for a chosen $\Lambda_{NS} \sim \mathcal{O}(\text{TeV})$. It follows that, while active neutrino masses remain small, the HNLs are relatively light and possibly detectable at colliders. Moreover, the unique $d = 6$ effective operator resulting from integrating out the HNLs does not depend on the LN violating parameters, thus describing possibly interesting phenomenological effects in both direct and indirect searches [44]. Although TeV scale HNLs is a very attractive feature of these constructions, it has to be pointed out that the texture in eq. (2.7) provides a good description of the low-energy neutrino data even for larger Λ_{NS} by accordingly rescaling the LN violating parameters.

Two popular models in this scenario are the ones obtained by setting $\epsilon m_S = \mu' = 0$, dubbed as Inverse Seesaw (ISS) [46, 47] or by imposing $\mu = \mu' = 0$, dubbed as Linear Seesaw (LSS) [48, 49], that predict the following active neutrino masses respectively

$$m_\nu^{\rm ISS} \simeq -\mu\,\frac{m_N m_N^T}{\Lambda_{NS}^2}\,, \qquad\qquad m_\nu^{\rm LSS} \simeq -\epsilon\frac{m_S\,m_N^T + m_N\,m_S^T}{\Lambda_{NS}}\,. \tag{2.9}$$

Notice that in the ISS case, it is not possible to describe successfully the neutrino spectrum and the PMNS mixing matrix with only two HNLs, as the product $m_N m_N^T$ has rank one. On the other hand, in the Linear Seesaw case, the light neutrino mass matrix has, instead, rank 2 and allows for a description of the neutrino sector compatible with data as discussed in ref. [50].

Before concluding this section, we generalise the charge assignment and discuss the spurion role as we did for the Type-I SS case. First of all, one key hypothesis of this setup is that $L(N_R) = -L(S_R) \neq 0$ and as a result the term associated to Λ_{NS} is automatically LN invariant, while the two Majorana terms proportional to μ and μ' always violate LN, as $L(\mu) = -2L(N_R)$ and $L(\mu') = -2L(S_R)$. To provide a mass for the active neutrinos, the charge of the lepton doublet should be fixed such that $L(L_L) = L(N_R)$: this guarantees that the term proportional to Y_N is invariant under LN.[1] All in all, a non-vanishing active neutrino mass would therefore involve μ and μ', although not necessarily the two at the same time. The ISS case is the example in which only the term proportional to μ is switched on as an explicit breaking of LN and a tree-level active neutrino mass is generated. On the other hand, although we may expect the same for μ', this is not the case: no tree-level contributions to the active neutrino masses arise in this case, but they arise at one-loop [51]. Focusing now

[1]The alternative choice $L(L_L) = L(S_R)$ leads to exactly the same physics, as indeed it is sufficient to exchange N_R with S_R to obtain the same neutral lepton mass matrix.

JHEP03(2024)094

on the Dirac terms, if we fix $L(L_L) = 1$ and $L(N_R) = -L(S_R) = n \neq \pm 1$, we conclude that both Y_N and Y_S should acquire a charge, $L(Y_N) = 1 - n$ and $L(Y_S) = 1 + n$, thus breaking LN. Notice that this is independent of the presence of the terms proportional to μ and μ'. This implies that the active neutrino masses necessarily contain the product of the two Dirac Yukawas, consistently with the explicit computation in the LSS mechanism.

An interesting alternative option with respect to the Inverse and Linear SS mechanisms is when $\mu = 0$, but both Y_S and μ' are added to the Lagrangian. As we will discuss in the next section, this may have a deep impact in the active neutrino mass generation and, moreover, represents the optimal setup for a massive Majoron.

2.2 The Extended Seesaw limit

In this section, we further exploit the spurionic approach in a modified LSS Lagrangian, which has been named as Extended Seesaw limit in ref. [52], whose physics case will be worked out in the next section. Using the same notation of section 2.1, we separate the neutral leptonic Lagrangian in a part that is invariant under LN and a part that explicitly violates it, once fixing for definiteness the LN charges as $L(L_L) = L(N_R) = 1$, $L(S_R) = -3$, $L(\Lambda_{NN}) = -2$ and $L(\Lambda_{NS}) = 2$:

$$-\mathscr{L}_{\rm LN} = \overline{L_L}\,\widetilde{H}\,Y_N\,N_R + \frac{\Lambda_{NN}}{2}\,\overline{N_R^c}\,N_R + \frac{\Lambda_{NS}}{2}\,(\overline{N_R^c}\,S_R + \overline{S_R^c}\,N_R) + \text{h.c.} \tag{2.10}$$

$$-\mathscr{L}_{\epsilon LN} = \epsilon\overline{L_L}\,\widetilde{H}\,Y_S\,S_R + \text{h.c.}\,. \tag{2.11}$$

The only term that explicitly breaks LN is the one proportional to ϵY_S that is assumed to be $\epsilon Y_S \ll Y_N$. On the other hand, once Λ_{NN} and Λ_{NS} acquire a background value, they represent two large Majorana masses such that $\Lambda_{NN} \sim \Lambda_{NS} \gg v_{\rm EW}$.

After SSB of the EW symmetry, the corresponding neutral lepton mass matrix reads:

$$-\mathscr{L}_{\nu\rm M}^{\rm ESS} \supset \frac{1}{2}\overline{\chi_L}\,\mathcal{M}_\chi^{\rm ESS}\chi_L^c + \text{h.c.} \qquad \text{with} \qquad \mathcal{M}_\chi^{\rm ESS} = \begin{pmatrix} 0 & m_N & \epsilon\, m_S \\ m_N^T & \Lambda_{NN} & \Lambda_{NS} \\ \epsilon\, m_S^T & \Lambda_{NS} & 0 \end{pmatrix}, \tag{2.12}$$

where Λ_{NN} plays the role that in the traditional ISS mechanism belongs to μ', although the similarities end here, as there is a tree-level contribution to the active neutrino masses proportional to Λ_{NN}. Indeed, the active neutrino mass matrix at tree level is given by

$$m_\nu^{\rm TL} = -\epsilon\frac{m_S\,m_N^T + m_N\,m_S^T}{\Lambda_{NS}} + \epsilon^2\,\frac{\Lambda_{NN}}{\Lambda_{NS}}\,\frac{m_S\,m_S^T}{\Lambda_{NS}}\,, \tag{2.13}$$

although the second term is typically negligible as $\epsilon \ll 1$ is assumed. On the other hand, this condition translates to an upper bound for the Majorana scale: for example, $\epsilon < 10^{-3}$ implies that $\Lambda_{NS} < 10^{12}\,\text{GeV}$, to reproduce the observed atmospheric mass splitting.

It is well known in the literature [51–54], that large values of Λ_{NN} and Λ_{NS} can generate a sizable mass splitting between the two HNL masses, implying non-negligible and possibly dangerous one-loop corrections to the tree-level result in eq. (2.13). The calculation and the discussion of the phenomenological consequences of such loop corrections will be detailed in the following subsection.

JHEP03(2024)094

2.2.1 Active neutrino masses at one-loop

Let us start by diagonalising the HNL sector of the mass matrix in eq. (2.12). The leading contribution, in the v_{EW}/Λ expansion, to the masses of the HNL states reads:

$$M_{N,S} = \frac{\Lambda_{NS}}{2}\left[\sqrt{4+\left(\frac{\Lambda_{NN}}{\Lambda_{NS}}\right)^2} \mp \left(\frac{\Lambda_{NN}}{\Lambda_{NS}}\right)\right] . \tag{2.14}$$

Notice that positively defined masses can be obtained by redefining the lightest eigenvector with a Majorana phase i.

The active neutrino mass matrix receives one-loop contributions from diagrams involving the HNLs and either the Higgs or the Z gauge boson. At leading order in v_{EW}/Λ one obtains [51–54]:

$$\delta m_\nu^{\rm 1L} = 2\,\frac{m_N\, m_N^T}{(4\pi v)^2}\,\frac{M_H^2+3M_Z^2}{M_N+M_S}\log\left(\frac{M_S}{M_N}\right) . \tag{2.15}$$

While in the degenerate limit, $M_S \sim M_N$, i.e. $\Lambda_{NN} \sim 0$, the Higgs and Z boson contributions cancel each other, when $\Lambda_{NN} \sim \Lambda_{NS}$ the HNLs mass splitting induces sizable one-loop corrections. Summing together the tree- and one-loop contributions, the neutrino mass matrix can be written as

$$m_\nu = m_\nu^{\rm TL} + \delta m_\nu^{\rm 1L} \equiv m_{T_1}(\mathbf{u}\mathbf{v}^T + \mathbf{v}\mathbf{u}^T) + m_{T_2}\mathbf{v}\mathbf{v}^T + m_L\mathbf{u}\mathbf{u}^T , \tag{2.16}$$

where the vectors $\mathbf{u}$ and $\mathbf{v}$

$$\mathbf{u} \equiv \frac{Y_N}{|Y_N|} \qquad , \qquad \mathbf{v} \equiv \frac{Y_S}{|Y_S|} , \tag{2.17}$$

define the directions in the flavour space and where the tree-level and one-loop overall numerical contributions m_{T_1}, m_{T_2} and m_L in terms of the Dirac Yukawas and Majorana mass terms read

$$m_{T_1} = -\epsilon\frac{|Y_N||Y_S|v_{\rm EW}^2}{2\Lambda_{NS}} \qquad , \qquad m_{T_2} = \epsilon^2\,\frac{\Lambda_{NN}}{\Lambda_{NS}}\,\frac{|Y_S|^2 v_{\rm EW}^2}{2\Lambda_{NS}} , \tag{2.18}$$

$$m_L = \frac{|Y_N|^2}{16\pi^2}\,\frac{M_H^2+3M_Z^2}{M_N+M_S}\log\left(\frac{M_S}{M_N}\right) . \tag{2.19}$$

To obtain the analytic expressions for the light neutrino mass eigenvalues, we generalise and adapt the procedure introduced in ref. [50], including the extra tree-level and one-loop contributions. The two non-zero eigenvalues read

$$\begin{aligned} |m_\pm|^2 = \frac{1}{2}\Big[& m_C^2 - \tau^2(2m_{T_1}^2 - m_{T_2}^2 - m_L^2) \\ & \pm\sqrt{\left(m_C^2 - \tau^2(2m_{T_1}^2 - m_{T_2}^2 - m_L^2)\right)^2 - 4\tau^4(m_{T_1}^2 - m_L m_{T_2})^2}\Big] , \end{aligned} \tag{2.20}$$

where

$$m_C \equiv |2m_{T_1} + \eta m_L + \eta^* m_{T_2}| , \qquad \eta \equiv \mathbf{u}^\dagger\mathbf{v} \equiv |\eta|e^{i\vartheta_\eta} , \qquad \tau^2 \equiv 1 - |\eta|^2 . \tag{2.21}$$

JHEP03(2024)094

Conventionally, we have chosen $m_{T_1} < 0$ and $\theta_\eta \in [-\pi/2, \pi/2]$. This has no impact on the results as the sign of m_{T_1} can be adjusted in m_C by a shift of π in the phase ϑ_η. Contrary to the case in ref. [50], the phase ϑ_η is a physical parameter to the presence of the extra tree- and loop-contributions: only neglecting $m_{T_2,L}$ it is possible to redefine away ϑ_η.[2] The vectors u and v are fixed to reproduce the PMNS mixing angles, following ref. [50]. As there are enough free parameters to correctly account for the observed values, they do not impose any constraints on the model[3] For the Normal Ordered (NO) and Inverted Ordered (IO) spectra, we thus have

$$\text{NO:} \qquad |m_1|^2 = 0\,, \qquad |m_2|^2 = |m_-|^2\,, \qquad |m_3|^2 = |m_+|^2\,, \tag{2.22}$$

$$\text{IO:} \qquad |m_1|^2 = |m_-|^2\,, \qquad |m_2|^2 = |m_+|^2\,, \qquad |m_3|^2 = 0\,. \tag{2.23}$$

We further define the ratio of the solar and atmospheric neutrino mass-splittings as in ref. [55]

$$r \equiv \frac{|\Delta m^2_{\text{sol.}}|}{|\Delta m^2_{\text{atm.}}|} \equiv \begin{cases} \dfrac{|\Delta m^2_{21}|}{|\Delta m^2_{31}|} = \dfrac{|m_-|^2}{|m_+|^2}\,, & \text{for the NO}\,, \\[2ex] \dfrac{|\Delta m^2_{21}|}{|\Delta m^2_{32}|} = \dfrac{|m_+|^2 - |m_-|^2}{|m_+|^2}\,, & \text{for the IO}\,. \end{cases} \tag{2.24}$$

In the limit $m_{T_2,L} \ll m_{T_1}$, the expression in eq. (2.20) greatly simplifies and reads

$$|m_\pm|^2 \approx m^2_{T_1}\,(1 \pm |\eta|)^2\,, \tag{2.25}$$

which matches with the result of ref. [50]. Along the same lines, it is convenient to extract the value of $|\eta|$ from the neutrino mass difference ratio:

$$|\eta| \equiv \frac{1-\sqrt{r}}{1+\sqrt{r}}\,, \qquad \text{for the NO}\,, \tag{2.26}$$

$$|\eta| \equiv \frac{1-\sqrt{1-r}}{1+\sqrt{1-r}}\,, \qquad \text{for the IO}\,. \tag{2.27}$$

These approximate expressions are valid given that, as it will turn out in our UV completed model, the contributions of $m_{T_2,L}$ are at most $\mathcal{O}(10\%)$ in the considered parameter space. Therefore, these will be the formulae used from now on.

3 The minimal massive Majoron Seesaw model

All the discussion in the previous section concerns the LN symmetry of the infrared (IR) theory. However, a theoretically intriguing assumption is that the Majorana mass terms in the low-energy Lagrangian of eq. (2.2) have a dynamical origin in the UV-theory, through the SSB of the $\mathrm{U}(1)_{\text{PQ}}$ at some scale $f_a \sim \Lambda \gg v_{\text{EW}}$, similarly to what happens in the SM where Dirac mass terms arise from the SSB of the $\mathrm{SU}(2)_L$ symmetry. In the following, we discuss

[2] Notice that, introducing a Majoron in this construction, even if $m_{T_2,L} \neq 0$, the Majoron potential dynamically relaxes such parameter to $\theta_\eta = 0$, as discussed in appendix C.

[3] They enter, however, in fixing the flavour structure of the Majoron couplings, see section 5.

JHEP03(2024)094

the embedding of a dynamical SSB mechanism in the models with two HNLs described in the previous section, respecting three "minimality" requirements: i) only renormalisable interactions are considered in the Lagrangian densities; ii) only one large (Majorana) scale is present and is associated with the SSB of the PQ symmetry, i.e. only one complex scalar field couples to the HNLs; and iii) only one (small) explicit LN and PQ-violating term is introduced. In particular, we assume that there is no other PQ symmetry-breaking term than the one in the Yukawa sector. We will see that, once satisfied these three conditions, a unique model that correctly describes the active neutrino spectrum and PMNS mixing also predicts a tight correlation between these masses (i.e. associated with the LN breaking) and the Majoron mass (i.e. resulting from the PQ breaking).

According to the previous criteria, the SM scalar spectrum is extended only by a single complex scalar field ϕ, endowed with a $\mathrm{U}(1)_{\mathrm{PQ}}$ global symmetry, that gets spontaneously broken by its non-vanishing vev, f_a. It is customary to define

$$\phi \equiv \frac{(f_a + \rho)}{\sqrt{2}} e^{ia/f_a} \,, \tag{3.1}$$

being ρ the radial mode and a the GB associated with the SSB of the PQ symmetry, hereafter dubbed as Majoron. The scale f_a is assumed to be much larger than the EW scale, $f_a \gg v_{\mathrm{EW}}$, in such a way that the radial field can be integrated out and the Majoron remains the only scalar light degree of freedom at low energies, besides the Higgs.

Although the RH neutrinos are gauge singlets, they can, in general, transform both under the LN and PQ symmetries and therefore can couple both with the SM leptons (and the Higgs) and the scalar field ϕ. Therefore, when the PQ symmetry gets spontaneously broken the Majorana mass terms for the RH neutrinos are dynamically generated. The manifestation of the LN breaking in the neutral lepton mass matrix of eq. (2.3) can be easily traced by introducing LN spurionic charges, as already illustrated in the previous section. Thus, to identify the specific LN-violating pattern, it is sufficient to impose a specific LN charge assignment to the neutral leptons and read the spurionic charges of the terms in the neutral lepton mass matrix. Giving a vanishing LN charge to the Higgs simplifies the exercise.

On the other hand, a different reasoning is necessary to identify the possible sources of the PQ symmetry breaking, as we will discuss in the next section. In principle one could also consider additional PQ-violating terms in the scalar potential, at the cost of washing out the Majoron-neutrino mass correlation studied in this paper, contrary to the minimality condition assumed from the beginning.

3.1 Spurionic analysis of the PQ symmetry

It is relatively easy to introduce the field ϕ in the SS realisations discussed in the previous section, giving rise to SSB of the LN. Accordingly to the minimality condition i) of having a renormalisable Lagrangian, we can write

$$\begin{aligned} -\mathscr{L}_{\mathrm{PQ}} = \; & \overline{L_L}\,\widetilde{H}\,Y_N\,N_R + \overline{L_L}\,\widetilde{H}\,Y_S\,S_R + \\ & + \frac{1}{2}\,\phi\left[Y_{NN}\,\overline{N_R^c}\,N_R + Y_{SS}\,\overline{S_R^c}\,S_R + Y_{NS}\,\left(\overline{N_R^c}\,S_R + \overline{S_R^c}\,N_R\right)\right] + \mathrm{h.c.}\,, \end{aligned} \tag{3.2}$$

JHEP03(2024)094

where the Dirac, $Y_{N,S}$, and Majorana, $Y_{NN,NS,\mathrm{SS}}$, Yukawa terms are large or small depending on the underlying LN symmetry assumed for each scenario. For example, the Linear Seesaw case is obtained, after the EW and PQ SSB, for

$$Y_S \to \epsilon Y_S\,, \qquad\qquad Y_{NN} = 0 = Y_{SS} \tag{3.3}$$

and identifying

$$m_N = \frac{Y_N}{\sqrt{2}} v_{\mathrm{EW}}\,, \qquad\qquad \epsilon m_S = \frac{\epsilon Y_S}{\sqrt{2}} v_{\mathrm{EW}}\,, \qquad\qquad \Lambda_{NS} = \frac{Y_{NS}}{\sqrt{2}} f_a\,, \tag{3.4}$$

with the "natural" hierarchy, from the LN charge assignment point of view, $\epsilon Y_S \ll Y_N$.

It is straightforward to observe that, besides the LN, the Lagrangian in eq. (3.2) possess an unbroken $\mathrm{U}(1)_{\mathrm{PQ}}$ symmetry, with charge assignment

$$PQ(L_L) = PQ(N_R) = PQ(S_R) = -PQ(\phi)/2\,. \tag{3.5}$$

As a consequence, the Majoron originated within the PQ SSB remains massless. This can be explicitly seen performing the following field redefinitions:

$$\chi_L \to e^{-\frac{i}{2}\frac{a}{f_a}} \chi_L\,, \tag{3.6}$$

that remove the Majoron dependence in all the Yukawa terms.[4] The Majoron dependence reappears then in the Lagrangian through the kinetic terms as derivative interactions, signalling the underlying presence of the GB shift symmetry.

In order to give a mass to the Majoron, small PQ-violating terms in the Lagrangian can be introduced:

$$-\mathscr{L}_{\epsilon\mathrm{PQ}} = \frac{1}{2}\,\phi^* \left[\epsilon Y_{NN}\, \overline{N_R^c}\, N_R + \epsilon Y_{SS}\, \overline{S_R^c}\, S_R + \epsilon Y_{NS} \left(\overline{N_R^c}\, S_R + \overline{S_R^c}\, N_R\right)\right], \tag{3.7}$$

being ϵY naturally tiny parameters "protected" by the PQ symmetry. It is impossible now to simultaneously eliminate the Majoron dependence from both the Yukawa Lagrangian in eq. (3.2) and that in eq. (3.7) by a field redefinition alike in eq. (3.6), implying the presence of shift symmetry violating terms in the theory and consequently a (loop generated) mass for the Majoron.

The additional terms introduced in eqs. (3.7) also contribute to the active neutrino masses, but clearly only through sub-dominant effects with respect to the leading contributions in eq. (3.2). However, this implies that the Majoron mass is not correlated to the active neutrino masses, or said otherwise the explicit PQ breaking can be considered as an *ad hoc* ingredient to provide the Majoron with a mass –equivalent to an explicit Majoron mass term in the scalar potential- rather than being a common feature of the Majoron and active neutrino mass generation mechanisms. For this reason, we do not dub as "minimal" this realisation and in particular it violates the minimality condition iii) as two independent explicit symmetry-breaking terms are present, one for the LN and the other for the PQ.

[4]The simultaneous redefinition of the RH charged lepton fields, $e_R \to e^{-\frac{i}{2}\frac{a}{f_a}} e_R$, ensures the removal of the Majoron dependence in the charged lepton Yukawa interaction. Being a vectorial transformation implies no generation of anomalous couplings with the gauge bosons.

JHEP03(2024)094

The choice of the Lagrangian in eqs. (3.2) and (3.7) is clearly not the only possible UV completion. In particular, changing the PQ charge assignment in eq. (3.5) implies that $\phi^{(*)}$ insertions may be different. The spurionic approach adopted in section 2 turns out to be very useful also in this case, to discuss the (formal) invariance of the different terms under the PQ symmetry and identify the minimal model. Thus, in what follows, we consider the general Lagrangian in eq. (2.2) and apply the spurionic analysis for the PQ symmetry as we did for the LN in the previous section.

First of all, given the structure of eq. (2.2), we notice that switching N_R with S_R gives physically equivalent configurations. Therefore, without any loss of generality, we simplify the spurionic discussion by fixing $PQ(L_L) = PQ(N_R)$, which implies the PQ invariance of the term proportional to Y_N. The spurionic charges of the other quantities entering eq. (2.2) read as:

$$\begin{aligned} PQ(Y_S) &= PQ(N_R) - PQ(S_R)\,, & PQ(\Lambda_{NS}) &= -PQ(N_R) - PQ(S_R) \\ PQ(\Lambda_{NN}) &= -2PQ(N_R)\,, & PQ(\Lambda_{SS}) &= -2PQ(S_R)\,. \end{aligned} \tag{3.8}$$

In particular, if $PQ(\Lambda_{ij}) = \pm PQ(\phi)$ then the corresponding term is a Yukawa-like interaction between the two HNL fields and the scalar $\phi^{(*)}$ (alike the terms proportional to Y_{NN}, Y_{SS} and Y_{NS} in eq. (3.2)); on the other hand, if $PQ(\Lambda_{ij}) = 0$ then we deal with a direct Majorana mass term; in all the other cases, $PQ(\Lambda_{ij}) \neq 0, \pm PQ(\phi)$ implies that it is not possible to write down the corresponding term at the renormalisable level.

We can now proceed with considering different hypotheses. First of all, if $PQ(N_R) = PQ(S_R)$, then $PQ(Y_S) = 0$ and therefore also the second Yukawa term proportional to Y_S is invariant under PQ. On the other hand, $PQ(\Lambda_{NN}) = PQ(\Lambda_{NS}) = PQ(\Lambda_{NN}) = -2PQ(N_R)$ and, by selecting $PQ(N_R) = -PQ(\phi)/2$, we end up with the Lagrangian in eq. (3.2), that is with a non-minimal model where the Majoron mass and the active neutrino masses are independent. Fixing $PQ(N_R) = +PQ(\phi)/2$ leads to an equivalent setup as indeed the corresponding Lagrangian is the one in eq. (3.2) by interchanging ϕ^* with ϕ. On the other hand, for any other choice of $PQ(N_R)$, the second line of eq. (3.2) is strictly forbidden.

We therefore continue our discussion assuming that $PQ(N_R) \neq PQ(S_R)$. In this case, independently from the exact values of the charges, the Yukawa term proportional to Y_S is not invariant under PQ. However, as already previously discussed, this term is necessary in order to obtain realistic active neutrino masses and therefore it must be introduced as an explicit breaking: we thus adopt the same notation as in the LSS with $Y_S \to \epsilon Y_S$ referring to the PQ symmetry breaking.

Next, if one of the two RH neutrinos has a vanishing PQ charge, then the corresponding Majorana HNL bilinear would be invariant under PQ and the associated term would be a direct mass. On the other hand, it would always be possible to fix the non-vanishing PQ charge of the other HNL such that a Yukawa-like Majorana term gets allowed in the Lagrangian. Explicitly, if $PQ(N_R) = 0$, the term proportional to Λ_{NN} is invariant under PQ and it enters the Lagrangian without any $\phi^{(*)}$ insertion. Then, there are two possibilities to give mass to the second HNL: either $PQ(S_R) = \mp PQ(\phi)/2$ or $PQ(S_R) = \mp PQ(\phi)$, corresponding to promoting to a Yukawa-like interaction the term with Λ_{SS} or that with

JHEP03(2024)094

Λ_{NS}. At the Lagrangian level and using the notation of eq. (2.3), these two cases read as

$$\begin{aligned} PQ(N_R) = 0 \quad \& \quad PQ(S_R) = \mp\frac{PQ(\phi)}{2} : \qquad \widehat{\Lambda} \longrightarrow \begin{pmatrix} \Lambda_{NN} & 0 \\ 0 & Y_{SS}\phi^{(*)} \end{pmatrix} \\ PQ(N_R) = 0 \quad \& \quad PQ(S_R) = \mp PQ(\phi) : \qquad \widehat{\Lambda} \longrightarrow \begin{pmatrix} \Lambda_{NN} & Y_{NS}\phi^{(*)} \\ Y_{NS}\phi^{(*)} & 0 \end{pmatrix} . \end{aligned} \tag{3.9}$$

The opposite situation with $PQ(S_R) = 0$ is very similar and would lead to

$$\begin{aligned} PQ(S_R) = 0 \quad \& \quad PQ(N_R) = \mp\frac{PQ(\phi)}{2} : \qquad \widehat{\Lambda} \longrightarrow \begin{pmatrix} Y_{NN}\phi^{(*)} & 0 \\ 0 & \Lambda_{SS} \end{pmatrix} \\ PQ(S_R) = 0 \quad \& \quad PQ(N_R) = \mp PQ(\phi) : \qquad \widehat{\Lambda} \longrightarrow \begin{pmatrix} 0 & Y_{NS}\phi^{(*)} \\ Y_{NS}\phi^{(*)} & \Lambda_{SS} \end{pmatrix} . \end{aligned} \tag{3.10}$$

All these models, however, are not minimal as they violate the minimality condition ii) as there are two different scales associated with the Majorana terms after the PQ SSB: the direct Majorana mass and f_a.

On the other hand, if none of the HNLs has a vanishing PQ charge but $PQ(N_R) = -PQ(S_R)$, the diagonal Majorana terms would have charges $PQ(\Lambda_{NN}) = -PQ(\Lambda_{SS}) = -2PQ(N_R)$ such that, taking $PQ(N_R) = \mp PQ(\phi)/2$, they can be written in the Lagrangian by multiplying by ϕ or ϕ^*. On the other hand, $PQ(\Lambda_{NS}) = 0$ and it enters as a direct Majorana mass. At the Lagrangian level, we can write

$$PQ(N_R) = -PQ(S_R) = -\frac{PQ(\phi)}{2} : \qquad \widehat{\Lambda} \longrightarrow \begin{pmatrix} Y_{NN}\phi & \Lambda_{NS} \\ \Lambda_{NS} & Y_{SS}\phi^* \end{pmatrix} \tag{3.11}$$

and equivalently for $PQ(N_R) = -PQ(S_R) = +PQ(\phi)/2$ interchanging ϕ^* with ϕ and viceversa. As for the previous two cases, also in this construction, there are two Majorana scales, Λ_{NS} and f_a, and therefore the model is not minimal for condition ii).

As the result of the discussion above, we further restrict the choice of the PQ charges of the HNLs such that $PQ(N_R) \neq \pm PQ(S_R)$ with both non-vanishing, preventing in this way any direct Majorana mass term in the Lagrangian. There are only two other possible setups that allow to give masses to both the HNLs and lead to the Seesaw mechanism. The first of them corresponds to promote the Majorana terms proportional to Λ_{NS} and to Λ_{SS} to be Yukawa-like interactions: the corresponding PQ charges and the Majorana block of the mass Lagrangian are

$$PQ(N_R) = -\frac{PQ(S_R)}{3} = -\frac{PQ(\phi)}{2} : \qquad \widehat{\Lambda} \longrightarrow \begin{pmatrix} 0 & Y_{NS}\phi^* \\ Y_{NS}\phi^* & Y_{SS}\phi \end{pmatrix} \tag{3.12}$$

or the equivalent setup

$$PQ(N_R) = -\frac{PQ(S_R)}{3} = +\frac{PQ(\phi)}{2} : \qquad \widehat{\Lambda} \longrightarrow \begin{pmatrix} 0 & Y_{NS}\phi \\ Y_{NS}\phi & Y_{SS}\phi^* \end{pmatrix} . \tag{3.13}$$

This construction does not suffer from the presence of multiple Majorana scales, as after the PQ SSB the non-vanishing entries are proportional to f_a, and thus it looks promising.

JHEP03(2024)094

However, the active neutrino mass matrix receives two different contributions at the tree level,

$$m_\nu \simeq -\sqrt{2}\frac{Y_{SS}}{Y_{NS}^2}\frac{m_N\, m_N^T}{f_a} - \sqrt{2}\epsilon\frac{m_N\, m_S^T + m_S\, m_N^T}{Y_{NS} f_a}\,, \tag{3.14}$$

where the first term dominates, unless specific tuning is present among the parameters. It follows that it is not possible to correctly describe the active neutrino masses and PMNS mixing as the dominant term has rank 1, thus ruling out this model.

3.2 The minimal massive Majoron Seesaw Lagrangian

The only case left unexplored identifies the minimal massive Majoron Seesaw (mmM) model where the Majoron mass and the active neutrino masses are indeed correlated. This model satisfies the three minimality conditions i)–iii) and describes realistic active neutrino masses and PMNS mixing. The PQ charges of the fields involved satisfy to

$$PQ(L_L) = PQ(N_R) = -\frac{PQ(S_R)}{3} = -\frac{PQ(\phi)}{2} \tag{3.15}$$

and the corresponding PQ conserving and explicitly violating Lagrangian densities read as

$$-\mathscr{L}_{\rm PQ}^{\rm mmM} = \overline{L_L}\,\widetilde{H}\,Y_N\,N_R + \frac{Y_{NS}}{2}\,\phi^*\left(\overline{N_R^c}\,S_R + \overline{S_R^c}\,N_R\right) + \frac{Y_{NN}}{2}\,\phi\,\overline{N_R^c}\,N_R + \text{h.c.}\,, \tag{3.16}$$

$$-\mathscr{L}_{\epsilon\rm PQ}^{\rm mmM} = \epsilon\overline{L_L}\,\widetilde{H}\,Y_S\,S_R + \text{h.c.}\,, \tag{3.17}$$

where as usual Y_N, Y_{NN} and Y_{NS} are assumed to be order one, while ϵY_S much smaller. Notice that this Lagrangian is invariant under the interchange of ϕ and ϕ^* as far as the sign of $PQ(\phi)$ in eq. (3.15) is accordingly flipped.

Focussing on the explicit PQ breaking, it is straightforward to check that neglecting the ϵY_S term, the Majoron dependence can be removed from these Yukawa-like interactions, reappearing only in derivative couplings, ending again with a massless Majoron model. Moreover, in this same limit, the active neutrino mass matrix has rank 1 and cannot generate the two observed neutrino mass differences. On the other hand, once this term is taken into consideration, it explicitly breaks both the PQ symmetry and the LN: the Majoron acquires a mass and the active neutrino masses can be described according to the observations, both types of masses being necessarily proportional to ϵY_S.

These equations closely look like the expressions in eqs. (2.10) and (2.11) of the Extended Seesaw context, and indeed, after the SSB of the EW and PQ symmetries, the resulting lepton mass matrix matches the one in eq. (2.12), with the mass terms explicitly given by

$$m_{N,S} = \frac{Y_{N,S}}{\sqrt{2}}v_{\rm EW}\,, \qquad \Lambda_{NN,NS} = \frac{Y_{NN,NS}}{\sqrt{2}}f_a\,, \qquad \Lambda_{SS} = 0\,. \tag{3.18}$$

We can now use the experimental data from neutrino oscillation experiments, adopting for definiteness the results presented in ref. [55] (including the SK atmospheric data) to constrain the parameter space of the mmM model by use of eqs. (2.25)–(2.27). In figure 1 we scan the parameter space Λ_{NS} *vs.* ϵY_S, running over the different Yukawa couplings taken in the "natural" range $|Y_i| \in [10^{-2}, 1]$, letting ϵ the only *ad hoc* "small" parameter. Their magnitude is represented by the coloured horizontal band: the smallest values are in blue, while the largest ones are in orange. In the coloured regions, the mass eigenstates are fixed

JHEP03(2024)094

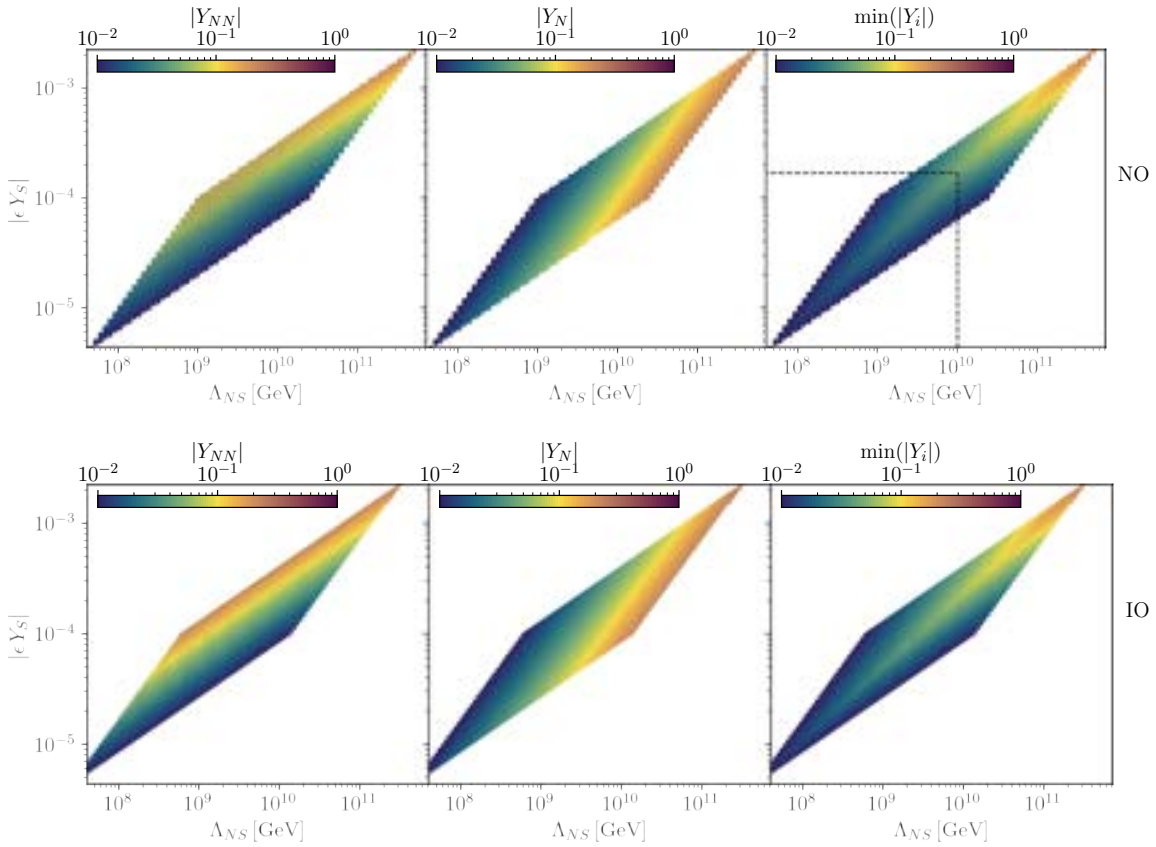

Figure 1. The colored region in the plots represents the allowed $\{\epsilon, Y_i, \Lambda_{NS}\}$ parameter space for which the condition $m_L \leq 0.1\, m_T$ is satisfied, assuming Normal Order (*top*) or Inverse Order (*bottom*), respectively. In the third upper plot the benchmark point $|\epsilon Y_S| = 1.7 \times 10^{-4}$, $|Y_{NN}| = |Y_N| = 0.06$, and $\Lambda = 10^{10}$ GeV is shown.

to reproduce both mass differences, by setting r and one mass splitting to their experimental central values, while variations within the corresponding 3σ ranges do not show qualitative changes. The loop contribution is required to be at most the 10% of the tree-level ones, to preserve the predictivity required by the hypothesis of this work. Moreover, ϵ satisfies the condition $\epsilon \leq 10^{-2} \min |Y_i|$, reflecting the soft explicit breaking of the LN.

These conservative conditions show a parameter space where the scale Λ_{NS} spans a relatively small range of values, $\Lambda_{NS} \sim 10^8 - 10^{11}$ GeV, where the Yukawa couplings are larger than 10^{-2}. As expected, relaxing any of the previous conditions enlarges the parameter space: e.g., requiring the loop contributions to be at most the 30% of the tree-level one, one would allow reaching scales of $\Lambda_{NS} \sim 10^{12}$ GeV with Yukawa couplings of order $|Y_i| \sim 0.7$.

Notice that the requirement of not going below 10^{-2} in the Yukawa couplings constrains the region of smaller Λ_{NS} values. This can be seen in the left and centre plots of figure 1, where $|Y_N|$ and $|Y_{NN}|$ need to be small in order to tame the loop contribution. As Λ_{NS} grows the loop contribution stops being so relevant, but as ϵ necessarily grows to fix the correct mass splitting, the constraint of $\epsilon \leq 10^{-2} \min |Y_i|$ exclude the upper sides of the rhomboid.

The next two sections are devoted to the study of the Majoron mass and its phenomenological constraints.

JHEP03(2024)094

4 One-loop contributions to the Majoron mass

Before calculating the one-loop contributions to the Majoron mass in the mmM scenario, it is useful to discuss a simpler model, similar to the one introduced in [56], to highlight some fundamental features.

4.1 Pseudo-GB mass radiative contributions in a toy model

We consider a Dirac fermion field ψ coupled to a complex scalar singlet ϕ through the interaction Lagrangian

$$-\mathscr{L} = y\,\phi\,\overline{\psi}_L\,\psi_R + \tilde{y}\,\phi^*\,\overline{\psi_L}\psi_R + \text{h.c.} \tag{4.1}$$

with y and $\tilde{y}$ reals. The fields ψ and ϕ have non-trivial transformation properties under a global U(1), spontaneously broken by ϕ getting a non-vanishing vev, f_a. It is clear from the above Lagrangian that, due to the simultaneous presence of y and $\tilde{y}$, there is no possible charge assignment for which the interaction Lagrangian could preserve any U(1) symmetry. One could assume that y-term is the symmetry preserving coupling and $\tilde{y}$-term is the (small) softly breaking one, but the opposite assumption is viable and leads to the same physical results. For the time being, without fixing a specific charge assignment and thus without identifying which term among y and $\tilde{y}$ is symmetry breaking, we just consider their product $y\,\tilde{y}$ to be a small quantity.

After SSB has occurred, the fermion mass term and coupling with the pseudo-GB a reads:

$$-\mathscr{L} \supset m_\psi \cos\left(\frac{a}{f_a}\right)\overline{\psi}\,\psi + i\,m'_\psi \sin\left(\frac{a}{f_a}\right)\overline{\psi}\,\gamma_5\,\psi\,, \tag{4.2}$$

$$\supset m_\psi\,\overline{\psi}\psi + i\,m'_\psi\frac{a}{f_a}\overline{\psi}\,\gamma^5\psi - \frac{m_\psi}{2}\left(\frac{a}{f_a}\right)^2\overline{\psi}\psi + \dots\,, \tag{4.3}$$

where m_ψ and m'_ψ are defined as

$$m_\psi \equiv \frac{y+\tilde{y}}{\sqrt{2}}\,f_a\,, \qquad\qquad m'_\psi \equiv \frac{y-\tilde{y}}{\sqrt{2}}\,f_a\,, \tag{4.4}$$

and in the second line, we have expanded in a/f_a and kept the two lowest order contributions that are the only relevant for a one-loop calculation.

As the simultaneous presence of y and $\tilde{y}$ explicitly breaks the U(1) symmetry, one expects a GB mass term to appear at loop level proportional to the product $y\,\tilde{y}$. Denoting with $-i\mathscr{M}(p^2)$ the sum of all one-particle-irreducible one-loop contribution to the GB scalar propagator, any positive contribution to $\mathscr{M}(p^2=0)$ corresponds to a positive shift of the GB mass. Such contributions can appear only from two types of loops, shown in figure 2: a) the Bubble diagram and b) the Balloon diagram. The Bubble diagram (*left*) needs two 3-point vertices, and therefore is proportional to m'^2_ψ, while the Balloon one (*right*) only involves a single 4-point vertex and is proportional to m_ψ.

JHEP03(2024)094

(a) *Bubble Diagram.* (b) *Balloon Diagram.*

Figure 2. Diagrams contributing to the 1-loop mass of the GB.

In dimensional regularization (with $d \equiv 4 - 2\varepsilon$), one obtains that the zero momentum contribution to the GB propagator reads:

$$\begin{aligned} -i\mathscr{M} &= -i\mathscr{M}_A - i\mathscr{M}_B \\ &= i\,\frac{m_\psi'^2}{f_a^2}\int \frac{\mathrm{d}^d k}{(2\pi)^d}\,\frac{\mathtt{Tr}\left[\gamma^5(\not{k}+m_\psi)\gamma^5(\not{k}+m_\psi)\right]}{(k^2-m_\psi^2)^2} + i\,\frac{m_\psi}{f_a^2}\int \frac{\mathrm{d}^d k}{(2\pi)^d}\,\frac{\mathtt{Tr}[\not{k}+m_\psi]}{k^2-m_\psi^2} \\ &= -i\,\frac{(-m_\psi^2\, m_\psi'^2 + m_\psi^4)}{4\pi^2 f_a^2}\left[1 - \log\left(\frac{m_\psi^2}{\mu_R^2}\right) + \frac{1}{\tilde{\varepsilon}_{UV}}\right] \end{aligned} \tag{4.5}$$

with the first (second) term referring to the bubble (balloon) diagram. In eq. (4.5), μ_R is the renormalisation scale and $\tilde{\varepsilon}_{UV}$ is defined as

$$\frac{1}{\tilde{\varepsilon}_{UV}} \equiv \frac{1}{\varepsilon_{UV}} - \gamma_E + \log(4\pi)\,, \tag{4.6}$$

with γ_E the Euler-Mascheroni constant.[5] The one-loop pseudo-GB mass, in the $\overline{\text{MS}}$-scheme, then reads

$$m_a^2 = \frac{y\tilde{y}\,(y+\tilde{y})^2}{4\pi^2} f_a^2\,, \tag{4.7}$$

confirming the dependence on the product between y and $\tilde{y}$, independently from the U(1) charge assignment, that is without having identified which one among y and $\tilde{y}$ does explicitly break the symmetry. On the other hand, if any of the two parameters is vanishing the Lagrangian is left with an accidental symmetry that protects the GB from acquiring a mass and indeed the expression in eq. (4.7) does vanish. This can be easily understood by writing the scalar field in the polar coordinates. Indeed, the two terms in eq. (4.1) would have exponentials with opposite signs and, only if either y or $\tilde{y}$ is vanishing, then it is possible to perform a ψ redefinition to reabsorb the GB dependence. In this case, the GB would reappear in the kinetic terms and only with derivative couplings, implying the presence of a shift symmetry that protects the GB from acquiring a mass term.

It is instructive to repeat the computation of the GB mass in the chirality-preserving basis, also known in the literature as *derivative basis*. Moreover, to make more evident the results of this exercise, we assume a specific charge assignment such that the y-term is U(1)-preserving, while $\tilde{y}$ is U(1)-breaking and we move to a more explicit notation with $\tilde{y} \to \epsilon\tilde{y}$, being ϵ a small

[5] Notice that the momentum zero computation is consistent with the fact that the GB is massless at tree level and therefore any correction to the kinetic term would effectively be translated into a 2-loop correction to its mass.

JHEP03(2024)094

parameter.[6] By performing the following field-dependent redefinition in the whole Lagrangian,

$$\psi \to e^{-i\gamma_5 a/2f_a}\,\psi\,, \tag{4.8}$$

the GB dependence is removed from the y-term and is only left in the $\tilde{y}$-term, and the relevant interactions read

$$\begin{aligned} -\mathscr{L} &\supset \frac{y\,f_a}{\sqrt{2}}\overline{\psi}\psi + \epsilon\frac{\tilde{y}\,f_a}{\sqrt{2}}\left[\cos\left(\frac{2a}{f_a}\right)\overline{\psi}\psi - i\,\sin\left(\frac{2a}{f_a}\right)\overline{\psi}\gamma_5\psi\right] - \frac{\partial_\mu a}{2f_a}\,\overline{\psi}\gamma^\mu\gamma_5\psi + \cdots \\ &\supset \frac{(y+\epsilon\tilde{y})\,f_a}{\sqrt{2}}\,\overline{\psi}\psi - \epsilon\frac{2\,\tilde{y}\,f_a}{\sqrt{2}}\left[\left(\frac{a}{f_a}\right)^2\overline{\psi}\psi + i\,\frac{a}{f_a}\overline{\psi}\gamma_5\psi\right] - \frac{\partial_\mu a}{2f_a}\,\overline{\psi}\gamma^\mu\gamma_5\psi + \cdots\,, \end{aligned} \tag{4.9}$$

where in the last line only the linear and quadratic terms in a/f_a have been kept. For a vanishing $\tilde{y}$, the a field has only derivative couplings reflecting its exact GB nature. Instead, for $\tilde{y}$ small, but different from zero, shift-breaking terms are present and lead to the one-loop pseudo-GB mass term.

In the derivative basis, the computation of the mass is much simpler as indeed i) diagrams with (one or two) derivative couplings never contribute to the GB mass as they always carry an external momentum dependence, and ii) the GB mass contribution is dominated by the balloon diagram,

$$-i\mathscr{M}_B = -i\,\epsilon\,\frac{y^3\,\tilde{y}\,f_a^2}{4\pi^2}\left[1 - \log\left(\frac{m_\psi^2}{\mu_R^2}\right) + \frac{1}{\tilde{\varepsilon}_{UV}}\right] + \mathcal{O}\left(\epsilon^2\right)\,, \tag{4.10}$$

being the bubble one suppressed by two powers of the small parameter ϵ. By expanding eq. (4.5) in ϵ and keeping the leading term, $(-m_\psi^2\,m_\psi'^2 + m_\psi^4) = y^3\tilde{y}f_a^4$ and we recover the result in eq. (4.10). This proves that moving to the derivative/chirality preserving basis, leaving the GB dependence only into the explicitly breaking term(s), is the most convenient one for what concerns the calculation of the contributions to the GB mass. Indeed, the computations reduce to only one topology of diagrams, the Balloon one, at the leading order in ϵ. This is indeed the choice that we will make in the next section for the mmM model.

4.2 Majoron mass in the Minimal Majoron model

In this section we calculate the one-loop contribution to the Majoron mass in the mmM model and the complete Yukawa Lagrangian relevant for this computation is the following:

$$\begin{aligned} -\mathscr{L}_{\rm Yuk} = \;& \overline{L_L}\,H\,Y_e\,e_R + \overline{L_L}\,\widetilde{H}\,Y_N\,N_R + \epsilon\,\overline{L_L}\,\widetilde{H}\,Y_S\,S_R + \\ &+ \frac{Y_{NS}}{2}\,\phi^*\left(\overline{N_R^c}\,S_R + \overline{S_R^c}\,N_R\right) + \frac{Y_{NN}}{2}\,\phi\,\overline{N_R^c}\,N_R + \text{h.c.} \end{aligned} \tag{4.11}$$

Once LN is spontaneously broken, the ϕ-radial model, ρ, acquires a large mass $m_\rho \approx f_a \gg v_{\rm EW}$, and therefore it can be safely integrated out and it is not expected to have any significant impact in the low-energy phenomenology we are interested in. In the following, only the lepton couplings with the light angular mode, a, are considered.

[6] Obviously the alternative assignment in which the symmetry is broken by the y-term would be perfectly equivalent.

JHEP03(2024)094

Armed with the toy-model discussion, the simplest approach to calculate the Majoron mass contributions is moving to the chirality preserving basis, leaving the Majoron dependence on the explicit PQ breaking term, where only the balloon diagram contributes at leading order in the small parameter ϵ. By means of the following field-dependent redefinition of the fermionic fields,

$$\{N_R,\, L_L,\, e_R\} \to \{N_R,\, L_L,\, e_R\}\, e^{-ia/(2f_a)}\,, \qquad\qquad S_R \to S_R\, e^{3ia/(2f_a)}\,, \tag{4.12}$$

the Majoron dependence in the second-line terms in eq. (4.11) is reabsorbed, without reappearing in the first two terms (i.e. the PQ conserving ones) of the first line. The only dependence on the Majoron field, after the redefinition in eq. (4.12), is left in the only PQ symmetry violating term of the first line, i.e. the one proportional to ϵY_S, and in the derivative couplings that originate from the fermion kinetic terms: all in all, the Lagrangian containing the Majoron interactions reads

$$\mathscr{L}_a = \frac{\partial_\mu a}{2f_a}\left(\overline{\nu}_L\gamma^\mu\nu_L + \overline{N}_R\gamma^\mu N_R - 3\,\overline{S}_R\gamma^\mu S_R\right) + \left(\epsilon\,\overline{\ell}_L\,\widetilde{H}\,Y_S\,S_R\,e^{2ia/f_a} + \text{h.c.}\right). \tag{4.13}$$

As all the SM leptons identically transform under the PQ, there is no tree-level Majoron coupling with the charged leptons and no anomalous gauge terms.

Before proceeding with the calculation of the one-loop contribution to the Majoron mass, it is convenient to write the Lagrangian in terms of the physical fields, that is the mass eigenstates of the neutral lepton mass matrix eq. (2.12) accounting for the parameter definitions in eq. (3.18). All the details of the straightforward procedure are reported in appendix A and for convenience, we only report here the leading contributions to the HNL masses in terms of the fundamental parameters of the mmM Lagrangian,

$$M_{N,S} = \frac{\Lambda_{NS}}{2}\left[\sqrt{4+\left(\frac{Y_{NN}}{Y_{NS}}\right)^2} \mp \left(\frac{Y_{NN}}{Y_{NS}}\right)\right]. \tag{4.14}$$

As in the chirality preserving basis the leading order contribution to the Majoron mass comes from the Balloon type diagram, the leading contribution to the Majoron mass comes from

$$-\mathscr{L}_a \supset \frac{|m_N||\epsilon m_S||\eta|}{2\sqrt{M_N\,M_S}(M_N+M_S)}\left(M_N\overline{S_R^c}S_R - M_S\overline{N_R^c}N_R\right)\frac{a^2}{f_a^2} + \text{h.c.}\,, \tag{4.15}$$

whose derivation can be found in appendix A. In fact, the SM neutrino contributions to the Majoron mass are proportional to the active neutrino masses and therefore are completely negligible. Moreover, the $\overline{S_R^c}N_R$ terms come with a linear coupling to the Majoron, and therefore, as learned from the toy model analysis, they contribute to m_a only through the bubble type of diagrams, thus being of $\mathcal{O}(\epsilon^2)$. However, in this model, a stronger statement regarding the Majoron mass can be made. The potential is constrained by symmetry arguments to be of the form

$$V(a) \propto |m_N||\epsilon m_S|\Lambda_{NN}\Lambda_{NS}\cos\left(\frac{2a}{f_a}\right), \tag{4.16}$$

JHEP03(2024)094

meaning that dimensionally the potential is already saturated by the necessary combination of EW- and Majorana-Yukawas (cfr. eq. (C.5)). The presence of extra EW-Yukawa factors in general, including dependence on ϵ, can only enter as a correction factor of the type $\propto (1 + |m_{N,S}|^2/f_a^2)$, meaning that it would be NLO in $1/f_a$ expansion. This implies that in the derivative basis, the balloon captures the full result of the amplitude at LO in f_a. The same statement is not valid in the toy model, where only one scale is present and thus no suppressions of the type $v_{\rm EW}/f_a$ are possible.

From the couplings in eq. (4.15), one can calculate the Balloon contribution to the Majoron mass in the $\overline{\rm MS}$ scheme. The result can also be derived employing the CW potential, as shown in appendix C in eq. (C.9). Assuming $v_{EW} \ll f_a$, in the NO case, the Majoron mass reads

$$m_a^2 = \frac{|\eta||m_N||\epsilon m_S|}{\pi^2}\frac{\sqrt{M_N M_S}}{M_N + M_S}\left[\frac{(M_S^2 + M_N^2)}{f_a^2}\log\left(\frac{M_S}{M_N}\right) + \right.$$
$$\left. + \frac{(M_S^2 - M_N^2)}{f_a^2}\left(\log\left(\frac{M_N M_S}{\mu_R^2}\right) - 1\right)\right]. \tag{4.17}$$

Let us notice that in a generic model with explicit PQ symmetry breaking one expects typically $m_a^2 \propto \epsilon f_a^2$. This happens, indeed, in the toy model described in section 4.1 as clearly revealed by eq. (4.10). Instead, with the specific symmetry-breaking pattern introduced for the mmM model, the Majoron mass for large f_a behaves as $m_a^2 \propto \epsilon\, v_{\rm EW}^2 \log f_a/\mu_R$, that is, m_a^2 asymptotically depends only logarithmically from the large PQ SSB scale, thus allowing a naturally lighter ALP.[7]

Assuming now also $m_L \sim m_{T_2} \ll m_{T_1}$ and by means of eqs. (2.25) and (2.26), the Majoron mass can be strictly connected with the neutrino mass splittings

$$m_a^2 \simeq \frac{\sqrt{|\eta||\Delta m_{32}^2|}}{2\,\pi^2}\frac{M_N M_S}{M_N + M_S}\left[\frac{(M_S^2 + M_N^2)}{f_a^2}\log\left(\frac{M_S}{M_N}\right) + \right.$$
$$\left. + \frac{(M_S^2 - M_N^2)}{f_a^2}\left(\log\left(\frac{M_N M_S}{\mu_R^2}\right) - 1\right)\right], \tag{4.18}$$

where, to understand the correct scale dependence in m_a^2 one has now to recall from eq. (2.18) that $\Delta m^2 \propto v_{\rm EW}^4/f_a^2$. The result for the IO scenario can be obtained by simply replacing $|\Delta m_{32}^2| \to |\Delta m_{21}^2|$ in eq. (4.18). To provide an intuitive idea of the Majoron mass behaviour in terms of the relevant model parameters, in figure 3 m_a as a function of the HNLs masses $M_{N,S}$ (*left*) and the Yukawas $Y_{NN,NS}$ (*right*) has been shown, with the different colour nuances indicating the Majoron mass (in keV) as reported on the scale on the right of the figure. The different black contours indicate, instead, the corresponding $m_L/\sqrt{\Delta m_{\rm atm}^2}$ values as an estimation of the relative size of the loop contribution with respect to the tree-level one. This gives an idea, similarly to figure 1, of how much the parameter space gets constrained for taming the one-loop contribution to the active neutrino masses. In grey, we estimate the region that could induce a $m_{T_2} > 0.1 m_{T_1}$. In terms of the HNL masses (*left plot*) this means that, in order to keep the one-loop vs tree-level ratio below 0.1, one needs either

[7] See also the discussion in ref. [40].

JHEP03(2024)094

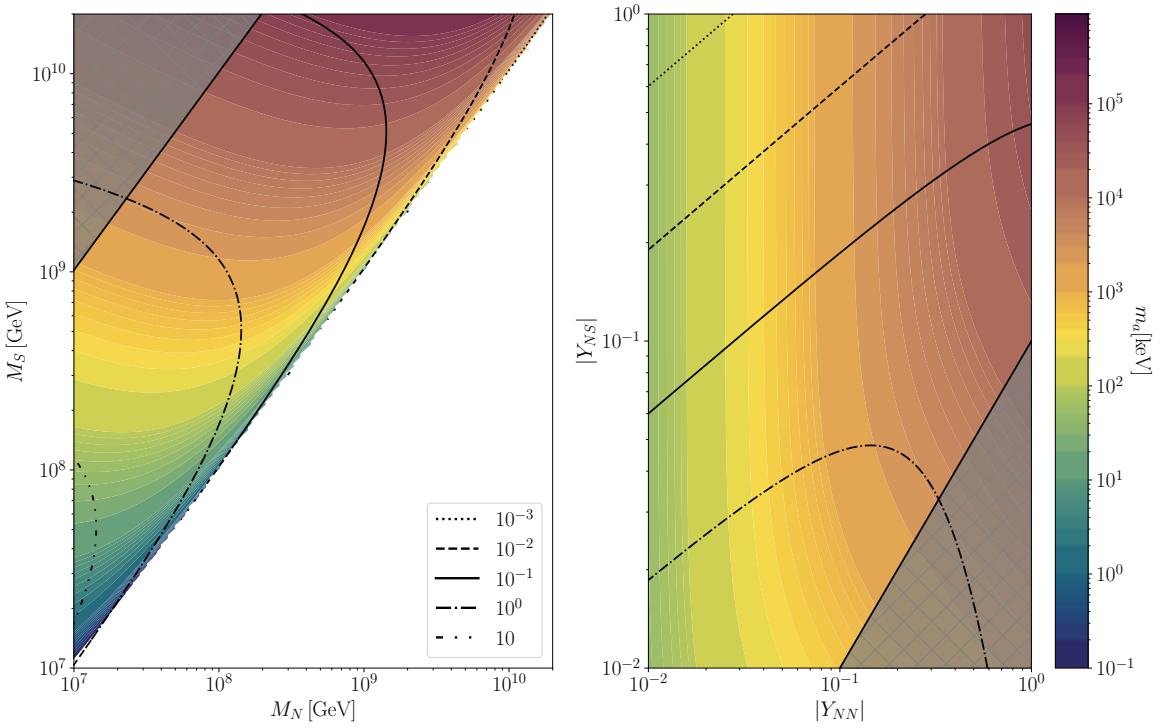

Figure 3. Dependence of the Majoron mass with respect to the (*left*) HNL masses $M_{N,S}$ and (*right*) the Yukawas $Y_{NN,NS}$, for $f_a = 10^{10}\,\text{GeV}$ and $Y_N = 0.01$. The different colours indicate the mass range of the Majoron, while the different black lines are contours of the $m_L/\sqrt{\Delta m^2_{\text{atm}}}$ ratio. The gray area bounds the region where $m_{T_2} > 0.1\, m_{T_1}$.

going close to the mass degeneracy region or increasing M_S above $\sim 10^9\,\text{GeV}$ for a fixed M_N, however, this last region would create a larger m_{T_2} contribution. The white region in the left plot of figure 3 corresponds to the inaccessible region once $M_S > M_N$ is chosen in eq. (2.14). The right plot of figure 3 represents the same information but as functions of the $Y_{NN,NS}$ Yukawas: one can notice here that for Yukawas $Y_{NN,NS} \sim \mathcal{O}(10^{-2})$ and for the chosen scale $f_a = 10^{10}\,\text{GeV}$, a Majoron mass around the keV scale is typically reproduced, while a $\sim 100\,\text{MeV}$ scale Majoron can be obtained for $\mathcal{O}(1)$ Yukawas couplings.

The second task is to identify the parameter space that satisfies the constraints mentioned in section 3.2, that is $\epsilon \ll 0.01 \min|Y_i|$ and $m_{T_2}, m_L \ll m_{T_1}$. The allowed parameter space is then shown in figure 4 with respect to one of the masses of the HNLs. The pair of HNLs needs to be non-degenerate, as otherwise $Y_{NN} = 0$ and the Majoron would become massless. However, a small tuning needs to be employed to control the size of the loop level. For this reason, the pair of HNLs is quasi-degenerate and we can plot the dependence for only one of the masses. On the plots of figure 4 we observe the dependence on the scale f_a (*left*), which shows a linear scaling $m_a \sim f_a$, this dependence is clear only when one fixes $\epsilon|m_S||m_N|$ to reproduce the neutrino masses, while if one keeps the dependence on the Yukawas (as in eq. (C.9)) this scaling is implicit. The range of f_a goes from $10^8 - 10^{11}\,\text{GeV}$ for masses of the Majoron between $1 - 5 \times 10^4\,\text{keV}$. We also see in figure 4 (*right*) the dependence of the mass with respect to the Yukawas showing that the region of the largest Yukawas corresponds to the heaviest Majoron.

JHEP03(2024)094

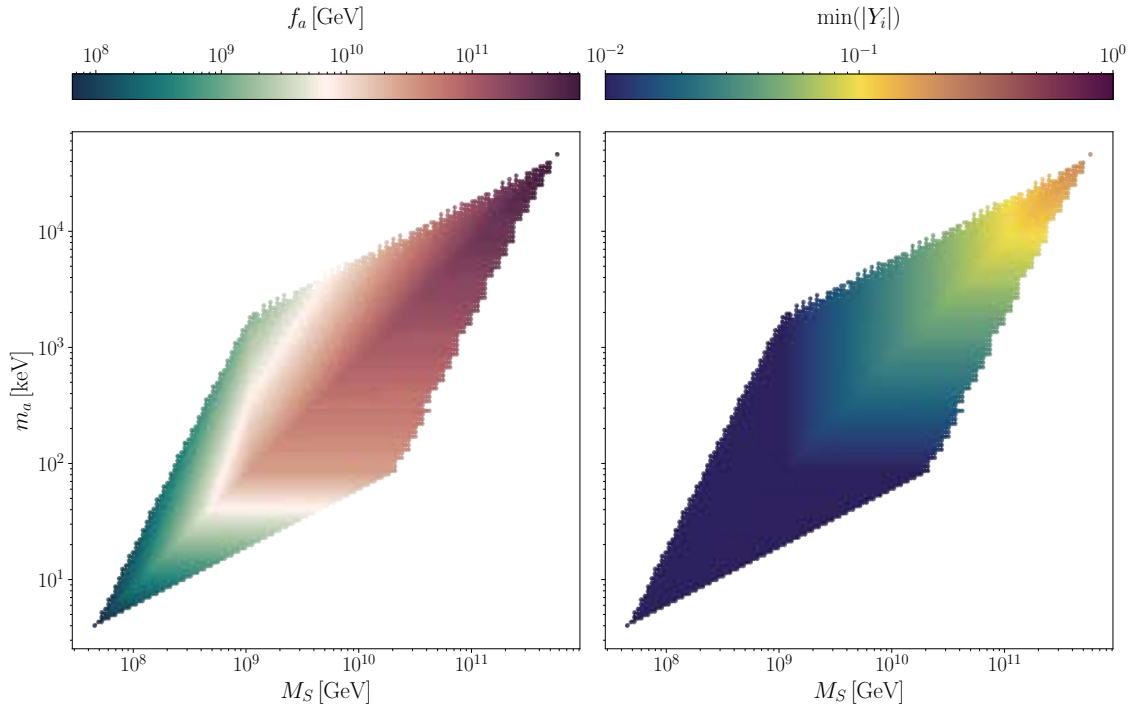

Figure 4. Majoron mass plotted as a function of M_S. Different colours indicate the dependence on the f_a scale (*left plot*), or on the min $|Y_i|$ value (*right plot*) as shown in the corresponding upper bars.

Note that this constrained space can be enlarged at the cost of relaxing our "natural" Yukawas, however at the cost of needing to control both loop and tree level extra contributions. This would be possible to accommodate the neutrino masses, but a loss in the predictivity of the Majoron mass would be expected.

5 Phenomenology of the minimal massive Majoron

In the previous section, it has been shown that the typical Majoron mass range, predicted by the mmM model, lies in the $[1,\, 5\times10^4]$ keV interval, i.e. slightly below the muon mass, with the typical SSB scale ranging between $[10^7, 10^{11}]$ GeV. In this section, the main phenomenological impact of the mmM model in particle and astroparticle/cosmological observables will be discussed.

The full mmM Lagrangian in the neutral lepton mass basis is described in appendix B. At tree-level the Majoron couples exclusively with neutral leptons, and clearly only the Majoron couplings with active neutrinos can be directly constrained by present experiments. Imposing that the observed neutrino oscillation mass differences and PMNS mixing angles are being reproduced by opportunely choosing the Dirac and Majorana Yukawas entries of the neutral lepton mass matrix, the lowest order[8] Majoron-active neutrino coupling (see for example eq. (B.7)) reads

$$\mathscr{L}_{a\nu\nu} = -\frac{i\,a}{2f_a}\overline{\nu_L}\, m_\nu\, \gamma_5\, \nu_L^c\,. \tag{5.1}$$

[8]Alternatively here one could use as m_ν the complete tree-level plus one-loop neutrino mass matrix calculated in eqs. (2.13) and (2.15).

JHEP03(2024)094

Couplings of the Majoron with charged SM leptons arise at one loop level through Z and W exchanges. For having a more compact notation, and matching with the existing literature [57, 58], it is useful to introduce the following adimensional hermitian coupling

$$K \equiv \frac{\hat{m}\hat{m}^\dagger}{v_{EW}^2} = \frac{m_N m_N^\dagger + \epsilon^2 m_S m_S^\dagger}{v_{EW}^2} = \frac{1}{2}\left(|Y_N|^2 uu^\dagger + \epsilon^2 |Y_S|^2 vv^\dagger\right) . \tag{5.2}$$

Since in our model the RH leptons couple simultaneously to ϕ and ϕ^*, see eq. (4.11), the Majoron-charged lepton couplings derived in [57–59] need to be accordingly modified. Therefore, the one-loop Majoron-charged leptons effective Lagrangian in the mmM model reads:

$$\mathscr{L}_{a\ell\ell} = \frac{i\,a}{16\pi^2 f_a}\bar{\ell}\left(M_\ell \,\mathrm{tr}\left[\widetilde{K}\right]\gamma_5 + 2\,M_\ell\,\widetilde{K}_H\,P_L - 2\,\widetilde{K}_H\,M_\ell\,P_R\right)\ell\,, \tag{5.3}$$

where M_ℓ is the diagonal charged leptons mass matrix and we have defined

$$\widetilde{K} = K + \frac{(\sigma-1)}{v_{\rm EW}^2}\left[m_N m_N^\dagger\left(1-R^2\right) + R\,\epsilon m_S m_N^\dagger + R^3\, m_N \epsilon m_S^\dagger + \epsilon^2 m_S m_S^\dagger\left(1+R^2\right)\right], \tag{5.4}$$

with $R = \Lambda_{NN}/\Lambda_{NS}$, $\widetilde{K}_H = (\widetilde{K} + \widetilde{K}^\dagger)/2$. In eq. (5.4) the parameter $\sigma = \pm 1$ has been introduced to switch easily between the models usually described in the literature ($\sigma = 1$) where the RH leptons are coupled solely to ϕ, from our model ($\sigma = -1$) where they are coupled simultaneously to ϕ and ϕ^*. Notice also that for $\sigma = -1$ but $R \ll 1$, one gets $\widetilde{K} \simeq -K$, that is, exactly the same coupling of the models with $\sigma = 1$ but with $a \to -a$. In other words, the $R \ll 1$ region of our model corresponds to a scenario where the RH leptons couple only to ϕ^*, as emerges looking at the Lagrangian of eq. (4.11). Finally, to match with (part of) the existing literature, bounds to the Majoron-electrons coupling are going to be expressed in terms of the dimensional parameter, g_{ae}, defined as

$$\mathscr{L}_{aee} = i\frac{m_e}{16\pi^2 f_a}\left(\mathtt{Tr}\widetilde{K}_H - 2(\widetilde{K}_H)_{ee}\right) a\,\bar{e}\,\gamma_5\,e \equiv i\,g_{ae}\,a\,\bar{e}\,\gamma_5\,e \tag{5.5}$$

We are not reporting here Majoron couplings with quarks and nucleons as the associated phenomenology, in our mmM scenario, is less compelling then the charged leptons one. In fact, Majoron couplings with quarks are flavour diagonal and therefore relevant bounds from flavour changing neutral currents observables (for example in $s \to d\,a$ or $b \to d\,a$ transitions) are not expected, being suppressed by two loops and by the relatively large scale f_a typically above 10^6 GeV (see for example the discussion in [60, 61]).

Majoron couplings with weak gauge bosons arise at one-loop level but with a $\mathcal{O}(1/f_a^2)$ suppression or at two-loops at $\mathcal{O}(1/f_a)$, therefore they are not phenomenology appealing. Conversely, $\mathcal{O}(1/f_a)$ two-loop contributions to the Majoron-photons couplings can be potentially relevant [58], contributing to the anomalous Lagrangian term

$$\mathscr{L}_{a\gamma\gamma} = -\frac{g_{a\gamma\gamma}}{4} a F_{\mu\nu}\widetilde{F}^{\mu\nu}\,. \tag{5.6}$$

A complete calculation of the two-loop Majoron-photons coupling is beyond the scope of this paper. We can, however, opportunely adapt the results of ref. [58] to reproduce an approximate $g_{a\gamma\gamma}$ suitable in the parameter space of interest for our model. From a careful

JHEP03(2024)094

inspection of the g_{aee} coupling of eq. (5.5) one realizes, that in the allowed parameter space the exact one-loop calculation is fairly approximated by the $R \ll 1$ expression within a 10% accuracy. Hence we assume, within the same range of validity, the following $g_{a\gamma\gamma}$ coupling

$$g_{a\gamma\gamma} \simeq -\frac{\alpha_{\rm em}}{8\pi^3 f_a}\left[\mathtt{Tr}K\sum_f N_c^f Q_f^2 T_3^f\, h\left(\frac{m_a^2}{4m_f^2}\right) + \sum_{\ell=e,\mu,\tau} K_{\ell\ell}\, h\left(\frac{m_a^2}{4m_\ell^2}\right)\right], \tag{5.7}$$

that is the result of [58] with a global minus sign indicating that RH leptons are predominantly coupled with ϕ^*. In eq. (5.7) f runs over all fermions, N_c is the number of colours, T_3^f is the weak isospin and

$$h(x) \equiv -\frac{1}{4x}\left[\log\left(1-2x+2\sqrt{x(x-1)}\right)\right]^2 - 1 \simeq \begin{cases} \dfrac{x}{3} & \text{for } x \to 0 \\ -1 & \text{for } x \to \infty \end{cases} \tag{5.8}$$

The dependence of the loop function $h(x)$ implies that the largest contributions come from the lightest generation of fermions, namely from electrons and up/down quarks. Furthermore, the anomalous coupling to photons (as well as to gluons) vanishes in the $m_a \to 0$ limit, showing that the lowest order amplitude originates from the $\Box a F\tilde{F}$ effective operator.

Bounds from Majoron-active neutrino coupling. Given the lightness and the feebly interacting nature of the Majoron, it constitutes an appealing candidate for DM [17, 21, 22, 37, 39, 40, 62–64]. An exhaustive analysis of the production of the Majoron relic abundance is beyond the scope of this work. For the rest of this paragraph, it will be assumed that Majoron is almost stable, represents the only DM component and predominantly decays into light neutrinos. The strongest available constraints, extracted from refs. [65, 66], are shown in figure 5, where we refer for the detailed labelling. Different colours indicate different $\min(|Y_i|)$ values as shown in the upper bar. As pointed out in the literature (see e.g. [65]), from DM-Majoron decays into neutrinos one bounds mainly the SSB scale f_a having only a mild dependence on the Yukawa couplings. Notice that by simply requiring the "naturalness conditions" introduced in section 3.2 (i.e. $\epsilon < 0.01 \times \min(|Y_i|)$ and $|Y_i| \in [10^{-2}, 1]$) and taming the loop contribution, our prediction lies just above the CMB bounds (purple) and on the left of the current neutrino experiments like SK (blue and orange areas), KamLand (red area) and Borexino (green area). Hence, scenarios with "relaxed naturalness conditions" are being already ruled out by present neutrino data. Future neutrino experiments like JUNO (dashed blue line) could, instead, start probing the region of interest for the mmM model.

Bounds on loop-induced Majoron couplings. Even if the Majoron does not constitute the totality of the observed DM, as assumed in the previous paragraph, it can be bound from other astrophysical and cosmological experiments as it would still contribute to the cosmological history of the universe via an irreducible freeze-in component [67]. In figure 6 (*top*) the bounds on the one-loop Majoron-electron couplings of eq. (5.3) are shown, as a function of the Majoron mass m_a and for different values of the SSB scale f_a (*left plot*) and $\min(|Y_i|)$ (*right plot*). Constraints from CMB, CRB and X-Rays (the cyan, green, and yellow regions respectively), derived in ref. [67], are shown. As reference the XENON1T [68] and XENONnT bounds [69] (darker red) are also plotted. All these data produce constraints

JHEP03(2024)094

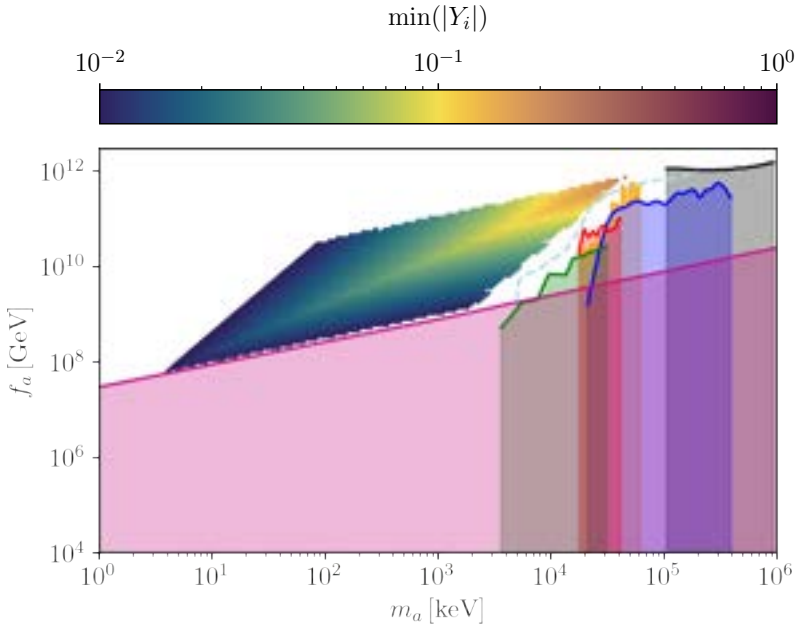

Figure 5. Constraints on Majoron DM. The DM bounds are mainly taken from ref. [65] and include CMB (*purple area*), neutrino experiments, namely Borexino (*green area*), KamLand (*red area*), SK (*blue area*) and projected JUNO (20yr) sensitivity (*dashed blue line*). Bounds from ref. [66], that include reinterpreted SK data (*orange area*) and atmospheric neutrinos data (*gray area*) are also included.

that are still at least two orders of magnitude away from the prediction of the mmM model represented by the two triangular regions in the lower part of the plots.[9]

Of higher interest are the cosmological bounds that can be derived on the Majoron-photon coupling of eq. (5.7), and that are shown in two lower plots in figure 6 as function of the Majoron mass m_a and for different values of the SSB scale f_a (*left plot*) and min(|Y_i|) (*right plot*). The particular shape of the mmM predicted region is due to the functional dependence on the fermion to Majoron mass ratios in the loop function $h(x)$ in eq. (5.8). In these plots, one can observe that, again, the effects of the irreducible Majoron production in CMB, CRB and X-Rays (the red, green and yellow regions respectively), are still far from the regions of interest. Stronger bounds to the Majoron-photon coupling can, instead, be obtained from the observation of galactic and Extragalactic Background Light (EBL) derived in ref. [71], and using XMM-Newton from [72], NuStar [73–75] and INTEGRAL [76]. These experiments are already able to constrain the upper part of the predicted area at the cost, however, of a thermalization temperature of the order of the Planck mass (see the discussion in ref. [71]) and only one coupling at a time.

As can be seen from the plots, $g_{a\gamma\gamma}$ grows with f_a. This can be understood from eq. (5.8), wherein the small x region (below the MeV) $g_{a\gamma\gamma} \propto m_a^2/f_a$ until reaching a "plateau" in the large x-region. From eq. (4.18) m_a is proportional to f_a, once the neutrino mass is given as an input, hence, $g_{a\gamma\gamma} \propto f_a$. This fictitious dependence, which resembles a non-decoupling effect, stems from the neutrino mass constraint and is not valid for arbitrarily large values of f_a: as $m_\nu \sim \epsilon |Y_N||Y_S| v_{\rm EW}^2/f_a$ an increase in f_a must be compensated by an increase in

[9]We acknowledge the use of the axion bounds repository for these plots [70].

JHEP03(2024)094

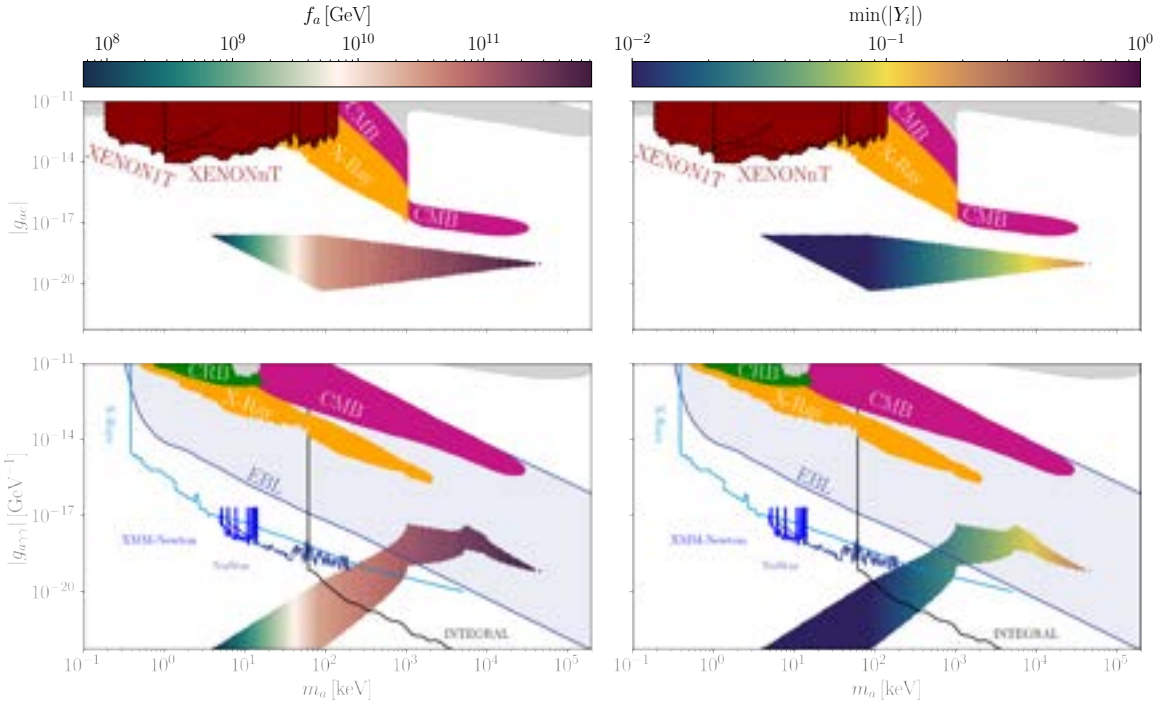

Figure 6. Constraints to Majoron-electron (*top*) and Majoron-photon (*bottom*) couplings. Predictions of the mmM model are plotted for different values of the SSB scale f_a (*left*) and min(Y_i) (*right*). Irreducible constraints from CMB, CRB and X-Rays (the cyan, green and yellow regions respectively), derived from ref. [67], are shown. In the upper plots, the constraints from XENON1T [68] and XENONnT [69] (dark red region) are also plotted, while in the lower plots bounds from galactic and extra-galactic photons emitted from Majoron decay are depicted, assuming the particle is the full amount of DM.

$|Y_{N,S}|$. Once the perturbativity limit $|Y_{N,S}| \leq 1$ is imposed, the artificial growth with f_a cannot continue for arbitrarily large values.

Bounds from LFV. In the mmM model, as can be seen from eq. (5.3), Majoron-charged lepton flavour-violating couplings are generated at 1-loop level, opening the possibility to study $\ell_i \to \ell_j a$ processes, which decay width reads

$$\Gamma(\ell_i \to \ell_j a) = \frac{|\widetilde{K}_{ji}|^2}{2048\pi^5 f_a^2 m_i^3} \sqrt{\lambda(m_i^2, m_a^2, m_j^2)} \left[(m_i^2 - m_j^2)^2 - m_a^2(m_i^2 + m_j^2)\right] , \tag{5.9}$$

where $\lambda(x^2, y^2, z^2)$ is the Källén function.

In the Majoron mass range predicted by the mmM model, i.e. $m_a \lesssim 5 \times 10^4$ keV $< m_\mu$, the strongest bounds come from the $\mu \to ea$ decay, while $\tau \to \mu a$ and $\tau \to ea$ decays would be relevant only for $m_a \gtrsim m_\mu$. In figure 7 the constraints from refs. [77, 78] on the LFV coupling $(\widetilde{K}_H)_{e\mu}$ defined in eqs. (5.4) are shown. We notice that both the present and future sensitivity of LFV experiments are still orders of magnitude far from testing the region of interest for the mmM model.

JHEP03(2024)094

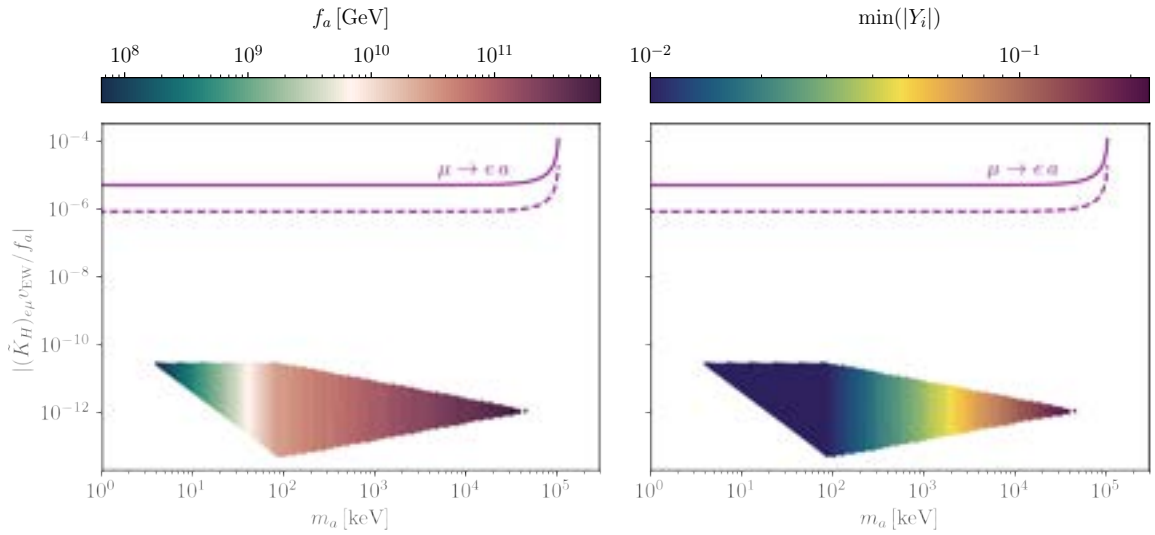

Figure 7. Present (*solid*) and future (*dashed*) 95% C.L. bounds on the flavour violating Majoron-e-μ coupling $K_{e\mu}$. The mmM model preferred region as functions of the different SSB scale f_a (*left*) and min($|Y_i|$) (*right*) are depicted.

6 Conclusions

The Majoron is traditionally considered as the would-be-Goldstone boson of the spontaneous breaking of the Lepton Number. The origin of its mass is an old problem and in this paper, we propose a scenario where it naturally arises without invoking Planck effects or extra ingredients behind those strictly necessary to correctly describe lepton masses and mixing.

The model is a high-scale Seesaw mechanism with two right-handed neutrinos with a mass texture that is very similar to the one associated with the so-called linear Seesaw. The heavy neutral lepton masses arise after the spontaneous symmetry breaking of a global Abelian symmetry, while the active neutrino masses can be correctly described only by introducing an explicit breaking of such symmetry. The Majoron is generated after the spontaneous breaking and acquires mass due to the explicit breaking. Although this may appear to be completely generic, we showed that it is not: not all the possible explicit breakings of the symmetry would lead to a mass for the Majoron.

We identified the unique, minimal model where the Majoron mass and the active neutrino masses are strictly tied together, by requiring three conditions to be satisfied: renormalisability of the model Lagrangian; only one Majorana scale that is associated with the spontaneous breaking of the Abelian symmetry; only one explicit breaking of this symmetry. The latter thus plays the role of both Lepton Number and PQ symmetry.

As a consequence of these conditions, only one scalar field ϕ transforming under the Abelian symmetry is introduced in the spectrum and, to guarantee a mass for the Majoron, both ϕ and ϕ^* enter the Lagrangian. In particular, this scalar field appears in the Majorana terms of the Lagrangian that represent the mass terms for the heavy neutral leptons, once it develops a vacuum expectation value. If these Majorana terms constitute the spontaneous symmetry-breaking sector, one of the Dirac terms explicitly violates the symmetry. The

JHEP03(2024)094

resulting neutral lepton mass matrix, after both LN/PQ and electroweak symmetry breaking, has already been studied in the pure neutrino context and undergoes the name of Extended Seesaw limit: it predicts potentially large one-loop contributions to the active neutrino masses that are kept under control only focusing in a parameter space where the two heavy neutral leptons have almost degenerate masses.

All in all, active neutrino masses and the lepton mixing can be correctly described with heavy neutral leptons with masses in the range $[10^7,\, 10^{12}]\,\text{GeV}$, when the Dirac and Majorana Yukawa couplings span the range $[10^{-2},\, 1]$, for both the normal and inverse ordering of the active neutrino mass spectrum.

The Majoron mass arises at one-loop and proportional to the active neutrino masses. We performed the explicit computation and confirmed the result through the CW potential, in the $\overline{\text{MS}}$-scheme. We found that the derivative or chirally preserving basis for the Majoron couplings greatly simplifies the computations. In our model, the Majoron mass turns out to scale logarithmically with the spontaneous symmetry breaking scale f_a. This is in contrast with the traditional QCD axion models where the mass is inversely proportional to f_a. Once inserting neutrino data as inputs and requiring natural values for the Yukawa couplings $\in [10^{-2},\, 1]$, we obtain a Majoron mass in the range $[1,\, 10^5]\,\text{keV}$ corresponding to $f_a \in [10^8,\, 10^{12}]\,\text{GeV}$.

This light and feebly interacting Majoron represents an appealing candidate for Dark Matter. We performed phenomenological analyses investigating the impact of its couplings with active neutrinos, charged leptons and photons, the last two being loop-induced. Majoron-neutrino interactions have an impact in the CMB and in oscillation neutrino experiments: the proper parameter space of the model lays just next to the excluded region by these experiments and therefore it would be directly probed once the experimental uncertainties decrease. Majoron couplings with electrons and photons are tested by CMB, CRB and X-Rays, but their sensitivities do not reach the proper parameter space of our model. The same holds for XENON1T and XENONnT (expected) bounds. For the specific case of the couplings with photons, the model could be probed from the observation of galactic and extra-galactic photon spectrum. Interestingly, the Majoron-photon coupling grows linearly with f_a in the examined parameter space, and therefore the first region that could be tested corresponds to the highest values of f_a and largest Majoron masses. Finally, our Majoron describes lepton flavour-violating processes, $\mu \to ea$, $\tau \to \mu a$ and $\tau \to ea$, but far from testing the proper parameter space of the model.

To summarise, the minimal massive Majoron Seesaw model represents the first example where the Majoron mass naturally arises from the same context where active neutrino masses and the lepton mixing are correctly described, without the necessity of introducing *ad hoc* new parameters or invoking high-scale-suppressed operators e.g. Planck-induced contributions. Its minimality conditions imply the uniqueness of the model and link the Majoron mass to the active neutrino masses providing a phenomenological viable scenario that could be probed by CMB, EBL, and oscillation neutrino experiments in the near future.

Acknowledgments

The authors thank Ilaria Brivio, Luca Di Luzio, Belén Gavela, Manuel González López, Álvaro Lozano Onrubia, Jorge Dasilva Golan, Jonathan Machado Rodríguez, Daniel Naredo Tuero and Giuseppe Lucente for useful discussions. AdG thanks Carlos A. Argüelles and the

group of Palfrey House for their hospitality and the stimulating working environment during which a core part of this work was realised. AdG also thanks J. Jaeckel and the Institute for Theoretical Physics of the University Heidelberg for relevant remarks to this work and the warm hospitality. The authors acknowledge partial financial support by the European Union's Horizon 2020 research and innovation programme under the Marie Skłodowska-Curie grant agreements No 860881-HIDDeN and 101086085-ASYMMETRY.AdG, LM and SR acknowledge partial financial support by the Spanish Research Agency (Agencia Estatal de Investigación) through the grant IFT Centro de Excelencia Severo Ochoa No CEX2020-001007-S and by the grants PID2019-108892RB-I00 and PID2022-137127NB-I00 funded by MCIN/AEI/ 10.13039/501100011033. The work of AdG and XPD was supported by the European Union's Horizon 2020 Marie Skłodowska-Curie grant agreement No 860881-HIDDeN. This article/publication is based upon work from COST Action COSMIC WISPers CA21106, supported by COST (European Cooperation in Science and Technology). This work was also partially supported by the Italian MUR Departments of Excellence grant 2023-2027 "Quantum Frontiers".

A ALP PQ-breaking interactions

In this appendix, we give some details regarding the Majoron PQ-breaking interactions in the lepton mass basis. This is necessary to calculate the Majoron mass in section 4. After rotating away the PQ-preserving terms, the only term relevant for the Majoron mass is

$$-\mathscr{L}_a \supset \epsilon\, \overline{L_L}\, \widetilde{H}\, Y_S\, S_R\, e^{2ia/f_a} + \text{h.c.}\,. \tag{A.1}$$

The block diagonalisation of the neutral mass matrix $\mathcal{M}_\chi$ can be performed through a unitary redefinition of the field vector χ_L [79]. As we are interested in interactions of $\mathcal{O}(\hat{\Lambda}^{-1})$, we expand the unitary matrix at second order in the mixing matrix Θ

$$\chi_L \to U_\chi\, \chi_L \qquad \text{with} \qquad U_\chi \simeq \begin{pmatrix} \mathbb{1} - \frac{1}{2}\Theta\Theta^\dagger & \Theta \\ -\Theta^\dagger & \mathbb{1} - \frac{1}{2}\Theta^\dagger\Theta \end{pmatrix}, \tag{A.2}$$

which requires at this order

$$\Theta \simeq \hat{m}\, \hat{\Lambda}^{-1} = \begin{pmatrix} m_N & \epsilon\, m_S \end{pmatrix} \begin{pmatrix} \Lambda_{NN} & \Lambda_{NS} \\ \Lambda_{NS} & 0 \end{pmatrix}^{-1} = \frac{1}{\Lambda_{NS}} \begin{pmatrix} \epsilon\, m_S & m_N - \epsilon\, m_S \dfrac{\Lambda_{NN}}{\Lambda_{NS}} \end{pmatrix}. \tag{A.3}$$

After this first diagonalisation, the fields get rotated, at LO in Θ, as

$$\begin{cases} \nu_L & \to & \nu_L + \Theta \begin{pmatrix} N_R^c \\ S_R^c \end{pmatrix} = \nu_L + \dfrac{\epsilon\, m_S}{\Lambda_{NS}} N_R^c + \dfrac{1}{\Lambda_{NS}} \left(m_N - \epsilon\, m_S \dfrac{\Lambda_{NN}}{\Lambda_{NS}} \right) S_R^c\,, \\ \begin{pmatrix} N_R^c \\ S_R^c \end{pmatrix} & \to & \begin{pmatrix} N_R^c \\ S_R^c \end{pmatrix} - \Theta^\dagger\, \nu_L = \begin{pmatrix} N_R^c \\ S_R^c \end{pmatrix} - \dfrac{1}{\Lambda_{NS}} \begin{pmatrix} \epsilon\, m_S^\dagger \\ m_N^\dagger - \epsilon\, m_S^\dagger \dfrac{\Lambda_{NN}}{\Lambda_{NS}} \end{pmatrix} \nu_L\,. \end{cases} \tag{A.4}$$

On the other side, the HNLs are not yet written in terms of mass eigenstates: we still need to diagonalise the 23 sector of the resulting mass matrix after the block diagonalisation. To

JHEP03(2024)094

do so, we perform a second field redefinition that only affects the neutral exotic states:

$$\begin{pmatrix} N_R & S_R \end{pmatrix}^T \to U_N \begin{pmatrix} N_R & S_R \end{pmatrix}^T \qquad \text{with} \qquad U_N = \frac{1}{\sqrt{M_N + M_S}} \begin{pmatrix} i\sqrt{M_N} & \sqrt{M_S} \\ -i\sqrt{M_S} & \sqrt{M_N} \end{pmatrix}, \tag{A.5}$$

obtaining the HNLs masses in eq. (2.14). The parameters $\Lambda_{NS,NN}$ can be written in terms of the HNL masses via

$$\Lambda_{NS} = \sqrt{M_N M_S}\,, \qquad\qquad \Lambda_{NN} = M_S - M_N\,. \tag{A.6}$$

Combining these field redefinitions we obtain the explicitly breaking term in the lepton mass basis:

$$\begin{aligned} -\mathscr{L}_a \supset \left(e^{2ia/f_a} - 1\right) \Bigg\{ & -\frac{1}{\sqrt{M_N M_S}} \overline{\nu_L} U^\dagger_{\text{PMNS}} \left(\epsilon m_S m_N^T - \left(\frac{\alpha^2 - 1}{\alpha}\right) \epsilon^2 m_S m_S^T \right) U^*_{\text{PMNS}} \nu_L^c \\ & - \frac{i}{\sqrt{(M_N + M_S)}} \left(\sqrt{M_S}\overline{\nu_L} U^\dagger_{\text{PMNS}} \epsilon m_S N_R - \sqrt{M_N}\overline{\nu_L} U^\dagger_{\text{PMNS}} \epsilon m_S S_R \right) \\ & + (\overline{N_R^c} N_R) \frac{1}{(M_N + M_S)} \left[\epsilon^2 m_S^\dagger m_S - \alpha \left(\epsilon m_N^\dagger m_S - \left(\frac{\alpha^2 - 1}{\alpha}\right) \epsilon^2 m_S^\dagger m_S \right) \right] \\ & + (\overline{S_R^c} S_R) \frac{1}{(M_N + M_S)} \left[\epsilon^2 m_S^\dagger m_S + \frac{1}{\alpha} \left(\epsilon m_N^\dagger m_S - \left(\frac{\alpha^2 - 1}{\alpha}\right) \epsilon^2 m_S^\dagger m_S \right) \right] \\ & + (\overline{N_R^c} S_R) \frac{i}{(M_N + M_S)} \left[\frac{1}{\alpha} \epsilon^2 m_S^\dagger m_S - \left(\epsilon m_N^\dagger m_S - \left(\frac{\alpha^2 - 1}{\alpha}\right) \epsilon^2 m_S^\dagger m_S \right) \right] \\ & - (\overline{S_R^c} N_R) \frac{i}{(M_N + M_S)} \left[\alpha \epsilon^2 m_S^\dagger m_S + \left(\epsilon m_N^\dagger m_S - \left(\frac{\alpha^2 - 1}{\alpha}\right) \epsilon^2 m_S^\dagger m_S \right) \right] \Bigg\} \\ & + \text{h.c.}\,, \end{aligned} \tag{A.7}$$

where we defined $\alpha \equiv \sqrt{M_S/M_N}$. The derivative couplings can be obtained similarly by employing the field redefinitions of eq. (A.4) in the Lagrangian of eq. (4.13) and are not going to be explicitly reported here.

Not all the interactions presented above are relevant to the LO prediction of the Majoron mass. First of all, as we are in the chirality preserving basis, only the Balloon diagram can provide relevant contributions at LO. This prompts us to neglect any term with powers of ϵ^2 and consider only diagonal couplings, leaving us with

$$-\mathscr{L}_a \supset \left[\frac{1}{2} \overline{\nu_L} m_\nu \nu_L^c + \frac{2\epsilon m_N^\dagger m_S}{\sqrt{M_N M_S}(M_N + M_S)} \left(M_N \overline{S_R^c} S_R - M_S \overline{N_R^c} N_R \right) \right] e^{2ia/f_a} + \text{h.c.}\,. \tag{A.8}$$

Moreover, as concluded in eq. (4.5) for the toy model, such contributions are proportional to the fermion running in the loop and therefore we can focus on the HNL couplings in eq. (A.8). The mixed $\overline{S_R^c} N_R$ term only contributes to the sub-leading Bubble diagram, while the active neutrino term contribution to the dominant Balloon diagram is proportional to the light neutrino masses, being therefore completely negligible. We can thus restrict our

JHEP03(2024)094

considerations to the following terms of the Lagrangian

$$-\mathscr{L}_a \supset \frac{2\epsilon\, m_N^\dagger m_S}{\sqrt{M_N\, M_S}(M_N+M_S)}\left(M_N\overline{S_R^c}S_R - M_S\overline{N_R^c}N_R\right)\frac{a^2}{f_a^2} + \text{h.c.}\,. \tag{A.9}$$

B Majoron and HNLs interactions

The interaction matrix with the Majoron can be compactly written down in block matrix form. After the block diagonalization has been carried out, to move to the mass basis, one must include the unitary matrix

$$U \equiv \begin{pmatrix} U_{\text{PMNS}} & 0 \\ 0 & U_N \end{pmatrix}, \tag{B.1}$$

where U_{PMNS} is the light neutrinos PMNS matrix and U_N is defined in eq. (A.5). The interactions in the mass basis reads

$$\mathscr{L}_a \simeq -\frac{1}{2}\overline{\chi_L}U^\dagger \mathcal{M}_a U^* \chi_L^c\,, \tag{B.2}$$

where

$$\mathcal{M}_a = \begin{pmatrix} (\mathcal{M}_a)_{11} & (\mathcal{M}_a)_{12} \\ (\mathcal{M}_a)_{21} & (\mathcal{M}_a)_{22} \end{pmatrix} \tag{B.3}$$

and its components are given by

$$(\mathcal{M}_a)_{11} \simeq -m_\nu^{\text{TL}} e^{i\sigma a/f_a} + \epsilon^2 m_S m_S^T \frac{\Lambda_{NN}}{\Lambda_{NS}}\left(e^{ia/f_a} - e^{i\sigma a/f_a}\right), \tag{B.4}$$

$$(\mathcal{M}_a)_{12} = [(\mathcal{M}_a)_{21}]^T \simeq \left(-e^{i\sigma a/f_a} m_N + \left(e^{ia/f_a} - e^{i\sigma a/f_a}\right)\epsilon m_S \frac{\Lambda_{NN}}{\Lambda_{NS}}\;\; \epsilon m_S e^{i\sigma a/f_a}\right), \tag{B.5}$$

$$(\mathcal{M}_a)_{22} \simeq \begin{pmatrix} \Lambda_{NN} e^{ia/f_a} & \Lambda_{NS} e^{i\sigma a/f_a} \\ \Lambda_{NS} e^{i\sigma a/f_a} & 0 \end{pmatrix}, \tag{B.6}$$

where we have introduced a parameter σ that helps us interpolate between the typical Majoron of the literature, $\sigma = +1$ all mass terms couple to ϕ, and other non-standard scenarios such as the mmM, where $\sigma = -1$, Λ_{NS} couples to ϕ^* while Λ_{NN} to ϕ. Expanding the exponential at LO, we thus have

$$(\mathcal{M}_a)_{11} \simeq \frac{ia}{f_a}\left[-\sigma m^{\text{TL}} + \epsilon^2 m_S m_S^T \frac{\Lambda_{NN}}{\Lambda_{NS}}(1-\sigma)\right], \tag{B.7}$$

$$(\mathcal{M}_a)_{12} = [(\mathcal{M}_a)_{21}]^T \simeq \frac{ia}{f_a}\left(-\sigma m_N + (1-\sigma)\,\epsilon m_S \frac{\Lambda_{NN}}{\Lambda_{NS}}\;\; \sigma\epsilon m_S\right), \tag{B.8}$$

$$(\mathcal{M}_a)_{22} \simeq \frac{ia}{f_a}\begin{pmatrix} \Lambda_{NN} & \sigma\Lambda_{NS} \\ \sigma\Lambda_{NS} & 0 \end{pmatrix}. \tag{B.9}$$

The interactions with gauge bosons can be derived similarly and in the mass basis they read

$$\mathscr{L}_Z \supset -\frac{g}{2\cos\theta_W}\overline{\chi_L}\not{Z}\, U^\dagger \begin{pmatrix} 1-\Theta\Theta^\dagger & \Theta \\ \Theta^\dagger & \Theta^\dagger\Theta \end{pmatrix} U\,\chi_L\,, \tag{B.10}$$

$$\mathscr{L}_{W^\pm} \supset -\frac{g}{\sqrt{2}}\overline{\chi_L} W^+ U^\dagger \begin{pmatrix} 1-\frac{1}{2}\Theta\Theta^\dagger & 0 \\ \Theta^\dagger & 0 \end{pmatrix} \ell_L \,, \tag{B.11}$$

$$\mathscr{L}_h \supset -\left(\frac{h}{v}\right) \overline{\chi_L} U^\dagger \begin{pmatrix} \hat{m}_\nu & \frac{1}{2}\hat{m} \\ \frac{1}{2}\hat{m}^T & \frac{1}{2}\left(\Theta^\dagger \hat{m} + \hat{m}^T \Theta^*\right) \end{pmatrix} U^* \chi_L^c \,, \tag{B.12}$$

where recall that

$$\Theta \simeq \hat{m}\,\hat{\Lambda}^{-1} = \frac{1}{\Lambda_{NS}} \left(\epsilon\, m_S \;\; m_N - \epsilon\, m_S \frac{\Lambda_{NN}}{\Lambda_{NS}}\right) , \tag{B.13}$$

and thus

$$\Theta\Theta^\dagger \simeq \frac{1}{\Lambda_{NS}^2}\left[\epsilon^2 m_S m_S^\dagger + \left(m_N - \epsilon m_S \frac{\Lambda_{NN}}{\Lambda_{NS}}\right)\left(m_N^\dagger - \epsilon m_S^\dagger \frac{\Lambda_{NN}}{\Lambda_{NS}}\right)\right] , \tag{B.14}$$

$$\Theta^\dagger\Theta \simeq \frac{1}{\Lambda_{NS}^2} \begin{pmatrix} \epsilon^2 m_S^\dagger m_S & \epsilon m_S^\dagger \left(m_N - \epsilon m_S \frac{\Lambda_{NN}}{\Lambda_{NS}}\right) \\ \left(m_N^\dagger - \epsilon m_S^\dagger \frac{\Lambda_{NN}}{\Lambda_{NS}}\right) \epsilon m_S & \left(m_N^\dagger - \epsilon m_S^\dagger \frac{\Lambda_{NN}}{\Lambda_{NS}}\right)\left(m_N - \epsilon m_S \frac{\Lambda_{NN}}{\Lambda_{NS}}\right) \end{pmatrix} . \tag{B.15}$$

C One-loop effective potential and Majoron mass

In this appendix we provide an alternative derivation of the Majoron mass, computing the full one-loop contribution to the scalar potential through the Coleman-Weinberg (CW) potential [41]. Accounting already for the trace over the Dirac indices, the fermionic contribution, in the $\overline{\text{MS}}$ scheme, reads

$$V_{\text{CW}} = -\frac{1}{2} \times \frac{1}{16\pi^2} \mathtt{Tr}\left[\left(\mathcal{M}_\chi \mathcal{M}_\chi^\dagger\right)^2 \left(\log\left(\frac{\mathcal{M}_\chi \mathcal{M}_\chi^\dagger}{\mu_R^2}\right) - \frac{3}{2}\right)\right] \tag{C.1}$$

where $\mathcal{M}_\chi \equiv \mathcal{M}_\chi(H,\phi)$ is the neutral mass matrix in eq. (2.12) including the dependence of the scalar fields H and ϕ. In the following a compact notation for the neutral mass matrix M_χ is going to be adopted:

$$\mathcal{M}_\chi(H,\phi) = \begin{pmatrix} 0 & \widehat{m}(H) \\ \widehat{m}(H)^T & \widehat{\Lambda}(\phi) \end{pmatrix} , \tag{C.2}$$

where $\widehat{m}$ and $\widehat{\Lambda}$ are the field-dependent Dirac and Majorana blocks inheriting the structure of the mass matrix in eq. (2.12). The overall factor 1/2 in front of the expression is due to the Majorana nature of the fermionic fields involved, which have half of the degrees of freedom of Dirac fermions.

We turn now to the explicit computation of the relevant traces. We consider only the terms containing the Majoron contribution. We find

$$\begin{aligned} \mathtt{Tr}\left[(\mathcal{M}_\chi \mathcal{M}_\chi^\dagger)^2\right] &= 2\mathtt{Re}\Big(\mathtt{Tr}\left[(\widehat{m}^\dagger \widehat{m})^2\right]\Big) + \mathtt{Tr}\left[(\widehat{\Lambda}^\dagger \widehat{\Lambda})^2\right] + 2\left(\mathtt{Tr}\left[\widehat{m}^\dagger \widehat{m} \widehat{\Lambda}^\dagger \widehat{\Lambda}\right] + \mathtt{Tr}\left[\widehat{m}^T \widehat{m}^* \widehat{\Lambda}\widehat{\Lambda}^\dagger\right]\right) \\ &\supset 2\,\epsilon\, Y_{NS}\, Y_{NN}\, v_{\text{EW}}^2 \left(Y_N^\dagger Y_S \phi^2 + Y_S^\dagger Y_N \phi^{*2}\right) \\ &\supset 2\,\epsilon\, Y_{NS}\, Y_{NN}\, |Y_N|\, |Y_S|\, |\eta|\, v_{\text{EW}}^2 f_a^2 \cos\left(\vartheta_\eta + \frac{2a}{f_a}\right) , \end{aligned} \tag{C.3}$$

JHEP03(2024)094

where in the last step we made use of the definitions in eq. (2.21). This confirms that the Majoron mass can only obtain a contribution when the four Y_i couplings are present and non-vanishing, and the leading contribution turns out to be linear in the LN breaking parameter ϵ. The computation of the log is far more problematic as one needs the eigenvalues of the full 5×5 matrix, $\mathcal{M}_\chi \mathcal{M}_\chi^\dagger$. However, recalling from the explicit computation that the one-loop diagrams contributing to the Majoron mass are proportional to internal lepton masses, we can safely neglect in the calculation the light active neutrino masses. Denoting with $\{\mu_i\}_{i=1}^5$ the eigenvalues of $\mathcal{M}_\chi \mathcal{M}_\chi^\dagger$, this allows to write

$$\mathtt{Tr}\mathcal{M}_\chi \mathcal{M}_\chi^\dagger \approx \mu_1 + \mu_2\,, \qquad\qquad \mathtt{Tr}(\mathcal{M}_\chi \mathcal{M}_\chi^\dagger)^2 \approx \mu_1^2 + \mu_2^2\,, \tag{C.4}$$

where $\mu_{1,2}$ represent the two large HNL masses. By solving the system in eq. (C.4) the CW potential for the Majoron field, in the $\overline{\text{MS}}$ scheme reads:

$$\begin{aligned} V_{\text{CW}} = &-\epsilon \frac{Y_{NS}\, Y_{NN}\, |Y_N|\, |Y_S|\, |\eta|\, v_{\text{EW}}^2\, f_a^2}{16\pi^2} \cos\left(\vartheta_\eta + \frac{2a}{f_a}\right) \times \\ &\times \left[\frac{(Y_{NN}^2 + 2Y_{NS}^2)}{Y_{NN}\sqrt{Y_{NN}^2 + 4Y_{NS}^2}} \text{Arcoth}\left(\frac{(Y_{NN}^2 + 2Y_{NS}^2)}{Y_{NN}\sqrt{Y_{NN}^2 + 4Y_{NS}^2}}\right) + \left(\log\left(\frac{Y_{NS}^2 f_a^2}{2\mu_R^2}\right) - 1\right)\right]. \end{aligned} \tag{C.5}$$

To obtain the final expression one has to use of the well-known algebraic identity:

$$\text{Arcoth}(x) = \frac{1}{2}\log\frac{x+1}{x-1}\,. \tag{C.6}$$

A few comments are in order. First of all, expanding the cosine, we would get a linear term for the Majoron, corresponding to a tadpole. To avoid it, we can perform a shift in the Majoron field

$$\frac{2a}{f_a} \to \frac{2a}{f_a} - \vartheta_\eta\,, \tag{C.7}$$

with a consequent appearance of $e^{\pm i\vartheta_\eta/2}$ term in eq. (4.11). As already mentioned, the couplings Y_{NS} and Y_{NN} can be made real by a proper redefinition of the leptons fields and, as a result, the ϑ_η phase would eventually end up in the Dirac Yukawa couplings. This is more evident in the chirality conserving basis in eq. (4.13), where the only term that would be affected by the Majoron shift is the LN explicit breaking term: the ϑ_η phase can be absorbed in the definition of Y_S,

$$Y_S\, e^{-i\vartheta_\eta} \to Y_S\,. \tag{C.8}$$

The net effect of this redefinition propagates to eq. (2.21), where the parameter η turns out to be a real number. This resembles what occurs with the QCD axion, a_{QCD}. As discussed by Vafa and Witten [80], the QCD vacuum energy has its minimum when $a_{\text{QCD}} \to a_{\text{QCD}} - \overline{\theta}$, where $\overline{\theta}$ includes a phase from the quark mass matrices. The latter, which is physical only in the presence of the axion, gets fixed by a minimum condition that also prevents the appearance of the axion tadpole. As the HNL sector is not coupled to SM gauge bosons, this shift does not induce any anomalous SM gauge boson coupling.

JHEP03(2024)094

By taking the second derivative on the CW potential, one automatically obtains the one-loop contribution to the Majoron mass:

$$m_a^2 = \epsilon \frac{Y_{NS}\, Y_{NN}\, |Y_N|\, |Y_S|\, |\eta|\, v_{\rm EW}^2}{4\pi^2} \times \\ \times \left[\frac{(Y_{NN}^2 + 2Y_{NS}^2)}{Y_{NN}\sqrt{Y_{NN}^2 + 4Y_{NS}^2}} \text{Arcoth}\left(\frac{(Y_{NN}^2 + 2Y_{NS}^2)}{Y_{NN}\sqrt{Y_{NN}^2 + 4Y_{NS}^2}} \right) + \left(\log\left(\frac{Y_{NS}^2 f_a^2}{2\mu_R^2} \right) - 1 \right) \right]. \tag{C.9}$$

References

[1] P. Minkowski, $\mu \to e\gamma$ *at a Rate of One Out of* 10^9 *Muon Decays?*, *Phys. Lett. B* **67** (1977) 421 [INSPIRE].

[2] M. Gell-Mann, P. Ramond and R. Slansky, *Complex Spinors and Unified Theories*, *Conf. Proc. C* **790927** (1979) 315 [arXiv:1306.4669] [INSPIRE].

[3] T. Yanagida, *Horizontal gauge symmetry and masses of neutrinos*, *Conf. Proc. C* **7902131** (1979) 95 [INSPIRE].

[4] R.N. Mohapatra and G. Senjanovic, *Neutrino Mass and Spontaneous Parity Nonconservation*, *Phys. Rev. Lett.* **44** (1980) 912 [INSPIRE].

[5] Y. Chikashige, R.N. Mohapatra and R.D. Peccei, *Spontaneously Broken Lepton Number and Cosmological Constraints on the Neutrino Mass Spectrum*, *Phys. Rev. Lett.* **45** (1980) 1926 [INSPIRE].

[6] Y. Chikashige, R.N. Mohapatra and R.D. Peccei, *Are There Real Goldstone Bosons Associated with Broken Lepton Number?*, *Phys. Lett. B* **98** (1981) 265 [INSPIRE].

[7] G.B. Gelmini and M. Roncadelli, *Left-Handed Neutrino Mass Scale and Spontaneously Broken Lepton Number*, *Phys. Lett. B* **99** (1981) 411 [INSPIRE].

[8] R.D. Peccei and H.R. Quinn, *CP Conservation in the Presence of Instantons*, *Phys. Rev. Lett.* **38** (1977) 1440 [INSPIRE].

[9] S. Weinberg, *A New Light Boson?*, *Phys. Rev. Lett.* **40** (1978) 223 [INSPIRE].

[10] F. Wilczek, *Problem of Strong P and T Invariance in the Presence of Instantons*, *Phys. Rev. Lett.* **40** (1978) 279 [INSPIRE].

[11] A.R. Zhitnitsky, *On Possible Suppression of the Axion Hadron Interactions* (in Russian), *Sov. J. Nucl. Phys.* **31** (1980) 260 [INSPIRE].

[12] M. Dine, W. Fischler and M. Srednicki, *A Simple Solution to the Strong CP Problem with a Harmless Axion*, *Phys. Lett. B* **104** (1981) 199 [INSPIRE].

[13] J.E. Kim, *Weak Interaction Singlet and Strong CP Invariance*, *Phys. Rev. Lett.* **43** (1979) 103 [INSPIRE].

[14] M.A. Shifman, A.I. Vainshtein and V.I. Zakharov, *Can Confinement Ensure Natural CP Invariance of Strong Interactions?*, *Nucl. Phys. B* **166** (1980) 493 [INSPIRE].

JHEP03(2024)094

[15] K. Choi and A. Santamaria, *17-KeV neutrino in a singlet-triplet majoron model*, *Phys. Lett. B* **267** (1991) 504 [INSPIRE].

[16] W. Chao, M. Jin, H.-J. Li and Y.-Q. Peng, *Axion-like Dark Matter from the Type-II Seesaw Mechanism*, arXiv:2210.13233 [INSPIRE].

[17] C. Biggio, L. Calibbi, T. Ota and S. Zanchini, *Majoron dark matter from a type II seesaw model*, *Phys. Rev. D* **108** (2023) 115003 [arXiv:2304.12527] [INSPIRE].

[18] C. Bonilla et al., *Dark matter from a radiative inverse seesaw majoron model*, *Phys. Lett. B* **847** (2023) 138282 [arXiv:2306.08453] [INSPIRE].

[19] K. Kannike, A. Kubarski, L. Marzola and A. Racioppi, *Pseudo-Goldstone dark matter in a radiative inverse seesaw scenario*, *JHEP* **12** (2023) 166 [arXiv:2306.07865] [INSPIRE].

[20] G. Gelmini, D.N. Schramm and J.W.F. Valle, *Majorons: A Simultaneous Solution to the Large and Small Scale Dark Matter Problems*, *Phys. Lett. B* **146** (1984) 311 [INSPIRE].

[21] V. Berezinsky and J.W.F. Valle, *The KeV majoron as a dark matter particle*, *Phys. Lett. B* **318** (1993) 360 [hep-ph/9309214] [INSPIRE].

[22] M. Lattanzi and J.W.F. Valle, *Decaying warm dark matter and neutrino masses*, *Phys. Rev. Lett.* **99** (2007) 121301 [arXiv:0705.2406] [INSPIRE].

[23] F. Bazzocchi, M. Lattanzi, S. Riemer-Sørensen and J.W.F. Valle, *X-ray photons from late-decaying majoron dark matter*, *JCAP* **08** (2008) 013 [arXiv:0805.2372] [INSPIRE].

[24] M. Lattanzi, S. Riemer-Sørensen, M. Tortola and J.W.F. Valle, *Updated CMB and x- and γ-ray constraints on Majoron dark matter*, *Phys. Rev. D* **88** (2013) 063528 [arXiv:1303.4685] [INSPIRE].

[25] F.S. Queiroz and K. Sinha, *The Poker Face of the Majoron Dark Matter Model: LUX to keV Line*, *Phys. Lett. B* **735** (2014) 69 [arXiv:1404.1400] [INSPIRE].

[26] R.Z. Ferreira and A. Notari, *Observable Windows for the QCD Axion Through the Number of Relativistic Species*, *Phys. Rev. Lett.* **120** (2018) 191301 [arXiv:1801.06090] [INSPIRE].

[27] F. Arias-Aragón et al., *Cosmic Imprints of XENON1T Axions*, *JCAP* **11** (2020) 025 [arXiv:2007.06579] [INSPIRE].

[28] F. Arias-Aragón et al., *Production of Thermal Axions across the ElectroWeak Phase Transition*, *JCAP* **03** (2021) 090 [arXiv:2012.04736] [INSPIRE].

[29] R.Z. Ferreira, A. Notari and F. Rompineve, *Dine-Fischler-Srednicki-Zhitnitsky axion in the CMB*, *Phys. Rev. D* **103** (2021) 063524 [arXiv:2012.06566] [INSPIRE].

[30] E.J. Chun and T.H. Jung, *Leptogenesis driven by majoron*, arXiv:2311.09005 [INSPIRE].

[31] W. Chao and Y.-Q. Peng, *Majorana Majoron and the Baryon Asymmetry of the Universe*, arXiv:2311.06469 [INSPIRE].

[32] M. Escudero and S.J. Witte, *A CMB search for the neutrino mass mechanism and its relation to the Hubble tension*, *Eur. Phys. J. C* **80** (2020) 294 [arXiv:1909.04044] [INSPIRE].

[33] F. Arias-Aragón, E. Fernandez-Martinez, M. González-López and L. Merlo, *Neutrino Masses and Hubble Tension via a Majoron in MFV*, *Eur. Phys. J. C* **81** (2021) 28 [arXiv:2009.01848] [INSPIRE].

[34] M. Escudero and S.J. Witte, *The hubble tension as a hint of leptogenesis and neutrino mass generation*, *Eur. Phys. J. C* **81** (2021) 515 [arXiv:2103.03249] [INSPIRE].

JHEP03(2024)094

[35] T. Araki et al., *Resolving the Hubble tension in a* $U(1)_{L_\mu - L_\tau}$ *model with the Majoron*, *PTEP* **2021** (2021) 103B05 [arXiv:2103.07167] [INSPIRE].

[36] E.K. Akhmedov, Z.G. Berezhiani, R.N. Mohapatra and G. Senjanovic, *Planck scale effects on the majoron*, *Phys. Lett. B* **299** (1993) 90 [hep-ph/9209285] [INSPIRE].

[37] I.Z. Rothstein, K.S. Babu and D. Seckel, *Planck scale symmetry breaking and majoron physics*, *Nucl. Phys. B* **403** (1993) 725 [hep-ph/9301213] [INSPIRE].

[38] R.N. Mohapatra and G. Senjanovic, *The Superlight Axion and Neutrino Masses*, *Z. Phys. C* **17** (1983) 53 [INSPIRE].

[39] P.-H. Gu, E. Ma and U. Sarkar, *Pseudo-Majoron as Dark Matter*, *Phys. Lett. B* **690** (2010) 145 [arXiv:1004.1919] [INSPIRE].

[40] M. Frigerio, T. Hambye and E. Masso, *Sub-GeV dark matter as pseudo-Goldstone from the seesaw scale*, *Phys. Rev. X* **1** (2011) 021026 [arXiv:1107.4564] [INSPIRE].

[41] S.R. Coleman and E.J. Weinberg, *Radiative Corrections as the Origin of Spontaneous Symmetry Breaking*, *Phys. Rev. D* **7** (1973) 1888 [INSPIRE].

[42] G.C. Branco, W. Grimus and L. Lavoura, *The Seesaw Mechanism in the Presence of a Conserved Lepton Number*, *Nucl. Phys. B* **312** (1989) 492 [INSPIRE].

[43] J. Kersten and A.Y. Smirnov, *Right-Handed Neutrinos at CERN LHC and the Mechanism of Neutrino Mass Generation*, *Phys. Rev. D* **76** (2007) 073005 [arXiv:0705.3221] [INSPIRE].

[44] A. Abada et al., *Low energy effects of neutrino masses*, *JHEP* **12** (2007) 061 [arXiv:0707.4058] [INSPIRE].

[45] K. Moffat, S. Pascoli and C. Weiland, *Equivalence between massless neutrinos and lepton number conservation in fermionic singlet extensions of the Standard Model*, arXiv:1712.07611 [INSPIRE].

[46] E.K. Akhmedov, M. Lindner, E. Schnapka and J.W.F. Valle, *Left-right symmetry breaking in NJL approach*, *Phys. Lett. B* **368** (1996) 270 [hep-ph/9507275] [INSPIRE].

[47] M. Malinsky, J.C. Romao and J.W.F. Valle, *Novel supersymmetric* SO(10) *seesaw mechanism*, *Phys. Rev. Lett.* **95** (2005) 161801 [hep-ph/0506296] [INSPIRE].

[48] R.N. Mohapatra, *Mechanism for Understanding Small Neutrino Mass in Superstring Theories*, *Phys. Rev. Lett.* **56** (1986) 561 [INSPIRE].

[49] R.N. Mohapatra and J.W.F. Valle, *Neutrino Mass and Baryon Number Nonconservation in Superstring Models*, *Phys. Rev. D* **34** (1986) 1642 [INSPIRE].

[50] M.B. Gavela, T. Hambye, D. Hernandez and P. Hernandez, *Minimal Flavour Seesaw Models*, *JHEP* **09** (2009) 038 [arXiv:0906.1461] [INSPIRE].

[51] A. Pilaftsis, *Radiatively induced neutrino masses and large Higgs neutrino couplings in the standard model with Majorana fields*, *Z. Phys. C* **55** (1992) 275 [hep-ph/9901206] [INSPIRE].

[52] J. Lopez-Pavon, S. Pascoli and C.-F. Wong, *Can heavy neutrinos dominate neutrinoless double beta decay?*, *Phys. Rev. D* **87** (2013) 093007 [arXiv:1209.5342] [INSPIRE].

[53] W. Grimus and L. Lavoura, *One-loop corrections to the seesaw mechanism in the multi-Higgs-doublet standard model*, *Phys. Lett. B* **546** (2002) 86 [hep-ph/0207229] [INSPIRE].

[54] D. Aristizabal Sierra and C.E. Yaguna, *On the importance of the 1-loop finite corrections to seesaw neutrino masses*, *JHEP* **08** (2011) 013 [arXiv:1106.3587] [INSPIRE].

JHEP03(2024)094

[55] I. Esteban et al., *The fate of hints: updated global analysis of three-flavor neutrino oscillations*, *JHEP* **09** (2020) 178 [arXiv:2007.14792] [INSPIRE].

[56] C.T. Hill and G.G. Ross, *Models and New Phenomenological Implications of a Class of Pseudogoldstone Bosons*, *Nucl. Phys. B* **311** (1988) 253 [INSPIRE].

[57] C. Garcia-Cely and J. Heeck, *Neutrino Lines from Majoron Dark Matter*, *JHEP* **05** (2017) 102 [arXiv:1701.07209] [INSPIRE].

[58] J. Heeck and H.H. Patel, *Majoron at two loops*, *Phys. Rev. D* **100** (2019) 095015 [arXiv:1909.02029] [INSPIRE].

[59] A. Herrero-Brocal and A. Vicente, *The majoron coupling to charged leptons*, *JHEP* **01** (2024) 078 [arXiv:2311.10145] [INSPIRE].

[60] A.W.M. Guerrera and S. Rigolin, *Revisiting $K \to \pi a$ decays*, *Eur. Phys. J. C* **82** (2022) 192 [arXiv:2106.05910] [INSPIRE].

[61] A.W.M. Guerrera and S. Rigolin, *ALP Production in Weak Mesonic Decays*, *Fortsch. Phys.* **71** (2023) 2200192 [arXiv:2211.08343] [INSPIRE].

[62] E.K. Akhmedov, Z.G. Berezhiani, G. Senjanovic and Z.-J. Tao, *Planck scale effects in neutrino physics*, *Phys. Rev. D* **47** (1993) 3245 [hep-ph/9208230] [INSPIRE].

[63] J.N. Esteves et al., *A_4-based neutrino masses with Majoron decaying dark matter*, *Phys. Rev. D* **82** (2010) 073008 [arXiv:1007.0898] [INSPIRE].

[64] S. Boulebnane, J. Heeck, A. Nguyen and D. Teresi, *Cold light dark matter in extended seesaw models*, *JCAP* **04** (2018) 006 [arXiv:1709.07283] [INSPIRE].

[65] K. Akita and M. Niibo, *Updated constraints and future prospects on majoron dark matter*, *JHEP* **07** (2023) 132 [arXiv:2304.04430] [INSPIRE].

[66] S. Palomares-Ruiz, *Model-independent bound on the dark matter lifetime*, *Phys. Lett. B* **665** (2008) 50 [arXiv:0712.1937] [INSPIRE].

[67] K. Langhoff, N.J. Outmezguine and N.L. Rodd, *Irreducible Axion Background*, *Phys. Rev. Lett.* **129** (2022) 241101 [arXiv:2209.06216] [INSPIRE].

[68] XENON collaboration, *Emission of single and few electrons in XENON1T and limits on light dark matter*, *Phys. Rev. D* **106** (2022) 022001 [arXiv:2112.12116] [INSPIRE].

[69] XENON collaboration, *Search for New Physics in Electronic Recoil Data from XENONnT*, *Phys. Rev. Lett.* **129** (2022) 161805 [arXiv:2207.11330] [INSPIRE].

[70] C. O'Hare, *cajohare/axionlimits: Axionlimits*, https://cajohare.github.io/AxionLimits/, July, 2020 [DOI:10.5281/zenodo.3932430].

[71] D. Cadamuro and J. Redondo, *Cosmological bounds on pseudo Nambu-Goldstone bosons*, *JCAP* **02** (2012) 032 [arXiv:1110.2895] [INSPIRE].

[72] J.W. Foster et al., *Deep Search for Decaying Dark Matter with XMM-Newton Blank-Sky Observations*, *Phys. Rev. Lett.* **127** (2021) 051101 [arXiv:2102.02207] [INSPIRE].

[73] K. Perez et al., *Almost closing the νMSM sterile neutrino dark matter window with NuSTAR*, *Phys. Rev. D* **95** (2017) 123002 [arXiv:1609.00667] [INSPIRE].

[74] K.C.Y. Ng et al., *New Constraints on Sterile Neutrino Dark Matter from NuSTAR M31 Observations*, *Phys. Rev. D* **99** (2019) 083005 [arXiv:1901.01262] [INSPIRE].

[75] B.M. Roach et al., *Long-exposure NuSTAR constraints on decaying dark matter in the Galactic halo*, *Phys. Rev. D* **107** (2023) 023009 [arXiv:2207.04572] [INSPIRE].

JHEP03(2024)094

[76] F. Calore, A. Dekker, P.D. Serpico and T. Siegert, *Constraints on light decaying dark matter candidates from 16 yr of INTEGRAL/SPI observations*, *Mon. Not. Roy. Astron. Soc.* **520** (2023) 4167 [arXiv:2209.06299] [INSPIRE].

[77] L. Calibbi, D. Redigolo, R. Ziegler and J. Zupan, *Looking forward to lepton-flavor-violating ALPs*, *JHEP* **09** (2021) 173 [arXiv:2006.04795] [INSPIRE].

[78] L. Di Luzio, A.W.M. Guerrera, X.P. Díaz and S. Rigolin, *On the IR/UV flavour connection in non-universal axion models*, *JHEP* **06** (2023) 046 [arXiv:2304.04643] [INSPIRE].

[79] M. Blennow and E. Fernandez-Martinez, *Parametrization of Seesaw Models and Light Sterile Neutrinos*, *Phys. Lett. B* **704** (2011) 223 [arXiv:1107.3992] [INSPIRE].

[80] C. Vafa and E. Witten, *Restrictions on Symmetry Breaking in Vector-Like Gauge Theories*, *Nucl. Phys. B* **234** (1984) 173 [INSPIRE].

JHEP03(2024)094

Fortschritte der Physik Progress of Physics
www.fp-journal.org

Probing HNL-ALP Couplings at Colliders

Arturo de Giorgi, Luca Merlo, and Jean-Loup Tastet*

Axion-like particles (ALPs) and heavy neutral leptons (HNLs) are both well-motivated extensions of the Standard Model. As ALPs couple to on-shell fermions proportionally to their masses, processes involving both types of particles may give rise, for TeV HNLs, to relevant phenomenology at colliders. In this work, we point out a particularly clean process, whose final state consists of four jets and two charged leptons, and we estimate its current and future sensitivity at the LHC. For on-shell HNLs, i) there is no dependence on the overall scale of the mixing between HNLs and the active neutrinos, making this process sensitive down to the type-I Seesaw line; ii) the signal strength of the process is sizable only as far as the HNL masses are below a few TeVs, contrary to what the proportionality to masses of the ALP couplings may suggest. Although ALPs and HNLs have been mainly studied independently in the literature, considering their interplay may lead to joint limits that are much stronger than those on the individual particles taken separately. This concise study paves the way for similar searches at colliders and other experiments.

1. Introduction

Axions and Axion-like particles (ALPs) experienced a revival of interest in the last years. From a more theoretical point of view, several studies appeared on axion constructions that extend the Peccei-Quinn model[1–3] and the original invisible axion models,[4–7] investigating possible axion flavour dynamics,[8–12] whose pioneering idea goes back to Ref. [13], or analysing the axion presence in composite Higgs frameworks,[14–16] or focusing on studying and enlarging the classical QCD axion parameter space,[17–24] showing that QCD axions may be much lighter or much heavier than in the classical scenario. Given the latter, we will adopt in the following the wording ALPs to refer to both QCD axions and to generic Goldstone bosons whose mass is not originated by non-perturbative QCD effects.

On the experimental side, the efforts pointed towards the construction of a consistent effective description of ALPs,[25–32] beyond the seminal study in Ref. [33], in order to investigate possible signals at low-energy facilities,[34–44] colliders[25,45–61] and in non-terrestrial environments.[62–65] Most of the analyses performed on collider data and from astrophysics deal with an on-shell ALP in the initial or final state of the considered processes, such as mono-Z, mono-W, and mono-Higgs searches or stellar cooling, and the associated bounds strongly depend on the ALP mass. The common aspect is that the associated Feynman diagram has only one single ALP coupling insertion and therefore the corresponding process amplitude is suppressed by only one power of the ALP characteristic scale f_a. On the other hand, the lack of observation of any tree-level flavour-changing process mediated by neutral currents leads to very strong bounds on ALP couplings, for example from meson oscillations and (semileptonic) meson decays. In this case, and in those few non-resonant ALP searches at colliders, the associated amplitude is suppressed by f_a^2 as the ALP appears as an internal line of the Feynman diagram.

Within the Standard Model (SM) framework with the addition of an ALP, it is always possible to express the ALP couplings to fermions in the chirality flip basis where the proportionality to the corresponding fermion mass becomes manifest. This implies that the heavier the fermion, the more enhanced is the corresponding coupling to the ALP. From here the idea is to study the implications of ALP couplings to Heavy Neutral Leptons (HNLs), typically introduced in Seesaw mechanisms[66–75] and with masses larger than the Electroweak (EW) scale. The idea of coupling an ALP to HNLs has not received much attention in the literature and only a few studies have appeared.[76–80]

Without entering into the details of any specific model of neutrino masses, HNLs are states composed of a mixture between the neutral components of the SM lepton Electroweak (EW) doublets and sterile leptons, singlets under the SM gauge symmetries: the matrix containing the mixings is typically labeled as $\boldsymbol{\Theta}$ and its entries are strongly bounded from global analyses on non-unitarity effects of the PMNS mixing matrix.[81–86] There exists a strong experimental program dedicated to searching for HNLs (see e.g. Refs. [87–89] for detailed reviews of existing and proposed searches), including at the CMS,[90–96] ATLAS[97–100] and LHCb[101] experiments at the LHC, where HNLs have been probed over a wide range of masses, in both the prompt and displaced regimes. As one of the main *renormalizable portals*[102–106] to new physics, HNLs are also a prime target for current and future searches at displaced detectors,[107–118] extracted beamlines,[119–136] colliders,[137–150] and cLFV experiments.[151,152]

A. de Giorgi, L. Merlo, J.-L. Tastet
Departamento de Física Teórica and Instituto de Física Teórica UAM/CSIC
Universidad Autónoma de Madrid
Cantoblanco, Madrid 28049, Spain
E-mail: arturo.degiorgi@uam.es

DOI: 10.1002/prop.202300027

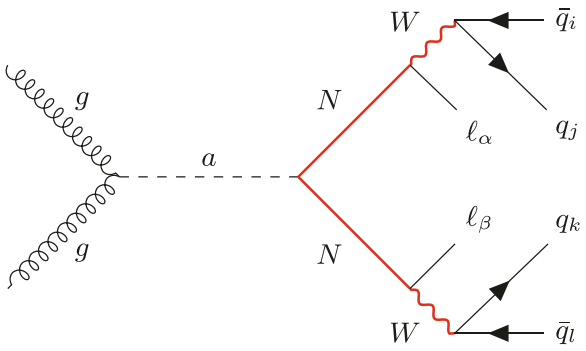

Figure 1. Feynman diagram of the JALZ-topology relevant for the study. The on-shell particles (besides final and initial states) are shown in red.

A number of reinterpretations have furthermore appeared, either to correct[153] the reported limits or to extend them[154–156] to non-minimal scenarios consistent with the observed lightness of neutrino masses.

In this letter, we identify a promising clean process that may shed light on the ALP couplings to HNLs and we study its sensitivity prospects at present and future colliders. The corresponding lobster-like Feynman diagram is shown in **Figure 1**. The ALP is produced off-shell through gluon fusion, which largely dominates over the other production mechanisms. The ALP then decays into two on-shell HNLs N, both of which subsequently decay into a charged lepton ℓ and an on-shell W gauge boson, whose final decay is into jets. The resulting final state consists of four jets and two charged leptons with same or opposite signs (j4ℓ2), which we refer to as the JALZ topology[1]. For HNLs with mass $M_N \gg M_W$, each W would be significantly boosted, resulting in an overlap between its two outgoing jets and making it harder to reconstruct the event unless a dedicated large-radius reconstruction[159] is used (see Appendix B).

This specific setup has the following advantages:

- the whole process is proportional to the HNL mass, thus the signal strength is sizeable;
- it is possible to adopt the narrow width approximation and then the branching ratios of the HNL decays do not depend on the overall scale of the mixing $\boldsymbol{\Theta}$, typically very small;
- the on-shellness of the two HNLs and the two W's, combined with the absence of light neutrinos, leads to a fully reconstructible final state with four *simultaneous* mass peaks. Not only we do not expect any Standard Model background with such a kinematic structure, but it could also significantly suppress the background from pileup jets that a process with four jets would otherwise suffer from.

With respect to other collider analyses, the JALZ topology is almost independent of the ALP mass and it is doubly suppressed by the ALP characteristic scale f_a, whose effect is however mitigated by the enhancement of the HNL mass. One may expect that the larger the HNL mass, the bigger would be the signal strength of the process, but this is not the case: due to the parton distribution functions of the colliding protons, the signal strength drops very fast for masses larger than $\sim \mathcal{O}(1.5)$ TeV.

In what follows, we will first introduce the parts of the ALP and HNL Lagrangian relevant to discuss the JALZ topology, then we will present the corresponding numerical analysis, and we will conclude with the sensitivity to the ALP-HNL coupling at colliders for different integrated luminosities as the main result of the letter.

2. The ALP-HNL Effective Lagrangian

Without entering into the details of a specific high energy theory, we will assume that a global symmetry, alike the Peccei-Quinn one, gets spontaneously broken at some large scale, giving rise to an ALP that couples to the SM spectrum, enlarged by n right-handed (RH) neutrinos, with $n \geq 2$. The latter provides lepton number violation that leads to masses for the active neutrinos at low energies: without focusing on a specific Seesaw mechanism, we will simply assume a minimal set of terms in the Lagrangian that describe the effective interactions at a scale where the HNLs are dynamical.

The effective Lagrangian that we will adopt for our analysis can be written as the sum of different terms:

$$\mathscr{L}^{\text{eff}} = \mathscr{L}_{\text{SM}} + \mathscr{L}_{\text{HNL}} + \mathscr{L}_a \,, \tag{1}$$

where the first term is the SM Lagrangian, the second contains the interactions of the HNL with the SM spectrum and the last describes the ALP couplings. More specifically,

$$\mathscr{L}_{\text{HNL}} = i\overline{N'_R}\not{\partial} N'_R - \left(\overline{L'_L}\widetilde{H}\boldsymbol{Y}_N N'_R + \frac{1}{2}\overline{N'^c_R}\boldsymbol{M}_N N'_R + \text{h.c.}\right), \tag{2}$$

where L'_L and H stand for the EW doublets of leptons and Higgs respectively, with $\widetilde{H} = i\sigma_2 H^*$, and N'_R are the RH neutrinos. The primes symbolise a generic flavour basis, where $\boldsymbol{M}_N$ and $\boldsymbol{Y}_N$ are $n \times n$ (symmetric) and $3 \times n$ matrices in the flavour space, respectively. After the EW symmetry breaking, the active neutrinos acquire small masses: in the canonical type-I Seesaw mechanism[66–72] their lightness results from the hierarchy between the Dirac and Majorana mass terms, while in the low-scale Seesaw variations[73–75,102,103] it follows from an approximately conserved lepton number[160–165] and the HNL masses can be close to the EW scale. Once the Higgs develops its vacuum expectation value (vev), $\langle H \rangle = v/\sqrt{2}$ with $v = 246$GeV, the neutral leptons mix, and the active neutrino mass term reads

$$\mathscr{L}_\nu \supset -\frac{1}{2}\overline{\nu''_L}\,\boldsymbol{m}_\nu\,\nu''^c_L + \text{h.c.}\,, \tag{3}$$

where in the Seesaw limit $v \ll ||\boldsymbol{M}_N||$,

$$\boldsymbol{m}_\nu = -\boldsymbol{\Theta}\,\boldsymbol{M}_N\,\boldsymbol{\Theta}^T \tag{4}$$

with the mixing matrix $\boldsymbol{\Theta}$ defined as

$$\nu'_L \equiv \nu''_L + \boldsymbol{\Theta} N'^c_R\,, \qquad \boldsymbol{\Theta} = \frac{v}{\sqrt{2}}\boldsymbol{Y}_N\,\boldsymbol{M}_N^{-1}\,. \tag{5}$$

[1] Such topology has been previously considered in Ref. [157] in the context of a Z'-portal to HNLs, and in Ref. [158] for the type-III Seesaw.

The HNL mass matrix can be identified with $\boldsymbol{M}_N$, neglecting small corrections proportional to the active neutrino mass matrix. Due to the mixing in Equation (5), the HNLs acquire couplings proportional to $\boldsymbol{\Theta}$ with the EW gauge and scalar bosons and with the other leptons.

The fermion mass basis is achieved by diagonalising the mass matrix of the charged leptons, $\boldsymbol{m}_\nu$, and $\boldsymbol{M}_N$,

$$\widehat{\boldsymbol{m}}_\nu = \boldsymbol{U}_\nu^\dagger \, \boldsymbol{m}_\nu \, \boldsymbol{U}_\nu^* , \qquad \widehat{\boldsymbol{M}}_N = \boldsymbol{U}_N^T \, \boldsymbol{M}_N \, \boldsymbol{U}_N , \tag{6}$$

and correspondingly the PMNS mixing matrix appears in the W–lepton currents. The associated mass eigenstates will be denoted as ν_L and N_R. As already mentioned, depending on the specific Seesaw realisation, N_R can be heavy ($\sim 10^{15}$ GeV) or very light ($\sim$ MeV). In the latter case, its phenomenological study is in general very promising in both direct and indirect searches. In the absence of any cancellation between the elements of $\boldsymbol{\Theta}$ in Equation (4), the light neutrino mass matrix is of order[2] $||\boldsymbol{m}_\nu|| \sim ||\boldsymbol{M}_N|| \cdot ||\boldsymbol{\Theta}||^2$, and conversely

$$||\boldsymbol{\Theta}||^2 \sim \frac{||\boldsymbol{m}_\nu||}{||\boldsymbol{M}_N||}. \tag{7}$$

Plotted as a function of the HNL mass(es) and taking $||\boldsymbol{m}_\nu|| \sim 50$ meV, this "Seesaw line" represents the naive expectation for the mixing matrix, in the absence of an approximate lepton number symmetry.

The last term in Equation (1) can be written as

$$\begin{aligned}\mathscr{L}_a =& \frac{1}{2}\partial_\mu a \, \partial^\mu a - \frac{1}{2} m_a^2 \, a^2 - \frac{a}{f_a} \sum_X c_{aXX} \, X^{\mu\nu} \widetilde{X}_{\mu\nu} + \\ & - \frac{\partial_\mu a}{f_a} \sum_{\psi'} \overline{\psi'} \boldsymbol{c}'_\psi \gamma^\mu \psi'\end{aligned} \tag{8}$$

where $X^{\mu\nu}$ is the field strength tensor of the SM gauge bosons and $\widetilde{X}_{\mu\nu}$ its dual, m_a is the generic ALP mass (that does not need to originate from non-perturbative QCD effects) and ψ' stands for any fermion field in the spectrum in the initial flavour basis, with $\boldsymbol{c}'_\psi$ the corresponding ALP-fermion coupling being a matrix in the flavour space. In the fermion mass basis, the ALP-HNL coupling contained in the second line in the previous expression reads

$$\mathscr{L}_a \supset - \frac{\partial_\mu a}{f_a} \, \overline{N_R} \, \gamma^\mu \, \boldsymbol{c}_N \, N_R \quad \text{with} \quad \boldsymbol{c}_N \equiv \boldsymbol{U}_N^\dagger \boldsymbol{c}'_{N_R} \boldsymbol{U}_N . \tag{9}$$

The latter coupling and the anomalous ALP-gluon coupling in Equation (8) are the basic ingredients necessary to discuss the JALZ process. The ALP couplings to charged fermions and active neutrinos have already been studied in the literature. The ALP couplings to one active neutrino and one HNL have not been investigated, but they are proportional to $\boldsymbol{\Theta}$ and therefore the associated signals are suppressed and harder to see at present and near-future colliders.

[2] The precise value depends on the number of HNLs, the neutrino mass ordering and the specific elements of $\boldsymbol{\Theta}$.

3. The Analysis

In the rest of the letter, we will discuss the phenomenology of the lightest HNL, dubbed N. Consistently, its mass will be denoted by M_N (not boldface), its couplings with the other leptons will only include the lepton family index and will be denoted by Θ_α, while the one with the ALP will be indicated as c_N (not boldface).

On-shellness: The on-shellness of the HNLs allows separating their production and decay using the narrow-width approximation. For a given combination of lepton flavours $\alpha, \beta \in e, \mu, \tau$ with any combination of charges:

$$\begin{aligned}\sigma_{\alpha\beta} \equiv \sigma(pp \to a^* \to & (N \to \ell_\alpha \bar{q}_i q_j)(N \to \ell_\beta q_k \bar{q}_l)) = \\ & = \frac{2}{S} \times \sigma(pp \to a^* \to NN) \times \\ & \times \mathrm{Br}(N \to \ell_\alpha \bar{q}_i q_j) \times \mathrm{Br}(N \to \ell_\beta q_k \bar{q}_l)\end{aligned} \tag{10}$$

where S is a symmetry factor equal to 2 if both HNL decays are identical and to 1 otherwise, and the 2 in the numerator is a combinatorial factor accounting for the presence of two HNLs. For a given choice of lepton flavours, α and β, Equation (10) shows that the cross-section scales as follows with the various parameters (excluding the HNL mass and neglecting the charged lepton masses):

$$\sigma_{\alpha\beta} \propto \frac{c_{agg}^2 c_N^2}{f_a^4} \frac{|\Theta_\alpha|^2 |\Theta_\beta|^2}{\Gamma_N^2} \propto \frac{c_{agg}^2 c_N^2}{f_a^4} \frac{|\Theta_\alpha|^2}{|\Theta|^2} \frac{|\Theta_\beta|^2}{|\Theta|^2} \tag{11}$$

where we have defined $|\Theta|^2 = \sum_{\alpha=e,\mu,\tau} |\Theta_\alpha|^2$ and used the proportionality of the total HNL width to $|\Theta|^2$. This shows that the cross-section is independent of the overall scale of the HNL mixings.

If we were to sum the cross-section over all three lepton flavours, the dependence on the mixing pattern $|\Theta_\alpha|^2/|\Theta|^2$ would disappear too (up to small finite-mass corrections). However, in practice, different lepton flavours come with different detection efficiencies, resulting in a residual dependence on the mixing pattern. Nevertheless, we should expect the sensitivity of the process to depend only weakly on the ratio of the three mixings. If, however, we were to consider separately the processes involving different combinations of charged lepton flavours, we could in principle constrain or even measure the relative values of the $\boldsymbol{\Theta}$ entries.

HNL lifetime: The expected number of signal events can be expressed as:

$$N_{\text{events}} = L_{\text{int}} \sigma \epsilon \tag{12}$$

with L_{int} denoting the integrated luminosity, σ the cross-section of the process, and ϵ the signal efficiency of the process. Despite the fact that the dependence on the overall $|\Theta|^2$ scale cancels out, as shown by Equation (11), if the HNL is long-lived, it can fly out of the detector, lowering the efficiency and reintroducing a dependence on $|\Theta|^2$. In particular, when the HNL lifetime becomes much larger than the size of the experiment r_{exp}, the efficiency (for each HNL) will have to include the probability of decaying within the detector, which asymptotically goes as $\Gamma_N r_{\text{exp}}/\gamma_N \propto |\Theta|^2/\gamma_N$, with γ_N the HNL boost that only depends on M_N. This would make the signal strength proportional to $|\Theta|^4$.

Table 1. Approximate relative frequencies of the various final states, classified according to the degree to which each HNL decay can be reconstructed, for $M_N \gg M_h$. "First" and "Second" denote the two HNLs produced in the ALP decay, in no particular order since they are indistinguishable.

First N \ Second N	Reconstructible	MET	Invisible
Reconstructible	10%		
MET	40%	40%	
Invisible	3%	6%	0.2%

Appendix A discusses the HNL lifetime in more detail and shows that for models of interest ($|\Theta|^2$ at or above the Seesaw line) and at the LHC, the HNLs can safely be considered as decaying promptly (see Figure 4), and therefore the signal strength is independent of the overall scale of the HNL mixings.

Other channels: The topology presented in Sect. 1 can lead to a number of different signatures, depending on the HNL decays and on the subsequent decays of the resulting on-shell bosons. When $M_N \gg M_h$, each HNL decays to $W : Z : h$ in proportions $\frac{1}{2} : \frac{1}{4} : \frac{1}{4}$, and each W decays hadronically (leptonically) about 2/3 (1/3) of the time. Out of all the final states, only the JALZ topology is in principle fully reconstructible, with no neutrinos in the final state. It corresponds to the lobster-like diagram shown in Figure 1, and will be the focus of this study. Because each HNL takes the fully reconstructible decay channel ℓjj about 1/3 of the time, this final state is realised in about 1/9 of the NN pairs produced through the coupling of HNLs to the ALP. This is in agreement with our numerical estimates, up to finite-mass effects that correct the decay widths when M_N is near the $\mathcal{O}(100\,\text{GeV})$ scale. Another $\approx 80\%$ of the final states resulting from the decay of the NN pair contain at least one neutrino — and will therefore lead to a signature with some missing transverse energy (MET). Half of them contain one fully reconstructible HNL decay, while the other half contains MET in both decays. If one can deal with the increased background resulting from not being able to reconstruct the mass of both HNLs, these could in principle be interesting search channels. In fact, similar topologies (mediated by on-shell fermions and vector bosons, and with off-shell gauge bosons instead of the ALP) have already been searched for at the LHC in the context of the type-III Seesaw and vector-like leptons, see e.g. Refs. [166–171], although in the models they consider, the production mechanism is not gluon fusion but Drell-Yan. **Table 1** summarises the relative frequencies of all the final states, classified in terms of whether each HNL decay is reconstructible, partially reconstructible (MET), or invisible.

Impact of partonic effects.: The effect of Parton Distribution Functions (PDFs) is very relevant. Not all the partons within the proton have the same energy. Denoting by $x_{1,2}$ the momentum fractions of the two partons, the total energy at their disposal is $\hat{s} \equiv x_1 x_2 s$. In order to produce two HNLs, the kinematic condition $\sqrt{\hat{s}} \geq 2M_N$ must hold. The area subtended by the PDFs, and that has to be convoluted with the partonic cross-section, gets reduced considerately at high momentum fraction. Therefore, as the mass of the HNL grows, the kinematic condition has little space to be satisfied, thus suppressing the final cross-section. To get a rough

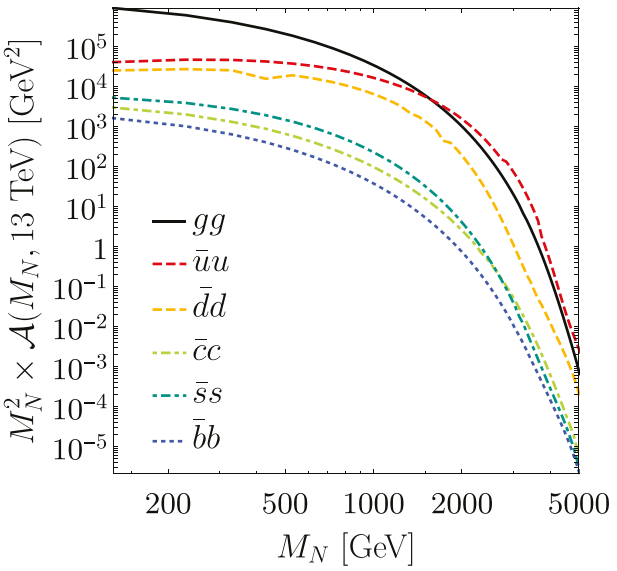

Figure 2. Scaling of the PDFs area times M_N^2 for different partons involved in the HNLs production as a function of M_N.

estimate of such an effect, we compute the area of the PDFs that must be convoluted with the partonic cross-section

$$\mathcal{A}_{g,q}(M_N, \sqrt{s}) \equiv \iint_{\sqrt{\hat{s}} \geq 2M_N} \mathrm{d}x_1 \mathrm{d}x_2 f_{g,q}(x_1) f_{g,\bar{q}}(x_2)\,, \tag{13}$$

where $f_i(x)$ are the PDFs. The result for $\sqrt{s} = 13$ TeV is shown in **Figure 2**. In this Figure, we have used the central values from the PDFs *MSTW 2008*.[172]

We have conveniently multiplied $\mathcal{A}$ by M_N^2 as this is the naively expected enhancement given by the ALP vertex.

Monte-Carlo event generation: The cross-sections are computed numerically using the `MadGraph5_aMC@NLO` (v3.4.1) Monte-Carlo event generator.[173] The Lagrangian defined in Sect. 2 is implemented in the `Mathematica`[174] package `FeynRules` (v2.3.41),[175] taking some inspiration from the `HeavyN`[176,177] and `ALP_linear`[25] models. Samples are generated for a number of HNL masses within the range [130, 5000] GeV. After numerically verifying that gluon fusion $gg \to a^*$ is the dominant production mechanism throughout this mass range, we neglect the remaining production modes. We use the PDF set `NNPDF40_nnlo_as_01180` from the NNPDF collaboration[178] through the `LHAPDF6` interface.[179] The ALP mass is set to a non-zero value of 1 GeV to avoid numerical stability issues, but is shown to have no effect on the cross-sections. We then parse the results file to aggregate the cross-sections for the various signatures of interest, using the scaling properties (11) as needed to interpolate between the various HNL mixing patterns (see Refs. [180] or [[155], section 3] for a description of this method).

4. The Projected Sensitivity

The JALZ topology is selected by requiring no neutrinos in the final state, and the projected single-event sensitivity of an LHC

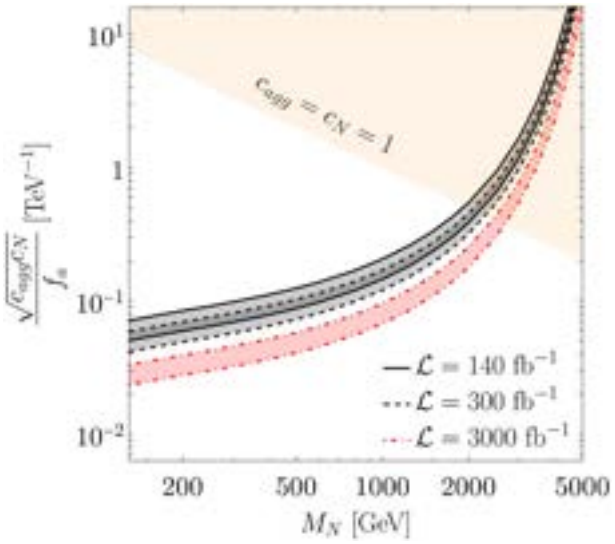

Figure 3. Sensitivity to NP couplings as a function of the HNL mass at LHC for different integrated luminosities at $\sqrt{s} = 13$ TeV, assuming perfect efficiency for electrons, muons, and jets. Above the lines, a number of events $N_{\text{events}} > 1$ is expected. For each colored band, the bottom line corresponds to the HNL mixing only with e and μ (best sensitivity), and the top one to mixing only with τ (worst sensitivity). The ratio of the two lines corresponds to $\sqrt{\epsilon_\tau}$. Any intermediate case is expected to lie within the band. Finally, the orange region shows where $f_a \leq M_N$ for $c_{gg} = c_N = 1$, where the theory is expected to become unreliable.

experiment is computed for various luminosity targets. The underlying assumption is that simultaneously reconstructing the two HNL masses, each from the momenta of a lepton and of a large-radius, W-tagged jet,[159] suppresses the background down to a negligible level (the correct combination of lepton and jet being selected by requiring the reconstructed HNL masses to agree). Using the scaling law in Equation (11), the projected sensitivity is then expressed in terms of $\sqrt{c_{agg}c_N}/f_a$ and the HNL mass.

Although summing Equation (11) over flavours leads to a cross-section that is completely independent of HNL parameters, in practice efficiencies differ for each flavour combination. This is particularly true for the tau lepton, whose leptonic modes account for 35% of decays and do not allow to identify the tau as such at the LHC. They would lead to a final state similar to the JALZ topology, but with missing transverse energy that may impede the reconstruction of the HNL mass. In what follows we will therefore focus on hadronically decaying taus τ_{h}, and we assume a further reconstruction/identification efficiency[3] of 80% for each tau, leading to an overall efficiency of $\epsilon_\tau \approx 0.5$.

The final result of the letter is in **Figure 3** where we show the sensitivity to the ALP couplings as a function of the HNL mass at the LHC for different integrated luminosities. The thickness of the sensitivity bands is defined considering HNL mixing with only electrons and muons (lower line), or only with the taus (upper line). Because these limits do not take into account signal efficiencies other than the tau's, we expect them to be slightly optimistic. In Appendix B, we apply a simple event selection, discuss the most important cuts at both low and high masses, and argue for the use of large-radius jet reconstruction to search for the JALZ topology.

[3] The reconstruction and identification efficiencies of tau leptons crucially depend on the chosen working point, i.e. on the required level of background rejection (see e.g. Ref. [181]). The favourable background conditions of the JALZ topology should allow for a high efficiency, hence the chosen value of 80%.

5. Concluding Remarks

The existence in Nature of ALPs from one side and of HNLs from the other is very well motivated. In this letter, we assume that both types of particles exist and interact with each other, and we point out an efficient discovery channel at colliders, whose final state consists of four jets and two charged leptons. When a non-resonant ALP produces two on-shell HNLs, with masses above the electroweak scale, the signal strength at present and near-future colliders is independent of the overall scale of the HNL mixing with the active neutrinos: this is particularly appealing as the elements of the $\boldsymbol{\Theta}$ matrix are constrained to be tiny. However, the signal strength still depends on the relative values of the $\boldsymbol{\Theta}$ entries. In case of not distinguishing between the charged leptons in the final state, the dependence on $\boldsymbol{\Theta}$ would completely disappear in the cross section, but a mild dependence in the signal strength remains due to the different efficiencies. On the contrary, in the event of an observation of this process, distinguishing between the charged leptons in the final state would provide constraints on $|\Theta_\alpha|/|\Theta_\beta|$ combinations.

Moreover, the analysis is independent of the ALP mass, thus applying to generic Goldstone bosons as well as to QCD axions, with f_a not too much larger than tens of TeV (a modification of the traditional QCD axion parameter space has been recently discussed in the literature[17–24]).

The standard lore for ALP-fermion couplings is that they are proportional to the corresponding fermion mass, thus naively implying that the larger the mass, the higher the signal strength of a process induced by such a coupling. However, we showed that the impact of the PDFs is very much relevant, leading to a drop of the signal strength (and of the sensitivity to the couplings) for HNL masses larger than a couple of TeV for LHC data with $\sqrt{s} = 13$TeV.

This study represents a first example of how a dedicated analysis of the interactions between ALPs and HNLs could shed light on the nature of these elusive particles. In particular, we showed that their interplay may lead to joint limits that are much stronger than those on the individual particles taken separately. It also paves the way for model building constructions and for additional searches at colliders and other types of experiments.

Appendix A: HNL Lifetime

For HNLs heavier than the Higgs, the decays to on-shell W's, Z's, and h's dominate, with rates:[182]

$$\Gamma(N \to W\ell_\alpha) \approx \frac{G_F M_N^3}{4\pi\sqrt{2}}|\Theta_\alpha|^2\left(1 - \frac{M_W^2}{M_N^2}\right)^2\left(1 + \frac{2M_W^2}{M_N^2}\right)$$

$$\Gamma(N \to h\nu_\alpha) \approx \frac{G_F M_N^3}{8\pi\sqrt{2}} |\Theta_\alpha|^2 \left(1 - \frac{M_h^2}{M_N^2}\right)^2 \tag{A1}$$

$$\Gamma(N \to Z\nu_\alpha) \approx \frac{G_F M_N^3}{8\pi\sqrt{2}} |\Theta_\alpha|^2 \left(1 - \frac{M_Z^2}{M_N^2}\right)^2 \left(1 + \frac{2M_Z^2}{M_N^2}\right),$$

where both particle and antiparticle final states are taken into account.

For $M_N \gg M_{W,Z,h}$, the HNL lifetime τ_N can be approximated as:

$$\tau_N^{-1} \approx \sum_\alpha \left[\Gamma(N \to W\ell_\alpha) + \Gamma(N \to Z\nu_\alpha) + \Gamma(N \to h\nu_\alpha)\right]$$

$$\cong \frac{G_F}{2\pi\sqrt{2}} M_N^3 |\Theta|^2 , \tag{A2}$$

where the total mixing angle has been defined as $|\Theta|^2 = \sum_{\alpha=e,\mu,\tau} |\Theta_\alpha|^2$.

The mean path of an on-shell HNL in the LAB frame largely affects the ability of a search to detect it. In what follows we perform a rough estimation of this quantity. The mean distance in the LAB frame $\lambda_{N,\mathrm{LAB}}$, is given by

$$\lambda_{N,\mathrm{LAB}} = \beta_N \gamma_N \tau_N = \sqrt{\frac{\hat{s}}{4M_N^2} - 1}\, \tau_N , \tag{A3}$$

where we have taken into account the fraction of energy delivered by the partons to the HNL. Averaging over this quantity:

$$\bar{\lambda}_{N,\mathrm{LAB}} = \frac{\iint_{\sqrt{\hat{s}} \geq 2M_N} \mathrm{d}x_1 \mathrm{d}x_2 f_g(x_1) f_g(x_2) \lambda_{N,\mathrm{LAB}}}{\iint_{\sqrt{\hat{s}} \geq 2M_N} \mathrm{d}x_1 \mathrm{d}x_2 f_g(x_1) f_g(x_2)} . \tag{A4}$$

The result can be seen in **Figure 4**.

Appendix B: Event selection

The projected sensitivity presented in this paper has been derived under the optimistic assumption of perfect acceptance. In this appendix, we test this assumption by applying a simple but typical selection (inspired by various type-III Seesaw and vector-like lepton searches that looked for similar topologies[166–171]) and by explicitly computing the signal efficiency. The leading lepton (defined as the lepton with the largest transverse momentum p_T) is required to have $p_T > 40$ GeV, and the subleading lepton to have $p_T > 15$ GeV. Both leptons are required to be within the pseudorapidity range $|\eta| < 2.5$ and to be separated from each other by $\Delta R > 0.4$. If the lepton pair has the same flavour but opposite signs (OSSF), its invariant mass is further required to be $m_{l^+l^-} > 110$ GeV to suppress background from Z decays. Jets (here quarks since we are performing the analysis at parton level) are required to have $p_T > 30$ GeV and to be within $|\eta| < 2.4$. We additionally require a separation $\Delta R > \Delta R_{jj}$ between any two jets (with a varying value of $\Delta R_{jj} = 0.001$, 0.2 or 0.4 in order to study its impact), as well as a separation of $\Delta R > 0.4$ between any given jet and lepton.

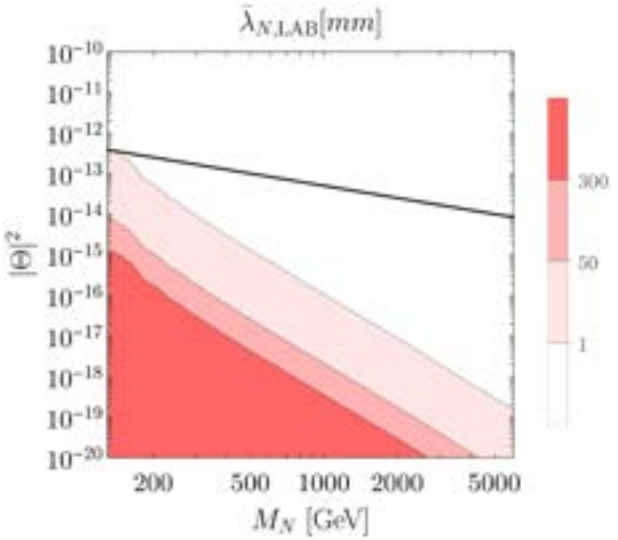

Figure 4. Contours of constant mean path of an HNL in the LAB frame as a function of M_N and of the total mixing angle. The black line indicates the naive Type-I Seesaw expectation $|\Theta|^2 = m_\nu / M_N$ with $m_\nu = 50$ meV. The contours correspond to typical scales in the ATLAS experiment, with 1 mm being a typical cut in a prompt search, the interval [50, 300] mm is covered by large radius tracking[183] while [1, 50] mm is best covered by a combination of standard and large radius tracking.

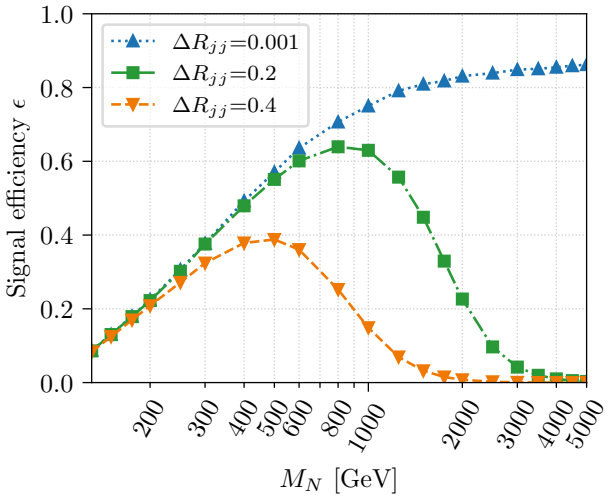

Figure 5. Signal efficiencies for the simple selection, as a function of the HNL mass M_N and the minimum distance ΔR_{jj} between any two jets.

The cuts are applied directly in MadGraph's `param_card.dat`, before generating the process `g g > n1 n1, n1 > j j l` with `l` denoting $e^\pm$ or $\mu^\pm$ but not $\tau^\pm$ (since the tau lepton efficiency has been treated separately) and `n1` denoting the HNL. We assume equal mixing of the HNL with all three flavours. The signal efficiency, computed as the ratio of the generated parton-level cross-sections with/without cuts, is plotted in **Figure 5** as a function of the HNL mass and ΔR_{jj}.

We observe that imposing a non-trivial ΔR separation between jets strongly suppresses the signal at higher HNL masses, while other cuts are subleading. In practice, because small-R jets are typically reconstructed with an angular size of $R = 0.4$, for two

jets to be resolved the parent partons will need to be separated by $\Delta R_{jj} \gtrsim 0.4$. The suppression then has a simple interpretation: the partons produced in the decay of a boosted W are collimated in the LAB frame and form a single boosted jet instead of two resolved jets. Therefore, in order to be sensitive to the JALZ process at large HNL masses, one should aim to reconstruct the hadronic decay products of each W as a single large-radius jet (with $R \approx 1$). Performing an analysis at the reconstructed level is outside the scope of the present letter, and is left for further study. For the time being, we shall assume that the two large-R, W-tagged jets can be successfully reconstructed with $\mathcal{O}(1)$ efficiency.

Following a similar analysis and enabling each cut one-by-one, we observe that the cuts responsible for the suppression at lower HNL masses are, in rough order from the most to least important: the p_{T} cuts on the jets, the minimum ΔR between a lepton and jet, and the p_{T} cut on the leading lepton. Then comes the Z veto and the $|\eta|$ requirements with a much smaller effect, while the remaining cuts are subleading. The p_{T} cuts largely depend on the specifics of the detector and trigger system and should be a prime target for optimisation by the search team. Regarding the minimum ΔR between a lepton and a jet, it might be possible to do away with this cut altogether by once again trying to reconstruct the W decays as large-radius jets possibly containing a lepton track. While the p_{T} cuts could already have been implemented in the present study, we shall leave the calculation of precise signal efficiencies to an upcoming study.

Acknowledgements

The authors acknowledge partial financial support by the Spanish Research Agency (Agencia Estatal de Investigación) through the grant IFT Centro de Excelencia Severo Ochoa No CEX2020-001007-S and by the grant PID2019-108892RB-I00 funded by MCIN/AEI/10.13039/501100011033, by the European Union's Horizon 2020 research and innovation programme under the Marie Skłodowska-Curie grant agreement No 860881-HIDDeN. JLT acknowledges partial support from the grant Juan de la Cierva FJC2021-047666-I funded by MCIN/AEI/10.13039/501100011033 and by the European Union "NextGenerationEU"/PRTR.

Data Availability Statement

None.

Conflict of Interest

The authors have declared no conflict of interest.

Keywords

axion, Axion-like particles, collider search, Heavy-neutral leptons, sterile neutrinos, JALZ

Received: January 28, 2023
Revised: January 28, 2023

[1] R. D. Peccei, H. R. Quinn, *Phys. Rev. Lett.* **1977**, *38*, 1440.
[2] S. Weinberg, *Phys. Rev. Lett.* **1978**, *40*, 223.
[3] F. Wilczek, *Phys. Rev. Lett.* **1978**, *40*, 279.
[4] A. R. Zhitnitsky, *Sov. J. Nucl. Phys.* **1980**, *31*, 260.
[5] M. Dine, W. Fischler, M. Srednicki, *Phys. Lett. B* **1981**, *104*, 199.
[6] J. E. Kim, *Phys. Rev. Lett.* **1979**, *43*, 103.
[7] M. A. Shifman, A. I. Vainshtein, V. I. Zakharov, *Nucl. Phys. B* **1980**, *166*, 493.
[8] Y. Ema, K. Hamaguchi, T. Moroi, K. Nakayama, *JHEP* **2017**, *01*, 096, [arXiv:1612.05492].
[9] L. Calibbi, F. Goertz, D. Redigolo, R. Ziegler, J. Zupan, *Phys. Rev. D* **2017**, *95*, 095009, [arXiv:1612.08040].
[10] F. Arias-Aragon, L. Merlo, *JHEP* **2017**, *10*, 168, [arXiv:1709.07039]. [Erratum: JHEP 11, 152 (2019)].
[11] F. Arias-Aragon, E. Fernandez-Martinez, M. Gonzalez-Lopez, L. Merlo, *Eur. Phys. J. C* **2021**, *81*, 28, [arXiv:2009.01848].
[12] F. Arias-Aragón, E. Fernández-Martínez, M. González-López, L. Merlo, *JHEP* **2022**, *09*, 210, [arXiv:2204.04672].
[13] F. Wilczek, *Phys. Rev. Lett.* **1982**, *49*, 1549.
[14] L. Merlo, F. Pobbe, S. Rigolin, *Eur. Phys. J. C* **2018**, *78*, 415, [arXiv:1710.10500]. [Erratum: Eur.Phys.J.C 79, 963 (2019)].
[15] I. Brivio, M. B. Gavela, S. Pascoli, R. del Rey, S. Saa, *Chin. J. Phys.* **2019**, *61*, 55, [arXiv:1710.07715].
[16] J. Alonso-González, L. Merlo, F. Pobbe, S. Rigolin, O. Sumensari, *Nucl. Phys. B* **2020**, *950*, 114839, [arXiv:1807.08643].
[17] L. D. Luzio, F. Mescia, E. Nardi, *Phys. Rev. Lett.* **2017**, *118*, 031801, [arXiv:1610.07593].
[18] L. D. Luzio, F. Mescia, E. Nardi, *Phys. Rev. D* **2017**, *96*, 075003, [arXiv:1705.05370].
[19] M. K. Gaillard, M. B. Gavela, R. Houtz, P. Quilez, R. D. Rey, *Eur. Phys. J. C* **2018**, *78*, 972, [arXiv:1805.06465].
[20] A. Hook, S. Kumar, Z. Liu, R. Sundrum, *Phys. Rev. Lett.* **2020**, *124*, 221801, [arXiv:1911.12364].
[21] L. D. Luzio, M. Giannotti, E. Nardi, L. Visinelli, *Phys. Rept.* **2020**, *870*, 1, [arXiv:2003.01100].
[22] L. D. Luzio, R. Gröber, P. Paradisi, *Phys. Rev. D* **2021**, *104*, 095027, [arXiv:2010.13760].
[23] L. D. Luzio, B. Gavela, P. Quilez, A. Ringwald, *JHEP* **2021**, *05*, 184, [arXiv:2102.00012].
[24] L. D. Luzio, B. Gavela, P. Quilez, A. Ringwald, *JCAP* **2021**, *10*, 001, [arXiv:2102.01082].
[25] I. Brivio, M. B. Gavela, L. Merlo, K. Mimasu, J. M. No, R. del Rey, V. Sanz, *Eur. Phys. J. C* **2017**, *77*, 572, [arXiv:1701.05379].
[26] G. Alonso-Álvarez, M. B. Gavela, P. Quilez, *Eur. Phys. J. C* **2019**, *79*, 223, [arXiv:1811.05466].
[27] M. B. Gavela, R. Houtz, P. Quilez, R. D. Rey, O. Sumensari, *Eur. Phys. J. C* **2019**, *79*, 369, [arXiv:1901.02031].
[28] M. Chala, G. Guedes, M. Ramos, J. Santiago, *Eur. Phys. J. C* **2021**, *81*, 181, [arXiv:2012.09017].
[29] J. Bonilla, I. Brivio, M. B. Gavela, V. Sanz, *JHEP* **2021**, *11*, 168, [arXiv:2107.11392].
[30] M. Bauer, M. Neubert, S. Renner, M. Schnubel, A. Thamm, *Phys. Rev. Lett.* **2021**, *127*, 081803, [arXiv:2102.13112].
[31] F. Arias-Aragón, C. Smith, *Phys. Rev. D* **2022**, *106*, 055034, [arXiv:2206.09810].
[32] F. Arias-Aragón, J. Quevillon, C. Smith, Axion-like ALPs, arXiv:2211.04489.
[33] H. Georgi, D. B. Kaplan, L. Randall, *Phys. Lett. B* **1986**, *169*, 73.
[34] E. Izaguirre, T. Lin, B. Shuve, *Phys. Rev. Lett.* **2017**, *118*, 111802, [arXiv:1611.09355].
[35] L. Merlo, F. Pobbe, S. Rigolin, O. Sumensari, *JHEP* **2019**, *06*, 091, [arXiv:1905.03259].
[36] M. Bauer, M. Neubert, S. Renner, M. Schnubel, A. Thamm, *Phys. Rev. Lett.* **2020**, *124*, 211803, [arXiv:1908.00008].
[37] M. Bauer, M. Neubert, S. Renner, M. Schnubel, A. Thamm, *JHEP* **2021**, *04*, 063, [arXiv:2012.12272].

[38] M. Bauer, M. Neubert, S. Renner, M. Schnubel, A. Thamm, *JHEP* **2022**, *09*, 056, [arXiv:2110.10698].
[39] A. W. M. Guerrera, S. Rigolin, *Eur. Phys. J. C* **2022**, *82*, 192, [arXiv:2106.05910].
[40] J. A. Gallo, A. W. M. Guerrera, S. Peñaranda, S. Rigolin, *Nucl. Phys. B* **2022**, *979*, 115791, [arXiv:2111.02536].
[41] J. Bonilla, A. de Giorgi, B. Gavela, L. Merlo, M. Ramos, The cost of an ALP solution to the neutral B-anomalies, arXiv:2209.11247.
[42] J. Bonilla, A. de Giorgi, M. Ramos, Neutral B-anomalies from an *on-shell* scalar exchange, arXiv:2211.05135.
[43] A. de Giorgi, G. Piazza, A lesson from $R_{\tau\tau}^{K^{(*)}}$ and $R_{\nu\nu}^{K^{(*)}}$ at Belle II, arXiv:2211.05595.
[44] A. W. M. Guerrera, S. Rigolin, ALP production in weak mesonic decays, arXiv:2211.08343.
[45] J. Jaeckel, M. Jankowiak, M. Spannowsky, *Phys. Dark Univ.* **2013**, *2*, 111, [arXiv:1212.3620].
[46] K. Mimasu, V. Sanz, *JHEP* **2015**, *06*, 173, [arXiv:1409.4792].
[47] J. Jaeckel, M. Spannowsky, *Phys. Lett. B* **2016**, *753*, 482, [arXiv:1509.00476].
[48] A. Alves, A. G. Dias, K. Sinha, *JHEP* **2016**, *08*, 060, [arXiv:1606.06375].
[49] S. Knapen, T. Lin, H. K. Lou, T. Melia, *Phys. Rev. Lett.* **2017**, *118*, 171801, [arXiv:1607.06083].
[50] M. Bauer, M. Neubert, A. Thamm, *Phys. Rev. Lett.* **2017**, *119*, 031802, [arXiv:1704.08207].
[51] A. Mariotti, D. Redigolo, F. Sala, K. Tobioka, *Phys. Lett. B* **2018**, *783*, 13, [arXiv:1710.01743].
[52] M. Bauer, M. Neubert, A. Thamm, *JHEP* **2017**, *12*, 044, [arXiv:1708.00443].
[53] C. Baldenegro, S. Fichet, G. von Gersdorff, C. Royon, *JHEP* **2018**, *06*, 131, [arXiv:1803.10835].
[54] N. Craig, A. Hook, S. Kasko, *JHEP* **2018**, *09*, 028, [arXiv:1805.06538].
[55] M. Bauer, M. Heiles, M. Neubert, A. Thamm, *Eur. Phys. J. C* **2019**, *79*, 74, [arXiv:1808.10323].
[56] M. B. Gavela, J. M. No, V. Sanz, J. F. de Trocóniz, *Phys. Rev. Lett.* **2020**, *124*, 051802, [arXiv:1905.12953].
[57] G. Haghighat, D. H. Raissi, M. MohammaDi Najafabadi, *Phys. Rev. D* **2020**, *102*, 115010, [arXiv:2006.05302].
[58] D. Wang, L. Wu, J. M. Yang, M. Zhang, *Phys. Rev. D* **2021**, *104*, 095016, [arXiv:2102.01532].
[59] J. Bonilla, I. Brivio, J. Machado-Rodríguez, J. F. de Trocóniz, *JHEP* **2022**, *06*, 113, [arXiv:2202.03450].
[60] F. A. Ghebretinsaea, Z. S. Wang, K. Wang, *JHEP* **2022**, *07*, 070, [arXiv:2203.01734].
[61] V. E. Vileta, B. Gavela, R. Houtz, P. Quilez, Discrete Goldstone Bosons, arXiv:2205.09131.
[62] F. D'Eramo, R. Z. Ferreira, A. Notari, J. L. Bernal, *JCAP* **2018**, *11*, 014, [arXiv:1808.07430].
[63] F. Arias-Aragón, F. D'eramo, R. Z. Ferreira, L. Merlo, A. Notari, *JCAP* **2020**, *11*, 025, [arXiv:2007.06579].
[64] F. Arias-Aragón, F. D'Eramo, R. Z. Ferreira, L. Merlo, A. Notari, *JCAP* **2021**, *03*, 090, [arXiv:2012.04736].
[65] F. D'Eramo, E. D. Valentino, W. Giarè, F. Hajkarim, A. Melchiorri, O. Mena, F. Renzi, S. Yun, *JCAP* **2022**, *09*, 022, [arXiv:2205.07849].
[66] P. Minkowski, *Phys. Lett. B* **1977**, *67*, 421.
[67] R. N. Mohapatra, G. Senjanovic, *Phys. Rev. Lett.* **1980**, *44*, 912.
[68] T. Yanagida, *Conf. Proc. C* **1979**, *7902131*, 95.
[69] S. L. Glashow, *NATO Sci. Ser. B* **1980**, *61*, 687.
[70] M. Gell-Mann, P. Ramond, R. Slansky, *Conf. Proc. C* **1979**, *790927*, 315, [arXiv:1306.4669].
[71] J. Schechter, J. W. F. Valle, *Phys. Rev. D* **1980**, *22*, 2227.
[72] J. Schechter, J. W. F. Valle, *Phys. Rev. D* **1982**, *25*, 774.
[73] R. N. Mohapatra, J. W. F. Valle, *Phys. Rev. D* **1986**, *34*, 1642.
[74] J. Bernabeu, A. Santamaria, J. Vidal, A. Mendez, J. W. F. Valle, *Phys. Lett. B* **1987**, *187*, 303.
[75] M. Malinsky, J. C. Romao, J. W. F. Valle, *Phys. Rev. Lett.* **2005**, *95*, 161801, [hep-ph/0506296].
[76] C. D. R. Carvajal, B. L. Sánchez-Vega, O. Zapata, *Phys. Rev. D* **2017**, *96*, 115035.
[77] A. Alves, A. G. Dias, D. D. Lopes, *JHEP* **2020**, *08*, 074, [arXiv:1911.12394].
[78] A. Dekker, E. Peerbooms, F. Zimmer, K. C. Y. Ng, S. Ando, *Phys. Rev. D* **2021**, *104*, 023021, [arXiv:2103.13241].
[79] S. Gola, S. Mandal, N. Sinha, ALP-portal majorana dark matter, arXiv:2106.00547.
[80] F. Arias-Aragón, E. Fernández-Martínez, M. González-López, L. Merlo, *PoS* **2022**, *EPS-HEP2021*, 207, [arXiv:2110.15698].
[81] P. Langacker, D. London, *Phys. Rev. D* **1988**, *38*, 886.
[82] S. Antusch, C. Biggio, E. Fernandez-Martinez, M. B. Gavela, J. Lopez-Pavon, *JHEP* **2006**, *10*, 084, [hep-ph/0607020].
[83] E. Fernandez-Martinez, M. B. Gavela, J. Lopez-Pavon, O. Yasuda, *Phys. Lett. B* **2007**, *649*, 427, [hep-ph/0703098].
[84] S. Antusch, O. Fischer, *JHEP* **2014**, *10*, 094, [arXiv:1407.6607].
[85] E. Fernandez-Martinez, J. Hernandez-Garcia, J. Lopez-Pavon, *JHEP* **2016**, *08*, 033, [arXiv:1605.08774].
[86] C. A. Argüelles, et al., 2022 Snowmass Summer Study, **2022**, *3*, arXiv:2203.10811.
[87] J. Beacham, et al., *J. Phys. G* **2020**, *47*, 010501, [arXiv:1901.09966].
[88] P. Agrawal, et al., *Eur. Phys. J. C* **2021**, *81*, 1015, [arXiv:2102.12143].
[89] A. M. Abdullahi, et al., 2022 Snowmass Summer Study, **2022**, *3*, arXiv:2203.08039.
[90] CMS Collaboration, Probing heavy Majorana neutrinos and the Weinberg operator through vector boson fusion processes in proton-proton collisions at $\sqrt{s} = 13$ TeV, arXiv:2206.08956.
[91] CMS Collaboration, A. Tumasyan, et al., *JHEP* **2022**, *07*, 081, [arXiv:2201.05578].
[92] CMS Collaboration, A. M. Sirunyan, et al., *Phys. Rev. Lett.* **2018**, *120*, 221801, [arXiv:1802.02965].
[93] CMS Collaboration, A. M. Sirunyan, et al., *JHEP* **2019**, *01*, 122, [arXiv:1806.10905].
[94] CMS Collaboration, V. Khachatryan, et al., *JHEP* **2016**, *04*, 169, [arXiv:1603.02248].
[95] CMS Collaboration, V. Khachatryan, et al., *Phys. Lett. B* **2015**, *748*, 144, [arXiv:1501.05566].
[96] CMS Collaboration, S. Chatrchyan, et al., *Phys. Lett. B* **2012**, *717*, 109, [arXiv:1207.6079].
[97] ATLAS Collaboration, Search for heavy neutral leptons in decays of W bosons using a dilepton displaced vertex in $\sqrt{s} = 13$ TeV pp collisions with the ATLAS detector, arXiv:2204.11988.
[98] ATLAS Collaboration, G. Aad, et al., *JHEP* **2019**, *10*, 265, [arXiv:1905.09787].
[99] ATLAS Collaboration, G. Aad, et al., *JHEP* **2015**, *07*, 162, [arXiv:1506.06020].
[100] ATLAS Collaboration, G. Aad, et al., *JHEP* **2011**, *10*, 107, [arXiv:1108.0366].
[101] LHCb Collaboration, R. Aaij, et al., *Phys. Rev. Lett.* **2014**, *112*, 131802, [arXiv:1401.5361].
[102] T. Asaka, S. Blanchet, M. Shaposhnikov, *Phys. Lett. B* **2005**, *631*, 151, [hep-ph/0503065].
[103] T. Asaka, M. Shaposhnikov, *Phys. Lett. B* **2005**, *620*, 17, [hep-ph/0505013].
[104] B. Patt, F. Wilczek, Higgs-field portal into hidden sectors, hep-ph/0605188.
[105] D. G. Cerdeno, A. Dedes, T. E. J. Underwood, *JHEP* **2006**, *09*, 067, [hep-ph/0607157].
[106] B. Batell, M. Pospelov, A. Ritz, *Phys. Rev. D* **2009**, *80*, 095024, [arXiv:0906.5614].

[107] FASER Collaboration, A. Ariga, et al., Technical Proposal for FASER: ForwArd Search ExpeRiment at the LHC, arXiv:1812.09139.
[108] F. Kling, S. Trojanowski, *Phys. Rev. D* **2018**, *97*, 095016, [arXiv:1801.08947].
[109] SHiP Collaboration, C. Ahdida, et al., SND@LHC, arXiv:2002.08722.
[110] D. Curtin, et al., *Rept. Prog. Phys.* **2019**, *82*, 116201, [arXiv:1806.07396].
[111] G. Aielli, et al., *Eur. Phys. J. C* **2020**, *80*, 1177, [arXiv:1911.00481].
[112] V. V. Gligorov, S. Knapen, B. Nachman, M. Papucci, D. J. Robinson, *Phys. Rev. D* **2019**, *99*, 015023, [arXiv:1810.03636].
[113] D. Dercks, H. K. Dreiner, M. Hirsch, Z. S. Wang, *Phys. Rev. D* **2019**, *99*, 055020, [arXiv:1811.01995].
[114] M. Bauer, O. Brandt, L. Lee, C. Ohm, ANUBIS: Proposal to search for long-lived neutral particles in CERN service shafts, arXiv:1909.13022.
[115] M. Hirsch, Z. S. Wang, *Phys. Rev. D* **2020**, *101*, 055034, [arXiv:2001.04750].
[116] J. L. Feng, et al., The Forward Physics Facility at the High-Luminosity LHC, arXiv:2203.05090.
[117] L. A. Anchordoqui, et al., *Phys. Rept.* **2022**, *968*, 1, [arXiv:2109.10905].
[118] S. Cerci, et al., *JHEP* **2022**, *2022*, 110, [arXiv:2201.00019].
[119] NA62 Collaboration, E. C. Gil, et al., *Phys. Lett. B* **2018**, *778*, 137, [arXiv:1712.00297].
[120] NA62 Collaboration, E. C. Gil, et al., *Phys. Lett. B* **2020**, *807*, 135599, [arXiv:2005.09575].
[121] NA62 Collaboration, E. C. Gil, et al., *Phys. Lett. B* **2021**, *816*, 136259, [arXiv:2101.12304].
[122] J.-L. Tastet, E. Goudzovski, I. Timiryasov, O. Ruchayskiy, *Phys. Rev. D* **2021**, *104*, 055005, [arXiv:2008.11654].
[123] E949 Collaboration, A. V. Artamonov, et al., *Phys. Rev. D* **2015**, *91*, 052001, [arXiv:1411.3963]. [Erratum: Phys.Rev.D 91, 059903 (2015)].
[124] W. Baldini, et al., SHADOWS (Search for Hidden And Dark Objects With the SPS), arXiv:2110.08025.
[125] W. Bonivento, et al., Proposal to Search for Heavy Neutral Leptons at the SPS, arXiv:1310.1762.
[126] SHiP Collaboration, M. Anelli, et al., A facility to Search for Hidden Particles (SHiP) at the CERN SPS, arXiv:1504.04956.
[127] S. Alekhin, et al., *Rept. Prog. Phys.* **2016**, *79*, 124201, [arXiv:1504.04855].
[128] SHiP Collaboration, C. Ahdida, et al., *JHEP* **2019**, *04*, 077, [arXiv:1811.00930].
[129] J.-L. Tastet, I. Timiryasov, *JHEP* **2020**, *04*, 005, [arXiv:1912.05520].
[130] SHiP Collaboration, C. Ahdida, et al., *Eur. Phys. J. C* **2022**, *82*, 486, [arXiv:2112.01487].
[131] DUNE Collaboration, A. A. Abud, et al., *Instruments* **2021**, *5*, 31, [arXiv:2103.13910].
[132] P. Ballett, T. Boschi, S. Pascoli, *JHEP* **2020**, *03*, 111, [arXiv:1905.00284].
[133] J. M. Berryman, A. de Gouvea, P. J. Fox, B. J. Kayser, K. J. Kelly, J. L. Raaf, *JHEP* **2020**, *02*, 174, [arXiv:1912.07622].
[134] I. Krasnov, *Phys. Rev. D* **2019**, *100*, 075023, [arXiv:1902.06099].
[135] P. Coloma, E. Fernández-Martínez, M. González-López, J. Hernández-García, Z. Pavlovic, *Eur. Phys. J. C* **2021**, *81*, 78, [arXiv:2007.03701].
[136] M. Breitbach, L. Buonocore, C. Frugiuele, J. Kopp, L. Mittnacht, *JHEP* **2022**, *01*, 048, [arXiv:2102.03383].
[137] Belle Collaboration, D. Liventsev, et al., Search for a heavy neutrino in tau decays at Belle, arXiv:2212.10095.
[138] FCC-ee study Team Collaboration, A. Blondel, E. Graverini, N. Serra, M. Shaposhnikov, *Nucl. Part. Phys. Proc.* **2016**, *273-275*, 1883, [arXiv:1411.5230].
[139] S. Antusch, E. Cazzato, O. Fischer, *Int. J. Mod. Phys. A* **2017**, *32*, 1750078, [arXiv:1612.02728].
[140] A. Blondel, et al., *Front. in Phys.* **2022**, *10*, 967881, [arXiv:2203.05502].
[141] Y.-F. Shen, J.-N. Ding, Q. Qin, *Eur. Phys. J. C* **2022**, *82*, 398, [arXiv:2201.05831].
[142] K. Mękała, J. Reuter, A. F. Żarnecki, *JHEP* **2022**, *06*, 010, [arXiv:2202.06703].
[143] S. Pascoli, R. Ruiz, C. Weiland, *JHEP* **2019**, *06*, 049, [arXiv:1812.08750].
[144] R. Ruiz, M. Spannowsky, P. Waite, *Phys. Rev. D* **2017**, *96*, 055042, [arXiv:1706.02298].
[145] S. Antusch, O. Fischer, A. Hammad, *JHEP* **2020**, *03*, 110, [arXiv:1908.02852].
[146] W. Rodejohann, *Phys. Rev. D* **2010**, *81*, 114001, [arXiv:1005.2854].
[147] K. M. Black *et al.*, Muon Collider Forum Report, arXiv:2209.01318.
[148] T. Bose, et al., Report of the Topical Group on Physics Beyond the Standard Model at Energy Frontier for Snowmass 2021, arXiv:2209.13128.
[149] G. Cvetic, C. S. Kim, *Phys. Lett. B* **1999**, *461*, 248, [hep-ph/9906253]. [Erratum: Phys.Lett.B 471, 471–472 (2000)].
[150] F. M. L. Almeida Jr., Y. A. Coutinho, J. A. Martins Simoes, M. A. B. do Vale, *Phys. Lett. B* **2000**, *494*, 273, [hep-ph/0008231].
[151] K. A. U. Calderón, I. Timiryasov, O. Ruchayskiy, Improved constraints and the prospects of detecting TeV to PeV scale Heavy Neutral Leptons, arXiv:2206.04540.
[152] A. Crivellin, F. Kirk, C. A. Manzari, *JHEP* **2022**, *12*, 031, [arXiv:2208.00020].
[153] B. Shuve, M. E. Peskin, *Phys. Rev. D* **2016**, *94*, 113007, [arXiv:1607.04258].
[154] A. Abada, N. Bernal, M. Losada, X. Marcano, *JHEP* **2019**, *01*, 093, [arXiv:1807.10024].
[155] J.-L. Tastet, O. Ruchayskiy, I. Timiryasov, *JHEP* **2021**, *12*, 182, [arXiv:2107.12980].
[156] A. Abada, P. Escribano, X. Marcano, G. Piazza, Collider Searches for Heavy Neutral Leptons: beyond simplified scenarios, arXiv:2208.13882.
[157] P. F. Perez, T. Han, T. Li, *Phys. Rev. D* **2009**, *80*, 073015, [arXiv:0907.4186].
[158] C. Biggio, F. Bonnet, *Eur. Phys. J. C* **2012**, *72*, 1899, [arXiv:1107.3463].
[159] ATLAS Collaboration, G. Aad, et al., *Eur. Phys. J. C* **2021**, *81*, 334, [arXiv:2009.04986].
[160] J. Kersten, A. Y. Smirnov, *Phys. Rev. D* **2007**, *76*, 073005, [arXiv:0705.3221].
[161] M. Shaposhnikov, *Nucl. Phys. B* **2007**, *763*, 49, [hep-ph/0605047].
[162] J. Gluza, *Acta Phys. Polon. B* **2002**, *33*, 1735, [hep-ph/0201002].
[163] K. Moffat, S. Pascoli, C. Weiland, Equivalence between massless neutrinos and lepton number conservation in fermionic singlet extensions of the Standard Model, arXiv:1712.07611.
[164] M. Drewes, J. Klarić, P. Klose, *JHEP* **2019**, *11*, 032, [arXiv:1907.13034].
[165] E. Fernández-Martínez, X. Marcano, D. Naredo-Tuero, HNL mass degeneracy: implications for low-scale seesaws, LNV at colliders and leptogenesis, arXiv:2209.04461.
[166] ATLAS Collaboration, G. Aad, et al., Phys. Rev. D **2015**, *92*, 032001, [arXiv:1506.01839].
[167] ATLAS Collaboration, G. Aad, et al., *JHEP* **2015**, *09*, 108, [arXiv:1506.01291].
[168] CMS Collaboration, A. M. Sirunyan, et al., *Phys. Rev. D* **2019**, *100*, 052003, [arXiv:1905.10853].
[169] CMS Collaboration, A. M. Sirunyan, et al., *JHEP* **2020**, *03*, 051, [arXiv:1911.04968].
[170] ATLAS Collaboration, G. Aad, et al., *Eur. Phys. J. C* **2021**, *81*, 218, [arXiv:2008.07949].
[171] ATLAS Collaboration, G. Aad, et al., *Eur. Phys. J. C* **2022**, *82*, 988, [arXiv:2202.02039].

[172] A. D. Martin, W. J. Stirling, R. S. Thorne, G. Watt, *Eur. Phys. J. C* **2009**, *63*, 189, [arXiv:0901.0002].
[173] J. Alwall, R. Frederix, S. Frixione, V. Hirschi, F. Maltoni, O. Mattelaer, H. S. Shao, T. Stelzer, P. Torrielli, M. Zaro, *JHEP* **2014**, *07*, 079, [arXiv:1405.0301].
[174] W. R. Inc., "Mathematica, Version 13.2." Champaign, IL, **2022**.
[175] A. Alloul, N. D. Christensen, C. Degrande, C. Duhr, B. Fuks, *Comput. Phys. Commun.* **2014**, *185*, 2250, [arXiv:1310.1921].
[176] D. Alva, T. Han, R. Ruiz, *JHEP* **2015**, *02*, 072, [arXiv:1411.7305].
[177] C. Degrande, O. Mattelaer, R. Ruiz, J. Turner, *Phys. Rev. D* **2016**, *94*, 053002, [arXiv:1602.06957].
[178] NNPDF Collaboration, R. D. Ball, et al., *Eur. Phys. J. C* **2022**, *82*, 428, [arXiv:2109.02653].
[179] A. Buckley, J. Ferrando, S. Lloyd, K. Nordström, B. Page, M. Rüfenacht, M. Schönherr, G. Watt, *Eur. Phys. J. C* **2015**, *75*, 132, [arXiv:1412.7420].
[180] Feebly-interacting particles: FIPs 2022 workshop report, In preparation (2023).
[181] ATLAS Collaboration, G. Aad, et al., *JHEP* **2020**, *11*, 163, [arXiv:2007.14811].
[182] M. Gronau, C. N. Leung, J. L. Rosner, *Phys. Rev. D* **1984**, *29*, 2539.
[183] ATLAS Collaboration, Performance of the reconstruction of large impact parameter tracks in the ATLAS inner detector.

Conclusions

This thesis focused on a compendium of papers whose guideline is the connection of HNLs with ALPs. Such a pair naturally arises in models featuring (at least) a complex singlet and heavy sterile neutrinos. If the symmetry is not exact, the ALP receives radiative contributions that identify preferred mass regions. Such a feature also generates interactions of the ALP to fermions, which manage to evade the proportionality of the coupling to the respective fermion masses. The simultaneous presence of such New Physics (NP) enhances their potential mutual discoveries. This makes them both theoretically well-motivated and experimentally appealing.

At the end of the three years of PhD studies, it is worth stopping for a moment and reflecting on the scientific values of the works of this thesis. Indeed, choosing not one but two types of NP at a time might seem an unrealistic guess. The situation worsens when studying even specific UV models or developing ideas from anomalies which might turn out to be caused by statistical fluctuations or systematics. The question I would like to raise as an objection and which now guides and has guided my path is: how likely is it that problems and puzzles that the SM faces can be solved in areas of the new physics that 1) cannot interact with each other and 2) cannot synergistically contribute to the solution of the same problem/puzzle? Above all, the opposite is also true, i.e. that even if we were interested in solving one of the puzzles mentioned, we could not ignore the problems that nevertheless remain, and we should consider what the interactions between these areas might be. While it is true that there are many combinations of new physics, it is not obvious that all of them can work together organically. The many aspects of this quest force us to look in more than one context at the same time: colliders still have the burden of exploring the Higgs mechanism, precision observables are testing the core of the SM, gravitational waves can see phase transitions and give signals of symmetry breaking, cosmic rays can give us information on the transparency of the universe and thus of new particles, etc.

Only a posteriori we will know whether these works will age well and prove useful to the community and my future research.

Conclusiones

Esta tesis se centra en un compendio de trabajos cuya guía es la conexión de los HNL con los ALP. Ambos surgen de forma natural en modelos que presentan (al menos) un singlete complejo y neutrinos estériles pesados. Si la simetría no es exacta, el ALP recibe contribuciones radiativas que identifican regiones de masa preferidas. Tal característica también genera interacciones del ALP con fermiones, que consiguen eludir la proporcionalidad del acoplo con las respectivas masas de los fermiones.La presencia simultánea de estas opciones de nueva física (NF) aumenta la posibilidad de un potencial descubrimiento mutuo, lo que las hace tanto teóricamente bien motivadas como atractivas experimentalmente.

Al final de los tres años de estudios de doctorado merece la pena detenerse un momento y reflexionar sobre sobre el valor científico de los trabajos de esta tesis. En efecto, elegir no uno sino dos tipos de NF a la vez puede parecer una suposición poco realista. La situación empeora cuando se estudian también modelos UV específicos o se desarrollan ideas a partir de anomalías que podrían resultar ser causadas por fluctuaciones estadísticas o sistemáticas. La pregunta que me gustaría plantear como objeción y que ahora guía y ha guiado mi camino es: ¿hasta qué punto es probable que los problemas y enigmas a los que se enfrenta el SM puedan resolverse en áreas de la nueva física que 1) no pueden interactuar entre sí y 2) no pueden contribuir sinérgicamente a la solución del mismo problema/enigma? Sobre todo, lo contrario también es cierto, es decir, aunque estuviéramos interesados en resolver uno de los rompecabezas mencionados anteriormente, no podríamos ignorar los problemas que, sin embargo, siguen existiendo, y deberíamos considerar cuáles podrían ser las interacciones entre estas áreas. Si bien es cierto que existen muchas combinaciones de nueva física, no es obvio que todas ellas puedan funcionar juntas de forma orgánica. Los múltiples aspectos de esta búsqueda nos obligan a mirar en más de un contexto al mismo tiempo: los colisionadores todavía tienen que explorar el mecanismo de Higgs, los observables de precisión están poniendo a prueba el núcleo del SM, las ondas gravitacionales pueden ver transiciones de fase y dar señales de ruptura de simetría, los rayos cósmicos pueden darnos información sobre la transparencia del

universo y, por tanto, de nuevas partículas, etc.

Sólo a posteriori sabremos si estos trabajos envejecen bien y resultan útiles a la comunidad y a mis futuras Investigaciones.

Acknowledgements

As always, the end of a journey deserves a moment to thank a number of people without whom it would not have been possible to come this far at the end of this PhD.

Firstly, I would like to thank my supervisor, Luca M., for having had faith in my abilities (and in my "creative" names), welcoming me into his group and guiding me with patience and passion through these years in the world of physics. I could not have hoped for more fertile ground to experience these three years.

Likewise, I would like to thank Belen, Enrique and Pilar. I vividly remember the interview for the position in HIDDeN. I can only express my sincerest gratitude for the trust you have placed in me and for the physics discussions I had with you. I express similar gratitude to Jose Miguel No, who kindly accepted to be part of the tribunal.

I thank my comrades of the office 308: Alejandro, Alvaro and Samuel, and earlier Fran and Judit. Your daily company has been a sweet source of good humour and stimulation for me. I am sure you will all find a happy path in life and I hope I have left you with good memories of Italy.

I could hardly omit a warm thought to my favourite PostDocs and lunch companions: Jean-Loup T., Maria R. and Javier L.: you rock! It started with donuts in the office and ended with a weekend at the beach, but I am sure we will see each other again, whether in the sunny south or the cloudy north.

Thanks also to Marta F. for the valuable Spanish lessons, to Victor and Jonathan for the exciting discussions at two in the morning at various conferences and to Jesus B. for many laughs during my first article here at IFT.

Many thanks also to Rebeca B. V. I will never forget your professionalism, kindness and patience in helping me with the bureaucracy!

Finally, thanks to all the other members of the IFT, PhDs, PostDocs and Seniors for the incredible working environment.

Many thanks to Stefan Pokorski: it was an honour and a pleasure to work and chat with you.

A hug to some friends and colleagues, Gioacchino P., Giuseppe L., and Xavier P.D.: there will be fun and much to work on!

As dulcis in fundo est, I would like to thank a number of people without whose support I would not be here today.

First of all, my family, my mother Stefania, my father Luigi and my sister Federica: the three big "S" of my life. It's not an understatement to say that without your encouragement, love and unconditional support I could not aspire to the title of Doctor today. Everything good that I am starts with you.

Secondly, a special thanks to Alberto L. for his evergreen friendship. Although he has been travelling the world in recent years (and showing me pictures of tropical paradises and turtles while I was in the office), he has never ceased to be a constant source of support and inspiration. Per aspera ad astra Amico mio!

The list of dear friends around the world that I have carried in my heart over the years is clearly long. I would like to mention Cecilia, Mario, Edison, Marco, Denis, Filippo, Maria, the Veneto clan, Giorgia and Nica.

Finally, I would like to thank a group of people I met in Rotaract Madrid Serrano: David, Laura, Dani, Patricia, Amira, Christian, Luis (Khaled) and Said (Zeit Zaitun), Emiliano, Juan Andrès, Sara, Andrea, Charlotte. You have been a second family to me, and to you I owe many of my sweetest memories, not only of Madrid.

'It has done me good,' said the fox, 'because of the colour of the wheat fields'. [1]

A.d.G. acknowledge partial financial support by the Spanish Research Agency (Agencia Estatal de Investigación) through the grant IFT Centro de Excelencia Severo Ochoa No CEX2020-001007-S and by the grant PID2019-108892RB-I00 funded by MCIN/AEI/10.13039/501100011033, by the European Union's Horizon 2020 research and innovation programme under the Marie Skłodowska-Curie grant agreement No 860881-HIDDeN.

[1] *Le Petit Prince*, A. de Saint-Exupéry, 1943.